

**STUDIES ON THE DYNAMICS OF ULTRAFAST PHOTOINDUCED
PROCESSES IN CONDENSED PHASE USING THIOFLAVIN-T AND
COUMARIN AS THE PROBES**

By

**PRABHAT KUMAR SINGH
BHABHA ATOMIC RESEARCH CENTRE**

*A thesis submitted to the
Board of Studies in Chemical Science Discipline*

*In partial fulfillment of requirements
For the degree of*

**DOCTOR OF PHILOSOPHY
of
HOMI BHABHA NATIONAL INSTITUTE**



November, 2010

Homi Bhabha National Institute

Recommendations of the Viva Voce Board

As members of the Viva Voce board, we certify that we have read the dissertation prepared by **PRABHAT KUMAR SINGH** entitled **Studies on the Dynamics of Ultrafast Photoinduced Processes in Condensed Phase using Thioflavin-T and Coumarin as the Probes** and recommend that it may be accepted as fulfilling the dissertation requirement for the Degree of Doctor of Philosophy.

Chairman- Prof. T. Mukherjee

Date:

Convener- Prof. H. Pal

Date:

Member 1- Prof. P. N. Bajaj

Date:

Member 2- Prof. D. K. Palit

Date:

External Examiner- Prof. Anindya Datta (IIT Bombay)

Date:

Final approval and acceptance of this dissertation is contingent upon the candidate's submission of the final copies of the dissertation to HBNI.

I hereby certify that I have read this dissertation prepared under our direction and recommend that it may be accepted as fulfilling the dissertation requirement.

Date: March 21, 2011

Place: Mumbai

Prof. H. Pal

(Guide)

STATEMENT BY AUTHOR

This dissertation has been submitted in partial fulfillment of requirements for an advanced degree at Homi Bhabha National Institute (HBNI) and is deposited in the Library to be made available to borrowers under rules of the HBNI.

Brief quotations from this dissertation are allowable without special permission, provided that accurate acknowledgement of source is made. Requests for permission for extended quotation from or reproduction of this manuscript in whole or in part may be granted by the Competent Authority of HBNI when in his or her judgment the proposed use of the material is in the interests of scholarship. In all other instances, however, permission must be obtained from the author.

Prabhat Kumar Singh

DECLARATION

I, hereby declare that the investigation presented in the thesis has been carried out by me. The work is original and has not been submitted earlier as a whole or in part for a degree / diploma at this or any other Institution / University.

Prabhat Kumar Singh

Dedicated to.....

*My Beloved
Mother*

ACKNOWLEDGEMENTS

Completing the PhD degree has been one of the most cherished dreams of my life right from the early days of my graduation. At the juncture of this milestone achievement, I would like to express my sincere gratitude to number of people to whom I am really indebted to for their help, support and motivation in all my endeavors. At the outset I wish to record my heartfelt gratitude and indebtedness to Prof. Swapnadip Thakur whose magical and inspiring teaching at the Masters deeply motivated me to choose research in chemistry as my scientific career.

I would like to express my deep and sincere gratitude to my guide, Prof. H. Pal for his invaluable guidance, constant encouragement, unstinted inspiration, keen interest and good wishes. His wide knowledge and his logical way of thinking on critical scientific problems have been of great value for me. I am also grateful to him for being patient while critically reviewing this thesis.

This thesis would not have been possible without the guidance, help, support, critical analysis and valuable suggestions from Dr. S. Nath who has been truly invaluable to me both on an academic and a personal level, for which I am extremely grateful. I am also thankful to him for sharing his excellent knowledge and scientific understanding with me. His enthusiasm, deep engagement in research and critical analysis strategy of experimental data has made a deep impression on me.

I wish to express my sincere thanks to my senior colleague Dr. M. Kumbhakar for his diversified help, fruitful scientific discussions and moral support offered to me from time to time throughout the course of the work. I also had the opportunity to discuss with Dr. G. B. Dutt and Dr. R. Ganguly whose work and knowledge on block copolymer-surfactant assembly has been very useful during the course of this work.

My special thanks goes to my colleague and my dear friend Ms. Mhejabeen Shaikh for her moral support, diversified help, and several funs which will always be remembered. She has been very patient while listening to me whenever I was excited about a new scientific idea.

It gives me immense pleasure to thank the members of the doctoral committee Prof. T. Mukherjee (Chairman), Prof. D. K. Palit (Member) and Prof. P. N. Bajaj (Member) for their critical review and suggestions during the progress review and pre-synopsis viva-voce.

It is my great privilege to acknowledge the trust and support extended by Prof. T. Mukherjee, Director, Chemistry Group and Dr. S. K. Sarkar, Head, RPCD since my joining this department.

I also gratefully acknowledge the help rendered by all the members of Molecular Photochemistry Section and Radiation & Photochemistry Division.

I express my heartfelt thanks to my special friends Arup Da, Aasis Da, Pradeep, Anirban, Rubel, Brindaban, Rajib, Chandralekha, Raghunath, Sandip, Sanjit, Sajal da and all others for their numerous help, support and enjoyable company for making the life more cheerful.

Today I really miss two of my very good friends Umang and Partha who were also my regular partners in the lonely evenings. I am sure their eternal souls will be very happy for me to achieve this success.

Finally, I owe my heartfelt gratitude and indebtedness to my grandparents, my parents, my elder sister Sandhya and beloved elder brother Sachin who have always encouraged me to follow my heart and inspired my inquisitive mind throughout my childhood and study career. It is their inspiration, encouragement, blessings and support that helped me to achieve what I am today.

November, 2010

Prabhat Kumar Singh
RPCD, BARC

The important thing in science is not so much to obtain new facts as to discover new ways of thinking about them

-William Lawrence Bragg

CONTENTS

	Page No.
SYNOPSIS	xv - xxxi
LIST OF FIGURES	xxxii-xlv
LIST OF TABLES	xlvi- xlvii
CHAPTER 1	
Introduction	
1.1. General Introduction: Photoinduced Processes	1-4
1.2. Intramolecular Configurational Changes in the Excited State	4-6
1.3. Dynamic Stokes' shifts and Solvent Relaxation Dynamics	6-8
1.4. Reverse Micelle and their General Characteristics	9-13
1.5. Cyclodextrins as Supramolecular hosts	13-15
1.6. Block Copolymers and their solution behavior	15-18
1.7. Motivation of the present work	18-22

CHAPTER 2

Instruments and Methods

2.1. Introduction	23
2.2. Ground-State Absorption Measurements	23-25
2.3. Steady-State Fluorescence Measurements	25
2.3.1. Correction of Emission Spectra	26
2.3.2. Fluorescence Quantum Yield Measurement	27
2.4. Fluorescence Lifetime Measurements	27-29
2.4.1. Basic Principles of TCSPC Technique	29-31
2.4.2. Important components of a TCSPC spectrometer	32-35
2.4.2.1. Time Calibration of the MCA channels in a TCSPC Spectrometer	35-36
2.4.2.2. Analysis of the fluorescence decay curves measured in a TCSPC instrument	36-37
2.5. Fluorescence Anisotropy Measurements	37-42
2.6. Fluorescence up-conversion Measurements	42-43
2.6.1. Basic principle of fluorescence up-conversion	43
2.6.1.1. Sum-frequency generation	43-46
2.6.1.2. Time resolution	47-48
2.6.2. Brief description of the present fluorescence up-conversion setup	48
2.6.2.1. The key features	48-50
2.6.2.2. Instrument response function	50-51

2.7. Cyclic Voltammetry and Differential Pulse Voltammetry	51-53
2.8. Quantum Chemical Calculations	53-54
2.9. Small Angle Neutron Scattering Measurements	54-56

CHAPTER 3

Ultrafast Bond Twisting Dynamics Studies on Amyloid Fibril Sensor Dyes Thioflavin-T and its Derivatives

3.1. Introduction	57-60
3.2. Experiments and Methods	60-62
3.2.1. Synthesis of ThT derivatives	62-64
3.3. Results and Discussion	64
3.3.1. Ground-state absorption and steady-state fluorescence studies of ThT and its derivatives Ia and Ib	64-67
3.3.2. Time-resolved fluorescence studies of Ia and Ib	68-69
3.3.3. Quantum chemical calculations for Ia and Ib	69-72
3.3.4. Time-resolved fluorescence studies of ThT in aqueous solution	72-76
3.3.5. Quantum Chemical Calculations for ThT	76-79
3.3.6. Studies on the Viscosity Effect of the Solvent upon the Bond Twisting Dynamics of ThT	79
3.3.6.1. Steady-state fluorescence studies	79-80
3.3.6.2. Time-resolved fluorescence measurements	80-90
3.3.7. Excited-State Dynamics of ThT in Amyloid Fibril	90-92
3.4. Conclusions	92-93

CHAPTER 4

Ultrafast Bond Twisting Dynamics of Thioflavin-T in Nanoconfined Water Pools

4.1. Introduction	94-96
4.2. Experiments and Methods	96-97
4.3. Results and Discussion	97
4.3.1. Ground-state absorption and steady-state emission studies	97-103
4.3.2. Time-resolved fluorescence studies	103-109
4.3.3. ThT in cationic reverse micelle	109-116
4.4. Conclusion	116-118

CHAPTER 5

Effect of β -CD Nanocavity on the Ultrafast Bond Twisting Dynamics of Thioflavin-T

5.1. Introduction	119-121
5.2. Experiments and Methods	121-122
5.3. Results and Discussion	122
5.3.1. Steady-state measurements	122-124
5.3.2. Time-resolved measurements	124-132
5.4. Conclusion	132

CHAPTER 6

Quantitative Distinction between Competing Intramolecular Bond Twisting & Solvent Relaxation Dynamics

6.1. Introduction	133-135
6.2. Experiments and Methods	135
6.3. Results and Discussion	135-145
6.4. Conclusion	145

CHAPTER 7

Effect of Electrostatic Interaction on the Probe Migration in Polymer-Surfactant Supramolecular Assembly: A Solvent and Rotational Relaxation Study

7.1. Introduction	146-149
7.2. Experiments and Methods	149-151
7.3. Results and Discussion	151
7.3.1. P123-CTAC system	151
7.3.1.1. Ground-state absorption and steady-state fluorescence studies	151-154
7.3.1.2. Solvent relaxation studies in P123-CTAC system	154-162
7.3.1.3. Rotational relaxation studies in P123-CTAC Systems	162-165
7.3.2. Studies on F88-CTAB mixed micellar system	165

7.3.2.1. Small angle neutron scattering (SANS) studies	166-167
7.3.2.2. Absorption and fluorescence studies in F88-CTAB system	167-169
7.3.2.3. Rotational relaxation Studies in F88-CTAB systems	169-172
7.3.2.4. Dynamic Stokes' shift measurements in F88-CTAC system	172-176
7.3.3. Studies on P105-CTAB mixed micellar systems	176-180
7.3.4. Effect of addition of SDS on the solute location in the polymer-surfactant assembly	180-181
7.3.5. Tuning the chemical reactivity in the nanocontainer	181-185
7.4. Conclusion	185-186

REFERENCES	187-205
-------------------	---------

LIST OF PUBLICATIONS	206-207
-----------------------------	---------

SYNOPSIS

It is well known that photoexcitation of a molecule generally induces changes in its electronic and geometrical structures, which in turn lead to the changes in its interactions with the nearby molecules and its environment. In many cases, the molecular interactions are greatly augmented in the excited electronic state where the energy of excitation is used partly as the driving force for the reaction dynamics, leading to various photophysical and photochemical processes, which include electronic charge redistribution,¹⁻³ electron and proton transfer,¹⁻⁶ large amplitude intramolecular torsional motions,⁷ trans-cis isomerization,^{8,9} intramolecular vibrational redistribution, intermolecular vibrational relaxation (vibrational cooling),^{10,11} internal conversion,^{12,13} solvation,^{1,2,14-16} etc. Ultrafast photoinduced intramolecular conformational changes are omnipresent in chemistry and biology. Extremely high reaction rates for such processes often faster than 10^{12} s^{-1} , arise mainly because the potential energy curve in the excited state, as a function of reaction coordinate, lacks an activation barrier. Such processes often constitute the nonradiative deactivation pathways for the excited state of the molecule leading to its very low emission quantum yield. These large amplitudes motion are strongly affected by the viscosity of the surrounding medium and thereby making such molecules as the potential probes to act as the viscosity sensors for various environments ranging from homogeneous to micro-heterogeneous media including biological systems. Control of these large amplitude intramolecular movements is a prerequisite for the development of the devices that would function through the motions at the molecular level.

Thioflavin-T (ThT), a benzothiazole based cationic dye, is one such molecule which is understood to have an ultrafast intramolecular relaxation process in its excited state mediated through large amplitude torsional motion. ThT is used as an extrinsic fluorescence sensor to monitor and estimate the formation of amyloid fibril, a filamentous form of protein responsible for several neurodegenerative diseases, like Alzheimer's and Parkinson's diseases.¹⁷⁻²⁰

Although ThT in water is very weakly fluorescent,²¹ it shows a remarkable enhancement in emission yield on its association with amyloid fibrils.¹⁷⁻²⁰ ThT is known to be very specific in its binding with amyloid form of the proteins with no significant interaction with other forms, namely, the folded or partially folded monomeric proteins.²² Detailed studies in several confined environments, like in amyloid fibril,^{17,22} polymer,²³ glass matrix,²⁴ etc., clearly indicate that the high local viscosity of the microenvironment around the dye is directly related to the observed fluorescence enhancement of ThT dye in these systems. However, understanding the basic molecular aspect of the process that is involved in the observed fluorescence enhancement of ThT in the above microenvironments has still remained elusive. Considering the molecular structure of ThT, it is hypothesized that in bulk water, due to the low viscosity of the medium, an intramolecular bond twisting process possibly takes place in the excited state of the molecule. This bond twisting process effectively introduces a very fast non-radiative decay channel for the excited ThT molecule resulting its extremely low fluorescence yield. In contrast, in a highly viscous medium, like in amyloid fibril, the above bond twisting process in the excited dye is significantly retarded, reducing its non-radiative decay channel. Accordingly there is a remarkable increase in the emission yield of ThT in a highly viscous medium and hence its fluorescence sensor ability in amyloid fibrils. In the present thesis a detailed study on the ultrafast fluorescence decay dynamics of the amyloid sensing dye, Thioflavin-T and two of its tailor made derivatives has been carried out in different solvents of varying viscosity to understand the basic molecular aspect responsible for the fluorescence sensing activity of ThT and to understand the different relaxation pathways of the excited ThT molecule.

Last two decades have witnessed the increasing significance of various organized assemblies on biological and photophysical processes. Reactants embeded in molecular assemblies like micelles, reverse micelles, cyclodextrins, vesicles, etc., achieve a greater

degree of organization compared to their geometries in homogeneous solution and can mimic many reactions in biosystems. They can also have potential applications in nanoparticle synthesis, pharmaceuticals and many other uses. The local viscosity/rigidity within the organized assemblies are appreciably different from that in the bulk liquid medium and as a result, these systems can alter the photoprocess of the entrapped molecule quite drastically. In the bulk state, water molecules form an extended intermolecular hydrogen-bonding network, which is highly dynamic in nature in terms of both bond lengths and H-bond partners, and accordingly this network structure fluctuations on picosecond to subpicosecond time scales.^{25,26} Because of the existence of this network, water is expected to be uniquely sensitive to the presence of a surface or its confinement in a nanostructure. Much of the importance of confined water comes about as many chemical and biochemical reactions do take place under similar situation. Thus, it is important to understand how the observed slower solvent relaxation dynamics in water nanodroplets influence the rate of various chemical reactions. Further, understanding the ultrafast dynamics of the photoexcited ThT molecule under different restricted microenvironments is very essential to understand the underlying molecular aspects responsible for the enhancement of the fluorescence emission yield of ThT in amyloid fibril. With this perspective, effect of the nanoconfined water in both anionic and cationic reverse micelles on the ultrafast torsional dynamics of the photoexcited ThT molecules has been investigated in detail. Extending this study further, the effect of bio-mimetic supramolecular encapsulation of ThT into β -cyclodextrin cavity on the excited state relaxation dynamics of the dye has also been investigated to understand the consequence of restricted environment on the fluorescence enhancement of the dye.

The dynamic response of the solvent molecules to the photoinduced changes in the charge distribution of the chromophoric solute molecule is of great research interest in photochemical sciences. Unlike electronic response, the dynamic response of the solvent

molecules is not instantaneous. The finite time required for the changes in solvent environment towards an electronic perturbation is crucial in determining the dynamics of the excited-state relaxation of the chromophoric dyes. The processes involved in such cases are quite complex in general and their propensity and manifestation are controlled by both intra- and intermolecular interactions of the dye and solvent environment. Wide varieties of fluorescence probes have been used to understand the solvent relaxation dynamics following dynamic Stokes' shift measurements and consequently to understand the nature of the local microenvironments. A judicious choice of a fluorescent probe for such solvent relaxation studies largely depends on the nature of the microenvironment under investigation. A major bottleneck in studying solvent relaxation dynamics with large probe molecules is the interference of several intramolecular processes in the excited probe that takes place in the similar time scale of the solvent relaxation dynamics. The competing intramolecular processes in the probe molecules that can significantly interfere the dynamic Stokes' shift measurement for solvent relaxation studies are the twisting of the functional groups around a bond, cis-trans isomerization, conformational change etc. Such an interference poses a tremendous challenge to the experimentalists in distinguishing various contributions of the different types of the relaxation processes in the observed results. In order to understand the actual dynamics of the solvent relaxation process, it is thus very essential to separate out the contribution of the interfering intramolecular processes in the probe from the solvent relaxation process. In the present thesis a methodology has been devised to quantitatively distinguish and separate out the effect of such a competing intramolecular process from the solvent relaxation process. The methodology has been demonstrated using three coumarin derivatives, namely coumarin-153 (C153), coumarin-481 (C481) and coumarin-152 (C152) in acetonitrile solution.

Dynamic Stokes' shift measurements for solvent relaxation study have been applied very extensively to understand the structure and dynamics of different chemical and biological

systems. For example, this method has been used to understand the nature of water molecules in different micro-heterogeneous media, like micelles,²⁷ reverse micelles, vesicles,²⁸ DNA,²⁹ protein,³⁰ pluronic- surfactant mixtures,³¹ etc. In the present thesis our major focus is to explore the pluronic-surfactant supramolecular assemblies using solvent relaxation dynamics as the tool. Pluronics are an important class of tri-block copolymers made up of poly ethyleneoxide (EO) and poly propyleneoxide (PO) blocks with general molecular formula $(EO)_n-(PO)_m-(EO)_n$. These water soluble tri-block copolymers have attracted considerable attention in last two decades partly because of their complex behavior in solution³²⁻³⁴ and partly because of their wide range of industrial applications, as detergent, lubricant and emulsifier.^{35,36} The unique behavior of the pluronics in aqueous solution and their low toxicity have made these polymers highly useful in many pharmaceutical formulations.^{37,38} In several industrial applications, pluronics are often used in combination with other low molecular weight ionic surfactants.³⁹ This feature has prompted experimental studies on the solution behavior of these mixed copolymer-surfactant systems.⁴⁰ Presence of two different classes of surfactants results in the formation of complex microheterogeneous systems whose properties and solution behavior are essential to be known to use them in a practical formulation. It is reported that some pluronic micelles form unique supramolecular assemblies in the presence of an ionic surfactant, for example, sodium dodecyl sulphate (SDS).^{41,42} In these supramolecular assemblies, it is understood that the hydrophobic chains of the SDS surfactant molecules are dissolved in the core of the pluronic micelles and the charged head groups of the SDS surfactants are resided at the peripheral region of the core projecting into the hydrated corona region of the micelles.⁴¹ Because of this unique structure of these assemblies, a charged layer is formed inside these mixed micelles. Accordingly, any solute having a charge opposite to that of the charged layer inside these supramolecular assemblies, can experience an electrostatic attraction towards the core-corona interface of the micelles. Such systems can thus provide a

wide range of microenvironments for the dissolved solutes. Because of the availability of wide range of microenvironments in these micelles, the solutes may also have quite different physical and chemical properties depending on their locations in the micelle. Thus, by changing the position of a solute in these micelles, it is possible to modulate the physical as well as the chemical properties of the solute in these microheterogeneous systems. In the present work we have studied the effect of ionic surfactant on the localization site of a solubilized molecule in a polymer-surfactant supramolecular assembly. Our aim is to see if the location of the solute in the micelle can be changed by changing the polymer-surfactant composition of the supramolecular systems. Additionally, we also investigate how the photophysical properties of the solubilized dye and the structure of water molecules around the dye in the micelle change with a change in the dye location in the supramolecular system, investigated using solvent relaxation dynamics as tool.

The results obtained for different systems investigated in the present research program have been presented and discussed in this thesis, to be submitted to the Homi Bhabha National Institute for the Ph.D. degree. For convenience of presentation, different aspects of the present work have been discussed in a systematic manner in seven different chapters of the thesis. The contents of the different chapters in the present thesis are briefly given below.

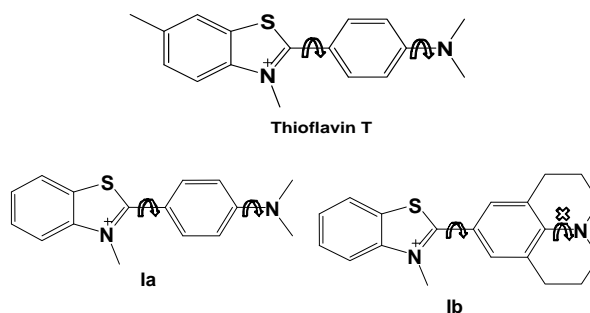
Chapter 1: This chapter of the thesis presents the basic aspects of photophysical and photochemical processes involving excited chromophoric molecules, with special emphasis to the photoinduced barrierless processes and solvent relaxation dynamics. This chapter also describes the general aspects of reverse micelles and cyclodextrins used as the confined medium in the present study. A detailed discussion on the aggregation behavior of the PEO–PPO–PEO type tri-block copolymer systems in aqueous solution is presented. The systems that have been chosen for the investigation in the present study are described in detail.

Brief note on the objective and motivation of the present work has also been discussed in this introductory chapter.

Chapter 2: Different instrumental techniques used in the present study to carry out different photophysical and photochemical measurements have been described briefly in this chapter. Working principle of the time-correlated single photon counting (TCSPC) spectrometer and fluorescence upconversion technique has been discussed in this chapter with some greater detail, as these techniques of time-resolved fluorescence measurements are quite involved. Basic principles of the other instrumental techniques used in the present study, e.g. absorption spectrophotometry, steady-state spectrofluorimetry, cyclic voltammetry, etc. have also been described briefly in this chapter. Chemical systems and their purification is also discussed in the chapter.

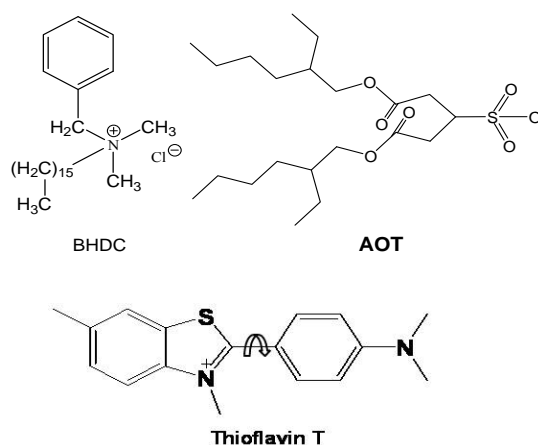
Chapter 3: This chapter presents the detail photophysical studies of two newly synthesized tailor made ThT derivatives. From the experimental results it is inferred that in these molecules intramolecular twisting of the groups around the C-N single bond is not responsible for their fluorescence sensing activity. This is also inferred to be true for their homologue, ThT, extensively used as the fluorescence sensing probe for amyloid fibrils. In all these molecules the twisting around the central C-C single bond between the benzothiazole and the anilino moieties appears to be mainly responsible for the observed fluorescence sensing activity of this class of molecules. Detail viscosity dependent studies show that the ThT derivative Ib (cf. scheme 3.1) with a julolidine substituent acts as a better sensor than the derivative Ia and ThT having free dialkyl amino substituent.(cf. Scheme 3.1). The better sensing activity of Ib as compared to Ia, is found to be due to the faster non-radiative decay rate for its excited state as compared to that of the latter. The faster non-radiative process in Ib is also supported by the results from quantum chemical calculations. For the first time we show from experimental

results that the bond twisting process in ThT takes place in the sub-picosecond time scale (570 fs in water). It is confirmed from the present study that the bond twisting in the excited states of these dyes actually takes place around the central C-C single bond, and not around the C-N single bond, and this process of bond twisting is barrierless in nature. Another important finding from the present study is that the twisted intramolecular charge transfer (TICT) state of ThT and its derivatives is weakly emissive in nature. Wavelength dependent decay kinetics have been observed for ThT in all the solvents studied. From the detailed studies of the time-resolved emission data it is inferred that the observed dynamic Stokes' shift and the increase in the spectral width with time for these system are due to the formation of the TICT state from the LE state of ThT molecule. Presence of any effect of solvent relaxation process on the observed ultrafast fluorescence dynamics has been neglected on the basis of the large reduction in the integrated emission intensity within the experimental time window of just few picosecond. The effect of viscosity on the LE to TICT conversion has been explored in detail. It is seen that the increase in the viscosity of the medium slows down the LE to TICT conversion, as manifested by the slower rate of increase in the spectral width or slower rate of decrease in the dynamic Stokes' shift on increasing the solvent viscosity. The fundamental informations obtained from the present study on the bond twisting dynamics of ThT and its derivatives are very useful to understand their fluorescence sensor activity in different restricted media. It is expected that the information obtained in the present study will help in the development of better fluorescence sensors based on ThT chromophore.



Scheme 3.1. Molecular structure of Thioflavin-T and its derivatives

Chapter 4: This chapter presents the results from the studies on the photophysical properties and the torsional relaxation dynamics of ThT in the nanoconfined water pools of anionic (sodium 1,4-bis(2-ethylhexyl) sulfosuccinate ; AOT) and cationic (benzyl-hexadecyl-dimethyl ammonium chloride ; BHDC) reverse micelles (RM). It is demonstrated that due to confinement, the torsional dynamics in the excited state of ThT becomes very sluggish. Due to this sluggish torsional motion, fluorescence enhancements of about 250 times have been observed in the anionic AOT/heptane/water reverse micelle at $w_0 = 1$ in comparison to that in bulk water. With an increase in the water pool size of the RMs, however, both fluorescence quantum yield and lifetime are seen to decrease non-monotonically. Such a decrease in the fluorescence quantum yield and lifetime has been attributed to the faster torsional motion in the larger water pools of the AOT reverse micelles. It is seen that the torsional motion remains restricted even in a very large water pool of the RMs. This result has been explained on the basis of the combined effect of the electrostatic interaction between the positively charged probe (ThT) and the negatively charged surfactant (AOT) head groups and the sluggish movement of water inside the RMs even if the water pool size of the RM is significantly large. High sensitivity of the fluorescence quantum yield and lifetime on the viscosity of the microenvironment in the RMs has been observed and can be useful to design an efficient molecular rotor based on ThT dye to monitor microviscosity.

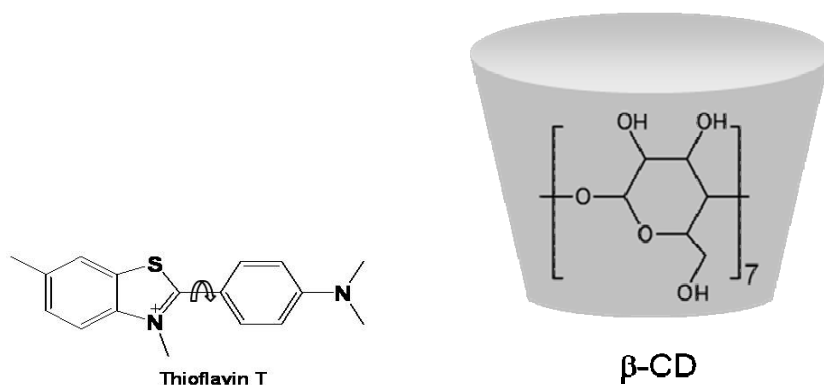


Scheme 4.1. Molecular structure of the chemicals

In cationic reverse micelle (BHDC/benzene/water), surprisingly it has been observed that the ThT is bound to the cationic interface even though large electrostatic repulsion was expected in the present case owing to the presence of positive charge on both the probe and the surfactant head group. The electrostatic interaction, which is normally expected to be much stronger than the other interactions like, hydrophobic interaction, π - π interaction, cation- π interaction etc. is understood to be largely minimized possibly due to the confinement of the large amount of charged counterions of the surfactant in a small confined volume of RMs. This result can have a far reaching implication in chemical and biological systems. From a conceptual and fundamental perspective, the results obtained here may herald various interesting applications. For instance, positively charged carriers for drugs are emerging as a promising option for pharmaceutical used owing to their very strong cellular interaction properties and good cellular uptake.⁴³ Therefore, one can foresee the design of a drug delivery system based on unconventional combination of a positively charged carrier (RM based) and a cationic drug with improved drug compatibility and drug stability. In fact, present results become even more appealing as Thioflavin-T itself is used as a model drug molecule in various studies.⁴⁴ Further, reverse micellar systems also hold strong promises as the nano-reactors for carrying out chemical reactions, nanosynthesis and catalysis, by exploiting its interfacial properties. So one

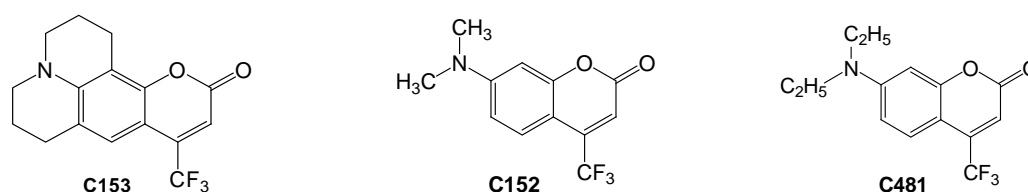
can imagine of the feasibility and/or improved efficiency of a chemical reaction between two similarly charged solutes at a charged interface (cationic in this case) owing to their localization and increased local concentration at the interface which is generally not contemplated.

Chapter 5: This chapter describes the excited-state torsional relaxation dynamics of ThT in β -CD nanocavity. ThT forms 1:1 inclusion complex with β -CD and such inclusion complex formation affects the torsional relaxation process of the excited ThT dye, leading to an enhancement of its fluorescence intensity. The longer average lifetime of ThT in the presence of β -CD also confirms the inclusion complex formation. TRES analysis indicates the presence of dynamic Stokes' shift as well as changes in the spectral shape with time. TRANES analysis shows the appearance of an iso-emissive point, suggesting the formation of an emissive TICT state. The decay of the peak frequency, growth in the width of the emission spectra and the decrease in the area under the emission spectra were found to be slower in the presence of β -CD compared to that of the bulk water. These substantiate the effect of confinement of β -CD cavity on the ultrafast bond-twisting dynamics of the amyloid fibril sensing dye ThT. Present results shine light on the behavior of the potential biological probe molecule ThT in the confined environment in very short time scale and can be relevant to the behavior of many similar molecules in chemical and biological nanocavity.



Scheme 5.1. Molecular structure of the chemicals

Chapter 6: This chapter describes a case study when an intramolecular relaxation process takes place in a timescale similar to that of the solvent relaxation process. Under these circumstances, the dynamic Stokes' shift of the probe can be modulated by the combined effect of these two relaxation processes. The results obtained here indicate that the intramolecular bond twisting process largely interfere with the dynamic Stokes' shift for coumarin-481 (C481) and coumarin-152 (C152), causing the observed solvent relaxation dynamics apparently faster, which is not the case of coumarin-153 (C153) dye. Following the procedure of time dependent changes in the integrated intensity of the time resolved emission spectra and using Einstein's theory of radiative decay rate, we are able to separate out the dynamics of the bond twisting process from the solvent relaxation process. This procedure can be applied to differentiate and quantitatively estimate the rate of an intramolecular relaxation process that is otherwise hidden or mingled up with the solvent relaxation process.



Scheme 6.1: Molecular Structure of the dyes

Chapter 7: This chapter presents the results on the modulation in the location of an anionic solute (Coumarin-343; C343) in a polymer-surfactant supramolecular assembly. It is demonstrated from the present study that the position of the anionic probe in the pluronic micellar phase can be changed by adding a positively charged co-surfactant cetyl trimethyl ammonium chloride (CTAC) or cetyl trimethyl ammonium bromide (CTAB). It is indicated from small angle neutron scattering (SANS) studies that the addition of ionic surfactant to the

pluronic micellar solution results in the formation of unique supramolecular assemblies where the hydrocarbon chain of the surfactant molecules reside in the core of the pluronic micelle and the ionic head group of the surfactant resides at the core-corona interface. The positively charged layer thus formed in the CTAC-pluronic and CTAB-pluronic mixed micelles pulls the anionic probe from the micellar surface to their interior. Because of the availability of wide range of microenvironments in these micelles, the solutes can display quite different physical and chemical properties depending on its location in the micelle. Thus, by changing the position of a solute in these micelles, it is possible to modulate the physical as well as the chemical properties of the solute in these microheterogeneous systems. Molecular structures of the pluronics, cationic surfactants and the probe dye are shown in scheme 7.1.



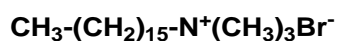
P123



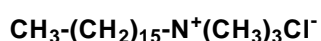
F88



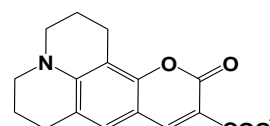
P105



CTAB



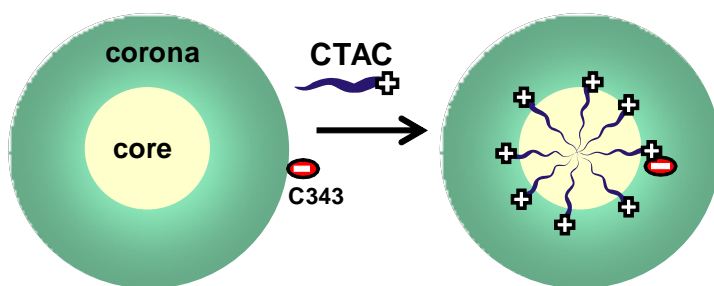
CTAC



C343 anion

Scheme 7.1.: Molecular structures of chemicals used in the present study

In one of the present systems, the probe migration has been shown to tune the redox potential of the solute by changing the composition of the supramolecular assembly. As the chemical reactivity of the solute largely depends on the redox potential, it can be controlled usefully by suitable selection of the composition of these supramolecular nanoreactors. Schematic presentation of the probe migration in a pluronic-surfactant supramolecular assembly is shown in scheme 7.2.



Scheme 7.2. Schematic representation of the changes in the location of an anionic solute with the addition of a cationic co-surfactant in a neutral pluronic micelle.

Present study further indicates that the effectiveness of a surfactant molecule to move a dissolved solute molecule from the surface to the interior of the micelle is largely determined by the thickness of the corona region, which in turn depends on the EO block size of the block polymer used. It can be inferred from the present study, that by a proper selection of the polymer and the ionic surfactant, a suitably charged solute can be placed at different locations inside the mixed micelles, simply by changing the concentration of the added ionic co-surfactant. From the studies with different pluronics it is indicated that the concentration of the ionic surfactant required to drag an oppositely charged probe molecule into the interior of the micelles is linearly correlated with the thickness of the corona region of the micelle used. By controlling the position of the solute in the micellar system, it is thus possible to tune the physical as well as chemical properties of the solute, which may have several applications, especially in the chemical synthesis and controlled drug release systems.

References

- (1) Bagchi, B. *Annu. Rev. Phys. Chem.* **1989**, *40*, 115.
- (2) Barbara, P. F.; Jarzeba, W. *Advan. Photochem.* **1990**, *15*, 1.
- (3) Bixon, M.; Jortner, J. *Chem. Phys.* **1993**, *176*, 467.
- (4) Chien, Y. Y.; Wong, K. T.; Chou, P. T.; Cheng, Y. M. *Chem. Commun.* **2002**, *23*, 2874.

- (5) Elsaesser, T. Ultrafast excited-state hydrogen transfer in the condensed phase. In *Ultrafast hydrogen bonding dynamics and proton transfer processes in the condensed phase*; Elsaesser, T., Bakker, H. J., Eds.; Kluwer Academic Publishers: Dordrecht: The Netherlands, 2002; pp 119.
- (6) Tolbert, L. M.; Solntsev, K. M. *Acc. Chem. Res.* **2002**, *35*, 19.
- (7) Rettig, W.; Maus, M. Conformational changes accompanying intramolecular excited-state electron transfer. In *Conformational Analysis of Molecules in Excited States*; Waluk, J., Ed.; Wiley-VCH: New York, 2000.
- (8) Liu, R. S. H. *Photochem. Photobiol. B: Biol.* **2002**, *76*, 580.
- (9) Rini, M.; Kummrow, A.; Dreyer, J.; Nibbering, E. T. J.; Elsaesser, T. *Faraday Discuss.* **2003**, *122*, 27.
- (10) Deng, Y.; Stratt, R. M. *J. Chem. Phys.* **2002**, *117*, 1735.
- (11) Owrutsky, J. C.; Raftery, D.; Hochstrasser, R. M. *Annu. Rev. Phys. Chem.* **1994**, *45*, 519.
- (12) Rini, M.; Holm, A. K.; Nibbering, E. T. J.; Fidler, H. *J. Am. Chem. Soc.* **2003**, *125*, 3028.
- (13) Yu, H. Z.; Baskin, J. S.; Zewail, A. H. *J. Phys. Chem. A* **2002**, *106*, 9845.
- (14) Bagchi, B.; Biswas, R. *Adv. Chem. Phys.* **1999**, *109*, 207.
- (15) Fainberg, B. D.; Huppert, D. *Adv. Chem. Phys.* **1999**, *107*, 191.
- (16) Fleming, G. R.; Cho, M. H. *Annu. Rev. Phys. Chem.* **1996**, *47*, 109.
- (17) Chiti, F.; Dobson, C. M. *Annu. Rev. Biochem.* **2006**, *75*, 333.
- (18) Gestwicki, J. E.; Crabtree, G. R.; Graef, I. A. *Science* **2004**, *306*, 865.
- (19) Gilead, S.; Gazit, E. *Angew. Chem. Int. Ed.* **2004**, *43*, 4041.
- (20) Mishra, R.; Winter, R. *Angew. Chem. Int. Ed.* **2008**, *47*, 6518.
- (21) Maskevich, A. A.; Stsiapura, V. I.; Kuzmitsky, V. A.; Kuznetsova, I. M.; Povarova, O. I.; Uversky, V. N.; Turoverov, K. K. *J. Proteome Res.* **2007**, *6*, 1392.

- (22) LeVine, H., III. *Protein Sci.* **1993**, *2*, 404.
- (23) Raj, C. R.; Ramaraj, R. *Photochem. Photobio.* **2001**, *74*, 752.
- (24) Schirra, R. *Chem. Phys. Letts.* **1985**, *119*, 463.
- (25) Cowan, M. L.; Bruner, B. D.; Huse, N.; Dwyer, J. R.; Chugh, B.; Nibbering, E. T. J.; Elsaesser, T.; Miller, R. J. D. *Nature (London)* **2005**, *434*, 199.
- (26) Eaves, J. D.; Loparo, J. J.; Fecko, C. J.; Roberts, S. T.; Tokmakoff, A.; Geissler, P. L. *Proc. Natl. Acad. Sci. U.S.A.* **2005**, *102*, 13019.
- (27) Shirota, H.; Tamoto, Y.; Segawa, H.; . *J. Phys. Chem. A* **2004**, *108*, 3244.
- (28) Duttachoudhury, S.; Kumbhakar, M.; Nath, S.; Pal, H. *J. Chem. Phys.* **2007**, *127*, 194901.
- (29) Andreatta, D.; Sen, S.; Lustres, J. L. P.; Kovalenko, S. A.; Ernsting, N. P.; Murphy, C. J.; Coleman, R. S.; Berg, M. A. *J. Am. Chem. Soc.* **2006**, *128*, 6885.
- (30) Pal, S. K.; Peon, J.; Zewail, A. H. *Proc. Natl. Acad. Sci. U.S.A.* **2002**, *99*, 1763.
- (31) Mandal, U.; Adhikari, A.; Dey, S.; Ghosh, S.; Mondal, S. K.; Bhattacharyya, K. *J. Phys. Chem. B* **2007**, *111*, 5896.
- (32) Alexandridis, P.; Hatton, T. A. *Colloids Surf. A* **1995**, *96*, 1.
- (33) Alexandridis, P.; Holzwarth, J. F.; Hatton, T. A. *Macromolecules* **1994**, *27*, 2414.
- (34) Chu, B.; Zhou, Z. Physical chemistry of polyoxyalkylene block copolymer surfactants. In *Nonionic surfactants*; Nace, V. M., Ed.; Marcel Dekker: New York, 1996; Vol. 60; pp 67.
- (35) Bahadur, P.; Riess, G. *Tenside, Surfactants, Deterg.* **1991**, *28*, 173.
- (36) Schmolka, I. R. *J. Am. Oil Chem. Soc.* **1980**, *59* 322.
- (37) Park, T. G.; Cohen, S.; Langer, R. *Parm. Res.* **1992**, *9*, 37.
- (38) Yokoyama, M. *Crit. Rev. Therapeutic Drug Carrier Syst.* **1992**, *9*, 213.

- (39) Pancheri, E. J.; Mao, M. H. K. Comprising anionic surfactant polymeric nonionic surfactant and betaine surfactant US Patent, 1992.
- (40) Tama, K. C.; Wyn-Jonesb, E. *Chem. Soc. Rev.* **2006**, 35, 693.
- (41) Ganguly, R.; Aswal, V. K.; Hassan, P. A.; Gopalakrishnan, I. K.; Kulshreshth, S. K. *J. Phys. Chem. B* **2006**, 110, 9843.
- (42) Jansson, J.; Schillen, K.; Nilsson, M.; Soderman, O.; Fritz, G.; Bergmann, A.; Glatter, O. *J. Phys. Chem. B* **2005**, 109, 7073.
- (43) Bilensoy, E. *Expert Opin Drug Deliv.* **2010**, 7, 795.
- (44) Hartig, W.; Paulke, B. R.; Varga, C.; Seeger, J.; Harkany, T.; Kacza, J. *Neuroscience Letters* **2003**, 338, 174.

LIST OF FIGURES

	Page No.
Figure 1.1	2
Schematic representation of the two possible energetic situations for photoinduced reaction involving the excited state reactant.	
Figure 1.2	3
The Jablonsky diagram showing different photophysical processes undergone by an electronically excited molecule. Straight arrows and wavy arrows represent the radiative and non-radiative processes, respectively. Abbreviations are: Abs -Absorption; IC -Internal Conversion; ISC -Intersystem Crossing; RISC -Reverse ISC; VR -Vibrational Relaxation; FI -Fluorescence; Ph -Phosphoresence; S_i -ith singlet state and T_i -ith the triplet state.	
Figure 1.3	6
Schematic presentation of a barrierless process	
Figure 1.4	7
Dynamic fluorescence Stokes' shift caused by solvent relaxation process following photoexcitation of the fluorescent probe.	
Figure 1.5	9
Reverse micelle structure	
Figure 1.6	10
Common surfactants used in the formation of reverse micelles	
Figure 1.7	13
Structure of cyclodextrins	
Figure 1.8	17
Schematic presentation of the formation of a block copolymer-surfactant complex	

Figure 2.1	25
Schematic of a double beam UV-vis spectrophotometer	
Figure 2.2	26
Schematic of a steady-state fluorescence spectrometer	
Figure 2.3	31
Schematic diagram of a Time Correlated Single Photon Counting Spectrometer	
Figure 2.4	33
Functioning of a TAC unit used in a TCSPC instrument. Start indicates the initiation of the charging process. Stop signal can arrive the TAC unit at any time within the TAC range following the arrival of the start pulse	
Figure 2.5	39
Creation of ground-state and excited state anisotropies from an isotropic distribution of molecules	
Figure 2.6	40
Schematic describing measurement of fluorescence anisotropy	
Figure 2.7	44
Schematic representation of sum frequency generation in a non-linear crystal	
Figure 2.8	47
Schematic representation of fluorescence decay measurement using fluorescence up-conversion technique	
Figure 2.9	49
The Schematic diagram of the femtosecond fluorescence up-conversion instrument developed in our department	

Figure 2.10

51

A typical instrument response function of the present fluorescence up-conversion instrument measured for 400 nm excitation light. The full-width at half maximum of the instrument response function is ~ 180 fs

Figure 2.11

52

(A) Cyclic voltammetric potential profile and (B) a typical cyclic voltammetric plot using glassy carbon electrode

Figure 2.12

53

(A) Potential profile of differential pulse voltammetry (B) the typical differential pulse voltammetric plot of Cd^{+2} reduction in aqueous solution

Figure 3.1

65

Ground-state absorption and steady-state fluorescence spectra of Ia (—) and Ib (- - - -) in aqueous solution. Absorption and emission spectra of ThT in water (.....) are also shown for comparison

Figure 3.2

67

Variation of fluorescence quantum yield (relative to that in acetonitrile solvent, ϕ_f^{ACN}) of Ia (Δ) and Ib (O) with the viscosity of the medium. Inset shows the variation in the emission yield for the low solvent viscosity region. Open symbol corresponds to acetonitrile-ethylene glycol mixtures and filled symbol corresponds to glycerol solution with different viscosity.

Figure 3.3

68

Transient fluorescence decays of Ia (- - - -, $\lambda_{\text{ex}} = 410$ nm, $\lambda_{\text{em}} = 490$ nm) and Ib (—, $\lambda_{\text{ex}} = 420$ nm, $\lambda_{\text{em}} = 510$ nm) in ethylene glycol solution. The instrument response function (IRF) is shown as the dotted curve.

Figure 3.4

70

The optimized chemical structures of Ia (A) and Ib (B)

Figure 3.5

71

Variation in the potential energy of Ia (Δ) and Ib (O) with the dihedral angle, θ_B , in their ground (S_0) and the first excited state (S_1). The energy is relative to the minimum of the ground-state energy.

Figure 3.6

72

The fluorescence decay profile for ThT in aqueous solution at different emission wavelengths: (1) 440 nm, (2) 490nm, (3) 530 nm and (4) 590 nm. Instrument response function (IRF) is also shown (.....). Inset: The fluorescence decay profile at 460 nm for ThT in aqueous solution at different excitation wavelengths: (O) 390 nm, (Δ) 430nm.

Figure 3.7

74

Time-resolved emission spectra (TRES) of ThT in water at different time following photexcitation. Inset shows the variation in the integrated area under the emission spectra with time.

Figure 3.8

75

Variation in the peak frequency (O) and the width (FWHM, Δ) of the emission spectrum with time

Figure 3.9

75

TRANES of ThT in water at different times (0.1 to 2 ps)

Figure 3.10

77

The ground-state optimized geometry for the ThT in water

Figure 3.11

77

Potential energies of ThT in the ground (S_0) and the excited (S_1) states as a function of the dihedral angle θ_A . The energy (expressed in eV) is relative to the minimum of the ground-state energy

Figure 3.12

79

(A) Ground-state and excited-state potential energy of ThT as a function of dihedral angle θ_B .
(B) Variation in the oscillator strength with the dihedral angle θ_B for the S_0 - S_1 transition of ThT in aqueous solution

Figure 3.13

80

(A) Changes in the emission spectra of ThT in ACN-EG solvent mixtures. (B) Changes in emission quantum yield (ϕ_f) of ThT with the increasing viscosity of the ACN-EG solvent mixtures

Figure 3.14

81

(A) Fluorescence transients at 490 nm (emission peak) for ThT in different ACN-EG solvent mixtures. The dotted line shows the IRF. (.....). (B) Variation in fluorescence lifetime of ThT with the viscosity of the solvent medium

Figure 3.15

82

Fluorescence transient decays of ThT in ACN at different emission wavelengths: (1) 440nm, (2) 490 nm, (3) 550 nm and (4) 600 nm. The dotted line shows the IRF

Figure 3.16

83

(A) Normalized time-resolved emission spectra (TRES) of ThT in ACN at (1) 0.05 ps, (2) 0.15 ps, (3) 0.4 ps, (4) 2 ps. The circles are the experimental data points and the solid lines are the lognormal fits to the data points. Inset: Variation in integrated area under the emission spectra with time. (B) Time-resolved area normalized emission spectra (TRANES) of ThT in ACN

Figure 3.17

83

Variation in the FWHM (\circ) and peak frequency (Δ) of ThT emission spectra in ACN with time

Figure 3.18

86

Fluorescence transients of ThT in EG at different emission wavelengths: (1) 440nm, (2) 490 nm, (3) 550 nm, (4) 600 nm. The dotted line shows the IRF

Figure 3.19

87

(A) Normalized time-resolved emission spectra (TRES) of ThT in EG at different times: (1) 0.1 ps, (2) 0.5 ps, (3) 3 ps and (4) 10 ps. The circles are the experimental data points and the solid lines are the lognormal fits to the data points. Inset: Variation in the area under the emission spectra with time. (B) Time-resolved area normalized emission spectra (TRANES) for ThT in EG

Figure 3.20

87

Variation in the FWHM of TRES with time in EG (○) and in 3:2 ACN-EG solvent mixture (Δ)

Figure 3.21

88

(A) Normalized time-resolved emission spectra (TRES) for ThT in ACN-EG solvent mixture at different time (1) 0.1 ps, (2) 0.2 ps, (3) 0.4 ps and (4) 2 ps. The circles are the experimental data points and the solid lines are the lognormal fits to the data points. Inset: Variation in the integrated area under the emission spectra with time. (B) Time-resolved area normalized emission spectra (TRANES) of ThT in 3:2 ACN-EG solvent mixture

Figure 3.22

89

Normalized steady-state emission spectra of ThT in three different solvents: Acetonitrile (—), ethylene glycol (.....) and glycerol (- - - - -)

Figure 3.23

91

(A) Steady-state emission spectrum of ThT in aqueous solution (.....) and in insulin amyloid fibril (—). (B) Emission decay traces for ThT in amyloid fibril at different emission wavelengths (1) 450, (2) 480, (3) 500, (4) 550 and (5) 600 nm. The decay trace at 490 nm for

ThT in aqueous solution (—) is also shown for comparison. The IRF is shown by the black dotted curve

Figure 3.24 92

(A) Intensity normalized TRES and (B) TRANES for ThT in amyloid fibril at different time (0.1, 0.3, 1, 2, and 6 ns)

Figure 4.1 98

(A) Ground-state absorption spectra of ThT in bulk water (—) and in AOT reverse micelle with $w_0=20$ (.....). (B) Steady-state emission spectra of ThT in bulk water (—) and in AOT reverse micelle at different w_0 : (- - - -) $w_0=1$, (.....) $w_0=4$ and (-.....-) $w_0=20$

Figure 4.2 100

(A) Steady-state emission spectra of ThT in bulk water and in AOT reverse micelle at different w_0 values. (B) Variation in the relative ϕ values of ThT in the reverse micelle with respect to that in water as a function of the w_0 of the reverse micelles

Figure 4.3 102

Variation in the fluorescence quantum yield (ϕ) of ThT with the viscosity (η) of the AOT reverse micelle

Figure 4.4 104

(A) Fluorescence decay traces of ThT in water (.....) and in AOT reverse micelle at different w_0 values. (B) Variation in the average fluorescence lifetime of ThT with the w_0 value of the reverse micelle

Figure 4.5 106

Transient fluorescence decay of ThT in normal AOT micelle at different AOT concentration. Inset shows the variation of fluorescence lifetime in normal AOT micelle with surfactant concentrations

Figure 4.6

107

Variation of fluorescence anisotropy for ThT molecule in the AOT reverse micelles at different w_0 : (Δ) $w_0=5$ and (\circ) $w_0=10$. Inset: The emission decay profile of ThT in AOT reverse micelle ($w_0=5$) at different excitation polarization: (—) parallel and (- - - -) perpendicular

Figure 4.7

109

Variation in the torsional rate constant (k_{tor}) of ThT dye with the w_0 value of the AOT reverse micelle

Figure 4.8

111

(A) Steady-state emission spectra of ThT in bulk water and in BHDC reverse micelle at different w_0 values. (B) Variation in the relative ϕ values of ThT in the reverse micelle with respect to that in water as a function of the w_0 of the reverse micelles

Figure 4.9

113

Variation in the relative ϕ values of ThT in the reverse micelle with respect to that in water as a function of the radius of water pool of AOT(\circ) and BHDC (Δ) RM

Figure 4.10

114

(A) Fluorescence decay traces of ThT in (1) BHDC and (2) AOT RM with $r_w = 1.1$ nm. (B) Variation in the average fluorescence lifetime of ThT with the r_w value for AOT(\circ) and BHDC (Δ) RM

Figure 4.11

115

Variation in the rate of bond twisting process with the size of the central water pool of AOT(\circ) and BHDC (Δ) RM

Figure 4.12

116

Fluorescence decay traces of ThT in water (—), AOT micelle (-.-.-.-.-) and BHDC micelle (-----) the dotted line represents the instrument response function (IRF)

Figure 5.1

123

(A) Steady-state emission spectra ($\lambda_{\text{ex}}=410$ nm) of Thioflavin-T ($7 \mu\text{M}$) at different β -CD concentrations: (1) 0.0 (2) 2.0 (3) 3.3 (4) 5.7 (5) 7.8 (6) 11.1 (7) 16.0 and (8) 18.0 mM. (B) Fluorescence titration curve (1:1 binding model) for ThT• β CD system

Figure 5.2

125

Fluorescence transient ($\lambda_{\text{ex}}=410$ nm, $\lambda_{\text{em}}=490$ nm) of ThT in water in the presence of different concentrations of β -CD: (1) 0.0, (2) 2.0, (3) 4.0, (4) 8.0 and (5) 18.0 mM. The dotted line shows the IRF. **Inset:** Variation in average lifetime (τ_{avg}) of ThT with increasing β -CD concentration.

Figure 5.3

126

Fluorescence transient of ThT in aqueous solution containing 15 mM β -CD at different emission wavelengths: (1) 440 nm, (2) 490 nm, (3) 540 nm, (4) 600 nm. The dotted line shows the IRF

Figure 5.4

127

(A) Time-resolved emission spectrum (TRES) of ThT in 15 mM β -CD solution at different times. The circles are the experimental data points and the solid lines are lognormal fit to the data points. **Inset:** Variation in area under the curve with time: ThT in water (Δ), ThT in 15 mM β -CD solution (\circ). (B). Intensity normalized TRES at different times

Figure 5.5

129

Time-resolved area normalized emission spectrum (TRANES) for ThT in 15 mM β -CD solution

Figure 5.6

131

Variation in the peak frequency with time for ThT in water (\circ) and in 15 mM β -CD solution (Δ)

- Figure 5.7** 132
Variation in the width of the spectrum (FWHM) with time for ThT in water (○) and in 15 mM β -CD solution (Δ)
- Figure 6.1** 136
Transient fluorescence decay for C153 at 470 and 630 nm. The dotted line shows the instrument response function (IRF)
- Figure 6.2** 137
Reconstructed time-resolved fluorescence spectra for (A) C153, (B) C481 and (C) C152. Spectra shown are for time 0.1-2 ps. The points in each panel indicate the wavenumbers where the transient emissions are recorded
- Figure 6.3** 138
Change in the mean frequency of the transient emissions with time for (○) C153, (□) C481 and (Δ) C152 in acetonitrile solution. Points are calculated from the reconstructed spectra and the solid lines are the multi-exponential fitting to the data points
- Figure 6.4** 139
Reconstructed transient fluorescence spectrum for (A) C153 and (B) C152 at different times (0.1-2 ps). Each spectrum have been moved along frequency axis to remove the time dependent spectral shift and the area under all spectra have been normalized for comparison
- Figure 6.5** 140
Changes in the spectral width of the emission spectra at different times for (○) C481 and (Δ) C152
- Figure 6.6** 143
Changes in the integrated intensity of (A) C153, (B) C481 and (C) C152 as a function of time. The solid lines are the fitted data according to the eq. 6.6. The dashed lines for coumarin-481 and coumarin-152 are the fitted data according to the eq. 6.7

Figure 7.1

152

Normalized absorption (A) and emission (B) spectra of C343 at different pH in water, pH=3.5 (·····), pH=9.5 (- - - - -), and in P123 micellar solution (—)

Figure 7.2

153

The absorbance vs pH plots for the peak position of the neutral form of C343 in water (○), P123 micellar solution (□) and P123-CTAC (△) mixed solution with [CTAC]/[P123] ratio of 0.4. Absorbances at the lowest pH used for the three systems were normalized to unity for comparison

Figure 7.3

154

Normalized steady-state emission spectra of C343 in P123 micellar solution at different CTAC/P123 molar ratio: 0 (—), 0.06 (·····) and 0.5 (- - - -)

Figure 7.4

155

Fluorescence transients of C343 in P123 micellar solution at the blue side (440 nm) and red side (610 nm) of C343 emission spectrum in P123 micelle. The dashed line represents the IRF

Figure 7.5

156

(A) Time-resolved emission spectra (TRES) and (B) Time-resolved area normalized emission spectra (TRANES) of C343 in P123 micellar solution

Figure 7.6

157

(A) Time-resolved emission spectra (TRES) and (B) Time-resolved area normalized emission spectra (TRANES) of C343 in P123 micellar solution at CTAC/P123 molar ratio of 0.5

Figure 7.7

158

Plot of the normalized mean frequency, ω_1 , for C343 dye in P123 micellar solution at different CTAC/P123 molar ratios

Figure 7.8

160

Variation in the (A) average solvation time and (B) percentage Stokes' shifts observed with the CTAC/P123 molar ratio

Figure 7.9

163

(A) Fluorescence anisotropy decay, $r(t)$, for C343 in water (\circ) and in P123 micelle at different CTAC/P123 molar ratio: (\triangle) 0.0 and (\square) 0.34. (B) Variation of the average rotational relaxation time, $\langle\tau_r\rangle$, for C343 in P123 micelle with varying CTAC/P123 molar ratio. Solid line is the best fitted smooth curve among the data points

Figure 7.10

167

SANS data of the F88 solutions with different CTAB/F88 molar ratio 0.0 (\square) and 0.5 (\circ). The solid lines are fit to the data using a mixed micellar model as discussed in text

Figure 7.11

168

Changes in absorbance of the C343 dye (at 450 nm) with the changes in the pH of the 5% w/v F88 solution

Figure 7.12

169

Steady-state emission spectra of C343 in 5% w/v F88 solution at different CTAB/F88 molar ratio: 0.0 (—) 0.1 (·····), 0.2 (- - - -) and 0.5 (— · — · —)

Figure 7.13

170

(A) Fluorescence anisotropy decay for C343 dye in water (\bullet) and in F88 micellar solution at different CTAB/F88 molar ratio: (\circ) 0.0, (\triangle) 0.1 and (\square) 0.3. (B) Variation of the average reorientation time for C343 dye in F88 micellar solution with the CTAB/F88 molar ratio

Figure 7.14

173

(A) Time-resolved emission spectra (TRES) and (B) time-resolved area normalized emission spectra (TRANES) of C343 in F88 micellar solution at different time (0.1 ns to 2 ns)

Figure 7.15

174

(A) Time-resolved emission spectra (TRES) and (B) time-resolved area normalized emission spectra (TRANES) of C343 in F88 micellar solution at CTAC/F88 molar ratio of 0.5 at different time (0.1 ns to 2 ns)

Figure 7.16

174

Plot of the percentage of Stokes' shift observed ($\Delta\omega_s^{\%obs}$) for C343 dye in the F88 micellar solution as a function of CTAC/F88 molar ratio

Figure 7.17

177

(A) Fluorescence anisotropy decay for C343 dye in water (o) and in P105 micellar solution at different CTAB/P105 molar ratio: (Δ) 0.0 and (\square) 0.25. (B) Variation of the average reorientation time for C343 dye in P105 micellar solution with the CTAB/P105 molar ratio

Figure 7.18

178

Figure shows the linear correlation between the limiting value of surfactant/polymer molar ratio and the thickness of corona region of the block copolymer

Figure 7.19

179

(A) Time-resolved emission spectra (TRES) and (B) Time-resolved area normalized emission spectra (TRANES) for C343 in P105 micellar solution

Figure 7.20

179

(A) Time-resolved emission spectra (TRES) and (B) Time-resolved area normalized emission spectra (TRANES) for C343 in P105 micellar solution at CTAB/P105 molar ratio of 0.4

Figure 7.21

180

Variation in the percentage Stokes' shift observed for C343 dye in P105 micellar solution with the CTAB/P105 molar ratio

Figure 7.22

181

The anisotropy decay for C343 in P105-SDS supramolecular assemblies at different SDS/P105 molar ratio : (—) 0 and (—) 0.3

Figure 7.23

183

(A) Differential pulse polarograms and (B) variation of the peak potential (V_p) of C343 in P123 micellar solution at different CTAC concentration. The CTAC/P123 molar ratios used are 0.0, 0.01, 0.02, 0.03, 0.05, 0.07, 0.10, 0.15 and 0.20. Solid line is the best fitted smooth curve among the data points.

Figure 7.24

184

Plot for the differences in the peak potentials ($V_p - V_p^0$) vs the differences in the reorientation times ($\langle \tau_r \rangle - \langle \tau_r^0 \rangle$) of C343 in P123 micellar solution obtained at different CTAC additions. V_p^0 & $\langle \tau_r^0 \rangle$ are the peak potential and average reorientation time of C343 in P123 micellar solution in the absence of CTAC and their values are -1.381V and 0.3 ns, respectively. The solid line is the best fitted straight line through the data points

LIST OF TABLES

	Page No.
Table 3.1	65
The emission quantum yield (ϕ_f) of ThT, Ia and Ib in different solvents	
Table 3.2	69
Average excited state lifetime of Ia and Ib in different solvents	
Table 3.3	81
Quantum yield and average lifetimes of Thioflavin-T in different acetonitrile–ethylene glycol solvent mixtures of varying viscosity	
Table 3.4	90
Time constants for the conversion of the LE to the TICT state of ThT in different solvents	
Table 4.1	99
Emission quantum yield, average excited state lifetime and torsional rate constant of ThT at different w_0 values	
Table 7.1	159
Solvation dynamics results and the estimates of the expected and the observed Stokes' shifts for C343 dye in CTAC/P123 mixed micellar system	
Table 7.2	164
Time-resolved anisotropy parameters with varying [CTAC]/[P123] molar ratio	
Table 7.3	167
The core radius (R_{cm}), the hard sphere radius (R_{hs}), the volume fraction (ϕ) and the polydispersity ($\Delta R_c/R_{cm}$) of the micelles in 5% w/v F88 solutions with different CTAB concentrations. The scattering length densities used to fit the data are $0.603 \times 10^{10} \text{ cm}^{-2}$, $0.343603 \times 10^{10} \text{ cm}^{-2}$ and $6.38603 \times 10^{10} \text{ cm}^{-2}$ for EO, PO and D ₂ O, respectively	

Table 7.4	170
Time-resolved anisotropy parameters with varying [CTAB]/[F88] molar ratio	
Table 7.5	175
Solvation parameters with varying CTAC/F88 molar ratio	
Table 7.6	177
Time-resolved anisotropy parameters with varying [CTAB]/[P105] molar ratio	
Table 7.7	180
Dynamic Stokes' shift of C343 in P105 micelle at different CTAB concentrations	

Chapter 1

Introduction

1.1. General Introduction: Photoinduced Processes

Study of chemistry encompasses the investigations of three major aspects i) synthesis ii) structure and iii) dynamics of chemical reactions. The major goal in the study of chemical dynamics is to develop an understanding of the elementary steps involved in a chemical reaction at a molecular level. An elementary process can be unimolecular if only one reactant molecule is involved or bimolecular if two reactant molecules participate in the reaction. Study of chemical dynamics is also to formulate the concepts governing the dynamics of the formation and dissociation of chemical bonds.

Interaction of electromagnetic radiation with molecules is often the method of choice to initiate and study the fast elementary processes. Photochemistry is concerned with reactions, which are initiated by active electronically excited molecules produced by the absorption of suitable radiation in the visible and near ultraviolet region of the electromagnetic spectrum. Absorption of photon makes some of the reactions to take place that are not feasible in dark because the energy acquired in the photoexcitation process favorably adds to the overall energy changes of the reaction. The situation is schematically shown in Fig.1.1. In case (a) of Fig. 1.1, the situation represents a kinetically slow exergonic dark reaction, but photo-excitation of any one of the reactant enables to overcome the activation barrier easily such that the reaction takes place with faster rate. Case (b) in Fig.1.1 corresponds to a reaction that cannot take place in

dark because of thermodynamic reason but light absorption makes the reaction thermodynamically feasible.

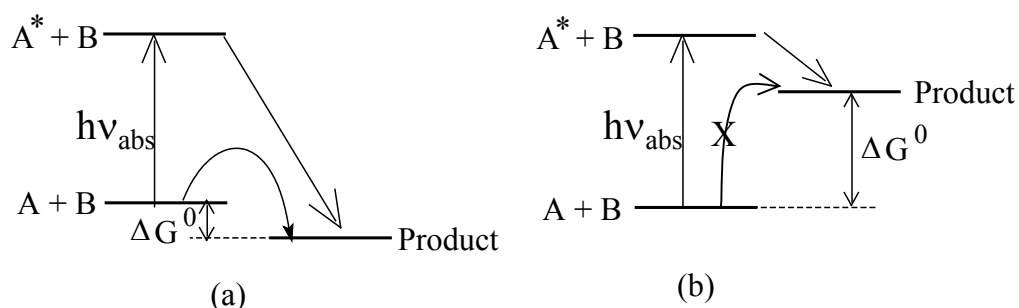


Figure 1.1. Schematic representation of the two possible energetic situations for photoinduced reaction involving the excited state reactant.

The absorption of electromagnetic radiation (time scale $\sim 10^{-15}$ sec) results in the excitation of an electron from a lower to a higher quantum state of the absorbing molecule. UV & VIS light absorption results in the excitation to the higher electronic state. After the excitation to a higher electronic state, a large solute molecule in solution can undergo various competitive relaxation processes. Schematic diagram of the possible molecular relaxation pathways in the excited molecules include internal conversion (IC), intersystem crossing (ISC), intramolecular vibrational relaxation (IVR), vibrational relaxation to thermalize with the bath (VR), radiative and nonradiative decay, solvent reorganization, bond reorganization, bond breaking, bond formation, proton/electron/energy transfer, etc. The schematic representations of the intramolecular relaxation pathways following excitation of the molecules are shown in Figure 1.2, which are commonly known as the Jablonsky diagram. Different relaxation processes take place in a wide range of time scales, e.g. few femtoseconds to milliseconds. These fundamental time scales are dictated by the rapidity of the nuclear or electronic rearrangements in the transition state. To understand the details of different fast elementary processes, it is necessary to monitor the short lived species formed after the light absorption.

With the advent of ultrafast laser technology it has become possible to study reaction dynamics with a sub-picosecond time resolution. Because of such time resolution, ultrafast processes can now be monitored in real-time. However, as laser pulses continue to shorten in time, the definition of ultrafast processes also evolves consequently. Several decades ago, when measurement using nanosecond light pulses were considered as the state of the art technique, ultrafast processes were defined as those occurring on that timescale. Today, most researchers would consider femtosecond, or atleast sub-picosecond processes as the ultrafast processes. One can imagine that the definition of ultrafast process is still to be refined further in the coming years. In relation to the present thesis, we would assign the term ultrafast to those processes that are required to be monitored by utilizing light pulses shorter than 100 ps. Ultrafast lasers have dramatically improved our ability to measure the motions of molecules that occur in unusually faster time scales. Thus, the timescales of molecular vibrations and rotations for small molecules lie in the femtosecond to picosecond regime and the direct measure of these dynamics is possible only through ultrafast laser spectroscopy techniques.

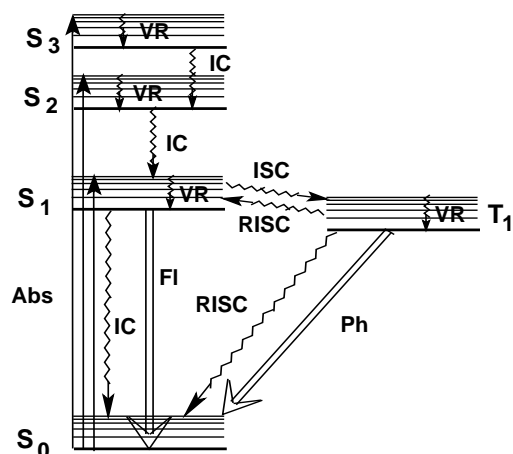


Figure 1.2. The Jablonsky diagram, showing different photophysical processes undergone by an electronically excited molecule. Straight arrows and wavy arrows represent the radiative and non-radiative processes, respectively. **Abbreviations are:** **Abs**-Absorption; **IC**-Internal Conversion; **ISC**-Intersystem Crossing; **RISC**-Reverse ISC; **VR**-Vibrational Relaxation; **FI**-Fluorescence; **Ph**-Phosphorescence; S_i -ith singlet state and T_i -ith the triplet state.

In this thesis we focus on the dynamics of first order photoinduced reactions in solution in which intramolecular configurational changes and solvent relaxation dynamics are of central interest. In the following we give a brief overview of the ultrafast intramolecular relaxation processes (which includes intramolecular configurational change) and solvent relaxation dynamics investigated following photoexcitation of suitable organic chromophoric molecules.

1.2 Intramolecular Configurational Changes in the Excited State

The traditional picture of a chemical reaction is that of a passage of the reactant over a high activation barrier to form the product. This picture of an elementary chemical reaction has played a key role in our understanding of many physical, chemical, and biological processes.^{1,2} However, it has become increasingly clear in recent years that there are many chemically and biologically important chemical reactions that proceed without the intervention of a high activation barrier along the reaction coordinate leading to the formation of the products.^{3,4} These barrierless chemical reactions also show rich and diverse dynamical behavior. Since barrierless chemical reactions are usually very fast (with time constants often in the picosecond range), detailed study of these processes required the development of ultrafast laser spectroscopy. Over the last few years it has become clear that there exist a rather large number of organic dye molecules whose photophysics in solution follow barrierless dynamics.⁵⁻¹⁵ In these molecules electronic excitation leads to intramolecular *configurational changes* due to large amplitude torsional motions of the functional groups. For some of these molecular systems, the synthesized structure may be tailored in such a manner that the functional groups are “bridged” or bonded, and torsional or twisting motions of the functional groups become impaired.¹⁶ Thus the influence of bridging on the dynamics of the twisting process can be selectively investigated. Also, the solvent has great influence on the rate of the intramolecular configurational changes. Now “collisional” friction (rather than “dielectric” friction as in solvation) largely affects the isomerization or twisting dynamics.¹⁶ The topic of functional group twisting has long been related to intramolecular charge transfer, hence the concept of a

twisted intramolecular charge transfer (TICT) state.¹⁷⁻¹⁹ For many systems, the TICT phenomenon has been studied in great detail,²⁰ however, relatively few ultrafast studies concerning TICT states have been reported, in part because TICT molecules are weakly fluorescent or nonfluorescent.²¹ Barrierless reactions are not limited only to twisting in the electronic excited state of dye molecules. Many activationless processes are found in the photoassisted isomerization. Isomerizations of stilbene and diphenylbutadiene in alcohol solvents are known to follow barrierless reaction pathways.²² Barrierless reactions are generally characterized by high reaction rates, exhibit a temperature dependence distinctly different from that of high barrier reactions, and are often strongly coupled to solvent viscosity. Actually, viscosity dependence has been often used to characterize the reaction mechanism of these reactions because in the absence of a barrier, solvent friction is the only impediment to the reaction.²³ Another important feature is that these reactions may depend on the initial conditions so that the wavelength of the excitation light may also play an important role in controlling the relaxation dynamics. Recent experimental and theoretical studies of electron transfer reactions have indicated that many intramolecular electron transfer reactions occur through activationless processes and are similar in many respects to the better known barrierless photochemical reactions.^{24,25} Barrierless reactions also seem to be common in biological processes. Agmon and Hopfield²⁶ have modeled the binding dynamics of CO to heme in myoglobin as a barrierless process. In nature, chromophores fulfill an important role in initiating signal transduction in a photoreceptor. After light absorption, the chromophore frequently undergoes ultrafast intramolecular conformational changes, for example, trans-cis isomerization, so the interaction of the chromophore with the protein environment is altered. At a later stage, this leads to the appearance of the signaling state and eventually the biological response. These phenomena have been extensively studied for rhodopsins,²⁷⁻²⁹ bacteriorhodopsins,³⁰ and phytochromes.^{31,32}

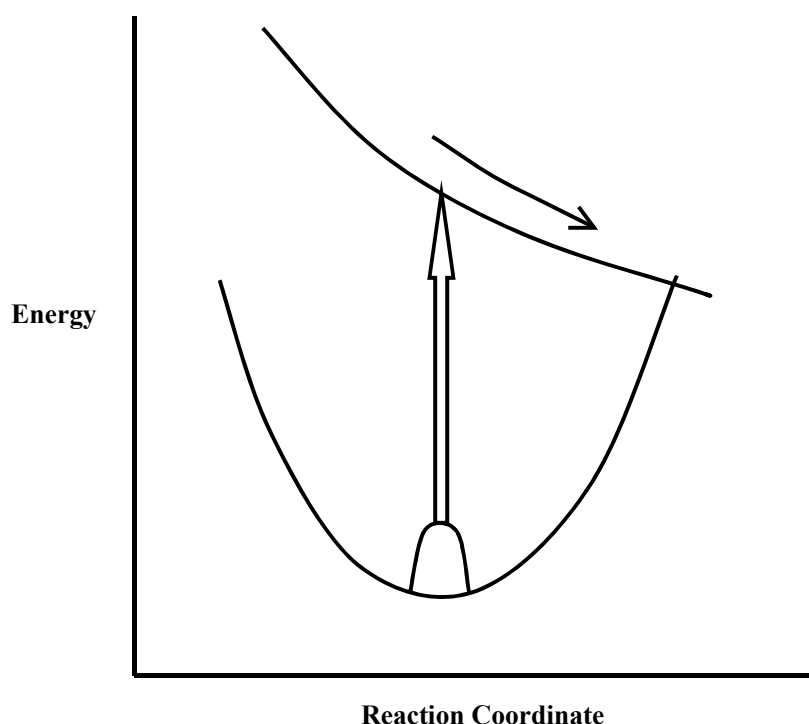


Figure 1.3. Schematic presentation of a barrierless process

1.3. Dynamic Stokes' shifts and Solvent Relaxation Dynamics

Dynamics of many chemical reactions in solution are strongly influenced by the dynamics of the solvents surrounding the reacting species. Studies of solvent relaxation processes are thus very important to gather a detailed understanding of the reaction dynamics in solution, especially the processes like electron transfer, charge transfer, proton transfer, conformational relaxation, etc. Besides other methods the time-dependent fluorescence Stokes' shifts measurements have been used extensively to understand solvent relaxation dynamics in large number of systems.³³⁻⁴⁵ On photoexcitation, the dipole moment of the probe molecule increases instantaneously. The polarisation of the surrounding solvent molecules responds to this dipole change in the solute and starts to reorganize around the new dipole. Therefore, the energy relaxation process, caused by the solvent reorganisation, shifts the fluorescence spectrum to longer wavelengths with time. The idea of solvent relaxation process has been conceptually illustrated in Figure 1.4. In the theoretical treatment of the solvent molecular relaxation by van der Zwan and Hynes,⁴⁶ it is assumed that the solute molecule in the excited

state is not polarizable (μ_e is constant during solvation) and that excited state reactions do not occur. In this approach it is thus assumed that the linear response theory applies for the solute/solvent systems.⁴⁷

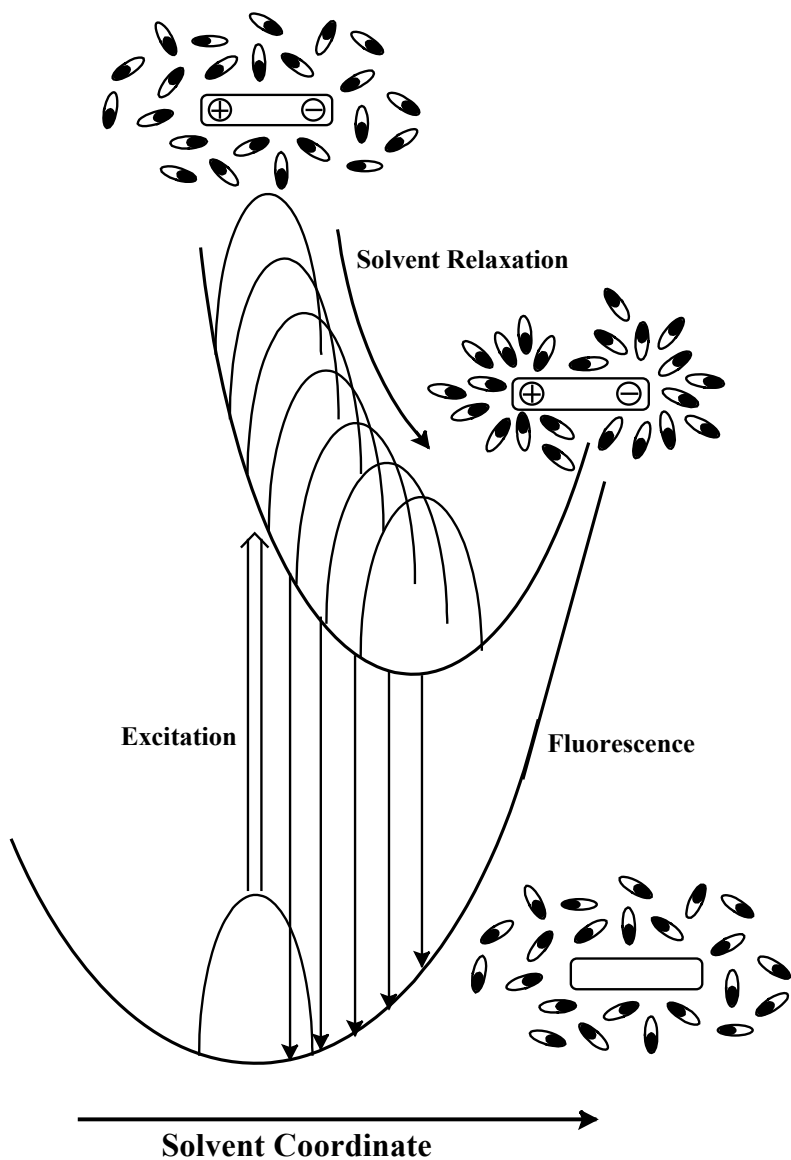


Figure 1.4. Dynamic fluorescence Stokes' shift caused by solvent relaxation process following photoexcitation of the fluorescent probe.

The reaction coordinate for the solvation process is considered to be represented by a so-called generalized solvation coordinate. In the case of a polar solvent the reaction coordinate is a measure for the nuclear solvent polarization that can be considered to be in equilibrium with an

effective dipole moment $\mu(t)$ of the solute molecule. Normalization leads to the relative coordinate $x(t)$, given as,

$$x(t) = \frac{\mu(t) - \mu_g}{\mu_e - \mu_g} \quad (1.1)$$

where μ_g and μ_e represent the ground and the excited state dipole moment.

The relaxation of the excited state population is usually studied by monitoring the temporal characteristics of the spectral response function (dynamic Stokes' shift):

$$C(t) = \frac{\nu(t) - \nu(\infty)}{\nu(0) - \nu(\infty)} \quad (1.2)$$

where $\nu(t)$, $\nu(\infty)$ and $\nu(0)$ are the fluorescence peak frequencies at times t , ∞ and 0, respectively.

For the measurements of the time resolved emission spectra (TRES), a set of fluorescence decays are collected at different wavelengths, covering the entire emission band of the probe. These decays are fitted using a suitable functional form (usually a multi-exponential function) to obtain the fitted curves $D(\lambda, t)$. The TRES spectra, $S(\lambda, t)$, are then constructed using the fitted decays, $D(\lambda, t)$, after their normalization with respect to the steady-state fluorescence spectrum, $S_0(\lambda)$, and applying the following relation.³⁸⁻⁴⁰

$$S(\lambda, t) = D(\lambda, t) \frac{S_0(\lambda)}{\int_0^{\infty} D(\lambda, t) dt} \quad (1.3)$$

To obtain smooth TRES, the data points obtained for the spectra $S(\lambda, t)$ using equation 1.5 are fitted following some line-shape function (usually log-normal function) for the emission band.³⁸⁻⁴⁰ The smooth TRES thus obtained are then used to estimate the emission maxima at different times and consequently to construct the dynamic Stokes' shift correlation function, $C(t)$. The function $C(t)$ thus obtained is the measure of the solvent relaxation dynamics.

1.4. Reverse Micelle and their General Characteristics

When a surfactant is introduced to a solution containing a polar and a nonpolar phase, it can lead to the formation of isolated droplets of the polar phase delineated from the nonpolar phase by the surfactant layer. When these droplets present a well-defined boundary and are isolated (Figure 1.5), we refer to them as reverse micelles (RMs).^{41,48-53} In some cases, a single surfactant is sufficient to encapsulate the polar solvent in the interior, whereas in some cases cosurfactants is required to stabilize the reverse micelle. Because a spherical form presents the minimum surface area-to-volume ratio, the average form of a RM is often spherical. However, other geometries such as ellipsoids or extended tubes are also possible.^{54,55} The most widely studied surfactant employed to form RMs is Aerosol OT (AOT; sodium 1,4-bis-2-ethylhexylsulfosuccinate) (*cf.* Figure 1.6)^{48,50,51,53,56} The geometry of this surfactant makes it especially effective for forming RMs in a wide range of nonpolar solvents, including alkanes, aromatic solvents, halogenated alkanes, and even supercritical solutions.^{48,50,51,53,56}

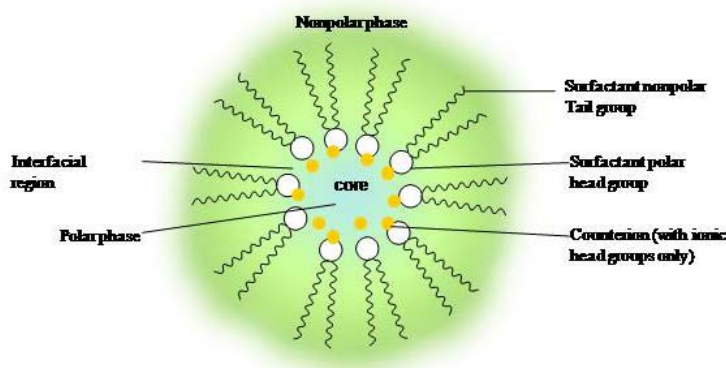
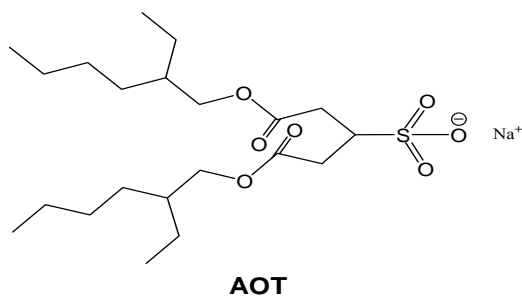
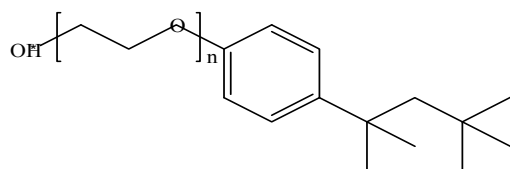
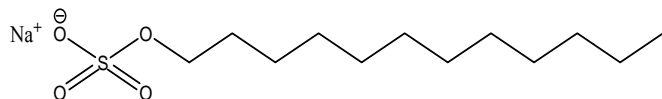


Figure 1.5. Reverse micelle structure

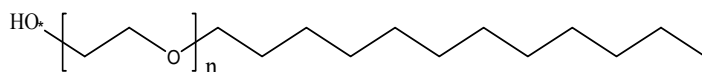




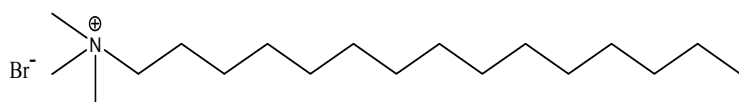
Triton X-100 (n~9.5)



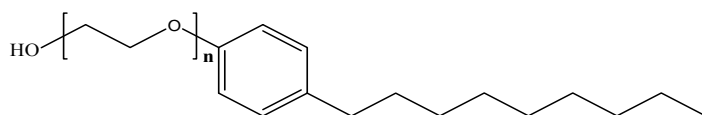
SDS (Sodium Dodecyl Sulphate)



Brij 30(dodecyl polyethylene glycol, n~4)



CTAB (cetyltrimethylammoniumbromide)



Igepal

Figure 1.6. Common surfactants used in the formation of reverse micelles.

Various other surfactants, nonpolar phases, and polar phases have also been explored; many of the common surfactants used are shown in Figure 1.6^{45,57-71}. RMs formed from surfactants other than AOT are significantly less well characterized but provide interesting comparisons. Researchers have characterized the structure and properties of the various RMs. One typical value used to characterize RMs is the molar ratio of the polar solvent to the surfactant, often represented as W_0 value. For water-containing RMs, $W_0 = [\text{H}_2\text{O}]/[\text{surfactant}]$. If the RMs are spherical, W_0 is directly proportional to the particle radius, as the interior comprises the volume, whereas the surfactant defines the surface area.⁷¹ Some RM systems, such as cetyl trimethylammonium bromide (CTAB), require an additional component, a cosurfactant, to the solution to achieve RM formation, usually a straight chain alcohol.^{57,59,63,66}

In recent years, these systems have attracted significant attention, predominantly because of their resemblance to biomembranes and their catalytic properties in chemical and enzymatic reactions. RM is an excellent model system that can provide interesting results about the effects of confinement on liquid properties. Often, analogies have been drawn between RMs and subcellular structures in biology.

One of the most fundamental questions posed by those studying RMs is, what is the nature of water in the water pool of RMs? Many previous studies utilizing vibrational spectroscopies revealed various ways that water in RMs differs from bulk water behavior⁷²⁻⁷⁹. However, the source of these differences (whether because of confinement or interactions with the often highly charged interfacial layer) remains a matter of debate. Also debatable is whether the water should be treated as a single species or as two or more separate populations. Extensive investigations on the influence of nanoconfinement on the structure and dynamics of water in RMs have led to a wealth of information on these systems. Initial investigations by NMR spectroscopy have shown that the average mobility of water in RMs is significantly slower due to the confinement effect. These studies, however, do not distinguish whether this slowing down holds for all of the water molecules present in RMs, or only for those present in the region of the surfactant head groups (interface). Recent studies employing techniques like vibrational echo and pump-probe spectroscopy,⁸⁰⁻⁸³ absorption,⁸⁴⁻⁸⁹ fluorescence,^{45,90-101} NMR,¹⁰²⁻¹⁰⁶ calorimetry,^{105,107} neutron scattering,^{85,108,109} molecular dynamics simulation,^{74,110-113} and so on have helped us in identifying different types of water in RMs, namely, water physically trapped between surfactant head groups, water directly bound (by the H-bonding) to the head groups, and relatively unperturbed bulklike water at the center of the RMs.^{75,79,86,87,90,114} A two-component core-shell model has thus been proposed to describe the differential properties of water located at the interface (between nonpolar and polar phase) and in the core of RMs.^{81,84,112,115} Spectrally resolved ultrafast mid-IR pump-probe spectroscopy on HDO/H₂O in RMs has distinctly demonstrated different mobilities for core and interfacial

water molecules as well as separation of their relative contributions.⁸⁰ Fluorescence experiments with suitable probes to understand the dynamics of the confined water molecules in RMs have shown that the nature of the water changes substantially as the size of the water droplet in RMs increases.^{45,90,91,95-99,101} In such studies, the possible uncertainty in the location of the probe in the heterogeneous media can sometimes impede inferences drawn on the structure and dynamics of the water confined in the nanoenvironment.¹¹⁶ However, as long as the primary goal of a study is to understand the gross behavior of the water pool under nanoconfinement and to determine how it influences the properties of a solute dissolved inside the nanoenvironment, photophysical investigation with suitable fluorescent probes is possibly still the most useful option. Photophysical properties, that is, fluorescence quantum yields, fluorescence lifetimes, spectral position, and so on, of a fluorescent probe directly depend on the nature of its immediate surroundings, namely, the polarity and the rigidity of the microenvironment around the probe, specific interactions of the probe with the surrounding solvents, and so on.¹¹⁷ Therefore, changes in photophysical parameters, if any, with the changes in the size of the RMs (i.e., W_0 value) can be utilized as a reporter for the changes in the properties of the nanoconfined water. At very low W_0 , almost all water molecules are present in the highly constrained Stern layer of the RMs, and are mainly engaged in hydrating the ionic head groups of the surfactant and the accompanying counterions. These are referred to as interfacial water. Structurally, the interfacial water resembles more closely to water monomers, either bound to or trapped among the surfactant head groups. With increasing W_0 value, as hydration of the interfacial region saturates, association of excess water molecules among themselves leads to the formation of nanodroplets of water inside the RMs, in which a truncated three-dimensional H-bonding network, quite similar to that of bulk water, prevails. Hence, the influence of the interfacial water on the properties of a dissolved solute is expected to be largely different from that of the water present in the RM core. Therefore, the influence of this transition on the physicochemical properties of the dissolved solute is equally

imperative for proper understanding of these microheterogeneous systems. Understanding the interaction of charged molecules with lipid interfaces is important in biology, chemistry, physics, and in other technical fields. Because most lipids are charged, interaction with a lipid surface depends at least in part on the Coulombic interaction and repulsion between charged species. The influence of nanoconfined water pools of reverse micelles upon the photophysical behaviour a biologically important probe ThT is the interest of the present thesis and has been discussed in Chapter 4.

1.5. Cyclodextrins as Supramolecular hosts

Cyclodextrins (CDs) are a class of cyclic oligosaccharides with six to eight D-glucose units linked by α -1,4-glucose bonds (*cf.* Figure 1.7), and their glucose units arranged in a way that the exterior surface of the CDs is covered by hydroxyl groups and is hydrophilic, while the cavity of the CD ring is hydrophobic. Significantly, the hydrophobic cavity of CDs, mostly in a truncated cone conformation, has a good capability to associate various inorganic/organic/biological molecules and ions in both aqueous solution and in the solid state to form stable host–guest inclusion complexes or supramolecular species. This unique property, along with satisfactory water solubility, low toxicity, easy preparation and low price, jointly enable the wide application of CDs in many fields of science and technology.^{118,119}

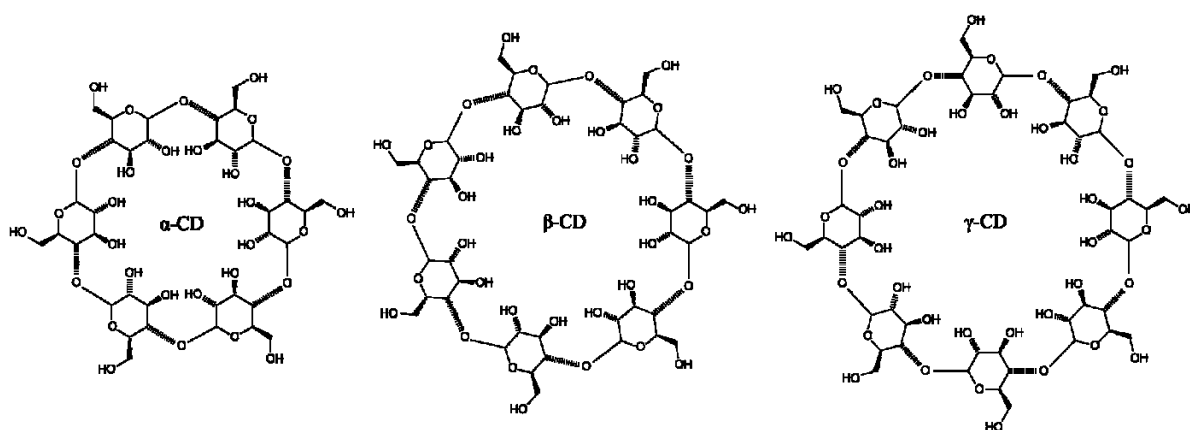


Figure1.7. Structure of cyclodextrins

Early studies on CDs were mainly focused on the investigation of CDs and their derivatives as molecular recognition receptors,^{120,121} drug delivery carriers,¹²² biomimetic catalysts,¹²³ and so on. CDs are extensively studied as not only excellent receptors for molecular recognition but also convenient building blocks to construct nanostructured functional materials, especially bioactive materials.¹²⁴ Between the 1970s through the beginning of the 2000s, many successful studies on the bioactivities of natural and simply modified CDs were reported. For example, reports by Bender,¹²⁵ Breslow,¹²⁶ Tabushi,¹²⁷ and Saenger¹²⁸ clearly demonstrated the capability of CDs as enzyme models. From then on, numerous studies showed that, after associating catalytically active groups with CDs, the resultant functionalized CDs can be used as artificial enzyme models to catalyze many biomimetic reactions.^{123,129} Moreover, CDs can also increase the utility of enzymes by increasing the availability of insoluble substrates,¹³⁰ can act as drug delivery agents,^{131,132} and can sense biological molecules.¹³³ All these properties are closely related to the inclusion complexation of model substrates within the hydrophobic cavity of CDs.

The most significant property of an inclusion complex is that a “host” component can admit a “guest” component into its cavity without forming any covalent bond. The study of inclusion complexes are important in fundamental research since it furnishes important clues regarding the noncovalent intermolecular forces that play at the molecular level. The CD molecules have an internal cavity accessible to the guest molecules of proper dimension through an opening of 4.5-5.3 Å, 6.0-7.0 Å, and 7.5-8.5 Å for α -CD, β -CD, and γ -CD, respectively; the depths of all remaining nearly the same (7.9 Å).^{125,134} Thus, depending on the cavity size, CDs are capable of encapsulating guest molecules of different dimensions, with different guest:CD stoichiometries. Therefore, the hydrophobic nanocavity of such hosts offers a unique opportunity for studying size-controlled nanoenvironment effects such as reduced degrees of freedom of the guest. The reduced polarity inside the CD cavity and the restricted

space influence the photophysical and photochemical properties of the probe.¹³⁵⁻¹³⁷ Many of these studies have revealed the formation of inclusion complexes of 1:1 and 1:2 type.^{135,138-140} Such preference in the formation of the well-defined nanoconjugates in microheterogeneous environments is of much interest to present day science. The effect of nanoconfinement of β -CD cavity on the photophysical behaviour will be discussed in Chapter 5.

1.6. Block Copolymers and their solution behavior

Pluronics are the triblock copolymers made up of poly ethyleneoxide (EO) and poly propyleneoxide (PO) blocks with general molecular formula $(EO)_n-(PO)_m-(EO)_n$. These water soluble non-ionic surfactants have attracted considerable attention in the last two decades partly because of their complex behavior in solution¹⁴¹⁻¹⁴⁶ and partly because of their wide range of industrial applications, as detergent, lubricant and emulsifier.¹⁴⁷⁻¹⁵³ Their unique behavior in aqueous solution and their low toxicity have made these polymers highly useful in many pharmaceutical formulations.^{147,149-153} These materials have also been extensively used as templates for the synthesis of the nano-structured materials.^{154,155}

Besides the absence of the polar head groups, unlike in the conventional surfactants, pluronics also form micelles in aqueous solution.¹⁴¹⁻¹⁴⁶ In case of $(EO)_n-(PO)_m-(EO)_n$ type of triblock copolymers, for example, the PO block is soluble in water below 288 K, but turns hydrophobic at elevated temperatures because of its diminishing hydrogen bonding interaction with water. In contrast, EO block is predominantly hydrophilic within the temperature range 273–373 K.¹⁴⁵ However, it must be noted that the solubility of EO block also decreases with temperature, but the effect is less pronounced compared to PO block. Due to the disparities in the relative solubilities of the two blocks, these triblock copolymers form aggregates in water above a critical micelle temperature (*cmt*) and a critical micelle concentration (*cmc*) with a core consisting of predominantly PO blocks and a corona made up of hydrated EO blocks. Thus, the self-assembly of block copolymers in solution can be initiated either by increasing the

concentration (via *cmc*) or by changing the temperature (via *cmt*). Both *cmc* and *cmt* are the fundamental parameters in characterizing the association properties of a given block copolymer-solvent system. In fact, for a number of block copolymers, a small increase in temperature, for example by 10 K, may result in a dramatic reduction of the *cmc* value by a factor of about 10-100.¹⁴² Such a striking temperature-dependence is rather unique for this class of polymeric surfactants, which is in contrast to that of the conventional non-ionic surfactants, wherein a rather weak temperature-dependence is observed. The *cmts* and *cmcs* of a number of aqueous triblock copolymers have been determined in a systematic manner by Alexandridis et al.¹⁴² It has become evident from their study that the copolymers with larger number of PO units formed micelles at lower concentrations, and for a given copolymer concentration, they have lower *cmts*. Other important micellar parameters such as aggregation number, hydrodynamic radius, and core radius are also available in the literature for the micelles formed with different triblock copolymers in water.^{156,157} In general, the aggregation number (N_{agg}) increases with increasing length of PO block and decreasing length of EO block. N_{agg} also increases with increasing temperature.¹⁴⁶ Importantly, an increase in N_{agg} with increasing temperature does not change the hydrodynamic radius significantly. This has been observed for a number of block copolymers such as F68,¹⁴⁶ P85,¹⁵⁸ P104,¹⁵⁹ P123,¹⁵⁹ and F127.¹⁵⁹⁻¹⁶¹ This dual effect of the temperature can be understood if we consider the fact that the dehydration of the EO block becomes increasingly important at elevated temperatures, which results in a more or less reduced coronal volume.

The micellization process and the structure of pluronic micelles have been studied extensively using different techniques, like neutron scattering,^{144,162-164} X-ray scattering,¹⁶⁵ light scattering,^{146,157,163,166} absorption¹⁶⁷ and fluorescence measurements.^{142,168,169} Though extensive studies have been carried out on the structural aspects of these micellar systems, studies on the dynamical processes in these micelles are very limited. Using fluorescence anisotropy measurements, Dutt et al. have reported on the rotational dynamics of a solubilized

probe in different phases of pluronic micelles.¹⁷⁰⁻¹⁷⁴ Grant et al. have demonstrated from anisotropy measurements that a suitable molecular probe can be used as a local reporter for the different regions of the copolymer micelles.^{175,176} Relaxation of the water molecules in different regions of pluronic micelles have recently been reported by Bhattacharya et al.¹⁷⁷⁻¹⁷⁹ and Kumbhakar et al.¹⁸⁰⁻¹⁸² All these studies indicate that the dynamical processes in these micelles largely depend on the EO and PO ratios of the polymer.

In several industrial applications, pluronics are often used in combination with low molecular weight ionic surfactants.^{183,184} This feature has prompted experimental studies on the solution behavior of these mixed surfactant systems.^{185,186} Presence of two different classes of surfactants results in the formation of complex microheterogeneous systems, whose properties and solution behavior are essential to be known to use them in a formulation. Interaction of pluronics with low molecular weight ionic surfactants like SDS, CTAC, etc. have been studied quite extensively by using light scattering,^{162,165,166} neutron scattering,¹⁶² and calorimetric methods.^{166,187-189} These studies show that at low ionic co-surfactant concentrations, the supramolecular assemblies are formed such that the hydrocarbon chains of the small ionic surfactants dissolve into the PO core of the pluronic micelles while their head groups are reside at the periphery of the core, pointing towards the hydrated corona region.¹⁶²

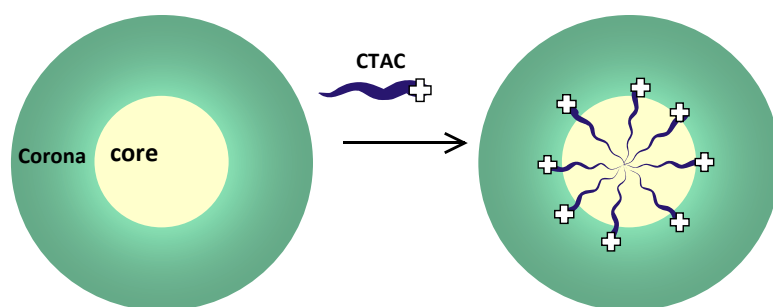


Figure 1.8. Schematic presentation of the formation of a block copolymer-surfactant complex
The usefulness of a polymer-surfactant system in an application is largely determined by the physical and chemical properties of the dissolved solutes in these supramolecular assemblies.

As these assemblies provide a wide range of microenvironments in a single phase, solubilized molecules can display a wide range of physical and chemical properties depending on their position in the micelle. To have a desired physical and chemical property of the solute, it is always a challenging task to place it at a suitable location in the micelle

1.7. Motivation of the present work

It is well known that photoexcitation of a molecule generally induces changes in its electronic and geometrical structures, which in turn lead to the changes in its interactions with the nearby molecules and its environment. Ultrafast photoinduced intramolecular conformational changes are omnipresent in chemistry and biology. Extremely high reaction rates for such processes, often faster than 10^{12} s^{-1} , arise mainly due to lack of an activation barrier. Such processes often constitute the nonradiative deactivation pathways for the excited state of the molecule leading to its very low emission quantum yield. These large amplitudes motion are strongly affected by the viscosity of the surrounding medium and thereby making such molecules as the potential probes to act as the viscosity sensors for various environments ranging from homogeneous to micro-heterogeneous media including biological systems. Control of these large amplitude intramolecular movements is a prerequisite for the development of the devices that would function through the motions at the molecular level.

Thioflavin-T (ThT), a benzothiazole based cationic dye, is one such molecule which is understood to have an ultrafast intramolecular relaxation process in its excited state mediated through large amplitude torsional motion.¹⁹⁰ ThT is used as an extrinsic fluorescence sensor to monitor and estimate the formation of amyloid fibril, a filamentous form of protein responsible for several neurodegenerative diseases, like Alzheimer's and Parkinson's diseases.¹⁹¹⁻¹⁹⁴ Although ThT in water is very weakly fluorescent,¹⁹⁵ it shows a remarkable enhancement in emission yield on its association with amyloid fibrils.¹⁹¹⁻¹⁹⁴ ThT is known to be very specific in its binding with amyloid form of the proteins with no significant interaction with other forms, namely, the folded or partially folded monomeric proteins.¹⁹⁶ Detailed studies in several

confined environments, like in amyloid fibril,^{191,196} polymer,¹⁹⁷ glass matrix,¹⁹⁸ etc., clearly indicate that the high local viscosity of the microenvironment around the dye is directly related to the observed fluorescence enhancement of ThT dye in these systems. However, understanding the basic molecular aspect of the process that is involved in the observed fluorescence enhancement of ThT in the above microenvironments has still remained elusive. Considering the molecular structure of ThT, it is hypothesized that in bulk water, due to the low viscosity of the medium, an intramolecular bond twisting process possibly takes place in the excited state of the molecule.¹⁹⁰ This bond twisting process effectively introduces a very fast non-radiative decay channel for the excited ThT molecule resulting its extremely low fluorescence yield.¹⁹⁵ In contrast, in a highly viscous medium, like in amyloid fibril, the above bond twisting process in the excited dye is significantly retarded, reducing its non-radiative decay channel. Accordingly there is a remarkable increase in the emission yield of ThT in a highly viscous medium and hence its fluorescence sensor ability in amyloid fibrils. In the present thesis a detailed study on the ultrafast excited state dynamics of the amyloid sensing dye, Thioflavin-T and two of its tailor made derivatives has been carried out in different solvents of varying viscosity to understand the basic molecular aspect responsible for the fluorescence sensing activity of ThT and to understand the different relaxation pathways of the excited ThT molecule.

Last two decades have witnessed the increasing significance of various organized assemblies on biological and photophysical processes. Reactants embeded in molecular assemblies like micelles, reverse micelles, cyclodextrins, vesicles, etc., achieve a greater degree of organization compared to their geometries in homogeneous solution and can mimic many reactions in biosystems. The local viscosity/rigidity within the organized assemblies are appreciably different from that in the bulk liquid medium and as a result, these systems can alter the photoprocess of the entrapped molecule quite drastically. Further, understanding the ultrafast dynamics of the photoexcited ThT molecule under different restricted

microenvironments is very essential to understand the underlying molecular aspects responsible for the enhancement of the fluorescence emission yield of ThT in amyloid fibril. With this perspective, effect of the nanoconfined water in both anionic and cationic reverse micelles on the ultrafast torsional dynamics of the photoexcited ThT molecules has been investigated in detail. Extending this study further, the effect of bio-mimetic supramolecular encapsulation of ThT into β -CD cavity on the excited state relaxation dynamics of the dye has also been investigated to understand the consequence of restricted environment on the fluorescence enhancement of the dye.

While in Thioflavin-T, there is negligible influence of solvent relaxation dynamics on its intramolecular configurational relaxation dynamics but there are several large solvatochromic probe molecules where the solvent relaxation dynamics and the intramolecular relaxation dynamics, occurring on a similar time scale, interfere with each other which occur on a similar time scale. Such competing intramolecular processes in the probe molecules that can significantly interfere the dynamic Stokes' shift measurement for solvent relaxation studies are the twisting of the functional groups around a bond, cis-trans isomerization, conformational change, etc. Such an interference poses a tremendous challenge to the experimentalists in distinguishing various contributions of the different types of the relaxation processes in the observed results. In order to understand the actual dynamics of the solvent relaxation process, it is thus very essential to separate out the contribution of the interfering intramolecular processes in the probe from the solvent relaxation process. In the present thesis a methodology has been devised to quantitatively distinguish and separate out the effect of such a competing intramolecular process from the solvent relaxation process. The methodology has been demonstrated using three coumarin derivatives, namely coumarin-153 (C153), coumarin-481 (C481) and coumarin-152 (C152) in acetonitrile solution.

Dynamic Stokes' shift measurements for solvent relaxation study have been applied very extensively to understand the structure and dynamics of different complex chemical and

biological systems. With this perspective, in this thesis, we chose to explore an interesting supramolecular assembly formed between pluronics and ionic surfactants using solvent relaxation dynamics as one of the tool. In several industrial applications, pluronics are often used in combination with other low molecular weight ionic surfactants.¹⁸³ This feature has prompted experimental studies on the solution behavior of these mixed copolymer-surfactant systems.¹⁸⁶ Presence of two different classes of surfactants results in the formation of complex microheterogeneous systems whose properties and solution behavior are essential to be known to use them in a practical formulation. It is reported that some pluronic micelles form unique supramolecular assemblies in the presence of an ionic surfactant.^{162,165} In these supramolecular assemblies, it is understood that the hydrophobic chains of the ionic surfactant molecules are dissolved in the core of the pluronic micelles and the charged head groups of the ionic surfactants are resided at the peripheral region of the core projecting into the hydrated corona region of the micelles.¹⁶² Because of this unique structure of these assemblies, a charged layer is formed inside these mixed micelles. Accordingly, any solute having a charge opposite to that of the charged layer inside these supramolecular assemblies, can experience an electrostatic attraction towards the core-corona interface of the micelles and move into the interior of the micelles. Such systems can thus provide a wide range of microenvironments for the dissolved solutes. Because of the availability of wide range of microenvironments in these micelles, the solutes may also have quite different physical and chemical properties depending on their locations in the micelle. Thus, by changing the position of a solute in these micelles, it is possible to modulate the physical as well as the chemical properties of the solute in these microheterogeneous systems. In the present work we have studied the effect of ionic surfactant on the localization site of a solubilized molecule in a polymer-surfactant supramolecular assembly. Our aim is to see if the location of the solute in the micelle can be changed by changing the polymer-surfactant composition of the supramolecular systems. Additionally, we also investigate how the photophysical properties of the solubilized dye and the structure of

water molecules around the dye in the micelle change with a change in the dye location in the supramolecular system, investigated using solvent relaxation dynamics as tool.

Chapter 2

Instruments and Methods

2.1. Introduction

This chapter gives an overview of the various experimental techniques that have been used to carry out the research work pertaining to the present thesis. To understand the dynamical processes in different polymer-surfactant assemblies, both steady-state and time-resolved photophysical measurements were carried out using absorption and fluorescence techniques. Rotational correlation times were evaluated using time-resolved fluorescence anisotropy measurements to understand the rotational diffusion of the probes in polymer-surfactant assemblies. Small Angle Neutron Scattering (SANS) studies were also carried out to characterize the polymer-surfactant complexes in some specific cases. Ultrafast processes like solvent relaxation dynamics and intramolecular relaxation in the excited probe molecules were investigated using state-of-the-art femtosecond time-resolved fluorescence up-conversion measurements. Important aspects of different instrumental techniques used in the present work are briefly described in the present chapter.

2.2. Ground-State Absorption Measurements

To understand the effect of light on chromophoric molecules, it is very important to know the detailed absorption and fluorescence emission characteristics of the systems under investigation. Optical absorption (ultraviolet-visible; UV-vis) spectroscopy is a widely used

technique to obtain information about the ground-state absorption characteristics of the chemical systems in terms of the wavelengths of the absorption bands and the extinction coefficients at different wavelengths. UV-vis absorption spectroscopy, being dependent on the electronic structure and the environment of the absorbing chromophore, allows the characterization or the identification of various chromophoric systems and their micro-environments. Changes in the solvent polarity, polarizability and hydrogen bonding characteristics often induce significant shift in the absorption spectra.¹⁹⁹⁻²⁰² Hence, this simple photochemical technique can provide many useful information regarding the nature of interactions between the ground-state of a chromophoric molecule and its surrounding environment. Measurements of the optical absorption spectra and thus to get knowledge about the absorbances of the experimental solutions in the ground-state are always very essential to adjust the concentration of the absorbing species in the solution for the purpose of their investigations using different other photochemical techniques.

The absorbance (A) of an absorbing species in a solution is directly proportional to the concentration (C) of the species and its molar extinction coefficient (ϵ_λ) at the measuring wavelength λ and is given by the equation 2.1.¹⁹⁹⁻²⁰²

$$A = \log\left(\frac{I_0}{I}\right) = \epsilon_\lambda Cl \quad (2.1)$$

where I_0 and I are the intensities of the incident and transmitted light, respectively, and l is the path length for the light beam passing through the sample. For absorbance measurements, the sample is usually kept in a quartz cuvette of 1 cm path length. For very concentrated solutions, thinner quartz cells are usually used with typical path length of either 0.1 or 0.2 cm.

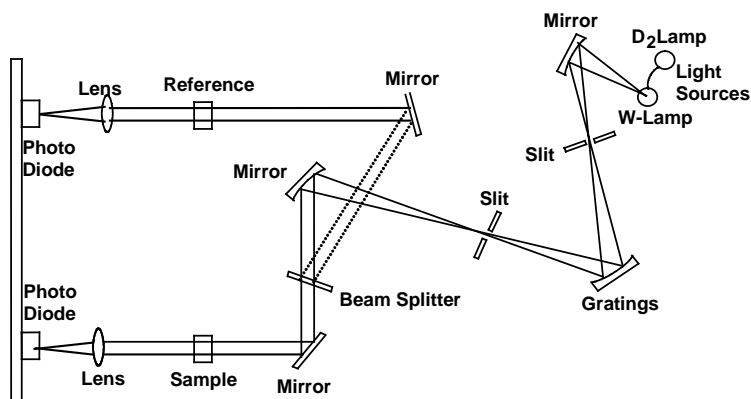


Figure 2.1 Schematic of a double beam UV-vis spectrophotometer

Ground-state optical absorption spectra for the chemical systems to be investigated in the present study were carried out using either of the two double beam UV-vis spectrophotometers available in the department, one from Shimadzu, kyoto, Japan (model 160A) and the other from Jasco, kyoto, Japan (model V530), available in the department. The wavelength range covered in both the spectrophotometers is 200-1100 nm. As the light sources, both the spectrophotometers use W-lamp for the 1100 to 350 nm region and a D₂ lamp for the 350-200 nm region. In both the spectrophotometers Si-photodiodes are used as the light detectors. The minimum wavelength resolution for the two spectrophotometers is 0.2 nm and lowest absorbance measurable is ~0.005. The schematic of a typical double beam UV-vis spectrophotometer is shown in Figure 2.1.

2.3. Steady-State Fluorescence Measurements

Fluorescence spectroscopy is a very simple but extremely powerful technique to investigate various photochemical processes that occur in the excited state of the chromophoric molecules. The intensity of the fluorescence emission, the fluorescence peak position (emission maximum), as well as the shape of the fluorescence spectrum are in general very sensitive to the environmental effects.^{199,201,202} In the present study steady-state fluorescence measurements (either fluorescence intensity, excitation spectra or emission spectra) were carried out using a Hitachi model F-4500 fluorescence spectrometer. The instrument uses a 150 watt continuous

powered high pressure xenon lamp as the excitation source and R-928F (Hamamatsu) photomultiplier tube (PMT) as the photodetector. Sample is excited in a 1 cm x 1 cm suprasil quartz cuvette and the fluorescence is collected and measured in a perpendicular direction with respect to the direction of the excitation beam. The wavelength range covered in the present instrument is 220 to 800 nm. The schematic of a typical steady-state spectrofluorimeter is shown in Figure 2.2.

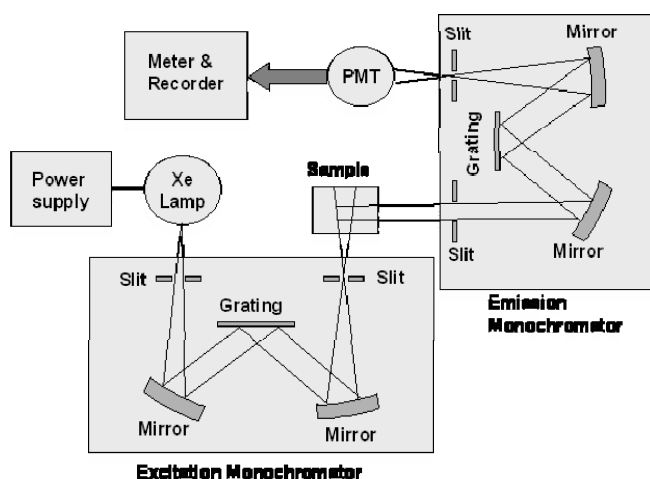


Figure 2.2. Schematic of a steady-state fluorescence spectrometer.

2.3.1. Correction of Emission Spectra

Emission spectra are often distorted due to the wavelength dependent efficiency of different components of the spectrofluorimeter e.g., monochromator, PMT etc., therefore it is necessary to know the wavelength-dependent efficiency of the detection system to calculate the corrected emission spectra. In the present work, spectrum of standard quinine sulfate solution were recorded and compared with the standard spectrum²⁰³ given in unit of photon/nm, to get the correction factors for the instrumental sensitivity. All the measured spectra for our sample have been multiplied by this correction term to get the corrected spectrum. The measured spectra, $I(\lambda)$, were in wavelength domain and have been converted to frequency domain $I(\nu)$, by using the following equation.²⁰³

$$I(\nu) = \lambda^2 I(\lambda) \tag{2.2}$$

2.3.2. Fluorescence Quantum Yield Measurement

Quantum yield of fluorescence ($\phi_{\text{fluorescence}}$) is defined as the ratio of the number of fluorescence photons emitted from the sample to the number of light quanta absorbed by the sample. Thus $\phi_{\text{fluorescence}}$ is expressed by the following equation.¹⁹⁹⁻²⁰²

$$\phi_{\text{fluorescence}} = \frac{\text{Number of Quanta Emitted}}{\text{Number of Quanta Absorbed}} \quad (2.3)$$

Since the determination of the absolute number of quanta absorbed and emitted by the sample is very difficult, the fluorescence quantum yield of a unknown sample is normally determined by using a comparative method,¹⁹⁹⁻²⁰² where the integrated emission intensity of the sample is compared with that of an optically matched (very close absorbance at the excitation wavelength) reference sample whose quantum yield is already known. Thus, keeping the excitation wavelength same for both the sample and the reference, the fluorescence quantum yield of the sample (ϕ_{sample}) can be expressed with respect to the quantum yield of the reference ($\phi_{\text{reference}}$) by using the equation 2.4.^{199,201,202}

$$\phi_{\text{sample}} = \frac{A_{\text{reference}}}{F_{\text{reference}}} \times \frac{F_{\text{sample}}}{A_{\text{sample}}} \times \frac{\eta_{\text{sample}}^2}{\eta_{\text{reference}}^2} \times \phi_{\text{reference}} \quad (2.4)$$

where $A_{\text{reference}}$ and A_{sample} are the absorbances at the excitation wavelength, $F_{\text{reference}}$ and F_{sample} are the integrated fluorescence intensities and $\eta_{\text{reference}}$ and η_{sample} are the refractive indices for the reference and the sample solutions, respectively.

2.4. Fluorescence Lifetime Measurements

Time-resolved fluorescence measurements are very essential to obtain information regarding the kinetics and dynamics of various photochemical processes involved in the deactivation of the excited molecules. Excitation of a sample containing fluorophoric molecules with a very short pulse of light results in an initial population (n_0) of fluorophores in the excited state. Since emission from the individual excited molecules is a random process, for a given time-

window following photoexcitation with an ultrashort light pulse each of the excited fluorophores should have the same probability to emit a fluorescence photon. This condition effectively results the excited state population to decay following a first order rate equation as,^{199-202,204-207}

$$\frac{dn(t)}{dt} = -(k_r + k_{nr})n(t) \quad (2.5)$$

where $n(t)$ is the number of excited molecules at time t following the very short pulse excitation of the sample, k_r is the radiative decay rate constant and k_{nr} is the nonradiative decay rate constant of the excited fluorophores. In an actual experiment, it is often difficult to know the exact number of the excited molecules present in the sample. However, knowing the fact that the fluorescence intensity is directly proportional to the number of excited molecules present in the solution, equation 2.5 can be simply expressed in terms of the time-dependent intensity $I(t)$ and the integration of the resulting equation gives us the expression for the fluorescence decay $I(t)$ as,

$$I(t) = I_0 \exp(-t / \tau_f) \quad (2.6)$$

where I_0 is the intensity at time zero and τ_f is the fluorescence lifetime of the sample and the latter is related to the radiative and nonradiative decay rate constants as,

$$\tau_f = \frac{1}{k_r + k_{nr}} \quad (2.7)$$

If the width of the excitation pulse is unusually short (δ -pulse) and the response time of the detection system is very fast compared to the fluorescence lifetime of the sample, the fluorescence lifetime can be obtained from the observed fluorescence decay by using the following two procedures. In the first method, the τ_f can be obtained simply by noting the time at which the fluorescence intensity decreases to $1/e$ of its initial value. In the other method, the lifetime can be determined from the slope of the plot of $\log I(t)$ versus t .^{199-202,204,205} In the cases where the fluorescence lifetime of the sample is quite short such that the excitation pulse

width and/or the response time of the detection system distorts the observed decay, it is not possible to apply the above two simple analysis procedures to obtain the fluorescence lifetime of the sample. In such cases, the observed fluorescence decays are analysed following a deconvolution procedure, which will be described in the latter part of this section. Regarding the fluorescence decay, however, it is important to mention here that since the excited fluorophores emit randomly, different molecules spend different length of times in the excited states. Thus, for an ensemble of excited molecules in the system, some may emit at very short times following the excitation but others may emit at times much longer than the measured fluorescence lifetime of the sample. Accordingly, the time distribution of these emitted photons actually represents the measured fluorescence decay curve of the experimental sample. It is thus evident that, the estimated lifetime from the observed fluorescence decay is actually the statistical average of the times that the excited molecules spend in the excited state.

As already mentioned, the time-dependent fluorescence measurement is very important to investigate the dynamics and mechanism of the photoinduced processes in the excited singlet (S_1) state of the molecules. Time-Correlated Single Photon Counting (TCSPC) technique is the most widely used experimental method to measure the time-dependent fluorescence of a sample in the nanosecond to picosecond time scales. In the present study a TCSPC spectrometer from Horiba Jobin Yvon IBH, UK (model Data Station Hub) was used to measure the fluorescence lifetimes of the samples under investigation. The important aspects related to the present TCSPC spectrometer are described in the following sections.

2.4.1. Basic Principles of TCSPC Technique

The instrument used in the present study for time-resolved fluorescence measurement works on the principle of Time-Correlated Single-Photon Counting (TCSPC), where each single photon emitted by the sample is detected following its excitation by a short light pulse.²⁰⁴⁻²⁰⁷ The

principle of TCSPC measurement relies on the fact that the time-dependent probability distribution of the single photon emission from an excited molecule following its excitation is equivalent to the time-dependent changes in the fluorescence intensity of the sample following its δ -pulse excitation.²⁰⁴⁻²⁰⁷ The schematic diagram of a typical TCSPC set up is shown in Figure 2.3.

According to Figure 2.3, an excitation pulse (optical pulse) from the pulsed excitation source is split into two parts, one part is used to excite the sample kept in the sample chamber and the other part of the light pulse is directed to a start PMT. The optical signal at the start PMT generates an electrical START pulse, which is then routed through a Constant Fraction Discriminator (CFD) to the START input of the Time to Amplitude Converter (TAC) unit to initiate its charging operation. On receiving the start pulse, the TAC continues to undergo charging linearly with time. The part of the optical pulse, which excites the sample, effectively gives rise to the emission photons. These photons are then detected one by one by the stop PMT (at the right angle to the direction of excitation) to generate electrical STOP pulses for each of the individual photons received. The STOP pulses thus generated in the stop PMT are also routed through a CFD and a variable delay line to the STOP input of the same TAC unit. On receiving the first STOP pulse, the TAC unit stops its charging operation and subsequently generates an electrical output pulse (TAC-output), having amplitude proportional to the time difference (Δt) between the START and the STOP pulses reaching the TAC unit. The TAC output pulse is then fed to the input of a Multichannel Analyzer (MCA) through an Analog-to-Digital Converter (ADC). The ADC generates a numerical value proportional to the height of the TAC output pulse and thus selects the corresponding memory address (channel) in the MCA, where a single count is added up.

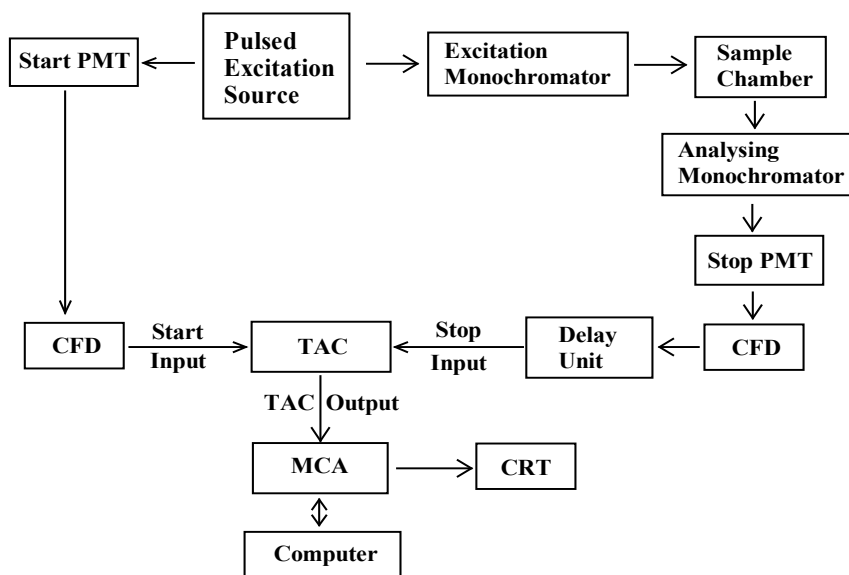


Figure 2.3. Schematic diagram of a Time Correlated Single Photon Counting Spectrometer.

The above cycle (from the triggering of the pulsed excitation light source to the data storage in the MCA) is repeated for a large number of times and thus a histogram of counts is collected in the MCA channels. The distribution of the counts against the channel number in the MCA then represents the fluorescence decay curve of the sample, provided the collection rate of the emission photons by the stop PMT is kept very low, only about 2% or less, compared to the repetition rate of the excitation pulses.²⁰⁴⁻²⁰⁷ This experimental condition effectively means that following an excitation pulse, in no circumstances more than one emission photon can be detected by the stop PMT. Thus, in the TCSPC measurement, for about 98% cases of the excitation pulses, though the sample is excited, there is effectively no emission photon that is directed to the stop PMT. Only about 2% cases of the sample excitations by the pulsed light source there is an effective emission of photon that is directed to the stop PMT and detected by the TCSPC setup. Such a low count rate is essential to maintain the time-dependent probability distribution of the photon emission from a single excited molecule following its excitation process. From the measured fluorescence decay curves, the fluorescence lifetimes of the samples are estimated following a suitable analysis procedure and introducing a proper time calibration for the MCA channels.²⁰⁴⁻²⁰⁸

2.4.2. Important components of a TCSPC spectrometer

The TCSPC instrument used in the present study is from Horiba Jobin Yvon IBH, UK, Model Datastation Hub. The important components of the present TCSPC instrument are as given below.

(a) Pulsed excitation source: Different light emitting diodes (LED's) and diode lasers, having different emission wavelengths between 373 nm to 636 nm are used as the excitation sources in the IBH machine. With 408 and 636 nm diode laser excitation and using the special stop PMT described latter, the instrument response function for the spectrometer is about 240 ps (FWHM). With the LED excitation sources, the instrument response function is about 1.2 ns (FWHM). The repetition rate for excitation pulses is usually kept at 1 MHz.

(b) Constant Fraction Discriminator (CFD): In a typical TCSPC instrument, the signals from the two PMTs (START and STOP PMTs) are routed through two independent CFDs to achieve the following two goals: (1) To improve the signal to noise ratio (S/N) by discarding the signals below a threshold height such that the counts recorded by the instrument are genuinely due to the photons detected by the PMTs and not due to spurious electrical noises. (2) To provide the correct timing information for the START and STOP inputs to the TAC unit such that the timing jitter in the detection is minimized. As the simple leading edge discriminators are always associated with significant timing errors, the CFDs are recognized to be the best suited discriminators for the TCSPC measurements to obtain accurate timing information for the START and STOP events.

(c) Variable Delay Line: A variable delay line is incorporated in the path of the STOP signal, between the CFD and the TAC, to intentionally delay the STOP pulse such that it reaches the TAC unit only after the START pulse and thus fruitfully counted by the TCSPC instrument. Moreover, by adjusting the variable delay line it is possible to trigger the TAC-

MCA combination effectively such that the measured fluorescence decay curve is placed and stored within the suitable range of the MCA channels.

(d) Time-to-Amplitude Converter (TAC): In TCSPC instrument the time-correlation between the START and STOP event is carried out by using the TAC unit. In fact, this unit is considered as the heart of the TCSPC instrument.^{204,206,209-211} On receiving the START pulse, following a preset delay (set in the TAC itself), a timing capacitor in the TAC start charging linearly with time from a constant current source. The charging is discontinued upon receiving a STOP pulse. Once the charging process is stopped, the TAC unit generates an output pulse (V_{TAC}) for which the amplitude is proportional to the charge accumulated on the TAC capacitor and consequently is a measure of the time-difference (Δt) between the arrivals of the START and STOP pulses to the TAC, because the charging process of the capacitor in the TAC is linear with time. Functioning of a TAC unit is schematically shown in Figure 2.4. Following a START pulse, if no STOP pulse is received (i.e. no emission photon detected) by the TAC within a predefined time period, called the "TAC range", the capacitor charging is automatically discontinued without recording the event and the TAC gets reset within a short time span making

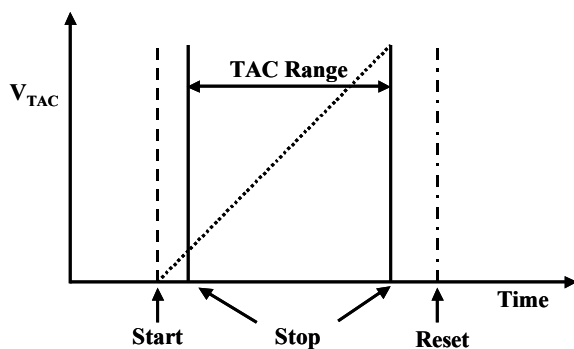


Figure 2.4. Functioning of a TAC unit used in a TCSPC instrument. Start indicates the initiation of the charging process. Stop signal can arrive the TAC unit at any time within the TAC range following the arrival of the start pulse.

the unit ready for the next START and STOP pulses. In the present TCSPC instrument the TAC range can be varied from 50 ns to 200 μ s. A suitable TAC range is judiciously selected

for a particular TCSPC measurement depending on the expected fluorescence lifetime of the sample used.

(e) Multichannel Analyzer (MCA): The MCA used in a TCSPC instrument can be operated either in the Pulse Height Analysis (PHA) mode (for measuring fluorescence decays) or in the Multichannel Scaling (MCS) mode (for measuring time-resolved emission spectra). The data stored in the MCA channels are transferred to a computer for further analysis and processing.

(f) The Start and the stop PMTs: In a typical TCSPC instrument where a nanosecond flash lamp with reasonably low repetition rate (~ 30 KHz) is normally used for sample excitation, the start and stop PMTs are used to get the respective signals for the TAC unit. In such instruments, an ordinary PMT with medium gain and reasonably low transit time can suitably be used to generate the START signals for the TAC unit, as a part of the light pulse (reasonably high intensity) is directly used to generate the START signal. In these cases, however, a special PMT with high gain and fast response time is required to be used to detect the emission photons from the sample. In TCSPC measurement, the spread in the transit time (the time difference between the emission of a photoelectron and its arrival to the anode) of the PMT has a pronounced effect on the time resolution achieved by the instrument. As the transit time becomes shorter, the spread of the transit time also becomes shorter, improving the time resolution of the TCSPC measurements. Accordingly, fast PMTs are always preferable for the TCSPC measurements. The important point to be noted, however, that the detected light level for the emission photons from the sample is inherently very low (due to the condition imposed for time-correlated single photon detection). Thus to detect the single emission photons effectively, the gain of the STOP PMT should be significantly high. To achieve a high gain for a PMT, one has to increase the number of dynodes for the PMT used. This, however, have a

detrimental effect to increase the transit time and consequently the transit time spread, which in turn reduces the time resolution of the TCSPC instrument.

Though in a typical TCSPC instrument, suitable start and stop PMTs are used to carry out the measurements in the present IBH instrument only a single PMT with very high gain and low transit time is used to detect the emission photons from the sample. Thus only photodetector used in the present instrument is a special Hamamatsu PMT, used in combination with a TBX4 module provided by IBH, UK, and is used with a peltier cooling. The detector is having a spectral response from ~300 to 800 nm. In this instrument the measurement is in fact made in a reverse mode, that is, the signal from the special PMT is used as a start pulse for the TAC unit and an electrical signal synchronized with the pulsed diode laser or LED is used as the stop pulses. This reverse mode is adopted especially for faster data collection using high repetition rate of the excitation pulses (1 MHz). This reverse mode of detection is essential to avoid unnecessary charging of the TAC unit by the high repetition rate excitation pulses. It is important to be added here that the present IBH TCSPC instrument has been recently updated by replacing the PMT detector with a MCP-PMT, whereby the instrument response function of the setup is improved to be about 100ps (FWHM) using diode lasers as the excitation sources. To be mentioned that in IBH machine a PC based card that incorporates both TAC and MCA are directly used for the data collection. PC monitor is directly used to display the measured decay curve. Suitable analysis software is used to fit the measured decay curves and thus to obtain the fluorescence lifetime of the samples.

2.4.2.1. Time Calibration of the MCA channels in a TCSPC Spectrometer

Time calibration of the MCA channels in a TCSPC spectrometer is done by using a number of accurately calibrated delay lines in the path of the STOP pulses.^{204,206,212} For this purpose, either the stop or the start signal is bifurcated into two parts, one is fed to the start input of the TAC and the other is routed through the precisely calibrated delay lines and then fed to the

stop input of the TAC. As both START and STOP inputs, of the TAC are originated from the same source, counts are collected only at a single channel of the MCA, determined by the TAC range used for the instrument and the known delay applied at the delay line in the path of the STOP pulse. For different known delays, the counts are thus collected at different channels of the MCA. The MCA data thus obtained are then transferred to a computer and the time calibration is calculated using a suitable analysis program.

2.4.2.2. Analysis of the fluorescence decay curves measured in a TCSPC instrument

As the light pulses used for the sample excitation in a TCSPC spectrometer is having a finite time width and the detection system is also having a finite response time, the experimentally measured fluorescence decay curve, $I(t)$, is effectively a convolution of the true fluorescence decay, $G(t)$, and the time profile of the excitation pulse, $P(t)$. Imagining the excitation pulse to be a combination of large number of δ -pulses, it is possible to express the observed decay, $I(t)$, as the convolution integral of $G(t)$ and $P(t)$ as,^{204-208,213-215}

$$I(t) = \int_0^t P(t') G(t - t') dt' \quad (2.8)$$

Experimentally one can obtain both $I(t)$ and $P(t)$. During analysis, a decay function $G(t)$ is first assumed for the sample and this function is convoluted with the observed $P(t)$ according to equation 2.8 to obtain a calculated curve $Y(t)$, which is then compared with the experimentally observed decay curve $I(t)$.^{204-206,213,214} The variables in the function $G(t)$ is iteratively changed until a good comparison (best fit) between the $Y(t)$ and $I(t)$ is obtained. The function $G(t)$ is usually assumed to be a sum of exponentials, such that,

$$G(t) = \sum_i B_i \exp(-t / \tau_i) \quad (2.9)$$

where B_i is the pre-exponential factor for the i^{th} component and τ_i is the corresponding fluorescence lifetime. The success of an analysis and accordingly the acceptance of a fit to the observed decay curve is determined from the judgement of the following statistical parameters.

(a) Reduced Chi-square (χ_r^2) values: The reduced chi-square (χ_r^2) is defined as,

$$\chi_r^2 = \frac{\sum_i W_i \{Y(i) - I(i)\}^2}{(n - p)} \quad (2.10)$$

where $Y(i)$ is the count at the i^{th} channel of the calculated curve, $I(i)$ is the count at the i^{th} channel of the experimentally measured curve, W_i [$=1/I(i)$], is the weighting factor of the counts in the i^{th} channel, n is the number of channels used for the decay to be analysed and p is the number of degrees of freedom in the decay function considered for the analysis (equals to the number of variables in the function $G(t)$). For a good fit, the χ_r^2 value should be very close to unity. Normally a χ_r^2 value between 1.00 to 1.20 is considered to represent a good fit.²⁰⁴⁻²⁰⁸

(b) Distribution of weighted residuals: To judge the success of an analysis of a TCSPC data set, the random distribution of the weighted residuals among the data channels is also considered to be an important criteria. The weighted residual for the i^{th} channel, r_i , is defined by equation 2.11.

$$r_i = \sqrt{W_i} \{Y(i) - I(i)\} \quad (2.11)$$

where W_i , $Y(i)$ and $I(i)$ are as defined earlier. For a good fit, the weighted residuals should be randomly distributed about the zero line for the whole range of the data channels used in the decay analysis.

2.5. Fluorescence Anisotropy Measurements

In a homogeneous solution, the ground-state fluorophores are all randomly oriented. When such an isotropic ensemble of chromophores is excited with a polarized light beam, an anisotropic distribution is generated in the excited state (also in the ground-state which is not considered here) due to the selective excitation of the suitably oriented chromophoric molecules in the solution. Thus, observation and measurement of fluorescence anisotropy is based on the photoselective excitation of fluorophores, which can be better understood in the following manner. Each fluorophore has within its molecular framework a fixed absorption and a fixed emission transition dipoles, that have very definite orientations with respect to the

molecular axis. The two transition dipoles in a molecule are usually separated from each other by an angle β . Those fluorophores preferentially absorb the excitation photons that have their absorption transition dipoles parallel to the electric field vector parallel to the polarized excitation light. The probability of absorption for a molecule for which its transition dipole is oriented at an angle θ is with respect to the direction of the electric field vector of the polarized light is proportional to $\cos\theta$. Therefore absorption is maximum when $\theta = 0^\circ$ and becomes negligible when θ approaches 90° .^{199,204,206,216} Thus, the excited state population obtained following the excitation of the sample by a polarized excitation pulse is not randomly oriented but highly anisotropic in nature. This preferential excitation of molecules creates an anisotropy in excited electronic state and this is schematically shown in Figure 2.5. Similarly, an excited molecule emits a photon preferentially with its electric field vector parallel to the emission transition dipole of the molecule. At any other angle θ , the probability of emission is again proportional to $\cos\theta$, where θ is the angle between the electric field vector of the emitted light and the emission transition dipole of the molecule. Thus, due to the selective excitation and emission, the fluorescence obtained following excitation with a polarized light is highly anisotropic in nature.

In dilute solution, where depolarization of the excited molecules via energy transfer among chromophoric components is very insignificant, the excited-state anisotropy of the system decays mainly due to the rotational relaxation of the excited species. The anisotropy measurements reveal the average angular displacement of the fluorophore that occurs between the absorption and the subsequent emission process. This angular displacement is dependent upon the rate and the extent of the rotational diffusion of the excited species during the lifetime of the excited state. As expected the rotational diffusion of a molecule depends upon its size and shape as well as on the viscosity or the rigidity of its local environment. Thus, studies on the fluorescence anisotropy have been utilized extensively to explore the local environment of

the chromophoric dyes as well as to investigate their interactions with various host molecules or supramolecular systems.

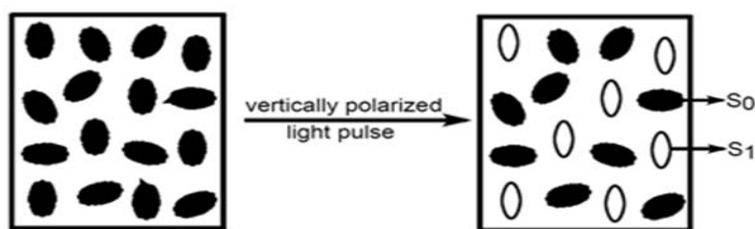


Figure 2.5. Creation of ground-state and excited state anisotropies from an isotropic distribution of molecules.

Fluorescence anisotropy can be measured using both steady-state and time-resolved fluorescence spectrometers. In the Steady-state measurement, the sample is illuminated with a continuous beam of plane polarized light, and the intensities of the fluorescence emission are recorded for both parallel and perpendicular polarizations of the emitted light with respect to the vertically polarized excitation light. In the time-resolved anisotropy measurement, the sample is excited with a vertically polarized pulsed excitation light source and the fluorescence decays are collected for both parallel and perpendicular polarizations of the emitted light with respect to the excitation polarization. The general measurement procedure of the fluorescence anisotropy (both steady-state and time-resolved) is illustrated in Figure 2.6. The sample is excited with the vertically polarized light, i.e. the electric vector of the excitation light is oriented along the z -axis. The emission from the sample is measured through a polarizer oriented either parallel (\parallel) or perpendicular (\perp) with respect to the excitation polarization. When the emission polarizer is oriented parallel to the excitation polarization, the observed intensity is labeled as I_{\parallel} . On the other hand, when the emission polarizer is oriented perpendicular to the excitation polarization, the observed intensity is designated as I_{\perp} . Since the response of the emission monochromator is not the same for the parallel and perpendicularly polarized light, the measured perpendicular component I_{\perp} is corrected by an

appropriate correction factor, known as G-factor, to rectify the polarization bias of the detection setup. Thus, from the measured I_{\parallel} and I_{\perp} values the steady-state anisotropy ($\langle r \rangle$) is calculated as,^{199,204,206,216}

$$\langle r \rangle = \frac{I_{\parallel} - GI_{\perp}}{I_{\parallel} + 2GI_{\perp}} \quad (2.12)$$

where the correction factor G, is obtained independently by keeping the excitation polarization horizontal i.e. along Y- axis and measuring the fluorescence intensities with the emission polarizer oriented vertical (I_{HV}), and horizontal (I_{HH}), respectively where the intensity ratio

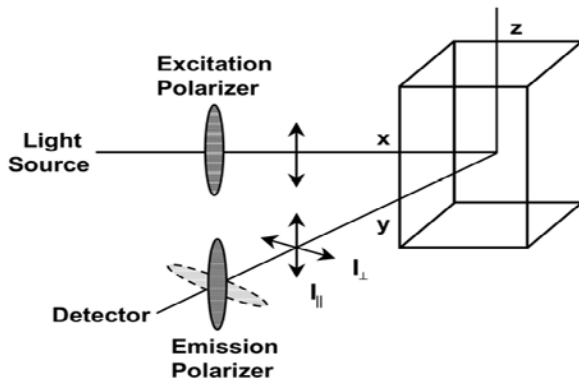


Figure 2.6 Schematic describing measurement of fluorescence anisotropy

I_{HV}/I_{HH} gives the measure of the G factor for the measuring emission wavelength. To be mentioned here that the G factor is not a fixed number for an instrument but is strongly dependent on the measuring emission wavelength. As indicated from the equation 2.12, anisotropy is a dimensionless quantity. Moreover, it is to be noted that the measured anisotropy is independent of the emission intensity of the sample. This is because the difference in the intensities for two emission polarization ($I_{\parallel} - GI_{\perp}$) is normalized by the total intensity of the sample, which can be easily shown to be equal to ($I_{\parallel} + 2GI_{\perp}$). Similar to steady-state anisotropy, the time-resolved fluorescence anisotropy is expressed as

$$r(t) = \frac{I_{\parallel} - GI_{\perp}(t)}{I_{\parallel} + 2GI_{\perp}(t)} \quad (2.13)$$

where I_{\parallel} and I_{\perp} are the two polarized fluorescence decays with emission polarizations parallel and perpendicular to the vertically polarized excitation light.

There exists a rather simple relationship between the steady-state and the time-resolved anisotropy parameters. The steady-state anisotropy is simply the average of the time-resolved anisotropy, weighted by the intensity decay of the sample. Thus the steady-state anisotropy $\langle r \rangle$ is given by the average of $r(t)$ weighted by $I(t)$ as,^{199,204,206,216}

$$\langle r \rangle = \frac{\int_0^{\infty} r(t)I(t)dt}{\int_0^{\infty} I(t)dt} \quad (2.14)$$

For a fluorophore, which displays a single exponential anisotropy decay with reorientation time τ_r , the function decay can be expressed as

$$r(t) = r_0 \exp(-t / \tau_r) \quad (2.15)$$

where r_0 is the initial anisotropy i.e. the anisotropy at $t = 0$ immediately after the δ -excitation pulse. Thus substituting $I(t)$ and $r(t)$ from equations 2.6 and 2.15 into equation 2.14 and on integration one can obtain,

$$\langle r \rangle = r_0 \left(\frac{\tau_r}{\tau_r + \tau_f} \right) \quad (2.16)$$

To be mentioned however, this expression is valid only if the intensity and anisotropy decays follow the single exponential functions. In most cases, however, intensity and anisotropy decays are more complex and cannot be fitted by the relations given by equations 2.6 and 2.15. The intensity decay of a fluorophore can follow a biexponential decay law when it is present in different environments (e.g. micelle bound and free dye) and is given by,

$$I(t) = a_1 \exp(-t / \tau_{f1}) + a_2 \exp(-t / \tau_{f2}) \quad (2.17)$$

where τ_{f1} and τ_{f2} are the two lifetimes associated with the decay of fluorescence and a_1 and a_2 values are the pre-exponential factors. A fluorophore usually displays different lifetimes in different environments. Thus, for the same fluorophore in different environments, the value of

a_i qualitatively represents the part of the fluorophores present in a particular environment. Similarly for fluorescence anisotropy a biexponential decay may be applicable as,²¹⁷⁻²²⁰

$$r(t) = r_0 [\beta_1 \exp(-t / \tau_{r1}) + \beta_2 \exp(-t / \tau_{r2})] \quad (2.18)$$

In this expression, τ_{r1} and τ_{r2} are the two time constants associated with the two decay component of the measured anisotropy and β_i represents the fractional fluorescence arising from each emitting species. More complex intensity and anisotropy decays are also possible and that are usually expressed as the sum of exponentials as,

$$I(t) = \sum_i a_i \exp(-t / \tau_i) \quad (2.19)$$

$$r(t) = r_0 \left[\sum_i \beta_i \exp(-t / \tau_i) \right] \quad (2.20)$$

For such complex decays the analysis and interpretation of the results are very difficult and are mainly done with lot of intuitions and modeling of the systems, as well as by gaining additional informations from other supporting measurements.

2.6. Fluorescence up-conversion Measurements

Using a technique like time-correlated single-photon-counting (TCSPC) in conjunction with a fast photomultiplier or MCP-PMT, it is possible to improve the time-resolution to some extent, in the range of about few tens of picoseconds,^{204,206,221} but a careful de-convolution analysis is required to obtain such a time-resolution for the TCSPC measurements. Another important technique for obtaining time-resolution better than 100 ps has been to use a streak camera.^{204,206,221} Single shot streak cameras offer a time-resolution better than ~10 ps. One of the drawbacks of using streak camera is that the spectral response of these cameras is limited by the spectral responses of their photocathodes, which typically do not extend beyond about 900 nm. In spite of this limitation, streak cameras remain the extremely convenient means for time-resolved luminescence measurements with time-resolutions in the range of ~10 ps.

Till date, the best way to get the time-resolution in the emission measurements comparable to the width of the excitation laser pulses appears to be the technique that uses the nonlinearity induced by the high energy laser pulses as the timing gate for the emission detection²²²⁻²²⁶. One of these nonlinear techniques, first introduced by Mahr and Hirsch,²²⁵ is the frequency mixing technique utilized for ultrafast time-resolved fluorescence measurements. In this technique, the emission from the sample is mixed with a part of the ultra-short laser light in a nonlinear crystal to generate the sum frequency or the difference frequency of the two mixing light. Since the mixing process takes place only during the temporal overlap of the ultra-short laser pulse with the fluorescence emission, this technique provides the best time-resolution, effectively comparable to the width of the ultra-short laser pulses used for the frequency mixing with fluorescence, provided that certain experimental conditions are satisfied during these measurements. The method of using sum-frequency generation to measure the ultrafast fluorescence decays of samples is the most widely used technique in the time-resolved fluorescence measurements and is commonly known as the fluorescence up-conversion technique.

2.6.1. Basic principle of fluorescence up-conversion

2.6.1.1. Sum-frequency generation

The basic concept of achieving ultra-short time resolution in the time-resolved fluorescence measurement by using the frequency mixing technique is illustrated in the following Figure 2.7. The emission light (frequency ω_{fl}) collected from the sample following its excitation with an ultra-short laser pulse and a suitably delayed intense laser pulse, known as the gate pulse (frequency ω_g), are focused into a thin nonlinear crystal whose optic axis is oriented at an appropriate angle with respect to the ω_g and ω_{fl} light beams. The sum-frequency photons (frequency ω_s) are generated only during that time for which the ultra-short gate pulse is present at the crystal along with the comparatively long lived fluorescence light. Thus, frequency mixing occurs only for a thin temporal slice of the fluorescence decay and

accordingly acts as a light gate, providing time-resolution quite comparable to the width of the gate pulses used.²²²⁻²²⁶

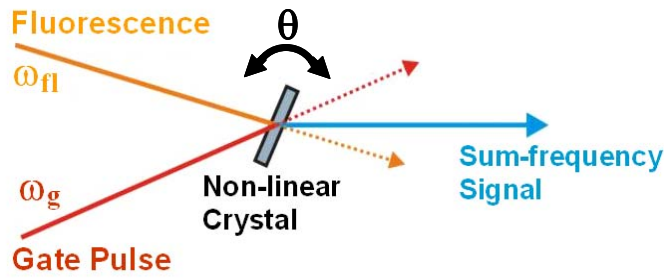


Figure 2.7. Schematic representation of sum frequency generation in a non-linear crystal.

The efficiency of the up-conversion process largely depends on the phase matching condition among the wave vectors (\vec{k}) of the different lights (ω_g , ω_{fl} , and ω_s) that interact in the nonlinear crystal.²²²⁻²²⁶ For the sum-frequency generation, two important criteria to be fulfilled are the “*energy conservation*” and the “*phase matching condition*” among the interacting lights in the nonlinear crystal. The energy conservation criterion gives us the following relation among the frequencies of the different light involved.

$$\omega_g + \omega_{fl} = \omega_s \quad (2.21)$$

Similarly, the phase matching condition suggests the following relation among all the wave vectors involved in the nonlinear phenomenon for the most efficient sum-frequency generation.

$$\vec{k}_s = \vec{k}_g + \vec{k}_{fl} \quad (2.22)$$

where \vec{k}_g , \vec{k}_{fl} and \vec{k}_s are the wave vectors for the gate, fluorescence and the sum frequency lights. In accordance with relation 2.22, the closeness to the phase matching condition for sum-frequency generation is often expressed by the parameter called phase mismatch, $\Delta \vec{k}$, and is expressed by the following equation.

$$\Delta \vec{k} = \vec{k}_s - (\vec{k}_g + \vec{k}_{fl}) \quad (2.23)$$

For the co-linear propagation of the gate and the fluorescence beams, the above expression for the phase mismatch for the sum-frequency generation can be simplified as,

$$\Delta \vec{k} = \vec{k}_s - (\vec{k}_g + \vec{k}_f) = \frac{1}{c}(n_s \omega_s - n_g \omega_g - n_f \omega_f) \quad (2.24)$$

where c is the velocity of light in vacuum and n_s , n_g and n_f are the refractive indices of the lights ω_s , ω_g and ω_f , respectively, in the non-linear medium. Obviously, the true phase matching condition suggests that the $\Delta \vec{k}$ value should be equal to zero. It is thus clear that the smaller is the $\Delta \vec{k}$ value, more closer is the situation for the true phase matching condition and accordingly the better should be the efficiency for the fluorescence up-conversion process. Such an ideal situation is, however, not possible to achieve practically, because none of the light beams used (e.g. ω_s , ω_g and ω_f) are monochromatic in nature. Thus, for all practical purposes in the fluorescence up-conversion measurements, the best efforts are made to achieve the lowest possible phase mismatch condition such that the intensity of the sum-frequency light becomes the maximum.²²²⁻²²⁶ To achieve this, the optical axis of the non-linear crystal is rotated with respect to the polarization direction and the direction of propagation of the gate and the fluorescence light pulses until the intensity of the sum-frequency light becomes the maximum for a selected ω_f value (i.e. the monitoring emission wavelength). The selection of ω_f or the monitoring emission wavelength is easily achieved by setting the wavelength of the monochromator in front of the photodetector corresponding to the sum-frequency light ω_s that is expected according to eq. 2.21 for the selected ω_f and the fixed ω_g for the gate pulses used. Thus, by selecting different emission wavelengths for the measurements and accordingly tuning the optical axis of the non-linear crystal for the maximum sum-frequency light for each of these selections, one can easily carry out the time-resolved fluorescence up-conversion measurements for a wide range of wavelengths covering the whole fluorescence spectrum of the sample. A proper selection of the non-linear crystal is, however, essential to achieve this

because different nonlinear materials have different spectral ranges for their suitability and efficiency to up-convert the fluorescence light by mixing it with the gate laser light. Among different non-linear crystals, the β -barium borate (BBO) is understood to be the most useful nonlinear crystal in the fluorescence up-conversion measurements, because it has a high transmittance over a wide spectral range (covering most of the UV-visible spectral region) and a reasonably high non-linear efficiency for the sum-frequency generation process.²²²⁻²²⁶

Since the beam size of the fluorescence collected from the sample is always quite large, it is always required to focus the fluorescence beam on to the non-linear crystal with a broad cone. Thus, the nonlinear crystal used for up-conversion measurement should have quite high phase matching acceptance angle, $\Delta\theta$, such that the maximum of the fluorescence light can be utilized in the up-conversion process.²²²⁻²²⁶ For a nonlinear crystal, the phase matching acceptance angle, $\Delta\theta$, is expressed by the following relation.

$$\Delta\theta = \frac{4\pi}{d} \left(\frac{\partial \Delta \vec{k}}{\partial \theta} \right) \quad (2.25)$$

where d is the thickness of the nonlinear crystal. It is evident from the above equation that the smaller the thickness of the crystal, the larger is the $\Delta\theta$ value. Thus, the thinner is the nonlinear crystal, the easier is the tuning of the crystal axis for the efficient sum-frequency generation. However, with very thin crystal the integrated intensity of the sum-frequency light becomes very low and accordingly the system becomes overall inefficient. Thus, in all practical systems, there is a compromise to select the optimum crystal thickness. Crystals with thickness of about 0.5 mm are quite commonly used in most fluorescence up-conversion measurements, without sacrificing much on the acceptance angle and at the same time not sacrificing much on the time resolution of the measurements.

2.6.1.2. Time resolution

In fluorescence up-conversion measurements, the time-dependent changes in the fluorescence intensity is obtained by recording the integrated sum-frequency intensity at the varying time delay of the gate pulse at the nonlinear crystal with respect to the excitation pulse and thereby scanning the whole fluorescence decay of the sample as shown in Figure 2.8. At any delay of the gate pulse, the intensity of the sum frequency light (I_s) is proportional to the correlation function of the fluorescence intensity (I_f) and the intensity of the gate light (I_g), and is given by the following equation.²²²⁻²²⁶

$$I_s(t) = \int_{-\infty}^{+\infty} I_f(t) I_g(t - \tau) dt \quad (2.26)$$

where τ is the time delay between the excitation and the gate pulses.

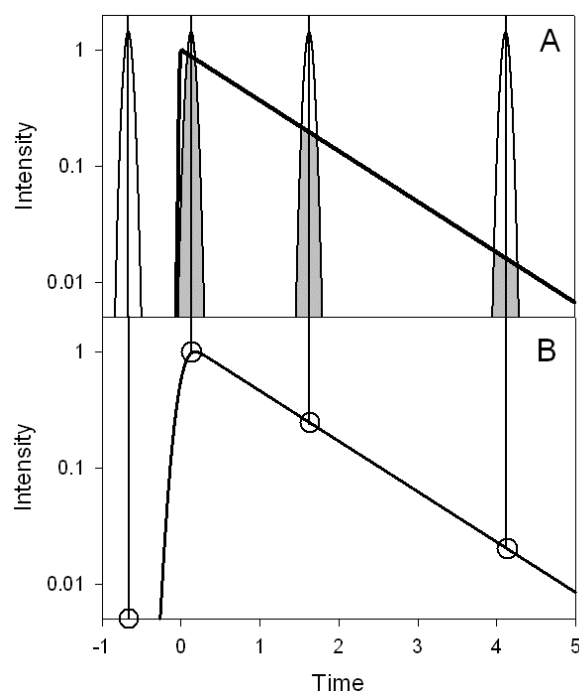


Figure 2.8. Schematic representation of fluorescence decay measurement using fluorescence up-conversion technique.

As the intensity of the gate pulse, I_g , remains constant at all the delays, the intensity of the sum frequency light at each delay position is effectively proportional to the intensity of the fluorescence light at that delay. Thus, pictorially, the value of the integral in eq. 2.26 at any delay position can be represented by the shaded area under the fluorescence curve in Figure

2.8. To obtain the full fluorescence decay profile, the delay τ for the gate pulse is scanned over the whole fluorescence decay and the integrated intensity of the sum frequency light at each delay is recorded for a fixed preset time period. Thus, the fluorescence up-conversion measurement is essentially an optical version of a boxcar sampler with time resolution determined by the pulse width of the gate pulses.

2.6.2. Brief description of the present fluorescence up-conversion setup

2.6.2.1. The key features

The block diagram of the femtosecond fluorescence up-conversion instrument developed in our department is shown in Figure 2.9. In this instrument a mode-locked Ti:sapphire oscillator (from CDP Inc. Russia) is optically pumped by a diode pumped solid state laser from Coherent (Verdi, 5W at 532 nm) to produce the ultra short laser pulses for the wavelength around 800 nm. The pulse duration of the present Ti:sapphire laser system is ~ 50 fs and it operates with a repetition rate of 82 MHz. Though 800 nm is the most commonly used laser wavelength for the Ti: sapphire oscillator, for the present laser it is also possible to tune the laser wavelength to a significant extent, namely for the wavelength range of 770-950 nm, as and when required for a particular experiment.

In the present up-conversion instrument, the output laser beam from the Ti:sapphire oscillator is first passed through a harmonic generator unit, where either the 2nd (around 400 nm) or the 3rd harmonic (around 266 nm) of the laser light is generated using suitable BBO crystals and by proper tuning of their optic axis for the required phase matching conditions. The higher harmonic light thus produced is separated from the residual fundamental light of the Ti:sapphire laser by using a dichroic mirror and is used for the excitation of the samples of our interest. The intensity of the higher harmonic light is normally kept reasonably low to ensure that the fluorescence intensity remains linearly dependent on the excitation laser

intensity. This is also required to minimize the photo-degradation of the samples during the measurements of the fluorescence decays.

In the actual experimental arrangement, the sample solution is kept in a rotating quartz cell of 1 mm thickness. The sample cell is rotated continuously during the measurement to prevent localized heating of the sample and consequently to minimize its photo-decomposition. A cut-off filter is used immediately after the sample cell to prevent the residual excitation light and/or Raman light to reach the detection system. The transient fluorescence originating from the sample is then focused onto an up-conversion crystal (0.5 mm thick BBO crystal), using two elliptical mirrors. The residual fundamental beam used as the gate pulse is first directed to an Optical delay line and subsequently focused onto the up-conversion crystal.

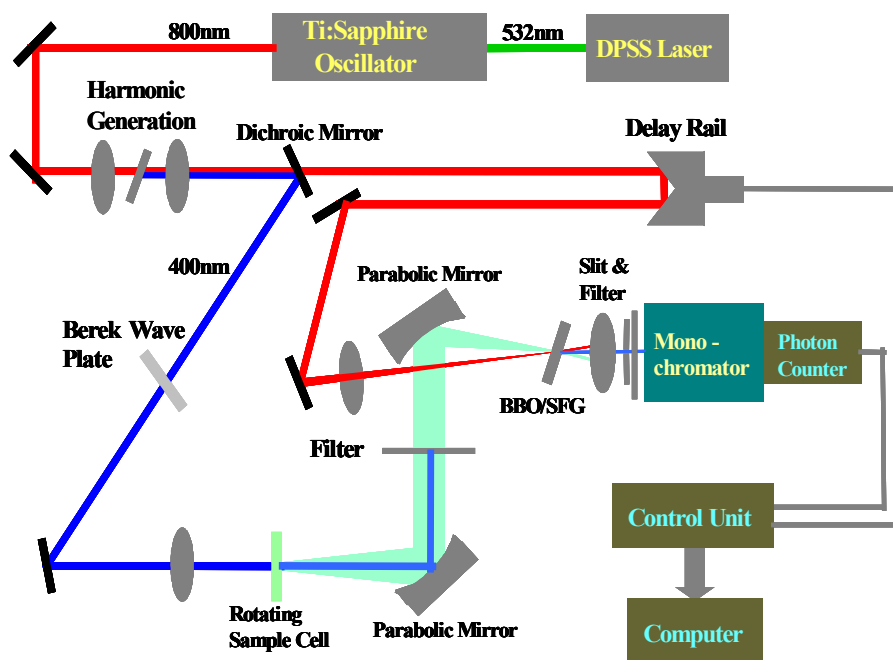


Figure 2.9. The Schematic diagram of the femtosecond fluorescence up-conversion instrument developed in our department.

A translational stage, driven by a stepper motor with a step size of $0.1 \mu\text{m}$, is used to change the delay of the gate pulse. Each step of the translational stage changes the optical path length of the gate pulse by $0.2 \mu\text{m}$, thus delaying the pulse by 0.66 femtosecond per step. The gate

pulse is focused onto the up-conversion crystal using a lens to mix with the fluorescence signal and thus to generate the sum-frequency or the up-converted signal. The upconverted light is focused onto a slit of a double monochromator after passing through a UV band pass filter (UG 11) that eliminates the gate and the unused fluorescence light but transmits the up-converted light. This up-converted light is finally detected by using a photomultiplier tube connected to a photon counting system (CDP Inc. Russia).

A variable wave plate (Berek Compensator) in the path of the excitation beam is used to control the polarization direction of the excitation pulses relative to the horizontally polarized gate pulses. Fluorescence up-conversion measurements are normally carried out under magic angle condition to avoid the rotational depolarization effect of the probe molecules on the observed fluorescence decays. For time-resolved fluorescence anisotropy studies, however, measurement are carried out with suitable polarizations of the excitation beams, adjusted by using the Berek compensator, such that the fluorescence decays corresponding to the parallel and perpendicular polarizations of the excitation pulses with respect to the horizontally polarized gate pulses are collected in the up-conversion setup. The two polarized fluorescence decays thus obtained are used accordingly to estimate the time-dependent anisotropy decay.¹¹⁷

2.6.2.2. Instrument response function

As already discussed, the fluorescence decay profiles of the samples at different wavelengths can be easily measured in the up-conversion instrument by simply setting the monochromator at the selected up-conversion wavelength and suitably tuning the optic axis of the nonlinear BBO crystal for maximum sum-frequency light. The fluorescence decay profiles thus measured for the samples at a given wavelength is a convolution of the sample response with that of the instrument response function (IRF). To extract the true sample response function or the actual fluorescence decay parameters of the sample, the measured fluorescence decay is to be de-convoluted with respect to the instrument response function of the setup. Thus, the

measurement of the IRF of the up-conversion setup is very essential to analyze the observed fluorescence decays, and this can be easily obtained by mixing the residual excitation light that passes through the sample with the gate pulse in the up-conversion crystal and measuring the concerned sum-frequency light, which is commonly referred as the cross-correlation light, by using the time-gated photon counter. The changes in the cross-correlation light intensity with the delay time of the gate pulse can be easily recorded similar to the measurements of the fluorescence decays and the temporal profile thus obtained for the cross-correlation light represents the IRF of the fluorescence up-conversion instrument. A typical IRF of the present setup is shown in Figure 2.10, which is found to be Gaussian in shape. In fact, the solid line in Figure 2.10 represents the actual Gaussian fit to the experimental data shown by symbols. The FWHM of the IRF for the present instrument is found to be ~ 180 fs at the full width at half maximum.

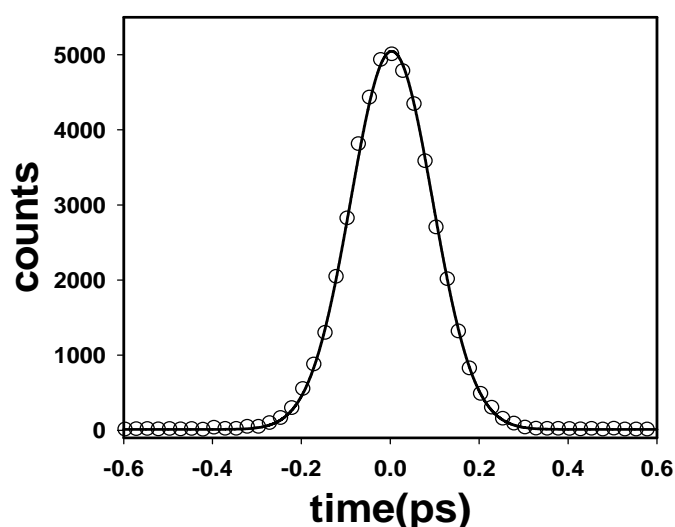


Figure 2.10: A typical instrument response function of the present fluorescence up-conversion instrument measured for 400 nm excitation light. The full-width at half maximum of the instrument response function is ~ 180 fs.

2.7. Cyclic Voltammetry and Differential Pulse Polarography

Cyclic voltammetry is the most widely used technique for acquiring qualitative information about electrochemical reactions. As a major application of this technique, redox potentials of

the electroactive species are determined using cyclic voltammetric measurements. A linear potential perturbation is applied in cycle to the working electrode (*cf.* Figure 2.11A). A typical response of a reversible electrochemical response is shown in Figure 2.11B. The cathodic (E_{pc}) and anodic peak (E_{pa}) potentials are the measure of the reduction and oxidation potential of the electroactive species. Similarly the measured current in the cathodic process and the anodic process are the measure of the electrokinetics of the respective processes. In majority of the cases cyclic voltammetry is used to measure the redox property to understand the electrochemical reactivity of the species in aqueous, non aqueous and in complex biological systems. However in case of lower solubility of the electroactive species in the reaction media, differential pulse polarography is used to obtain the redox property of the system.

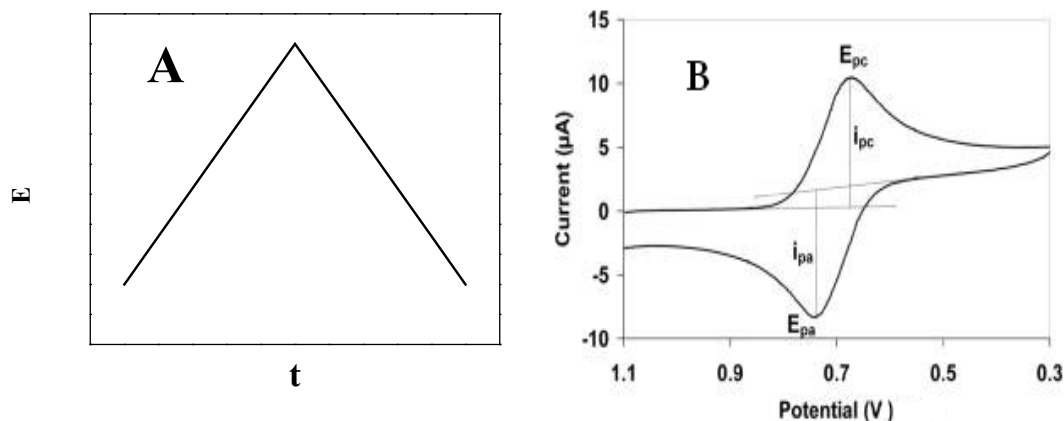


Figure 2.11. (A) Cyclic voltammetric potential profile and (B) a typical cyclic voltammetric plot using glassy carbon electrode.

Differential pulse polarography is one of the best pulsed voltammetric techniques for detection of samples at lower concentration. In this technique square shaped voltage pulses of constant heights is applied along with the DC voltage step. A typical differential pulse profile is shown in Figure 2.12A. As can be seen from this figure, the current is sampled at the beginning of the pulse and at the end of the pulse. The difference in these two currents is plotted against the DC voltage to produce the differential pulse voltammogram as shown in

Figure 2.12B. Such differential current measurement makes the technique less prone to the double layer charging effect.

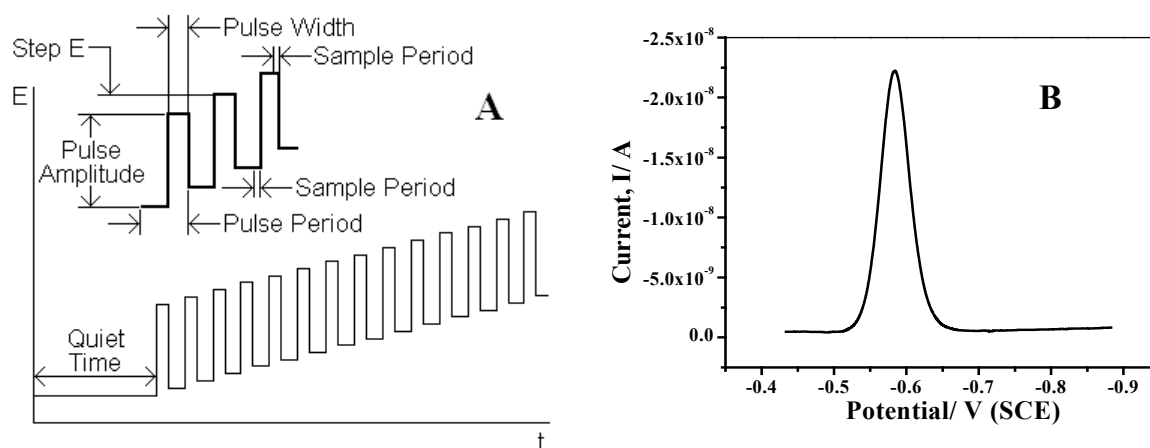


Figure 2.12. (A) Potential profile of differential pulse voltammetry (B) the typical differential pulse voltammetric plot of Cd^{2+} reduction in aqueous solution.

In the present thesis the peak potentials of the coumarin-343 at different surfactant to polymer ratios were measured by using differential pulse polarography using Eco chemie potentiostat, AUTOLAB-100, fitted with the VA663 stand comprising of static mercury drop electrode (SMDE) as the working, glassy carbon rod as the counter and saturated calomel (SCE) as the reference electrodes. Experimental data acquisition was carried out using a GPES-4.9 software. Polarographic scans were carried out for the potential window from -1.0 V to -1.5 V, with the modulated pulse amplitude of 25 mV and step potential of 3 mV. The potentials applied and measured in this report are with respect to SCE. In the present systems 0.1 M KCl was used as the supporting electrolyte and the test solution was purged with high purity nitrogen gas for 15 minutes before every electrochemical scan. Polarographic scans were taken in quiescent condition keeping 10 seconds equilibration times. All electrochemical experiments were carried out at 25⁰C.

2.8. Quantum Chemical Calculations

The ground state geometry optimization was performed using the density functional theory (DFT). Becke's three parameter hybrid exchange function with the Lee-Yang-Parr gradient corrected correlated functional (B3LYP)^{227,228} was used in conjunction with 6-311+G(d,p)

basis set as implemented in the GAUSSIAN-03 software package.²²⁹ Conductor-like polarizable continuum model (CPCM)²³⁰ was used to incorporate the effect of the bulk solvent. TDDFT method using B3LYP/6-311+ G(d,p) basis set was used to calculate the energy in the excited state of the molecules.

2.9. Small Angle Neutron Scattering Measurements

Small Angle Neutron Scattering (SANS) is a technique routinely used for structural studies on the nanometer length scales (1-300 nm). Typical samples consist of macromolecules or colloids in solution and the measurements are performed in situ. The technique provides information on the size and shape of the nanometer size objects in the solution as well as their inter-particle interactions. The neutrons interact with the nuclei in the sample and the interaction depend on the nature of the isotope of the concerned element. Hydrogen and deuterium have very different scattering length and this can be exploited in contrast variation measurements in which it is usual that part of the molecule in the solution is deuterated. It is also usual to change the scattering length density of the solvent by mixing deuterated and protonated solvents. The technique requires a neutron source, i.e. a nuclear reactor or an accelerator based spallation source and therefore the experiments are performed at large scale facilities. In the present thesis to understand the nature of interaction between the block copolymer and cationic surfactant (CTAB), Small Angle Neutron Scattering measurements were carried out with the polymer solution (in D₂O) in the absence and in the presence of CTAB. Neutron scattering measurements were carried out using the facility at DHRUVA reactor, Trombay, INDIA. The mean incident wavelength (λ) of the neutron was 5.2 Å with $\Delta\lambda/\lambda = 15\%$. The scattered neutrons were measured for the scattering vector (q) range of 0.02-0.3 Å⁻¹. The measured SANS data were corrected for the background, the empty cell contribution and the transmission, and were presented on an absolute scale using the standard

protocols.²³¹ Correction due to the instrumental smearing was also taken into account throughout the data analysis.²³¹

The differential scattering cross section per unit volume ($d\Sigma/d\Omega$) of a monodisperse micelle as a function of scattering vector (q) can be expressed as²³²

$$d\Sigma/d\Omega (q) = NF_{\text{mic}}(q)S(q) + B \quad (2.27)$$

where N is the number density of the micelles, B is a constant representing the incoherent background scattering mainly from the hydrogen atoms present in the sample, $F_{\text{mic}}(q)$ is the form factor, determined by the size and the shape of the scatterers, and $S(q)$ is the structure factor, accounting for the inter-particle interaction. Structurally, pluronic micelles can be considered as the core-shell particles with different scattering length densities for the PPO core and the PEO shell. In the present SANS analysis, $F_{\text{mic}}(q)$ was considered for a spherical micelle as formulated by Pedersen,²³³ and it depends on the radius of the hydrophobic micellar core. The structure factor, $S(q)$ is a function of the micellar volume fraction ϕ , which is related to the hard sphere radius (R_{hs}) as^{164,234,235}

$$\phi = \frac{C4\pi R_{\text{hs}}^3}{3N_{\text{agg}}} \quad (2.28)$$

where C is the concentration of the pluronic in w/v % and N_{agg} is the aggregation number, which can be determined from the knowledge of the core size.²³⁶ The analytical form of $S(q)$ factor for the block copolymer micelles was obtained from the analytical solution of the Ornstein-Zernike equation in the Percus-Yevick approximation, employing the hard sphere potential.²³⁷

For polydispersed micelles, eq. 2.27 can be written as

$$\frac{d\Sigma}{d\Omega}(q) = \int \frac{d\Sigma}{d\Omega}(q, R) f(R) dR + B \quad (2.29)$$

In the present study, the polydispersity in the micellar size was accounted by Schultz distribution as given by the following equation,²³⁸

$$f(R) = \left(\frac{z+1}{R_{cm}} \right)^{z+1} R_{cm}^z \exp \left[- \left(\frac{z+1}{R_{cm}} \right) R_{cm} \right] \frac{1}{\Gamma(z+1)} \quad (2.30)$$

where Γ is the gamma function, R_{cm} is the mean core radius of the micelles and the parameter z is a function of the width (ΔR_c) of core radius, defined by the following equation,

$$z = (R_{cm}/\Delta R_c)^2 - 1 \quad (2.31)$$

The mean core radius (R_{cm}), the polydispersity for the core radius ($\Delta R_c/R_{cm}$), the micellar volume fraction (ϕ) and the hard sphere radius (R_{hs}) of the micelles are the fitting parameters in the analysis of the SANS data. Using this analysis, the different micellar parameters has been determined for F88-CTAB mixed micellar system which has been discussed in Chapter 7.

Chapter 3

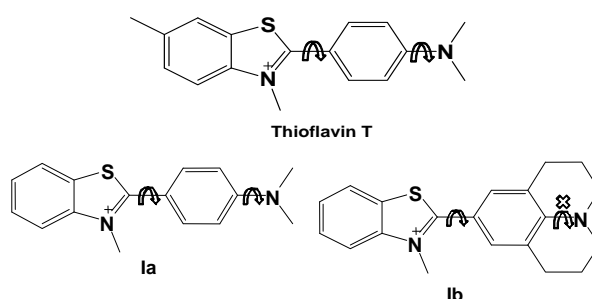
Ultrafast Bond Twisting Dynamics Studies on Amyloid Fibril Sensor Dyes Thioflavin-T and its Derivatives

3.1. Introduction

Thioflavin-T (ThT), a benzothiazole based cationic dye, is used as an extrinsic fluorescence sensor to monitor and estimate the formation of amyloid fibril, a filamentous protein form responsible for several neurodegenerative diseases, like Alzheimer's and Parkinson's disease.¹⁹¹⁻¹⁹⁴ Although ThT in water is very weakly fluorescent,^{195,239} it shows a remarkable enhancement in emission yield on its association with amyloid fibril.^{191-194,196,240,241} ThT is also known to be very specific in its binding with amyloid form of the protein with no significant interaction with other forms, namely, the folded or partially folded monomeric proteins.^{196,242} Although the underlying mechanism for the large fluorescence enhancement of ThT on its association with amyloid fibril is not clear, several hypothesis have been proposed to explain this observation. Khurana et al.²⁴³ have proposed that the formation of a kind of micelle of ThT in the amyloid fibril is mainly responsible for the observed emission enhancement for the dye. Formation of ThT excimer in amyloid fibril has also been proposed by Groenning et al.²⁴⁴ However, such association of charged species is a matter of debate. Recently, an optical microscopic study has however, clearly demonstrated that there is no association of ThT

molecules in amyloid fibril and the observed emission enhancement is due to the incorporation of monomeric ThT molecule within the fibril structure.²⁴⁵

Detailed studies in several confined environments, like in amyloid fibril,^{191,196,241,246-249} polymer,¹⁹⁷ glass matrix,¹⁹⁸ etc., clearly indicate that the high local viscosity of the microenvironment around the dye is directly related to the observed fluorescence enhancement of ThT in these systems. However, understanding the actual molecular process, that is related to the observed fluorescence enhancement of ThT in these microenvironments remains still elusive. Considering the molecular structure of ThT (*cf.* Scheme 3.1), it is hypothesized that in bulk water, due to the low viscosity of the medium, some intramolecular bond twisting process might take place in the excited state of the ThT molecules which effectively introduces a very fast nonradiative decay channel for the excited dye resulting its extremely low fluorescence yield.¹⁹⁰ In contrast, in a highly viscous media, like in amyloid fibril, the bond twisting process in the dye is substantially retarded, reducing the nonradiative decay channel for the dye and hence a remarkable increase in its emission yield.²⁵⁰⁻²⁵² In some reports it is also proposed that the bond twisting process in ThT is associated with the large intramolecular charge transfer from the anilino moiety of the dye to its benzothiazole moiety.^{190,253} Such a charge transfer, associated with the bond twisting in the dye effectively results in the formation of a twisted intramolecular charge transfer (TICT) state in the excited ThT molecules.



Scheme 3.1. Molecular structure of Thioflavin-T and its derivatives

From the molecular structure of ThT (*cf.* Scheme 3.1), it is clearly evident that there are two possible bond twisting, one occurring around C-N single bond (*i.e.* twisting of the amino (NR₂)

group) and/or the other occurring around central C-C single bond (*i.e.* twisting of the anilino (PhNR₂) group) can take place in this molecule. Twisting around any one of these bonds can introduce the nonradiative decay channel in the excited state of ThT, causing a very low emission yield. There are several reports in the literature on organic dyes with N-alkylated anilino groups where it is shown that the twisting of either the N-alkylated amino group or that of the whole anilino group can cause the enhanced nonradiative decay of the excited dye resulting a large reduction in their emission yields. For example, in several tri-phenyl methane dyes with amine substitutions, it is reported that the twisting of the anilino group in their excited state is responsible for their low emission yield.^{254,255} For *para*-(*N,N*-dialkylamino) benzylidenemalononitriles, however, based on experimental evidence as well as from theoretical calculations, it was shown that the twisting of both the amino group as well as the anilino group contribute significantly towards the nonradiative decay channel of this molecule in its excited states.²⁵⁶ Very recently, Saha *et al.*²⁵⁷ have shown that in dimethylaminostyrylbenzothiazole, having a close structural relation with ThT, only the twisting of the amino group is responsible for the fast nonradiative decay in its excited state. Based on these literature reports, it is expected that for ThT, twisting of either of the two bonds, as depicted in Scheme 3.1, can be responsible for the ultrafast nonradiative decay channel in its excited state. In order to use ThT or some of its derivatives as an efficient fluorescence sensor for different microenvironment, including that of amyloid fibril, it is very essential to identify the bond, which is responsible for its ultrafast nonradiative decay channel. This information might also help to develop much better sensor based on the ThT structure. In order to disentangle this issue, we designed and synthesized two ThT derivatives, Ia and Ib (see Scheme 3.1 for molecular structures), with the presumption that the lack of a methyl group in the benzothiazole moiety, as is present in ThT, would not cause any significant effect on the fluorescent properties of the derivatives in comparison to that of ThT. Between the two ThT derivatives synthesized, the compound Ia can have twisting around both the bonds. However, due to the presence of a

julolidine group, compound Ib would prohibit twisting of the Ph-NMe₂ bond, but allow twisting around the central C-C bond (benzothiazole-aniline) only. Detailed steady-state and time-resolved photophysical studies of Ia and Ib along with ThT in different solvents have been carried out to identify the bond responsible for the sensory activity of ThT class of molecules. Detailed excited state dynamics of ThT in amyloid fibril media has also been explored.

Studies on the photophysical properties of ThT in different solvents indicate that its emission yield is largely dependent on the viscosity of the medium.^{250,258} This feature characterizes ThT to act as a molecular rotors, because the changes in its fluorescence yield can be used to estimate the viscosity of different microenvironment. Understanding the effect of viscosity on the relaxation pathways in the excited ThT molecule might help to comprehend the underlying mechanism for the enhancement of the fluorescence emission yield of ThT in different confined media. With this in mind, we have investigated on the excited state relaxation dynamics of ThT in solvents of varying viscosity, using femtosecond fluorescence upconversion technique.

3.2. Experiments and Methods

ThT was purchased from Sigma as the chloride salt and used after repeated recrystallization from methanol. The purity of the recrystallized ThT was checked through NMR spectra.²⁵⁹ All the solvents were of spectroscopic grade (Spectrochem, India) and were used as received. Ground-state absorption measurements were carried out using a Shimadzu spectrophotometer (model UV-160A) and the steady-state fluorescence measurements were made in a Hitachi spectrofluorimeter (model F-4500). The emission spectra were corrected for the wavelength dependent instrument responses as discussed in Chapter 2 (*cf.* Section 2.3.1). The fluorescence quantum yield (ϕ_f) of ThT in different solvents were determined by comparative method (*cf.* Section 2.3.1, Chapter 2) using Coumarin 481 (C481) dye in acetonitrile ($\phi=0.08^{174}$) as the reference. Viscosity of mixed solvent were calculated using the following equation,²⁶⁰

$$\ln(\eta_{mix}) = \sum_i w_i \ln \eta_i \quad (3.1)$$

where η_{mix} is the viscosity of the mixture, η_i and w_i is the viscosity and weighting factor of the i^{th} component, respectively.

Bovine Insulin was purchased from Sigma-Aldrich, USA and was used as received. Bovine insulin is well known to form fibril at low pH and at elevated temperature.²⁶¹ Solutions of bovine insulin (2mg/ml) in 20 % acetic acid was freshly prepared and was incubated at 70^o C for 24 h in a glass vial under stirring. Freshly prepared stock solution of ThT in nanopure water was added to fibrillar solution to make a final concentration of ThT to 5 μ M and was incubated at room temperature for 1 h before final measurement.

Time-resolved fluorescence measurements were carried out using a femtosecond fluorescence upconversion and TCSPC instrument discussed earlier (*cf.* Chapter 2). In the present study the second harmonic of Ti-sapphire laser pulses (410 nm, 50 fs, 88 MHz) was used for the sample excitation in fluorescence upconversion measurement while 405nm LED was used as excitation source in TCSPC instrument. For the construction of the time-resolved emission spectra (TRES), the fluorescence transients were recorded at 10 nm intervals across the steady-state emission spectrum of ThT. All these fluorescence transients were fitted with a tri-exponential function using the iterative convolution method. Time-resolved emission spectra (TRES) were reconstructed using the best fitting parameters of the fluorescence decays measured at different wavelengths following the method proposed by Maroncelli and Fleming.³⁹ In the present study, the experimental data points for the each reconstructed TRES was fitted using the lognormal function of the following form.³⁹

$$I(\nu) = a \exp \left[-\ln(2) \left\{ \frac{1}{b} \ln \left(1 + \frac{2b(\nu - \nu_p)}{w} \right) \right\}^2 \right] \quad \text{if } \frac{2b(\nu - \nu_p)}{w} > -1$$

$$= 0 \quad \text{if } \frac{2b(\nu - \nu_p)}{w} \leq -1 \quad (3.2)$$

where, the amplitude, a , the peak frequency, ν_p , the width parameter, w , and the asymmetry parameter, b , are the adjustable parameters. The full width at half maximum (FWHM) of the

emission spectra were calculated from width parameter, w , and the asymmetry parameter, b , by using the following equation,³⁹

$$FWHM = w \frac{\sinh(b)}{b} \quad (3.3)$$

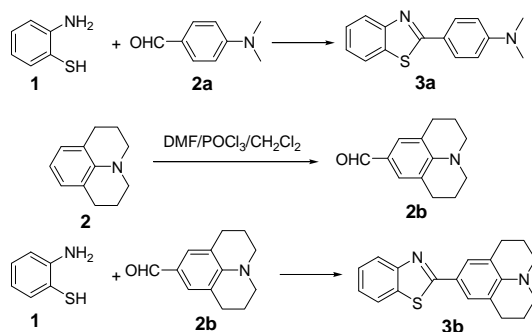
Because of the very long fluorescence lifetime of ThT in amyloid fibril media, time-resolved fluorescence measurement were carried out using a time-correlated single-photon-counting (TCSPC) based instrument from IBH, Glasgow, U.K. ThT in amyloid fibril was excited with a 408-nm diode laser (1 MHz,). The fluorescence from the sample was collected at right angles to the excitation source and detected using a microchannel plate (MCP) detector. The IRF of the TCSPC instrument was measured by collecting the scattered light from a TiO₂ suspension in water and was found to be ~100 ps.

The ground-state geometry optimization of the studied molecules were performed using the density functional theory (DFT) (*cf.* Section 2.7, Chapter 2). The energy of the first excited singlet state (S_1) was determined as the sum of the ground-state (S_0) energy and the transition energy. The energy (expressed in eV) is relative to the minimum of the ground-state energy.

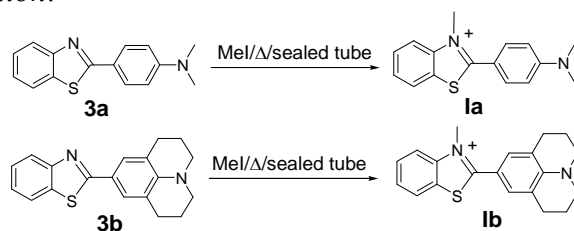
3.2.1. Synthesis of ThT derivatives

All anhydrous reactions were carried out under an argon atmosphere, using freshly dried solvents. The organic extracts were dried over anhydrous Na₂SO₄. The ¹H NMR (200 MHz) spectra were recorded with a Bruker AC-200 spectrometer.

Microwave assisted condensation reaction:



Methylation reaction:



Scheme 3.2: Synthesis of **1a** and **1b**

Synthesis of 9-Formyljulolidine (2b): To a magnetically stirred solution of julolidine (**2**) (0.5 g, 2.88 mmol) and DMF (0.27 mL, 3.46 mmol) in dry CH₂Cl₂ (5 mL) under Ar was injected POCl₃ (0.29 mL, 3.17 mmol). After 1 h, when the substrate was fully consumed (checked through TLC), the mixture was treated with aqueous 2M NaOH solution, and the mixture extracted with Et₂O (3 × 5 mL). The ether layer was washed with water (2×10 mL) and brine (1×5 mL), and dried. Removal of solvent in vacuum followed by column chromatography (silica gel, 0-5% Et₂O/hexane) of the residue furnished pure **2b**. Yield: 90%; ¹H NMR (CDCl₃): δ 1.97-2.06 (m, 4H), 2.81 (t, *J* = 6.2 Hz, 4H), 3.31 (t, *J* = 5.8 Hz, 4H), 7.28 (s, 2H), 9.63 (s, 1H).

Synthesis of 2-(4'-Diaminophenyl)benzothiazole (3a) and julolidinyl benzothiazole (3b): The aldehyde **2a** or **2b** (3 mmol) and 2-aminothiophenol **1** (6.0 mM) in Et₂O (10 mL) and silica gel (3.0 g) were thoroughly mixed to make slurry, and concentrated under vacuum to obtain the respective solid pre-adsorbed materials, which were individually exposed to microwave irradiation (600 W power) for 10 min. The completion of the reaction was checked by taking an aliquot of the sample, extracting with Et₂O and carrying out TLC analysis of the ether extract. The solid was extracted with Et₂O (30 mL), the ether extract concentrated in vacuum, and the residue was column chromatographed (silica gel, 0-15% EtOAc/hexane) to obtain the respective 2-arylbenzothiazoles **3a** and **3b**. **3a**: Yield: 90%; ¹H NMR (CDCl₃): δ 3.05 (s, 6H), 6.74 (d, *J* = 9.0 Hz, 2H), 7.25-7.34 (m, 1H), 7.40-7.48 (m, 1H), 7.84 (d, *J* = 7.8 Hz, 1H), 7.95-8.01 (m, 3H). **3b**: Yield: 68.5%; ¹H NMR (CDCl₃): δ 1.92-2.04 (m, 4H), 2.81 (t, *J* = 6.2 Hz,

4H), 3.26 (t, $J = 5.8$ Hz, 4H), 7.26-7.32 (m, 1H), 7.39-7.46 (m, 1H), 7.59 (s, 2H), 8.03 (d, $J = 8.0$ Hz, 1H), 7.79 (d, $J = 8.0$ Hz, 1H).

Synthesis of the dyes Ia and Ib: A mixture of **3a** or **3b** (each 0.2 g) and MeI (2 equivalent) was heated at 120 °C in a sealed tube for 4 h. The mixture was concentrated in vacuum, and the crude products were washed successively with acetone (3 mL) and Et₂O (3 mL) and recrystallized from ethanol. **Ia:** Yield: 63%; ¹H NMR (DMSO-d₆): δ 3.10 (s, 6H), 4.22 (s, 3H), 6.97 (d, $J = 8.4$ Hz, 2H), 7.75-7.83 (m, 4H), 8.28-8.38 (m, 2H). **Ib:** Yield: (60%); ¹H NMR (DMSO-d₆): δ 1.86-1.91 (m, 4H), 2.72-2.78 (m, 4H), 3.54 (m, 4H), 4.18 (s, 3H), 7.38 (s, 2H), 7.64-7.83 (m, 2H), 8.09-8.12 (m, 1H), 8.26-8.30 (m, 1H).

3.3. Results and Discussion

3.3.1. Ground-state absorption and steady-state fluorescence studies of ThT and its derivatives Ia and Ib

The ground-state absorption and steady-state fluorescence spectra of ThT derivatives Ia and Ib in aqueous solution are shown in Figure 3.1. As indicated in the figure, both absorption and emission spectra of Ib is significantly red shifted with respect to those of Ia. This red shift in absorption and emission spectra of Ib as compared to that of Ia is possibly due to the fact that the difference in the ground and the excited state dipole moment is higher for the former dye as compared to that in the latter. The more polar nature of the dye Ib as compared to that of dye Ia is due to the presence of julolidine group in the former. The red shift in the absorption maxima in dye Ib than that of dye Ia is also supported from the quantum chemical calculations (discussed later). Similar red shifts in the absorption and emission spectra due to the introduction of the julolidine group have also been observed in coumarin derivatives.²⁶² As anticipated, the absorption and the emission spectral characteristics of Ia in water (and also in other solvents) are quite similar to that of ThT (*cf.* Figure 3.1). This clearly supports our assumption on the inconsequential role of the methyl substituent in the benzene ring of the benzothiazole moiety in the photophysical properties of the ThT molecules.

Fluorescence quantum yield (ϕ_f) values measured for both the ThT derivatives in different solvents are listed in Table 3.1. The ϕ_f values of ThT in different solvents are also presented in Table 3.1 for comparison. It is evident from Table 3.1 that the quantum yield of ThT and Ia are quite comparable in all the solvents studied. This result indicates that ThT and its derivative Ia have similar photophysical behavior, which is consistent with our inference from the absorption and emission spectral studies. Henceforth the dye Ia is thus considered as the representative of ThT and its photophysical properties is compared with those of Ib.

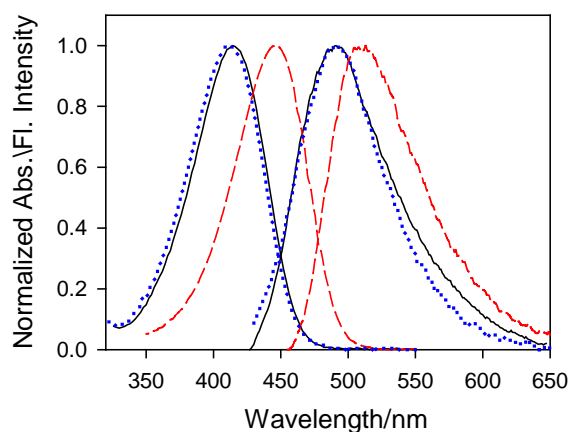


Figure 3.1. Ground-state absorption and steady-state fluorescence spectra of Ia (—) and Ib (- - -) in aqueous solution. Absorption and emission spectra of ThT in water (· · · ·) are also shown for comparison.

Table 3.1. The emission quantum yield (ϕ_f) of ThT, Ia and Ib in different solvents

Solvent	Quantum yield (ϕ_f) $\times 10^4$		
	ThT	Ia	Ib
Water	1.0 \pm 0.2	1.0 \pm 0.2	0.84 \pm 0.2
Acetonitrile	1.4 \pm 0.15	1.45 \pm 0.2	0.84 \pm 0.15
Ethylene Glycol	17.5 \pm 0.5	16.1 \pm 0.4	10.1 \pm 0.5

It is clearly indicated from Table 3.1, the introduction of the julolidine group in Ib that prevents the twisting around the C-N bond, does not cause any appreciable change in the emission yield of the dye as compared to that of Ia and ThT. However, it is seen from Table 3.1 that the ϕ_f of Ib is always relatively low as compared to that of Ia and ThT in all the solvents studied. As reported in the literature, the restriction of the bond rotation in ThT in viscous environment, like in amyloid fibril, is the reason for the large enhancement (~ 1000 times) in the fluorescence yield.^{191,196,241,246-249,258} If the restriction in the rotation around C-N bond was responsible for this sensing activity of ThT, one would expect a large increase in the ϕ_f for Ib in comparison to that of Ia and ThT. Lack of such an observation clearly suggests that the twisting around the C-N bond is not responsible for the sensory activity of ThT and its derivatives. This, in turn, reveals that the twisting around the central C-C single bond (*i.e.* the twisting of the anilino group) must be responsible for the fluorescence sensing activity of ThT dye.

If the sensing activity of ThT is related to the C-C bond twisting process, the emission quantum yield of both Ia and Ib should be highly dependent on the viscosity of the medium. To investigate this aspect, we measured the ϕ_f values of Ia and Ib in different acetonitrile-ethylene glycol solvent mixtures where the viscosity of the medium is changed over a wide range,²⁶⁰ but the polarity of the medium remains almost in the similar range (dielectric constant of acetonitrile and ethylene glycol is ~ 37).²⁶³ As charge transfer (CT) is reported to take place in the excited state of these molecules,¹⁹⁰ to see the viscosity effect the polarity of the medium was needed to maintain at the similar range. To see the fluorescence enhancement at higher viscosity region, the ϕ_f values of the two dyes were also measured in glycerol medium at different temperatures.^{264,265} It is to be mentioned here that for ThT it is reported that its fluorescence quantum yield in solvents with significantly high dielectric constants, like acetonitrile, methanol and water is almost independent of the solvent polarity.¹⁹⁵ In the present study, we also find similar fluorescence quantum yields for Ia and Ib dyes in water and

acetonitrile solvents (*cf* Table 3.1). Thus, it is expected that in this high solvent polarity region the CT mediated non-radiative de-excitation of the excited Ia and Ib molecules is not affected that significantly by the small changes in the solvent polarity. Thus, a marginally higher dielectric constant of glycerol ($\epsilon \sim 42.5$) as compared to that of acetonitrile and ethylene glycol should not affect the fluorescence quantum yield of these dye, rather the viscosity of the solvent will play a significant role in modulating their photophysical behaviour.

The variation in fluorescence quantum yields (relative to that in acetonitrile) of Ia and Ib with the viscosity of the medium is shown in Figure 3.2. It is clearly indicated from the inset of Figure 3.2 that in the low viscosity region (< 20 cP) the fluorescence enhancement due to the increase in the viscosity is very similar for both of the dyes. However, a substantial difference in the fluorescence enhancement is observed in the region of higher solvent viscosity, where the rate of change in the fluorescence quantum yield with the solvent viscosity is relatively higher for Ib, compared to that for Ia. This result clearly demonstrates that the molecule Ib is a relatively better viscosity sensor than molecule Ia.

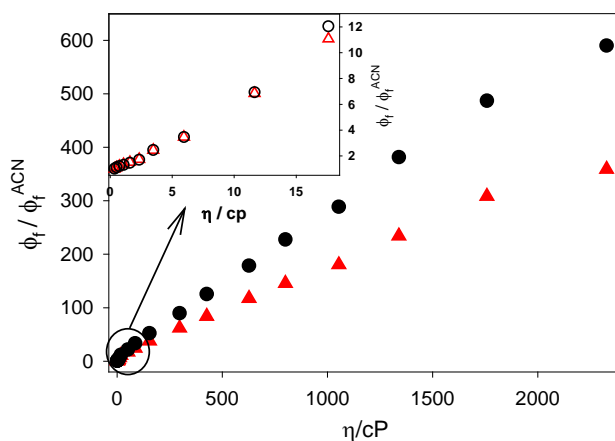


Figure 3.2. Variation of fluorescence quantum yield (relative to that in acetonitrile solvent, ϕ_f^{ACN}) of Ia (Δ) and Ib (O) with the viscosity of the medium. Inset shows the variation in the emission yield for the low solvent viscosity region. Open symbol corresponds to acetonitrile-ethylene glycol mixtures and filled symbol corresponds to glycerol solution with different viscosity.

3.3.2. Time-resolved fluorescence studies of Ia and Ib

The fundamental issue that determines the sensing activity of a dye is the competition between the radiative and nonradiative (due to the bond twisting) decay processes in the excited state of the dye molecules. The fluorescence quantum yield, ϕ_f , of a dye is defined by the following equation.

$$\phi_f = \frac{k_f}{k_f + k_{nr} + k_{nr}^{tor}} = \tau_f k_f \quad (3.4)$$

where k_f is the radiative rate constant, k_{nr} is the nonradiative rate constant for the processes other than bond twisting process, k_{nr}^{tor} is the nonradiative rate constant due to the bond twisting process and $\tau_f (= 1/(k_f + k_{nr} + k_{nr}^{tor}))$ is the excited state lifetime of the dye. In a less viscous solvent, e. g. water, the intramolecular bond twisting process is very fast and thus leads to a higher value for k_{nr}^{tor} , resulting in a very short τ_f value for the present dyes. Because of the very high k_{nr}^{tor} value, ϕ_f is also seen to be very low in low viscosity solvents. However, in highly viscous media, the bond twisting process is retarded significantly, resulting in a lower k_{nr}^{tor} value and subsequently a higher ϕ_f value for the dyes.

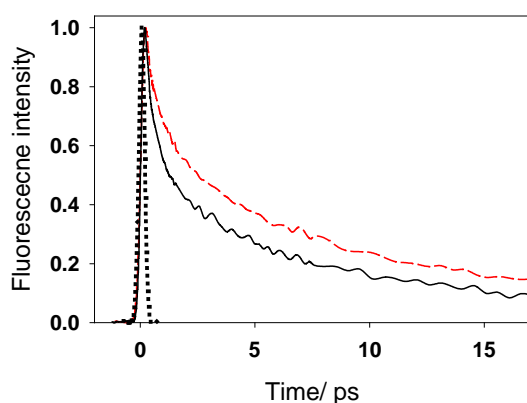


Figure 3.3. Transient fluorescence decays of Ia (---, λ_{ex} = 410 nm, λ_{em} = 490 nm) and Ib (—, λ_{ex} = 420 nm, λ_{em} = 510 nm) in ethylene glycol solution. The instrument response function (IRF) is shown as the dotted curve.

Thus, to understand the differences in the sensing activity of Ia and Ib, time-resolved fluorescence measurements were carried out in different solvents using the fluorescence upconversion technique. Both the dyes show multi-exponential fluorescence decay behavior at their emission maxima in all the solvents studied. Multi-exponential decay kinetics for the barrierless bond twisting process is well known in the literature.^{266,267} The representative fluorescence decays of Ia and Ib in ethylene glycol are shown in Figure 3.3, while their estimated average fluorescence lifetimes in different solvents are presented in Table 3.2. It is evident from Figure 3.3 and Table 3.2 that the average lifetime of Ia is always longer as compared to that of Ib in all the solvents studied. The observed ultrafast decay is known to be due to the torsional motion in the ThT dyes.²³⁹ Thus, the present results clearly indicate that the torsional motion is relatively faster in the dye Ib, compared to that in Ia. Accordingly, the k_{nr}^{tor} value is always higher for Ib as compared to that of Ia irrespective of the solvents used. Because of the larger value of k_{nr}^{tor} and hence, shorter value of τ_f , the increase in fluorescence yield due to an increase in the solvent viscosity is expected to be relatively higher for dye Ib than Ia, as observed experimentally in the present study.

Table 3.2. Average excited state lifetime of Ia and Ib in different solvents

Solvent	Fluorescence lifetime, (ps)	
	Ia	Ib
Water	0.59	0.48
Acetonitrile	0.41	0.30
Ethylene Glycol	12.4	11.8

3.3.3. Quantum chemical calculations for Ia and Ib

To understand the reason behind the faster bond twisting dynamics in Ib as compared to that in Ia, detailed quantum chemical calculations were carried out. The structures of both the molecules were optimized, and the optimized structures are shown in Figure 3.4. From the

optimized structures, it is evident that both the molecules are non-planar in nature, with the benzothiazole moiety of the molecules undergoing a twist of about 40° for Ia and about 36° for Ib, with respect to the plane of anilino moiety. Vertical transition energies were also calculated for the optimized geometry for these two molecules and are found to be ~ 3.055 eV (406 nm) and 2.893 eV (428 nm) for Ia and Ib, respectively. These values correspond reasonably well with the experimentally observed absorption maxima (412 nm and 440 nm for Ia and Ib respectively) of the two molecules.

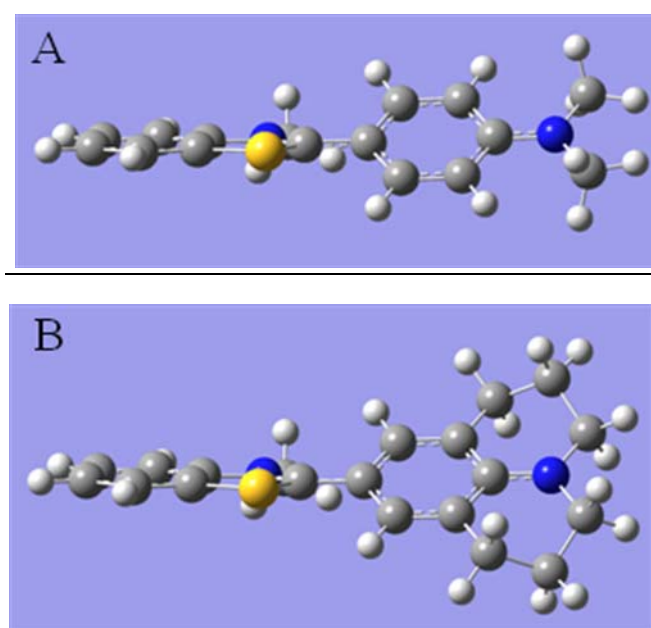


Figure 3.4. The optimized chemical structures of Ia (A) and Ib (B).

To understand how the dihedral angle (θ_B) between the benzothiazole and the anilino moieties affect the potential energy surface of the two molecules, both ground and excited state potential energies were calculated at different values of θ_B and are plotted as a function of the twist angle in Figure 3.5. It is evident from Figure 3.5 that for both the dyes, the locally excited state (with $\theta_B=36^\circ$ for Ia and 40° for Ib) produced due to photoexcitation, is not energetically minimum in the potential energy surface. Thus, both the molecules undergo bond twisting around the C-C single bond between the benzothiazole and the anilino moiety to attain a θ_B

value of $\sim 90^\circ$ in their excited state to attain the minimum in the potential energy surface. This feature is qualitatively very similar to that obtained for the ThT molecules in the gas phase.¹⁹⁰

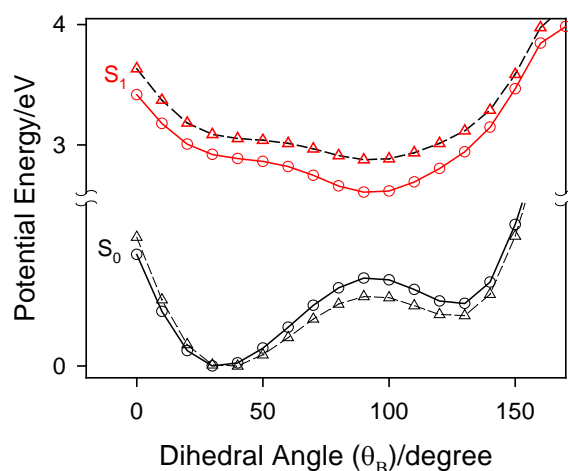


Figure 3.5. Variation in the potential energy of Ia (Δ) and Ib (O) with the dihedral angle, θ_B , in their ground (S_0) and the first excited state (S_1). The energy is relative to the minimum of the ground-state energy.

Although the qualitative nature of the potential energy surfaces of Ia and Ib are very similar, there are distinct quantitative differences between them. These quantitative differences in the potential energy surfaces of Ia and Ib can explain the observed differences in the excited state dynamics of these two molecules. It is to be noted from the Figure 3.5 that the energy stabilization due to bond twisting process in the excited state is relatively higher for the dye Ib than Ia, suggesting the twisting process occurs faster in the former molecule than the latter. Further, the excited state potential energy surface in the region of $\theta_B = 40-90^\circ$ is relatively steeper for Ib as compared to that of Ia. This feature also suggests a faster bond twisting process in the dye Ib as compared to that of Ia. In addition, it is also evident from the Figure 3.5 that the energy gap between the S_1 and S_0 states in the twisted configuration (*i.e.* $\theta_B = 90^\circ$) is relatively less for Ib as compared to that in Ia. This lower energy gap between the S_1 and the S_0 state also causes the nonradiative process to be more efficient in Ib than in Ia. Thus, because of all the above factors, the fluorescence lifetime of Ib is expected to be shorter as compared to that of Ia, as observed experimentally. Therefore, the results of the quantum chemical calculation is in good agreement with the observed experimental results and supports the role

of the bond twisting process around the central C-C single bond to cause the extremely low fluorescence quantum yield of the ThT and its derivatives.

3.3.4. Time-resolved fluorescence studies of ThT in aqueous solution

The fluorescence decays of ThT in water were recorded at different emission wavelengths and are shown in Figure 3.6. At emission maxima (490 nm), the decay is very fast and follows a non-exponential function. Following a multi-exponential fitting, the average lifetime was calculated and is found to be ~ 1 ps (*cf.* equation 2.17, Chapter 2). As indicated from this figure, the decays are also found to be strongly dependent on the monitoring wavelengths. Thus, a fast decay is observed at the blue edge and a fast growth followed by a relatively slow decay is observed at the red edge of the emission spectrum. It is further observed that the transient decays at the blue edge of the spectrum (below the emission peak at 490 nm) are independent of the excitation wavelength (*cf.* inset of Figure 3.6). This suggests that there is no major contribution of the vibrational relaxation in the observed fluorescence decays. We thus infer that the wavelength dependent changes in the fluorescence decays might be due to either solvent relaxation dynamics or an ultrafast intramolecular process takes place in the excited dye molecule.

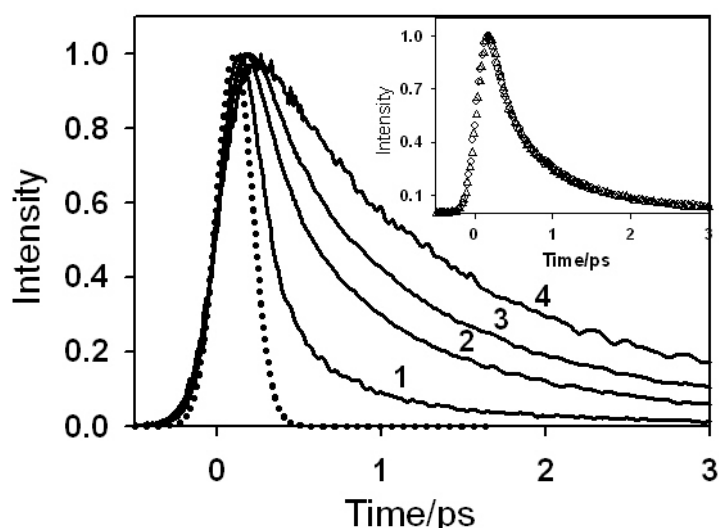


Figure 3.6. The fluorescence decay profile for ThT in aqueous solution at different emission wavelengths: (1) 440 nm, (2) 490nm, (3) 530 nm and (4) 590 nm. Instrument response function (IRF) is also shown (.....). Inset: The fluorescence decay profile at 460 nm for ThT in aqueous solution at different excitation wavelengths: (O) 390 nm, (Δ) 430nm.

To explore the photoinduced processes further in the present systems, the wavelength dependent fluorescence decays were used to construct time-resolved emission spectra (TRES) following the standard procedure reported by Maroncelli et. al.³⁹ The TRES thus obtained for ThT dye in water are shown in Figure 3.7 after normalization to the same peak intensity. It is seen from this figure that there is a gradual red shift in the emission spectra with time. Such dynamic Stokes' shift are often associated with solvent relaxation dynamics around the excited fluorophore. For the present system, however, it is indicated from the following considerations that the solvent relaxation process is not the main reason for the observed changes in the TRES. In the case of solvent relaxation, the TRES should show dynamic Stokes' shift without any appreciable reduction in the fluorescence intensity because excited state population does not change due to solvent relaxation process. For the present system, however, in contrary to the above expectation, there is a substantial decrease in the excited state population within the small experimental time span (upto 2 ps) following photoexcitation. This is clearly indicated by the plot of the integrated area under the emission spectra with time, shown in the inset of Figure 3.7, where the initial intensity decreases by ~90% of its initial value within the time span of ~ 2 ps following photoexcitation. Such an observation clearly suggests that the observed dynamics Stokes' shift in the present case is not related to the solvent relaxation process. Absence of any significant effect of solvent relaxation in the present system is also suggested by the fact that the peak position of the steady-state emission spectra of ThT is almost similar in a nonpolar (chloroform, $\epsilon=4.8$) and in a highly polar (water, $\epsilon=78.5$) solvent. The lack of any significant solvatochromism in the steady-state emission spectra clearly indicates that the dynamic stokes' shift observed for ThT is not due to the solvent relaxation process.

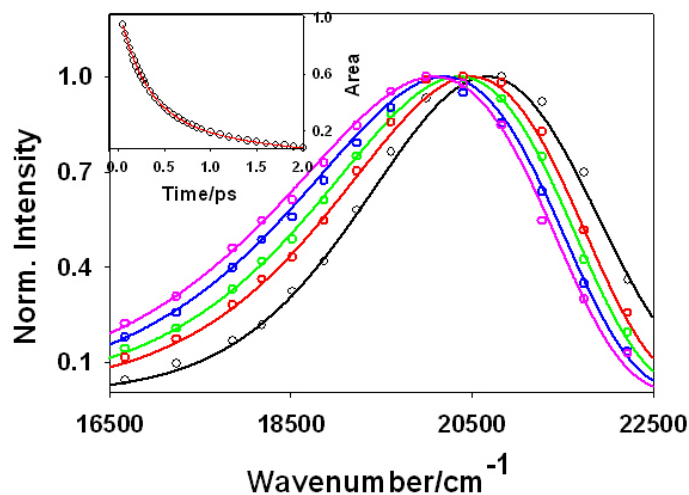


Figure 3.7. Time-resolved emission spectra (TRES) of ThT in water at different time following photexcitation. Inset shows the variation in the integrated area under the emission spectra with time.

A critical inspection of the TRES in Figure 3.7 indicates that along with the frequency shift there is also a significant spectral broadening with time. It is seen that the spectral broadening primarily occurs at the red edge of the spectra, while the shape at the blue edge effectively remains unchanged. These changes in the spectral shape is also corroborated by the changes in the asymmetry parameter (b), obtained from fitting the experimental data in the TRES with a lognormal function. Thus, the asymmetry parameter is seen to change from -0.18 at 50 fs to -0.41 at 2ps. Time dependent changes in the peak frequency of the emission spectra are shown in Figure 3.8. About 600 cm^{-1} Stokes' shift is observed within 2 ps time span following photoexcitation. Changes in the peak frequency with time are seen to follow an exponential kinetics with a time constant of $\sim 575 \pm 25$ fs. The changes in the spectral width (FWHM) with time are also presented in Figure 3.8. Interestingly, the width of the spectra shows a very fast growth, with time constant, very similar ($\sim 560 \pm 30$ fs) to that observed for the change in the peak frequency. These results thus suggest that the same photoinduced process is responsible for both the observed dynamic Stokes' shift and the changes in the spectral shape with time.

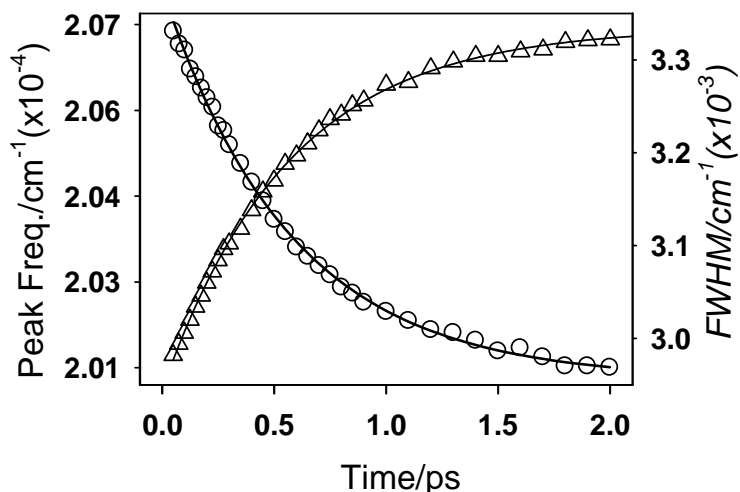


Figure 3.8: Variation in the peak frequency (O) and the width (FWHM, Δ) of the emission spectrum with time.

To get more insight of the present system, we also constructed the time-resolved area normalized emission spectra (TRANES),^{268,269} as are shown in Figure 3.9. The appearance of an isoemissive point in TRANES is clearly indicated in Figure 3.9 and such an observation suggests the presence of two emissive species in the system.^{268,269} We propose that following photoexcitation, the local excited (LE) state of ThT molecule undergoes an ultrafast intramolecular twisting process with a time constant of ~ 570 fs to generate a new emissive species in the system. To be mentioned here that similar observations have also been made earlier for hemicyanine²⁷⁰ and benzothiazole dyes²⁷¹ and explained on the basis of the formation of a new twisted emissive species from the local excited state of the dyes.

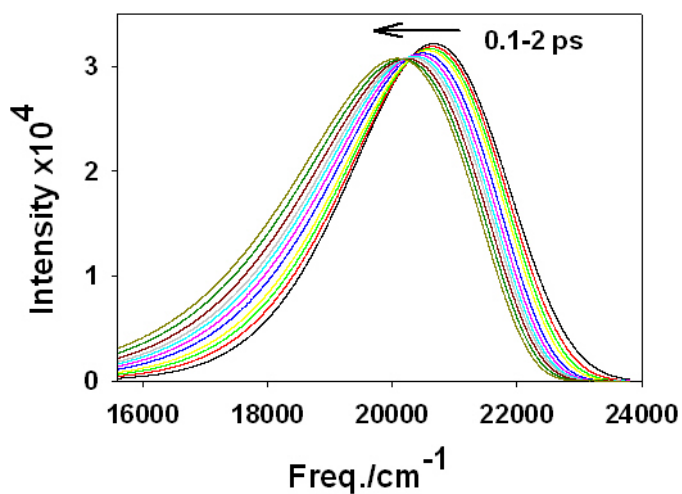


Figure 3.9. TRANES of ThT in water at different times (0.1 to 2 ps).

Dynamic Stokes' shift associated with the formation of twisted conformer in the excited state is also reported for several other dyes.^{272,273} Thus our proposition of the formation of a twisted emissive state for ThT is in accordance with these literature reports. It is interesting to note here that, in the literature, it is suggested that the twisted configuration in the excited state of ThT is non-emissive in nature.²⁷⁴ Our results, however, clearly suggest that the twisted configuration of ThT is in fact emissive in nature, though its emission yield could be much lower than that of the LE state, as indicated by the very fast decay of the integrated fluorescence intensity with time for the TRES (*cf.* inset of Figure 3.7) and also supported by the very low value of oscillator strength in the twisted configuration (*cf.* Figure 3.12B, discussed in the next section). The proposition of the involvement of a twisted configuration of the ThT in the excited state is further supported by the fact that the fluorescence quantum yield of ThT is highly dependent on the viscosity of the medium.^{239,253} It is suggested that the ultrafast bond twisting process introduces an efficient nonradiative decay channel for the excited ThT molecules resulting a very low fluorescence quantum yield for the dye in water as well as in other less viscous solvents. Similar reduction in the emission yield due to the formation of twisted configuration in the excited state is well known for several other dyes.^{16,20,272,275,276}

3.3.5. Quantum Chemical Calculations for ThT

To further support our proposition of the bond twisting process, we carried out a detailed quantum chemical calculations. The ground-state optimized geometry of ThT molecule in water is shown in Figure 3.10. It is evident from Figure 3.10 that the ThT molecule in its ground-state is in a twisted configuration. Thus, the plane containing the benzothiazole ring makes an angle (θ_B) of $\sim 39^\circ$ with respect to the plane containing the dimethylanilino ring. This partially twisted configuration of ThT is in agreement with the results reported in the literature.^{277,278}

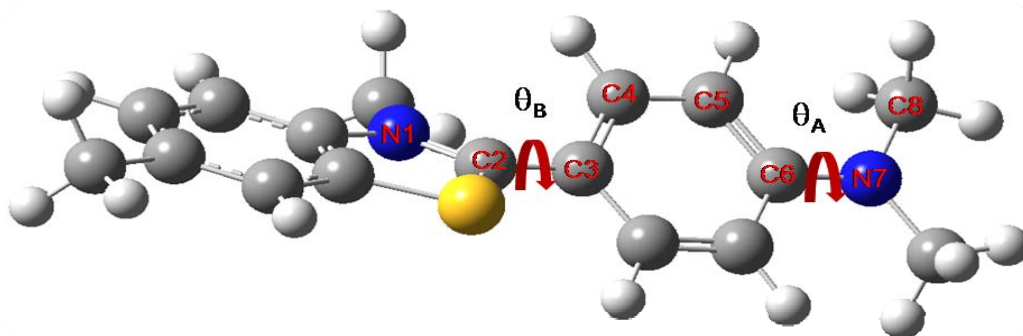


Figure 3.10. The ground-state optimized geometry for the ThT in water.

The potential energy surface for both ground and excited states of ThT were calculated as a function of the dihedral angle for both central C-C and terminal C-N single bonds (θ_A and θ_B ; *cf.* Figure 3.10). Figure 3.11 shows the variations in the potential energies for both ground and excited state of ThT in water as a function of the dihedral angle θ_A . It is evident from the optimized structure of ThT (*cf.* Figure 3.10) and also from Figure 3.11 that in the ground-state the dihedral angle between the dimethylamino group and the benzene ring (θ_A) is zero i.e. the two groups are in same plane. The excited state potential energy surface indicates that the configurations with $\theta_A=0^\circ$ and 90° are of comparable energy but separated by a reasonably high energy barrier (~ 0.29 eV).

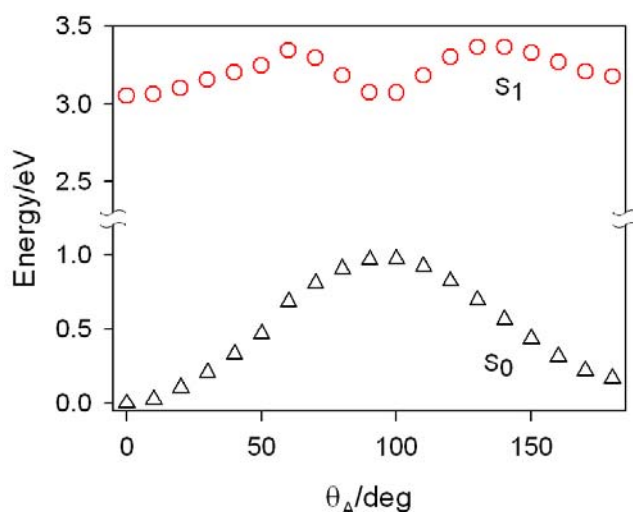


Figure 3.11. Potential energies of ThT in the ground (S_0) and the excited (S_1) states as a function of the dihedral angle θ_A . The energy (expressed in eV) is relative to the minimum of the ground-state energy.

Hence, the interconversion between the configurations with $\theta_A=0^\circ$ and 90° is highly unlikely in the excited state of the dye. These results thus suggest that the twisting around the C-N single bond in the excited state of ThT is not feasible, which is in line with our observation and discussion presented in the previous section (*cf.* Section 3.3.3)

Ground and excited state potential energy surfaces were also calculated as a function of the dihedral angle θ_B and the results are shown in Figure 3.12A. It is evident from Figure 3.12A, that the LE state (with $\theta_B=39^\circ$) has only a quasi minimum and the most stable configuration in the excited state is the fully twisted configuration with $\theta_B=90^\circ$. Thus, it can be inferred that following photoexcitation the ThT molecule undergoes a twisting around the C-C single bond to attain the fully twisted configuration (with $\theta_B=90^\circ$). It is also important to note from Figure 3.12A that the transition from the LE state to twisted state is a barrierless process. Due to this barrierless nature of the twisting process it is expected to occur in an ultrafast time scale as observed experimentally (*cf.* Figure 3.8). Thus, the results from quantum chemical calculations directly support our results from femtosecond fluorescence upconversion studies and suggest that ultrafast process in the excited state of the ThT occurs due to the twisting around the C-C single bond (θ_B) joining the benzothiazole moiety and dimethylanilino ring of the molecule. Figure 3.12B shows the variation in the oscillator strength for the transition between the excited state and the ground-state for ThT as a function of dihedral angle θ_B . From this figure it is seen that there is a substantial decrease in the radiative rate while the molecule undergoes twist around the C-C bond. For example the oscillator strength decreases from 1.1 at $\theta_B=39^\circ$ to 0.01 at $\theta_B=90^\circ$. This result clearly indicates that the twisted state is very weakly emissive as compared to that of the LE state. This result is also supported from the experimental observation that there is substantial reduction in the emission intensity during the twisting process.

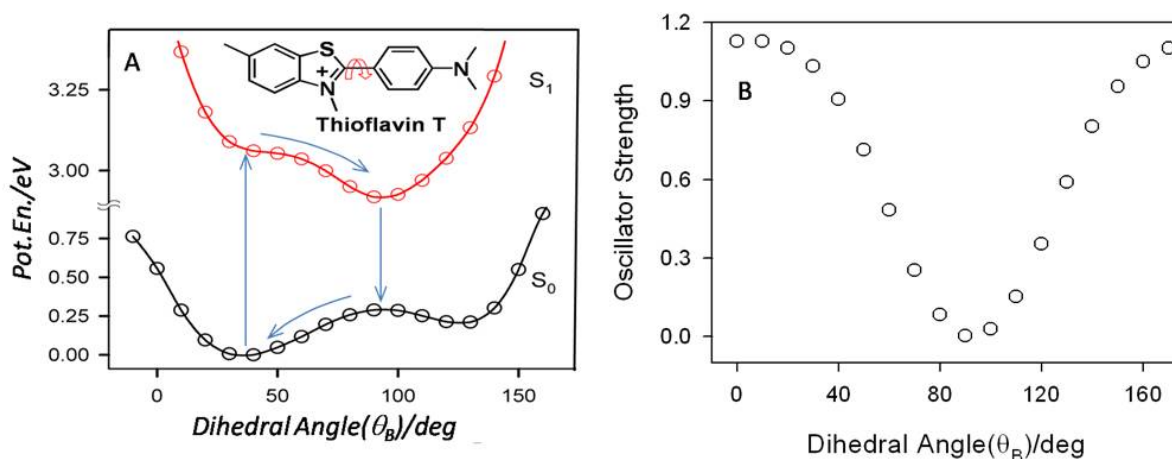


Figure 3.12: (A) Ground-state and excited-state potential energy of ThT as a function of dihedral angle θ_B . (B) Variation in the oscillator strength with the dihedral angle θ_B for the S_0 - S_1 transition of ThT in aqueous solution.

3.3.6. Studies on the Viscosity Effect of the Solvent upon the Bond Twisting Dynamics of ThT

3.3.6.1. Steady-state fluorescence studies

As discussed in Section 3.1, ThT has the characteristics of molecular rotor such that the viscosity of the surrounding environment has a pronounced effect on the fluorescence quantum yield (ϕ_f) of the dye. In the present study effect of solvent viscosity of the photophysical properties of ThT has been investigated in detail using acetonitrile (ACN)-ethylene glycol (EG) solvent mixtures for which viscosity changes systematically but the polarity remains quite similar. Figure 3.13A shows the changes in the emission spectra of ThT in different ACN-EG solvent mixtures. As indicated from this figure, the emission intensity increases gradually with an increase in the EG percentage in the solvent mixture. The ϕ_f values of ThT in these solvent mixtures were estimated using a comparative method and values are presented in Table 3.3 along with the viscosity of the solvent mixtures. The variation in ϕ_f values with the viscosity of the medium are shown in Figure 3.13B. It is evident from this figure that with an increase in the viscosity the ϕ_f of ThT increases gradually. The increase in the ϕ_f value with the increasing viscosity of the medium is suggestive of the diffusive torsional motion in the excited

state of ThT molecule to cause a fast nonradiative deexcitation in low viscosity solvents resulting a very low fluorescence quantum yield of the dye.^{253,279}

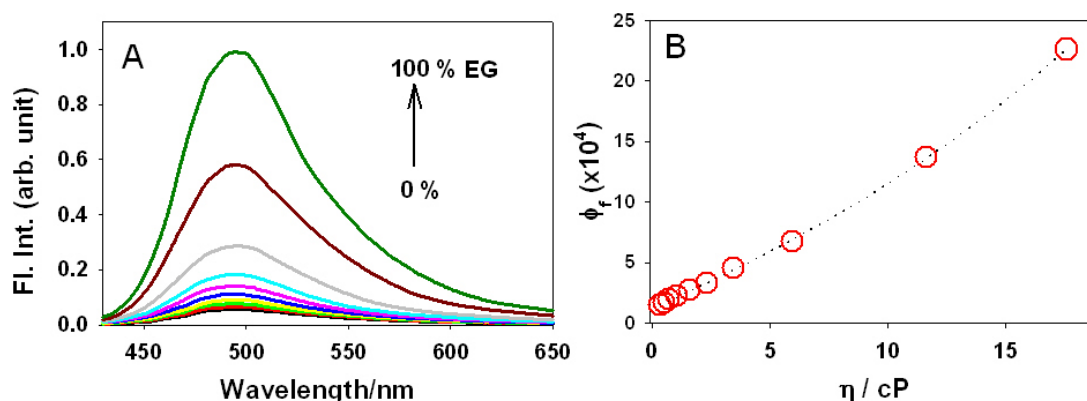


Figure 3.13. (A) Changes in the emission spectra of ThT in ACN-EG solvent mixtures. (B) Changes in emission quantum yield (ϕ_f) of ThT with the increasing viscosity of the ACN-EG solvent mixtures.

3.3.6.2. Time-resolved fluorescence measurements

Fluorescence decays of ThT were measured at the emission peak (490 nm) in ACN, EG, as well as in ACN-EG solvent mixtures. Fluorescence decay traces for different solvent mixtures using fluorescence upconversion measurements are shown in Figure 3.14A. The excited state decay of ThT in ACN is seen to be very fast. As mentioned earlier, the ultrafast decay in the excited state of ThT is due to the ultrafast torsional motion around the central C-C single bond.^{190,239} All the decays are seen to follow a non-exponential kinetics. The decay traces were fitted with a tri-exponential function and the average lifetimes were calculated using the fitted decay parameters (*cf.* equation 2.17, Chapter 2). The average lifetime of ThT in ACN is found to be 0.61 ps. It is evident from Figure 3.14A that as we increase the viscosity of the medium, the excited state decay becomes slower. Thus, the average lifetime of ThT in EG is found to be 17.64 ps, which is much larger as compared to that in ACN. The average excited state lifetime of ThT in different solvent mixtures are presented in Table 3.3 and its variation with the viscosity of the medium is shown in Figure 3.14B. This result suggests that the frictional force, which increases with an increase in the viscosity of the medium, causes a retardation in the nonradiative deexcitation channel caused by the torsional motion in the excited ThT molecule.

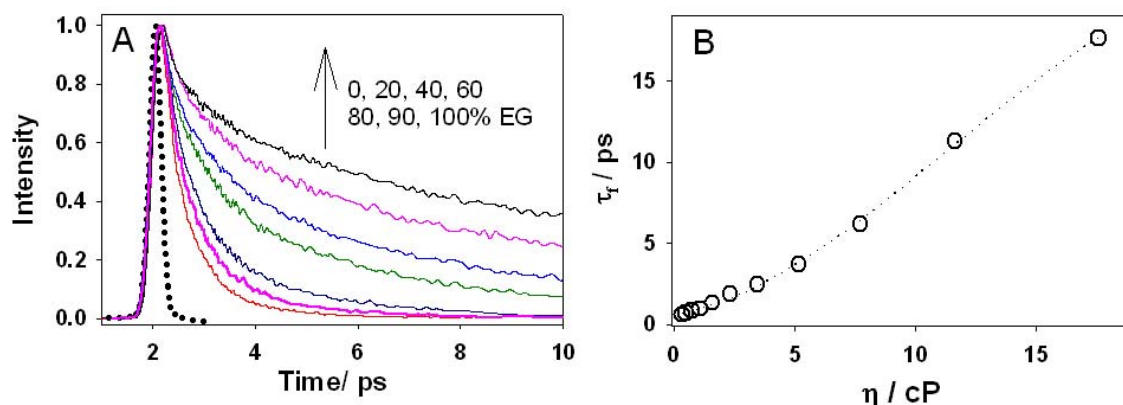


Figure 3.14. (A) Fluorescence transients at 490 nm (emission peak) for ThT in different ACN-EG solvent mixtures. The dotted line shows the IRF. (.....). (B) Variation in fluorescence lifetime of ThT with the viscosity of the solvent medium.

Table 3.3. Quantum yield and average lifetimes of Thioflavin-T in different acetonitrile–ethylene glycol solvent mixtures of varying viscosity.

% of ethylene glycol	Viscosity (η) / cp	Quantum Yield (ϕ) $\times 10^4$	Avg. lifetime (τ_f) / (ps)
0	0.35	1.42	0.61
10	0.51	1.66	0.71
20	0.74	1.91	0.86
30	1.08	2.22	1.00
40	1.59	2.66	1.36
50	2.34	3.32	1.88
60	3.47	4.53	2.48
75	5.95	6.73	4.81
90	11.64	13.65	11.30
100	17.60	22.59	17.64

This result is in line with the measurement of the ϕ_f of ThT as described in the previous section. Detail time-resolved studies were carried out for ThT in ACN to gain insight of the ultrafast fluorescence decay dynamics in the excited state. For this purpose, fluorescence transient decays at different emission wavelengths were collected for the dye in ACN and are

presented in Figure 3.15. It is evident from Figure 3.15 that the fluorescence decays are strongly dependent on the emission wavelength. At the blue edge of the emission spectrum, the transient decay has a very fast decay time component, which increases with an increase in the monitoring wavelength.

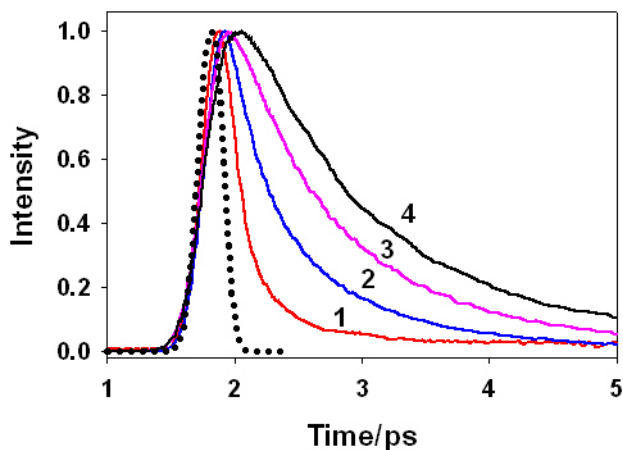


Figure 3.15. Fluorescence transient decays of ThT in ACN at different emission wavelengths: (1) 440nm, (2) 490 nm, (3) 550 nm and (4) 600 nm. The dotted line shows the IRF.

The TRES obtained for ThT in ACN are shown in Figure 3.16A after intensity normalization. It is evident from Figure 3.16A that with time the emission spectra slowly shift towards the lower frequency. A dynamic Stokes' shifts of $\sim 750\text{ cm}^{-1}$ have been observed in ACN within a span of 2 ps following photoexcitation. The inset of Figure 3.16A shows the variation in the integrated area under the emission curve at different time. From this figure it is very evident that the dynamics Stokes' shift in the present case is strongly associated with a large decrease in the emission intensity. In the present case the initial intensity is found to decrease by $\sim 93\%$ only within 2 ps following excitation. This large reduction in the emission intensity clearly indicates that the observed dynamic Stokes' shift is not due to the solvent relaxation process, as discussed earlier in section 3.3.4 for the dye solution in water. Non-exponential and wavelength dependent emission decay behavior are previously reported for compounds that undergo barrierless intramolecular relaxation including bond-twisting, cis-trans isomerization etc. in the excited state.^{266,280-285} Thus, drawing an analogy with the previous reports, we

propose that the observed dynamics Stokes' shift for ThT in ACN is mainly due to an intramolecular relaxation process that takes place in the excited state of the dye.

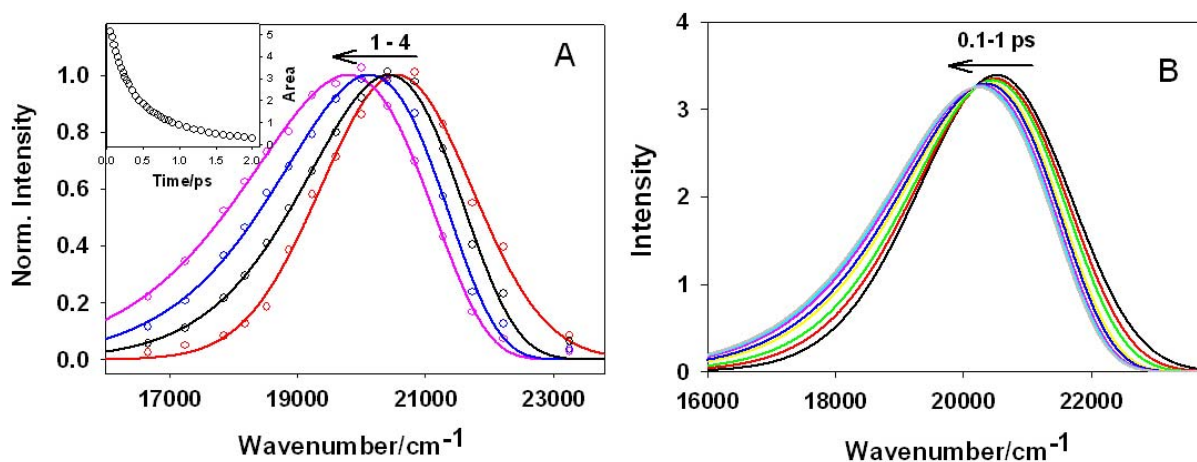


Figure 3.16. (A) Normalized time-resolved emission spectra (TRES) of ThT in ACN at (1) 0.05 ps, (2) 0.15 ps, (3) 0.4 ps, (4) 2 ps. The circles are the experimental data points and the solid lines are the lognormal fits to the data points. Inset: Variation in integrated area under the emission spectra with time. (B) Time-resolved area normalized emission spectra (TRANES) of ThT in ACN.

It is evident from Figure 3.16A that along with the changes in the spectral position there is also distinct broadening in the emission spectra with time. In the present case, the asymmetry parameter (b in eqn. 3.4) is seen to change from -0.11 at 100 fs to -0.39 at 2 ps. Similar asymmetric spectral change at the red side of the emission spectra has also been observed earlier for photoactive yellow protein.²⁸¹ From the time-resolved area normalized emission spectra (TRANES) shown in Figure 3.16B, it is evident that there is also a clear isoemissive point for the ThT dye in ACN solution.

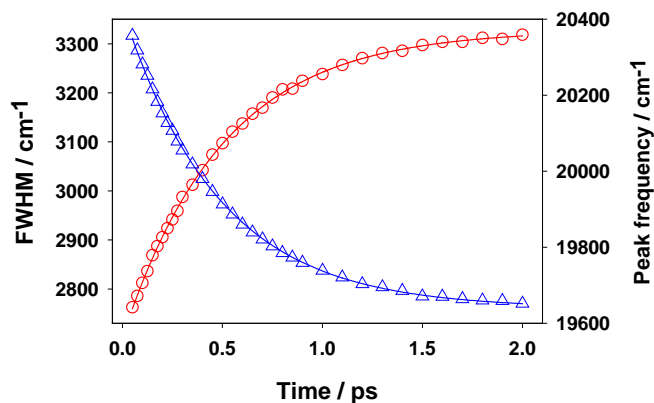


Figure 3.17. Variation in the FWHM (○) and peak frequency (Δ) of ThT emission spectra in ACN with time.

The variation of peak frequency with time for the TRES of ThT dye in ACN is presented in Figure 3.17. Variation in the peak frequency is seen to follow an exponential kinetics with a time constant of 490 ± 35 fs. The change in the spectral width (FWHM) with time is also presented in Figure 3.17. It is evident that the width of the emission spectra shows a very fast growth and also follows an exponential kinetics with time constant of 500 ± 40 fs. These two comparable time constants for the changes in the peak frequency and the spectral width clearly indicate that the same intramolecular process in the excited ThT is responsible for the observed dynamic Stokes' shift as well as the changes in the spectral width. A similar observation has also been made earlier in section 3.3.4 for ThT in water solution.

Present results clearly indicate that the observed dynamics Stokes' shift in ThT molecule in ACN solution is not due to the solvent relaxation process. If the observed dynamic Stokes' shift would have been due to the solvent relaxation, the shape of the spectra, in general, was expected to remain unchanged. Observed results thus clearly indicate that some intramolecular ultrafast relaxation process is taking place in ThT which is responsible for the time-dependent changes in the spectral characteristics. The appearance of an isoemissive point in the TRANES and the gradual increase in the FWHM of the emission spectra is indicative of the fact that there is a formation of a new emissive species in the excited state of ThT. Similar changes in the peak frequency and the width of the emission spectra were also seen for ThT in aqueous solution (*cf.* Section 3.3.4). Further, such changes in the peak frequency and the spectral width are reported in the literature for those molecules where the bond twisting takes place in the excited state.^{270,282} The increase in the width of the spectra has been explained on the basis of the formation of emissive TICT state for these molecules. By drawing an analogy, we also propose that in the present case, the ThT molecule undergoes an ultrafast bond twisting process following its photoexcitation. Detail quantum chemical calculations show that there is a decrease in the radiative rate while the molecule undergoes twists around the C-C single bond.²⁷⁹ Due to this decrease in the radiative rate in the TICT state, as compared to the local

excited (LE) state, a large drop in the emission intensity is observed due to the bond twisting process in ThT.

The formation of an emissive TICT in the excited state of ThT is a consequence of bond twisting process and hence provides a unique opportunity to directly observe the formation of TICT from the LE state and also to estimate the TICT formation constant. Hence, it is interesting to see how the conversion of the LE to the TICT state is affected by the viscosity of the solvent medium. To address this inquisitiveness we carried out detailed time-resolved fluorescence studies in neat EG and in a ACN-EG solvent mixture. These results are discussed in the following subsections.

Time-resolved fluorescence studies of ThT in Ethylene Glycol: Fluorescence decays for ThT in EG at different emission wavelengths are shown in Figure 3.18. It is seen from this figure that similar to the observation in ACN, the fluorescence decay of ThT in EG also depends on the monitoring wavelength. However, on comparison of Figure 3.15 and Figure 3.18, it is indicated that the fluorescence decay in EG is much slower as compared to that in ACN for all the monitoring wavelengths. The TRES constructed from the wavelength dependent decay traces in EG are presented in Figure 3.19A. It is seen that that the transient emission spectra slowly shift towards the lower frequency with time. Qualitatively, the spectral features of the transient emission spectra in EG are very similar to that in ACN except that the decrease in the integrated emission intensity of the emission spectra is found to be much slower in EG as compared to that in ACN. The changes in the integrated emission intensity with time are shown in the inset of Figure 3.19A. Thus, the integrated emission intensity decreases from its initial value by ~55% within the time span of 2 ps, while the corresponding decrease in ACN was about 93%. The decrease of emission intensity by 55% in 2 ps time is also a considerably larger reduction. We thus infer that the observed dynamic spectral shift for ThT in EG is not due to the solvent relaxation process but due to the intramolecular twisting process.

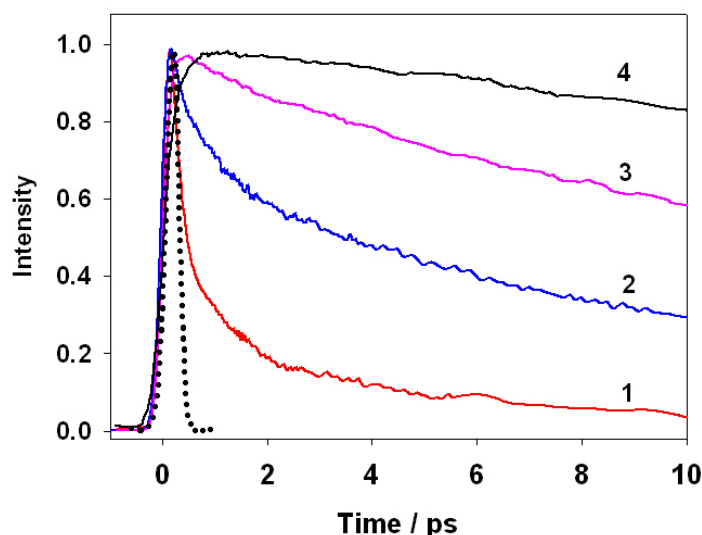


Figure 3.18. Fluorescence transients of ThT in EG at different emission wavelengths: (1) 440nm, (2) 490 nm, (3) 550 nm, (4) 600 nm. The dotted line shows the IRF.

TRANES constructed for ThT in EG, as shown in Figure 3.19B, also possess an isoemissive point similar to that in ACN solution. Thus, the present results also indicate the presence of two emissive species for ThT in EG solution. By drawing an analogy with the results in ACN, we propose that in EG also ThT undergoes a bond twisting process in the excited state to form the TICT state, which is weakly emissive in nature. To estimate the time constant for the LE to TICT conversion, the changes in the spectral width with time were calculated from TRES and are presented in Figure 3.20. It is evident from this figure that the width (FWHM) of the spectra of ThT in EG gradually increases with time. It is found that the spectral width variation follows a single exponential kinetics with a time constant of 1.8 ps. This time constant for the conversion of the LE to TICT state in EG is thus much longer than that observed in ACN solution (~ 0.5 ps). The increase in the time constant for the LE to TICT conversion in EG is due to much higher viscosity of EG ($\eta=17.6$ cp) than that of ACN ($\eta=0.35$ cp). Due to the higher viscosity, the bond twisting process becomes much retarded in EG than in ACN. These results clearly support our proposition that the changes in the spectral width are due to the bond twisting process in the excited state of ThT molecule.

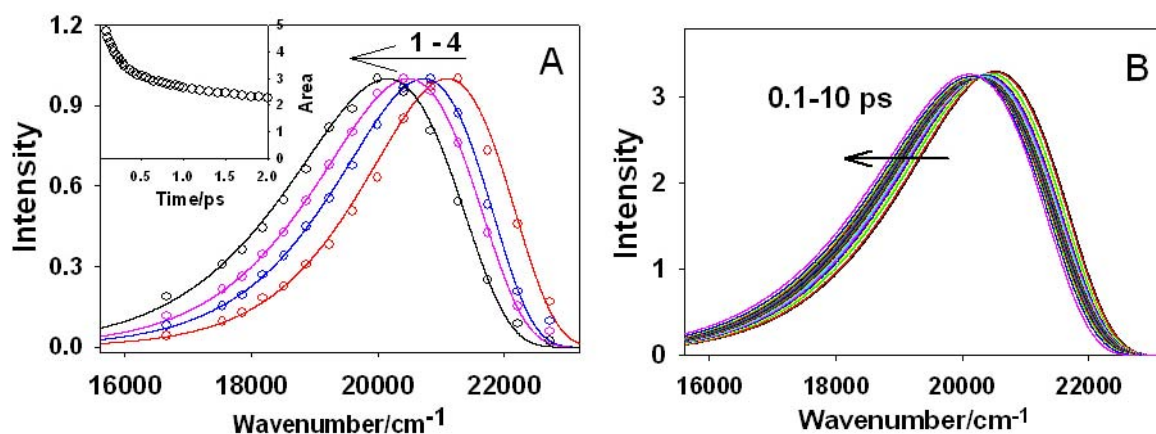


Figure 3.19. (A) Normalized time-resolved emission spectra (TRES) of ThT in EG at different times: (1) 0.1 ps, (2) 0.5 ps, (3) 3 ps and (4) 10 ps. The circles are the experimental data points and the solid lines are the lognormal fits to the data points. Inset: Variation in the area under the emission spectra with time. (B) Time-resolved area normalized emission spectra (TRANES) for ThT in EG.

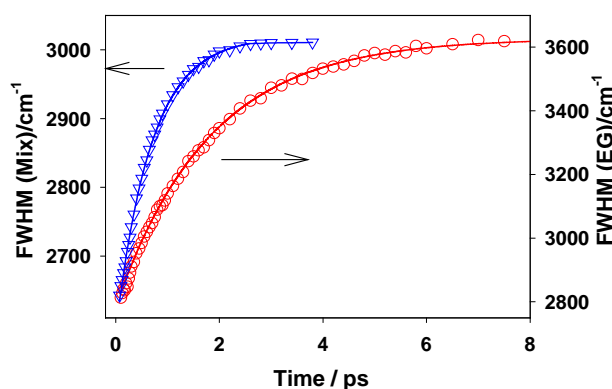


Figure 3.20. Variation in the FWHM of TRES with time in EG (○) and in 3:2 ACN-EG solvent mixture (Δ).

Time-resolved fluorescence studies of ThT in ACN-EG Mixture: To see the effect on the bond twisting dynamics of ThT molecule at an intermediate viscosity, the time-resolved emission studies were carried out in an ACN-EG (3:2 v/v) solvent mixture. The TRES and TRANES constructed from the wavelength dependent decay traces for ThT in ACN-EG solvent mixture are shown in Figure 3.21. It is evident from Figure 3.21A that similar to that in ACN and EG solvent, a dynamics Stokes' shift is evident in ACN-EG mixed solvent also. Thus, Stokes' shift of $\sim 780 \text{ cm}^{-1}$ has been observed in ACN-EG mixture within a time span of 2 ps following photoexcitation. The integrated emission intensity was found to decrease from its initial value by $\sim 83\%$ within the 2 ps time span (*cf.* inset of Figure 3.21A). It is also to be noted from Figure 3.21B that similar to ACN and EG solution, the TRANES in ACN-EG

mixture also shows an isoemissive point. Thus, in line with the proposition made earlier, bond twisting results in the formation of the emissive TICT state in ACN-EG solvent mixture.

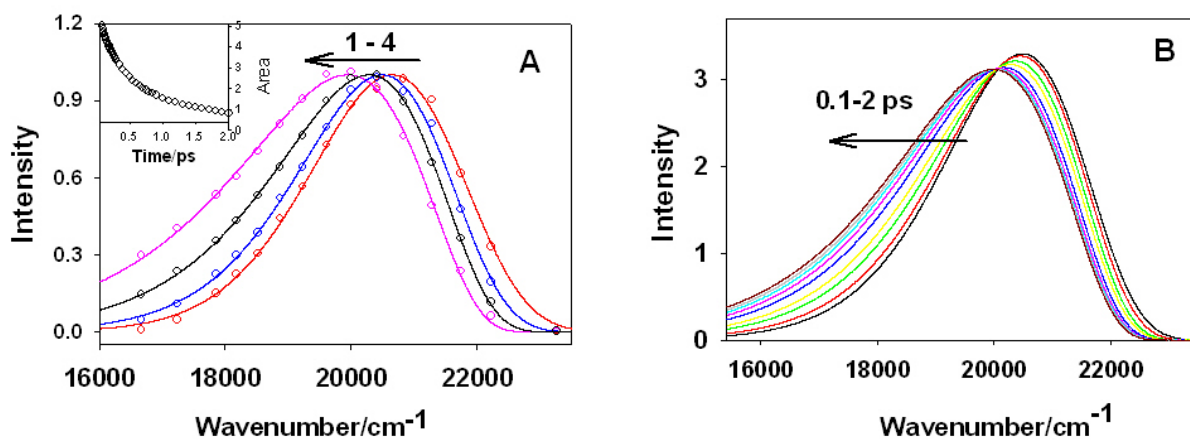


Figure 3.21. (A) Normalized time-resolved emission spectra (TRES) for ThT in ACN-EG solvent mixture at different time (1) 0.1 ps, (2) 0.2 ps, (3) 0.4 ps and (4) 2 ps. The circles are the experimental data points and the solid lines are the lognormal fits to the data points. Inset: Variation in the integrated area under the emission spectra with time. (B) Time-resolved area normalized emission spectra (TRANES) of ThT in 3:2 ACN-EG solvent mixture.

However, due to the lower viscosity of the ACN-EG solvent mixture as compared to that of EG, the bond twisting process is relatively faster in the present case as compared to that in EG. This is also supported from the rate of change in the spectral width with time. Figure 3.20 shows the plot of FWHM vs. time for ACN-EG solvent mixture along with that observed in EG. The variation in FWHM in ACN-EG mixture also follows a single exponential kinetics with a time constant of 0.7 ps, which is much lower compared to that in EG (1.8 ps) but significantly higher than that in ACN. The time constant for the LE to TICT state conversion in all the solvents studied are presented in Table 3.4. It is evident from Table 3.4 that an increase in the viscosity significantly slows down the formation of the TICT state from the LE state of ThT.

Present time-resolved fluorescence studies in different solvents of varying viscosity clearly indicate that the ThT molecule undergoes bond twisting process following photoexcitation, resulting in the formation of the TICT state, which is weakly emissive in

nature. The emissive nature of the TICT state is further confirmed from the changes in the shape of the emission spectra in solvents with different viscosities. The steady-state emission spectra of ThT in ACN, EG and highly viscous glycerol solvent are shown in Figure 3.22 after intensity normalization at the peak position. It is clearly evident from Figure 3.22 that as the viscosity of the medium is increased there is a spectral narrowing, specially at the red edge of the emission spectra. This result clearly indicates that as the viscosity of the solvent increases the contribution of the TICT state, which emits at the red edge of the observed emission spectra, also decreases concomitantly, causing a spectral narrowing at the red edge of the observed emission spectra. Thus, we can infer from the present study that the rotational motions of the anilino and the benzothiazole moiety around the central C-C single bond play an important role in the relaxation of the excited state of ThT molecule. As the viscosity increases, torsional motion in the ThT molecule gets retarded. This retardation in the bond rotation affects the LE to TICT conversion, as manifested by slower increase in the spectral width and the slower dynamic Stokes' shift. The decrease in the integrated emission intensity with time also follows the expected trend with the changing viscosity of the solvent media.

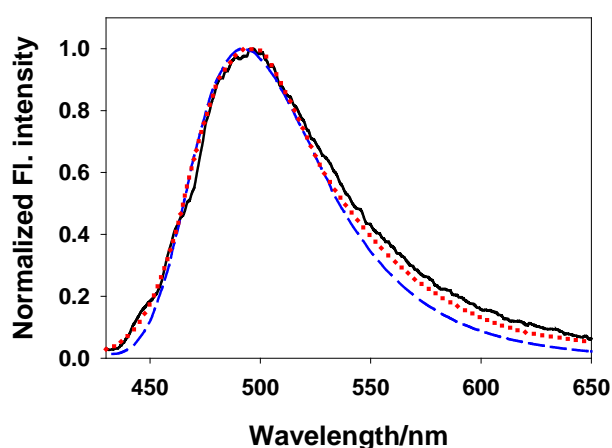


Figure 3.22. Normalized steady-state emission spectra of ThT in three different solvents: Acetonitrile (—), ethylene glycol (·····) and glycerol (- - - - -)

Table 3.4. Time constants for the conversion of the LE to the TICT state of ThT in different solvents.

Solvent	Viscosity (η) / cp	Time constant (fs)
ACN	0.35	490
ACN-EG (3:2)	1.59	700
EG	17.6	1800

3.3.7. Excited-State Dynamics of ThT in Amyloid Fibril

To understand the fate of the observed ultrafast bond twisting process in ThT molecule inside amyloid fibril, detailed time-resolved emission studies have been carried out in insulin fibril. Figure 3.23A shows the enhancement in the emission of ThT due to its incorporation in the amyloid fibril media. A large enhancement (~ 160 times) in the emission in the presence of fibrillar media indicates the incorporation of the dye inside the amyloid fibril. Fluorescence decay traces for ThT in amyloid fibril at different emission wavelengths were recorded and are shown in the Figure 3.23B. For comparison the emission decay trace for ThT in bulk water measured at 490 nm by TCSPC instruments is also shown in Figure 3.23B. It is evident from the Figure 3.23B that the lifetime of ThT in aqueous solution is instrument limited. It is further to be noted from Figure 3.23B that the emission lifetime of ThT has significantly increased due to its incorporation inside the amyloid fibril. Thus, the average emission lifetime measured in amyloid fibril is found to be 1.3 ns, which is around three order of magnitude higher as compared to that in the bulk water (~ 1 ps). The increase in the emission lifetime of ThT is also substantiated by the large enhancement in the emission intensity in amyloid fibril as compared to that in bulk water (*cf.* Figure 3.23A). Comparing the emission lifetime of ThT in bulk water and that in amyloid fibril it can be inferred that the bond twisting process in the excited state of ThT molecule is substantially retarded due to its incorporation in the latter media. Further, it is to be noted from Figure 3.23B that in contrary to that in bulk water, the emission decay is

found to be, almost independent of the interrogated emission wavelength. This result thus indicates the absence of any considerable extent of bond twisting process in the excited state of ThT in amyloid fibril.

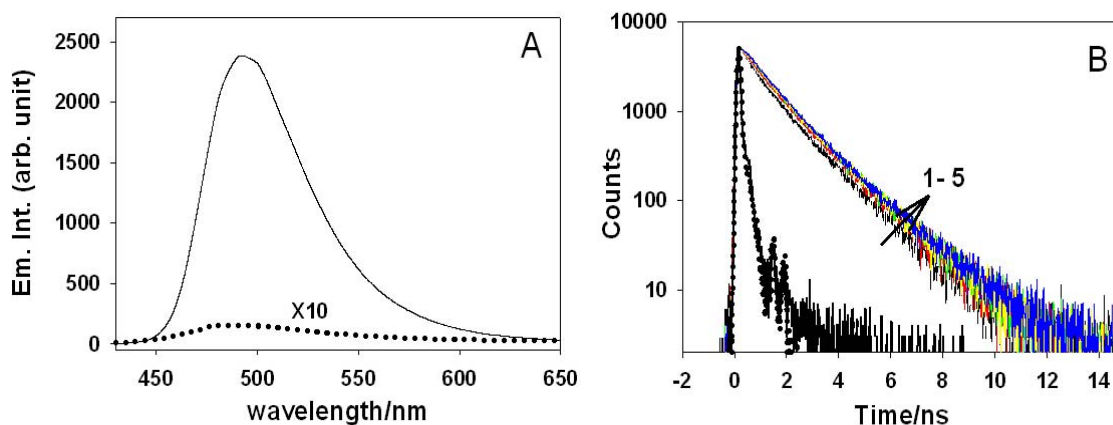


Figure 3.23: (A) Steady-state emission spectrum of ThT in aqueous solution (.....) and in insulin amyloid fibril (—). (B) Emission decay traces for ThT in amyloid fibril at different emission wavelengths (1) 450, (2) 480, (3) 500, (4) 550 and (5) 600 nm. The decay trace at 490 nm for ThT in aqueous solution (—) is also shown for comparison. The IRF is shown by the black dotted curve.

TRES generated from the wavelength dependent decay traces for ThT in amyloid fibril is shown in Figure 3.24A after intensity normalization. It is clearly indicated from this figure that unlike in bulk water, there is merely any dynamic Stokes' shift present in the amyloid fibril. Further, the shape of the emission spectrum is seen to be invariable with time. Because of this fact the width of the emission spectrum is also found to be independent of time. Thus, the absence of dynamics Stokes' shift and the absence of any variation in the spectral shape (i.e. width of the spectra) clearly indicates that unlike in bulk water, the bond twisting process is largely retarded in the amyloid fibril. TRANES for ThT in amyloid fibril is also shown in the Figure 3.24B. It is evident from Figure 3.24B (*cf.* inset of Figure 3.24B), that there is no isoemissive point indicated in the present case. Absence of such isoemissive point suggests that ThT do not form any twisted state, a weakly emissive state, when it is incorporated in the amyloid fibril medium. Thus, the present results clearly demonstrate that the bond twisting process in the excited state of ThT molecule gets substantially retarded in amyloid fibril due to the very high microviscosity around the probe.

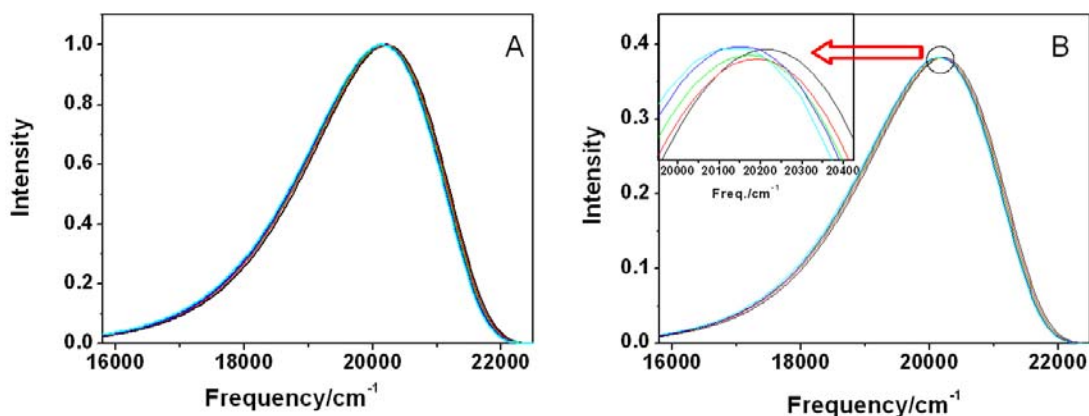


Figure 3.24: (A) Intensity normalized TRES and (B) TRANES for ThT in amyloid fibril at different time (0.1, 0.3, 1, 2, and 6 ns).

3.4. Conclusions

In conclusion, from detail photophysical studies of two newly synthesized ThT derivatives, it is inferred that the C-N single bond twisting is not responsible for the sensing activity of ThT and its derivatives. The twisting around the central C-C single bond between the benzothiazole and the anilino moieties appears to be mainly responsible for the observed fluorescence sensing activity of these dyes. Detail viscosity dependent studies show that the dye Ib with a julolidine substituent acts as a better viscosity sensor than dye Ia (*cf.* Scheme 3.1). The better sensing activity of Ib as compared to Ia, is found to be due to the faster nonradiative decay rate in the excited state of the former as compared to that of the latter. The faster nonradiative process in Ib is also predicted by the quantum chemical calculations. For the first time we show from experimental results that the barrierless bond twisting process in ThT takes place in the sub-picosecond time scale (570 fs in water). Another important finding from the present result is that the TICT state of ThT is weakly emissive in nature. Wavelength dependent decay kinetics has been observed for ThT in all the solvents studied. From detailed analysis of the time-resolved data it is shown that the observed dynamic Stokes' shift and the increase in the spectral width with time is associated with the formation of the TICT state from the LE state of ThT molecule. Presence of any effect of solvent relaxation process on the observed excited

state dynamics has been discarded on the basis of the large reduction in the integrated emission intensity within the experimental time window. The effect of viscosity on the LE to TICT conversion has been explored in detail. It is seen that the increase in the viscosity of the medium slows down the LE to TICT conversion. In amyloid fibril media, the bond twisting process was found to be largely retarded leading to negligible dynamic Stokes' shift and disappearance of isoemissive point in the TRANES. The fundamental information obtained in the present study on the bond twisting dynamics of ThT is very useful to understand its fluorescence sensor activity in different restricted media. It is expected that the information obtained in the present study will help in the development of a better fluorescence sensors based on the ThT chromophore.

Chapter 4

Ultrafast Bond Twisting Dynamics of Thioflavin-T in Nanoconfined Water Pools

4.1. Introduction

The presence of a highly anisotropic interface separating the polar aqueous part from the nonpolar oil region is the key microstructural feature common to various membrane mimetic supramolecular aggregates such as micelles, reverse micelles, microemulsions and vesicles. These supramolecular systems have attracted significant attention of the researchers for quite long primarily because of their resemblance to biomembranes and their catalytic properties in chemical and enzymatic reactions. These systems bear the molecular heterogeneity owing to the amphiphilic nature of the surfactant molecules which form the interface between the water and the nonaqueous solvent. Understanding the interaction of charged molecules with lipid interfaces is important in biology, chemistry and other applied areas. Because most lipids are charged, interaction of a charged species with the lipid surface depends at least in part on the Coulombic interaction. Several models have been used for the characterization of lipid interfaces including simple systems such as reverse micelles and liposomes.^{52,56}

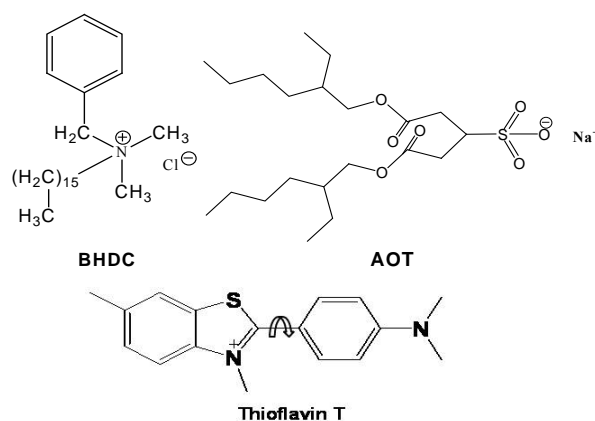
Reverse micelles (RM) are the self-assembled lipid structures that form in nonpolar media.^{48,49,56,286,287} At the appropriate concentrations, surfactant molecules demarcate polar solvent pools (mostly water) from nonpolar solvent region. It is well known that the structure,

dynamics and physicochemical properties of water molecules confined in a nanometer sized space of RMs are substantially different from those of the bulk water. Water molecules at the interfacial region of the RM are quite immobilized due to their involvement in the hydration of the surfactant head groups and are commonly known as the bound water.⁴⁸ On the other hand, the water molecules at the core of the water pool behave quite similar to the bulk water and are known as the free water. Interestingly, the size of the water pool in the most RMs can be changed systematically in a controlled manner just by changing the water to surfactant molar ratio ($w_0 = [\text{H}_2\text{O}]/[\text{surfactant}]$). For spherical RMs, w_0 is known to be directly proportional to the micellar radius.⁴⁸ It is evident that the water/AOT/oil RM is very useful to provide nanometer size confined water pools and has been extensively studied as a model system to mimic the water in biological systems, like water in proteins, in bio-membranes, etc, to understand the chemical and biological processes in such confined environment.

Among others the anionic surfactants, aerosol-OT (AOT; sodium 1,4-bis-2-ethylhexylsulfosuccinate), is known to be the best to form stable RMs in different nonpolar media. AOT has a well-known V-shaped molecular geometry and it forms stable RMs in the absence of any cosurfactant. In addition, it has the ability to solubilize a large amount of water with w_0 values as large as 40 to 60 depending upon the surrounding nonpolar medium, and the temperature. However, the water pool size in the RM depends mainly only on w_0 .^{48,52,288}

In the previous chapter we have discussed on the ultrafast bond twisting process in excited Thioflavin-T (ThT) molecule which is strongly dependent on the the viscosity of the solvent medium. Retardation in the bond-twisting process in ThT is also believed to be responsible for amyloid fibril sensing activity of the dye. Therefore, understanding the ultrafast dynamics in ThT molecule under different restricted environments is very essential to reveal the underlying mechanism for the large fluorescence enhancement of ThT in amyloid fibril. In the present study, we have investigated the confinement effect of AOT RMs on the ultrafast

torsional dynamics of the photoexcited ThT molecules. Rate constants for the torsional motion of the dye have been estimated from the femtosecond fluorescence upconversion measurements and the results have been correlated with the properties of the water pools in the RMs. Further to understand the effect of the head group charge of the surfactants on the localization site of ThT in the RMs, we have extended our study to a cationic RM formed by Benzyl hexadecyl dimethyl ammonium chloride (BHDC) in benzene.



Scheme 4.1. Molecular structure of the chemicals

4.2. Experiments and Methods

The source and purification of Thioflavin T (ThT) is already discussed in Chapter 3. AOT was obtained from Sigma-Aldrich and purified by boiling its methanolic solution with activated charcoal. Charcoal was removed by hot filtration and AOT was recovered by removing methanol under vacuum. Because of the hygroscopic nature of AOT, its water content was determined through the Karl-Fischer titration method. The sample had a [water]/[AOT] molar ratio of 0.67 very similar to the value reported earlier.^{289,290} BHDC was purchased from sigma and was used as received. Heptane and benzene was purchased from Spectrochem (India) and was freshly distilled before use. Nano pure water (conductivity less than $0.1 \mu\text{S cm}^{-1}$) was obtained from Millipore Milli Q system. The surfactant concentration was kept at 0.2 mol dm^{-3} throughout the present study. Water was systematically added to the surfactant solution in

heptane and benzene to prepare the RM with appropriate w_o value. Concentration of ThT was kept very low ($\sim 10\mu\text{M}$) so that the possibility of having more than one ThT molecule per reverse micelle is negligible. The instrument used for ground-state absorption, fluorescence and ultrafast fluorescence and anisotropy decays are discussed in chapter2. The fluorescence quantum yield of ThT in AOT reverse micelles were determined by comparative method (*cf.* Section 2.3.1, Chapter 2) using Coumarin 481 (C481) dye in acetonitrile ($\phi=0.08^{174}$) as the reference.

Time-resolved fluorescence measurements were carried out using a femtosecond fluorescence upconversion instrument (FOG 100, CDP Inc. Russia) which has been described in detail in Chapter 2. For transient depolarization measurements, samples were excited with vertically and horizontally polarized excitation laser pulses using different angles for Berek compensator. In the present setup, since the horizontally polarized gate pulse is mixed with the fluorescence light, the measured sum frequency signal for horizontally polarized excitation measures I_p and that for vertically polarized excitation measures I_{\perp} . Accordingly, fluorescence anisotropy decay $r(t)$ was calculated as²⁰¹

$$r(t) = \{I_p(t) - I_{\perp}(t)\} / \{I_p(t) + 2I_{\perp}(t)\}. \quad (4.1)$$

The measured decay traces were fitted with a multi-exponential function using the standard convolute-and-compare nonlinear least square procedure.²⁰⁶ Emission from ThT was monitored at the peak position of its emission spectrum, 490 nm. Each decay was collected at least for two times to see the reproducibility of the measurements.

4.3. Results and Discussion

4.3.1. Ground-state absorption and steady-state emission studies

The ground-state absorption spectra of ThT were recorded in the confined water pool of AOT reverse micelles in heptanes and are shown in the Figure 4.1A. The absorption spectrum of ThT in bulk water is also shown in Figure 4.1A for comparison. The absorption maximum of

ThT in water is at ~ 411 nm. This is in good agreement with the reported results.^{195,198,258} It is to be noted that due to its confinement in AOT reverse micelles, the absorption spectra of ThT show a large bathochromic shift. The observed bathochromic shift in the absorption spectra of ThT can be explained on the basis of the confinement of the dye in the water pool where the effective polarity experienced by the probe is much less as compared to that in the bulk water. It has been reported that ThT undergoes a bathochromic shift with the decrease in the polarity of the medium.^{195,258}

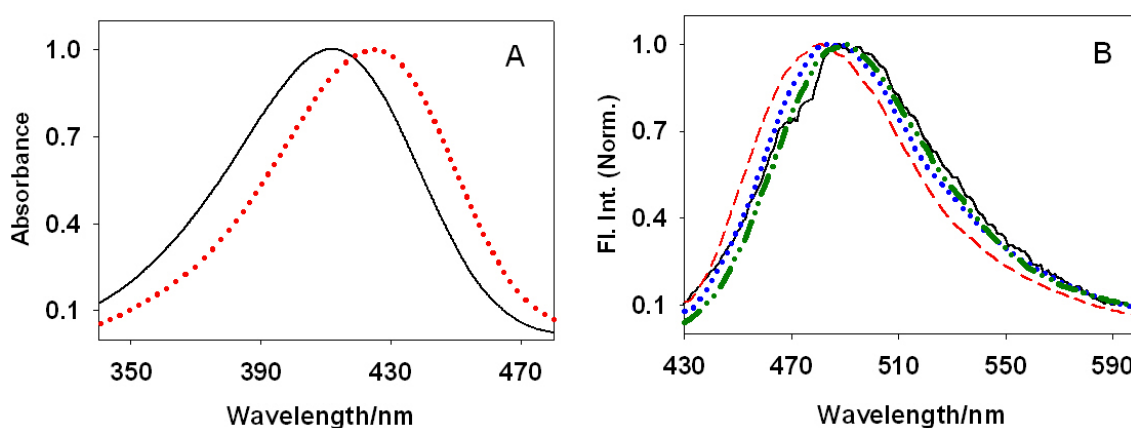


Figure 4.1. (A) Ground-state absorption spectra of ThT in bulk water (—) and in AOT reverse micelle with $w_0=20$ (.....). (B) Steady-state emission spectra of ThT in bulk water (—) and in AOT reverse micelle at different w_0 : (---) $w_0=1$, (.....) $w_0=4$ and (-.-.-) $w_0=20$.

The observed bathochromic shift in the reverse micelle could also be due to the electrostatic interaction between the cationic ThT and the anionic head group of AOT molecules. Such a bathochromic shift due to the electrostatic interaction of a cationic dye in SDS micellar solution has also been reported by Kumar et. al.²⁹¹ Present results clearly indicate that the ThT dye is solubilized in the confined water pool of the AOT RM.

Steady-state emission spectra of ThT were also recorded in AOT reverse micelles at different w_0 values and typical such spectra are shown in Figure 4.1B after normalization at the peak intensity. For comparison, the emission spectrum of ThT in bulk water is also shown in the same figure. According to Figure 4.1B, the emission band of ThT shows a small hypsochromic shift in the reverse micelle as compared to that in bulk water. The presence of

hypsochromic shift in the reverse micelle clearly indicates that the ThT molecules are confined in the reverse micelle and the effective polarity around the probe is much lower than that of the bulk water. This result is in agreement with the reported result, where it has been shown that the confinement of ThT in the hydrophobic environment results in a small but definite hypsochromic shift in the fluorescence spectra in comparison to that in bulk water.¹⁹⁷ It is to be noted from Figure 4.1B that the extent of hypsochromic shift gradually decreases as we increase the water content, i.e. w_0 value of the reverse micelle. These reduction in the hypsochromic shift might be due to the increase in the micropolarity experienced by the ThT molecule or due to the increase in the degree of hydration of the ThT molecule with an increase in the water content of the RM.

Table 4.1. Emission quantum yield, average excited state lifetime and torsional rate constant of ThT at different w_0 values.

w_0	ϕ	Avg. lifetime (ps)	$k_{\text{tor}} \times 10^{10}$ (sec^{-1})
1	0.0255	166.0	0.59
2	0.0155	121.4	0.81
3	0.0086	88.0	1.13
4	0.0059	60.3	1.65
5	0.0046	47.8	2.08
6	0.0039	37.8	2.64
7	0.0035	30.2	3.30
8	0.0029	23.8	4.18
10	0.0026	19.4	5.15
15	0.0023	17.9	5.56
20	0.0022	17.7	5.65
25	0.0021	17.1	5.83
30	0.0020	16.8	5.93

Figure 4.2A shows the changes in the emission intensity of ThT in AOT RM as a function of the w_0 values. It is indicated from Figure 4.2A that although the spectral position changes only nominally with the change in the w_0 values, there is a remarkable decrease in the observed emission intensity with increasing w_0 . The emission quantum yields (ϕ) of ThT was measured in the reverse micelles at different w_0 values and the results are presented in Table 4.1. The quantum yield at $w_0=1$ is estimated to be around 0.0255 and that for the bulk water medium is found to be ~ 0.0001 . This result indicates that there is an enhancement of ~ 250 fold in the emission yield of ThT in reverse micelle as compared to that in the bulk water. Such a large enhancement in the emission yield of ThT has not been observed in any other confined geometry, except in amyloid fibril. Figure 4.2B shows the variation in the relative ϕ values of ThT (with respect to water) as a function of the w_0 . As indicated from Table 4.1 and Figure 4.2B, the maximum enhancement in ϕ is observed in the reverse micelle with $w_0=1$ and on further addition of water, the emission yield decreased quite sharply. The decrease in the emission yield is prominent up to w_0 value of ~ 10 and beyond this w_0 , the changes in the emission intensity were nominal and attained a kind of saturation limit.

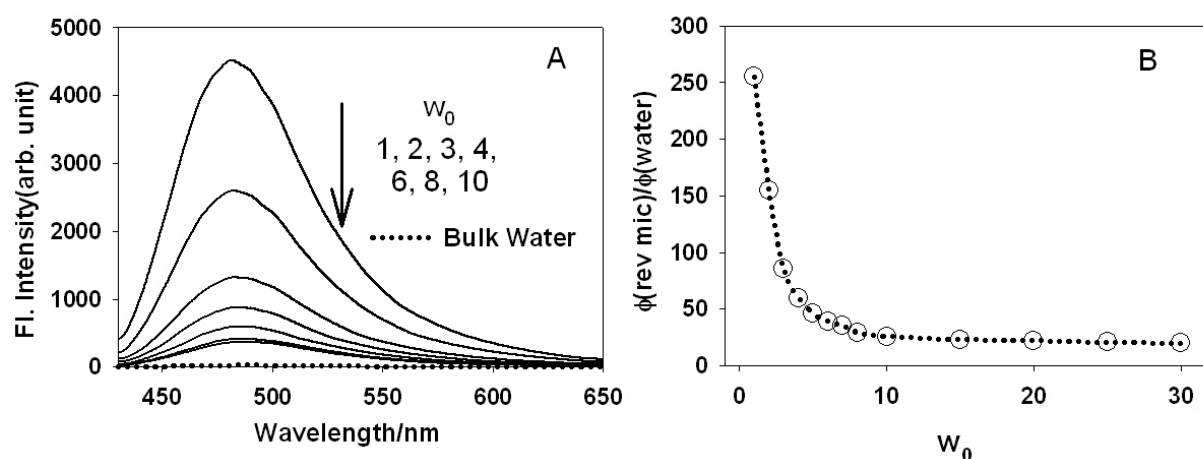


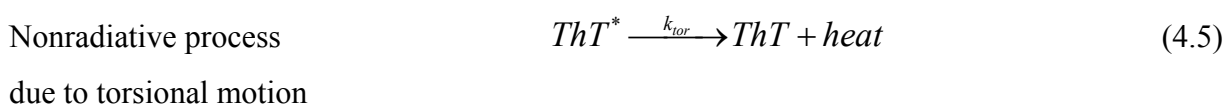
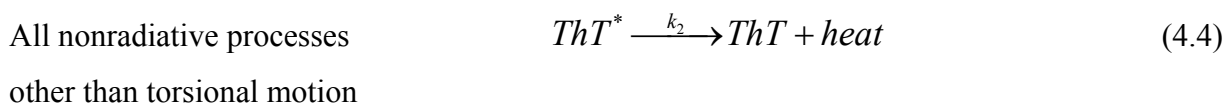
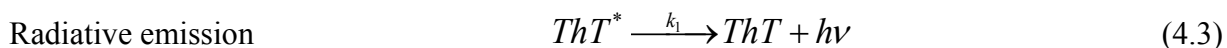
Figure 4.2. (A) Steady-state emission spectra of ThT in bulk water and in AOT reverse micelle at different w_0 values. (B) Variation in the relative ϕ values of ThT in the reverse micelle with respect to that in water as a function of the w_0 of the reverse micelles.

The emission yield of ThT is known to be highly sensitive to the viscosity of the medium.²⁵³ It has been shown in Chapter 3 that the free ThT molecules undergo a very fast bond twisting process in the photoexcited state around its central C-C single bond and this fast torsional motion introduces a strong nonradiative deexcitation channel, which is responsible for the low emission yield of the ThT molecule in low viscous solvents.^{190,279,292} However, in rigid media, the torsional motion in ThT becomes restricted and thus decreases the nonradiative decay process. This restriction in the torsional motion thus results in an increase in the emission quantum yield of ThT in highly viscous media.^{253,292,293}

Because of the large inhomogeneity in the reverse micelles, other processes, like the changes in the probe location or a change in the degree of hydration with the change in the water pool size of AOT micelles may also change the measured fluorescence quantum yield of the probe. To check whether the observed changes in the ϕ values are due to the changes in the microviscosity experienced by the probe or due to the other factors, we analyzed our experimental data in the following way. It is well established that if any torsional motion takes place in the excited state of a molecule, its ϕ value can be expressed with the following relationship,^{275,276,294,295}

$$\frac{1}{\phi} = 1 + \frac{k_2}{k_1} + \frac{k_{tor}}{k_1} \quad (4.2)$$

where, the rate constants k_1 , k_2 and k_{tor} are due to the following photophysical processes.



Since the torsional motion is basically a rotational diffusion, it should follow the Debye-Stokes-Einstein equation and its rate constant, k_{tor} , can be given by the following expression.

$$k_{\text{tor}} \propto \frac{T}{\eta} \quad (4.6)$$

where, T is the absolute temperature and η is the viscosity of the medium. Thus, substituting k_{tor} in equation 4.2 by expression 4.6, one obtains,

$$\frac{1}{\phi} = A + B \frac{1}{\eta} \quad (4.7)$$

where, $A = 1 + \frac{k_2}{k_1}$, $B = \frac{aT}{k_1}$ and a is the proportionality constant. At a given temperature, A and B should be the constant parameters.

Our experimental data was analyzed in light of equation 4.7. The viscosity of the AOT water pool at different w_0 values are obtained from the results reported by Hasegawa et al.²⁹⁶ To be mentioned that Hasegawa et al. has determined the viscosity of AOT reverse micelle using a cationic probe.²⁹⁶ Thus, the location of the probe used by Hasegawa et al. can be assumed to be quite similar to that of the present cationic dye, ThT. The variation of ϕ values with the viscosity of the microenvironment in the reverse micelles is shown in Figure 4.3.

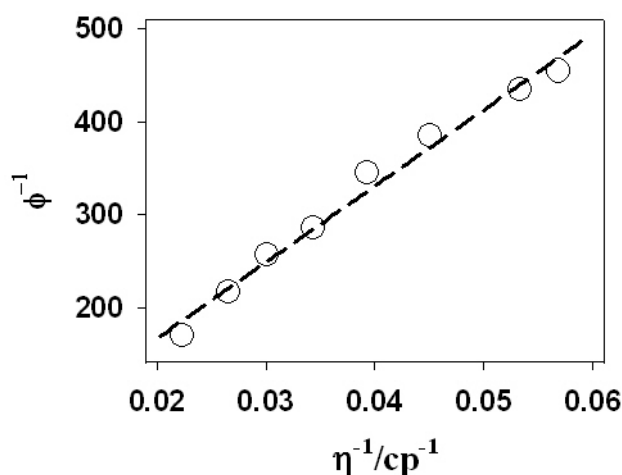


Figure 4.3. Variation in the fluorescence quantum yield (ϕ) of ThT with the viscosity (η) of the AOT reverse micelle.

It is evident from Figure 4.3 that the $(1/\phi)$ values changes linearly with $(1/\eta)$ as predicted by equation 4.7. Such a linear correlation clearly indicates that the kinetics in the photoexcited state of ThT in AOT reverse micelles are mainly governed by the processes described by

equations 4.3-4.5. In other words, the variation of the quantum yield is mainly governed by the changes in the local viscosity around the probe molecule. If there were any other processes, like the changes in the location of the dye or the changes in the degree of hydration of the probe due to the changes in the w_0 values, then we would not have expected a linear correlation in the $1/\phi$ vs. $1/\eta$ plot as shown in Figure 4.3.

The higher fluorescence yield of ThT in all the reverse micelle as compared to water can be simply explained on the basis of the decreased torsional motion of the dye in the rigid microenvironment of the reverse micelles. The ThT molecules experience the most rigid environment at $w_0=1$ and thus show the maximum emission yield. However, with an increase in the w_0 value, the microviscosity inside the water pool decreases rapidly and this is readily reflected by the rapid decrease in the emission yield. It is reported in the literature that the microviscosity at the interface of AOT RM varies only marginally beyond $w_0=10$.^{296,297} This is also supplemented by the present results, where it is seen that the emission yield of ThT attained a kind of limiting value for the w_0 values greater than 10.

4.3.2. Time-resolved fluorescence studies

It is a general perception that the fluorescence lifetime measurements can give the direct insight of the torsional motion involved in an excited dye. Thus, to understand the effect of water pool size of the reverse micelles on the torsional dynamics of the ThT dye we carried out the time-resolved fluorescence measurements using femtosecond fluorescence upconversion technique. Figure 4.4A shows the temporal decay profiles (measured at the emission peaks, 490 nm) of the excited ThT molecules in AOT reverse micelles at different w_0 values. To compare the lifetime values of ThT in reverse micelles with that in bulk water, we have also measured the fluorescence decay of ThT in aqueous solution and is also shown in Figure 4.4A.

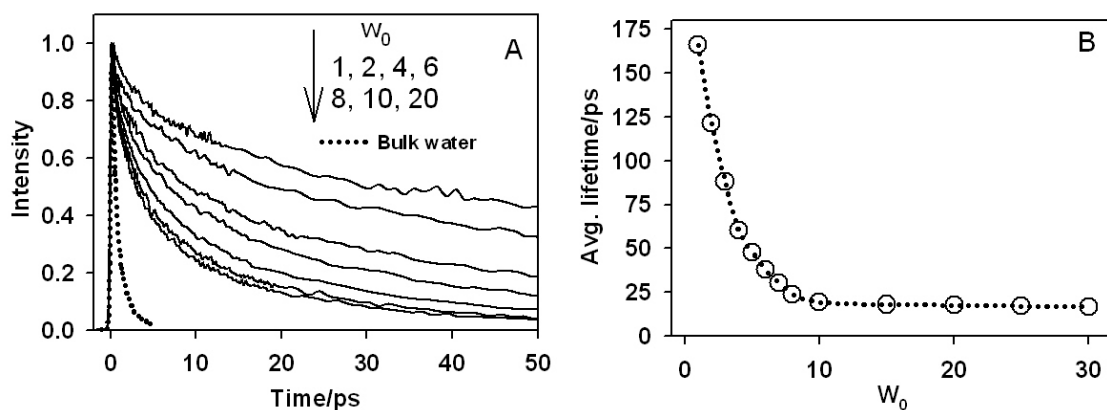


Figure 4.4. (A) Fluorescence decay traces of ThT in water (.....) and in AOT reverse micelle at different w_0 values. (B) Variation in the average fluorescence lifetime of ThT with the w_0 value of the reverse micelle.

It is evident from Figure 4.4A that the fluorescence decay of ThT in reverse micelles are much slower for all w_0 values investigated in comparison to that in bulk water. Decay traces of ThT in all the cases are found to follow a multi-exponential kinetics. Similar multi-exponential kinetics were also reported for many other fluorophores in the water nano pools of reverse micelles. The multi-exponential nature of the fluorescence decay in the confined water environment is believed to be due to the heterogeneity in the reverse micelles. Thus, it is not possible to assign the individual decay components to any specific processes in the molecule. Hence, average fluorescence lifetime was calculated at each w_0 value to have a single characteristic parameter that represents the gross dynamical feature of the excited state of the dye in a particular w_0 value of the reverse micelles. The average fluorescence lifetimes of ThT as estimated in the reverse micelles at different w_0 values are listed in Table 4.1. Figure 4.4B shows the changes in the average lifetime of ThT in the reverse micelles as a function of the w_0 values. Figure 4.4B clearly indicates that the lifetime of the ThT in the reverse micelle decreases quite sharply with an increase in the w_0 value. The average lifetime of ThT in the smallest water pool ($w_0=1$) investigated in the present study is more than two orders of magnitude higher as compared to that in bulk water. Such a large increase in the emission lifetime in the confined water pool suggests that the ThT molecule resides in an environment

that provides strong frictional force and thus resist the torsional motion of the dye responsible for the fast radiationless decay channel in the bulk water.

Even at the highest w_0 value used in the present study, where the water molecules in the centre of the water pool is known to behave quite similar to the bulk water,^{298,299} the emission lifetime of ThT is seen to be much higher than that in the bulk water. This observation is attributed to the fact that there is a strong electrostatic interaction between the ThT cation and the anionic sulphonate head group of AOT. Present results thus clearly indicate that even at the highest w_0 value, the ThT molecule prefers to stay near the interface than going deep inside the core of the water pool.

To understand the effect of the electrostatic interaction between the ThT cation and the sulphonate head group of AOT on the fluorescence decay time, we also measured the lifetime of ThT in AOT normal micelle at different surfactant concentrations. The concentration of the AOT was always kept higher than its critical micellar concentration, $4 \times 10^{-3} \text{ mol dm}^{-3}$.²⁹⁶ In the normal AOT micelle, the ThT cation is expected to reside on the surface of the micelle due to the electrostatic attraction with the negatively charged surfactant head group. Figure 4.5 shows the decay traces for the ThT in AOT normal micelles at different surfactant concentrations. It is clearly indicated from Figure 4.5 that the lifetime of ThT does not vary with the concentration of the AOT. The average lifetime of ThT estimated in these normal AOT micelles is found to be around 11 ps (*cf.* inset of Figure 4.5). It is important to note that the lifetime of ThT in normal micelle is slightly lower than that in the reverse micelle with the highest w_0 value (~17 ps). These results suggest that the increase in the fluorescence lifetime of ThT in the reverse micelle is not only due to the electrostatic interaction between the ThT cation and the negatively charged surfactant head group, but also due to the presence of some bound water in the interface region even at the highest w_0 value. Hasegawa et. al. have shown through the fluorescence depolarization measurements that the microviscosity experienced by a cationic probe in AOT reverse micelle is quite high even at a very high w_0 value than that in the bulk

water.²⁹⁶ Thus, the presence of such bound water in reverse micelles is suggested to be responsible for the large frictional forces that retard the torsional motion of the ThT molecule. Present results are also in agreement with the results obtained from the solvent relaxation study which showed that even at the higher w_0 value of the reverse micelles the movement of the water molecules are quite restricted as compared to that in bulk water.^{99,300} Molecular dynamic simulation on the confined water pool shows that due to the confinement, the motion of the water molecules is restricted by a factor of 2-5 as compared to that in bulk water.⁹⁹ This constraint in the water movement is expected to cause an increase in the local viscosity and consequently a longer fluorescence lifetime of the ThT dye present in the water pool of the reverse micelle. Thus, we infer that large increase in the fluorescence lifetime as observed in small water pool, is mainly due to the combination of two factors, the electrostatic interaction between ThT cation and the negatively charged surfactant head group and the effect of the constrained water molecules at the surfactant-water interface that are quite less mobile as compared to those in bulk water.

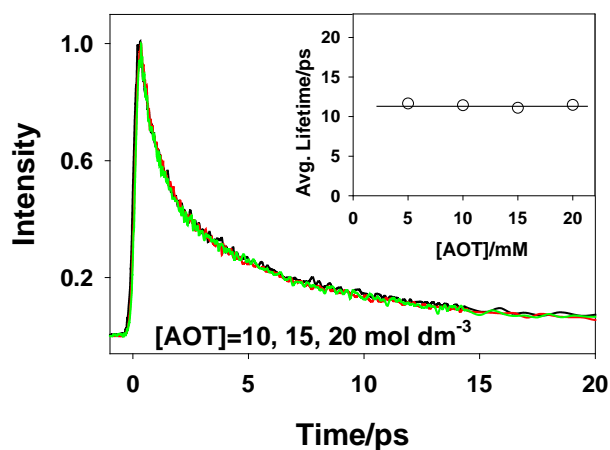


Figure 4.5. Transient fluorescence decay of ThT in normal AOT micelle at different AOT concentration. Inset shows the variation of fluorescence lifetime in normal AOT micelle with surfactant concentrations.

To further understand the nature of the torsional dynamics in the ThT molecule, time-resolved fluorescence depolarization measurements were carried out in AOT reverse micelles at different w_0 values. The changes in the fluorescence anisotropy with time in AOT reverse

micelles for two different w_0 values (5 and 10) are shown in Figure 4.6. It is evident from this figure that there is no appreciable decrease in the anisotropy of ThT within its excited state lifetime. Further, the anisotropy value as well as its temporal behavior is seen to be independent of the w_0 values of the reverse micelles. This result clearly indicates that there is no appreciable rotational motion of the whole ThT molecule within its excited state lifetime. This is also in accordance with the slow rotational relaxation dynamics reported for other dyes in the restricted AOT environment.^{99,301} Present result clearly indicates that the torsional motion present in the ThT molecule do not cause any effect on the depolarization process as seen for other molecules.³⁰²⁻³⁰⁴ Present result is also in agreement with the reports of Stsiapura et al.,²⁵³ where the authors have shown that the degree of polarization for ThT in glycerol is very high and remains constant across the emission spectrum. The high value of anisotropy, which remains unchanged within the excited state lifetime of ThT molecule can be explained on the basis of the following consideration. The transition dipole of ThT is directed along its long molecular axis.²⁵³ Thus, the torsional motion of the aminobenzene ring do not cause any change in the direction of the transient dipole. Because of this reason, the torsional motion in the ThT molecule do not cause any change in the anisotropy for the excited dye.

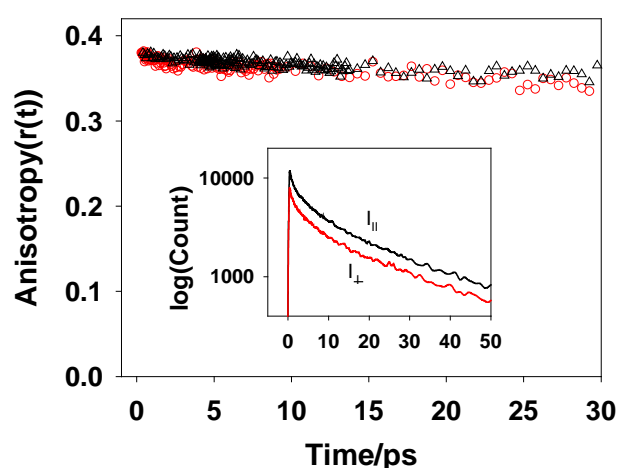


Figure 4.6. Variation of fluorescence anisotropy for ThT molecule in the AOT reverse micelles at different w_0 : (Δ) $w_0=5$ and (\circ) $w_0=10$. Inset: The emission decay profile of ThT in AOT reverse micelle ($w_0=5$) at different excitation polarization: (—) parallel and (---) perpendicular.

As mentioned above, the decrease in the decay lifetime and emission yield with an increase in the w_0 value of the reverse micelles is mainly due to the enhancement in the nonradiative torsional motion in the ThT molecule. Thus, we have calculated the rate constant for all possible nonradiative processes (k_{nr}) using following relation,

$$k_{nr} = k_2 + k_{tor} = \frac{1-\phi}{\tau_f} \quad (4.8)$$

where τ_f and ϕ are the average lifetime and emission quantum yield, respectively, of the dye. The total nonradiative rate constant, k_{nr} , thus calculated is presented in Table 4.1. It is also evident from equation 4.8 that the nonradiative rate constant, k_2 , can be calculated from the intercept of the plot shown in Figure 4.3. The intercept value of 3.04 is obtained from the plot of $1/\phi$ vs. $1/\eta$ (*cf.* Figure 4.3). The average value of radiative rate constant, k_1 , estimated from the measured τ_f and ϕ values are found to be $1.2 \times 10^8 \text{ s}^{-1}$. Using this value of k_1 , the value of k_2 is calculated to be $2.45 \times 10^8 \text{ s}^{-1}$. The total nonradiative rate constant k_{nr} , as calculated using equation 4.8, are in the range of $0.6-6 \times 10^{10} \text{ s}^{-1}$ (*cf.* Table 4.1), which is almost two order of magnitude higher than the k_2 value. This result clearly indicates that the nonradiative process in the present system is mainly governed by k_{tor} , i.e. the torsional motion in the ThT molecule. The variation of k_{tor} with the w_0 values of the reverse micelles is shown in Figure 4.7. It is clearly evident from this figure that the changes in the k_{tor} values with the changing w_0 values of the reverse micelles are not monotonic. The k_{tor} value increases quite rapidly with the initial increase in the w_0 values. However, beyond $w_0=10$, the increase in the k_{tor} is very nominal. Similar trends were also observed for the fluorescence quantum yields and the excited state lifetimes of the dye. Such a change in the torsional rate constant can easily be correlated to the changes in the nature of the water pools with changing w_0 values. As mentioned earlier, and also supported from the IR measurements,³⁰⁵ the water molecules are mainly bound to the surfactant head group for $w_0 < 10$. Beyond this w_0 value, it is basically the fraction of free water

molecules in the water pool which increases with an increase in w_0 value. In accordance to this the viscosity at the interface of the reverse micelle tend towards a limiting value at higher w_0 values though at the lower w_0 values it decreases very sharply with the change in the water content of the reverse micelles.

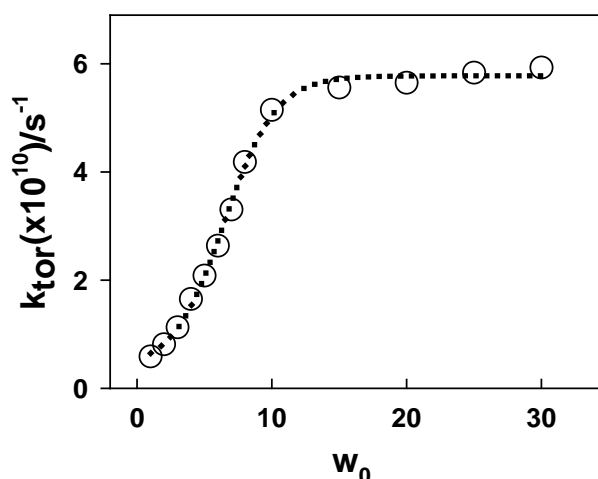


Figure 4.7. Variation in the torsional rate constant (k_{tor}) of ThT dye with the w_0 value of the AOT reverse micelle.

Present results indicate that the fluorescence quantum yield and lifetime of the ThT molecule is highly sensitive to the viscosity of its surrounding environment. The fluorescence quantum yield and lifetime of the ThT molecule follows exactly the similar trend as that of the viscosity of the medium. Thus, ThT can act as a very efficient molecular rotor for complex microheterogeneous media as compared to other fluorophore reported in the literature.^{275,306}

4.3.3. ThT in cationic reverse micelle

The study of encapsulation of molecules and their interaction with the RM interface is important in its own right both from fundamental and applied point of view. A range of molecules have been used by researchers to disclose details about pH,³⁰⁷ microviscosity,²⁹⁶ and polarity,³⁰⁸ among others, in confined environments, such as cells, micelles, and nanoporous materials. In general the molecular probes are selected for their spectroscopic features and the ability to interpret the observations made. Experiments exploiting molecular probes to understand micro- and nanoscopic structures in confined environments depend on the location

of the probe, often assuming the location based on a particular characteristics.^{49,52,309-315} Thus, determination of the probe location is important for analyzing the results of different relaxation dynamics. In general, the location of a solute within a RM is difficult to determine unambiguously. In the literature, the general interpretation is that charged molecules reside in the most polar environment available, such as in aqueous phase, while less polar molecules may reside in the micellar interface.⁴⁹ We have seen that in case of AOT reverse micelle, electrostatic interaction between the ThT and the surfactant head groups dominates even at the higher water content in the reverse micelle. However due to the likelihood of encompassing different type of interactions, for example, hydrophobic, H-bonding, dipole-dipole, etc. in RM, the electrostatic interaction may be surmounted by the precedence of other forces. To verify this aspect in the RM, in the present study, we have investigated the location of the positively charged ThT molecule in a cationic RM and the results are compared with those in the anionic RM. From the basic perception of electrostatic interaction it is expected that the positively charged molecules will prefer to reside at the centre of the water pool of the cationic RM to minimize the electrostatic repulsion with the high positive charge density at the interface. In contrast, in anionic reverse micelle, the positively charged probe is expected to reside at the water-surfactant interface due to the strong electrostatic attraction with the interfacial negative charge. Astonishingly a reverse trend is observed in the present study by using cationic reverse micelle, as are discussed in this section.

From our studies in AOT reverse micelle and from the literature reports, ThT is suggested to act as an efficient molecular rotor to determine the viscosity of different microenvironments.^{195,253,293} As discussed in the previous section that if the microviscosity around the ThT molecule increases, the nonradiative bond twisting process of ThT gets retarded on increasing its surrounding viscosity and consequently there is an increase in its fluorescence quantum yield and its emission lifetime. Hence, through fluorescence quantum

yield and excited state lifetime measurements, it is quite possible to predict the strength of binding of the ThT molecule with its surrounding media. In the present study, BHDC has been used as the model surfactant for cationic RM and benzene is used as bulk organic solvent media. Emission spectra of ThT in cationic RM were recorded at different w_0 values. Figure 4.8A shows the emission spectra for ThT in BHDC reverse micelle at different w_0 . It is evident from this figure that the emission intensity of ThT decreases with an increase in the size of the central water pool. The variation in the emission quantum yield of ThT with the w_0 of BHDC RM is shown in the Figure 4.8B. The decrease in the emission yield of ThT with increase in the water pool size is due to the fact that the microviscosity around the ThT molecule decreases with an increase in the water content in the RM. From Figure 4.8B it is indicated that the emission yield decreases gradually upto w_0 value of 10 and remains invariant on further increase in the w_0 value. This behavior can be rationalized if the probe ThT resides at the interface of the RM. At very low water content, most of the water molecules in the RM are involved in hydrating the head groups of the surfactants.^{316,317}

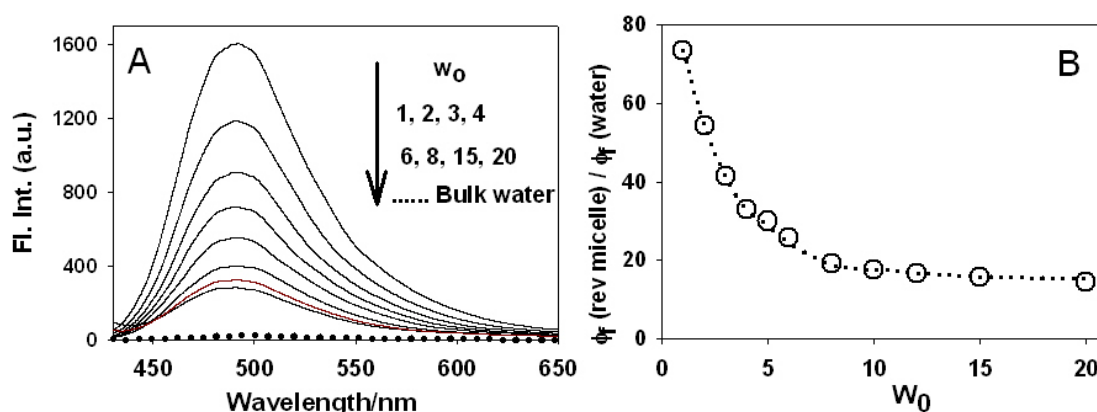


Figure 4.8. (A) Steady-state emission spectra of ThT in bulk water and in BHDC reverse micelle at different w_0 values. (B) Variation in the relative ϕ values of ThT in the reverse micelle with respect to that in water as a function of the w_0 of the reverse micelles.

With the increase in the water content the hydration of the surfactant head group increases with a concomitant decrease in the microviscosity at the interfacial region. However, after complete hydration of the head groups of the surfactants, further added water contributes to the increase in the free water in the central water pool without affecting the hydration of the head group

region.^{316,317} Thus, after certain w_0 value, there will be no change in the microviscosity at the interfacial region and consequently the emission yield of ThT decreases and attains a limiting value at higher w_0 values. It is to be noted from the Figure 4.8B that even at the highest w_0 value of 20, the emission quantum yield of ThT in BHDC RM is substantially higher (~ 20 times) than that in the bulk water. This result clearly indicates that even in large water pool, the probe molecule prefers to reside at the interface of the RM rather than in the central water pool. This is quite surprising from the viewpoint of electrostatic interaction, because the positive charge on the probe, should experience an electrostatic repulsion from the positively charged interface of the RMs. Thus, the probe ThT was expected to avoid the interfacial region of the cationic RM and should move towards the central water pool on increasing the w_0 value. Such movement of the charged molecular species from the charged interface to central water pool is infact well documented in the literature.

Although we have seen that the probe resides at the interfacial region of AOT/heptane/water reverse micellar system but the external organic solvent can also modify the interfacial rigidity owing to its extent of penetration in the interfacial region and solubility of water in the external organic solvent at the interfacial region.^{318,319} So to consider the effect of external organic solvent we carried our measurements in AOT/benzene/water system also and the results are compared with BHDC/benzene/water system. Further the radius of the water pool varies differently with w_0 for AOT/benzene/water and BHDC/benzene/ water system so a meaningful comparison should include the same water pool radius for AOT and BHDC reverse micelle rather than same w_0 value. The variation of the emission quantum yield of ThT in AOT/benzene/water RM with the size of the central water pool is shown in the Figure 4.9. It is evident from Figure 4.9 that qualitatively ThT behaves quite similarly in both BHDC and AOT reverse micelle. However, the emission quantum yield of ThT is always higher for BHDC RM as compared to that in AOT RM. This large emission yield of ThT in the BHDC RM clearly

indicates that despite having the positive charge, ThT is more strongly associated with the positively charged interface than with the negatively charged interface. This result is a clear indication of violation of principle of electrostatic interaction in the present RM systems.

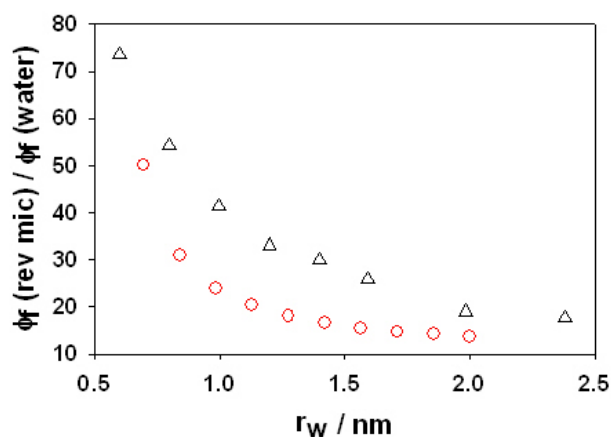


Figure 4.9. Variation in the relative ϕ values of ThT in the reverse micelle with respect to that in water as a function of the radius of water pool of AOT(O) and BHDC (Δ) RM.

To understand the reason behind the observed discrepancy in the measured emission quantum yield, time-resolved emission measurements were carried out in both types of RMs. As mentioned in Chapter 3, the excited state lifetime of ThT is very short (~ 1 ps) due to the ultrafast barrierless bond twisting process in its excited state. However, the lifetime increases significantly due to its association with different confined environments. Thus, the increase in the excited state lifetime of ThT is a signature of the retardation of the bond twisting process. The excited state decay traces recorded for ThT in BHDC and AOT RMs with water pool size of 1.1 nm are shown in Figure 4.10A. The average lifetime thus measured for ThT in BHDC and AOT reverse micelle with 1.1 nm water pool size are 52 ps and 32 ps respectively. Such longer lifetime as compared to that in bulk water clearly indicates that the bond twisting process in ThT is considerably retarded in both type of RMs. However, the relatively longer lifetime of ThT in BHDC RM as compared to that in AOT RM clearly indicates that the association of the ThT with the interfacial region of RM is more stronger for the BHDC RM as

compared to that in the AOT RM. These time-resolved measurements again goes against the consideration of electrostatic interaction.

The variation of the excited state lifetime of ThT with the central water pool size is presented in Figure 4.10B. It is to be noted that the excited state lifetime decreases with the increase in the size of the central water pool for both type of RMs. However, the lifetime attains a constant value at a larger water pool size. Thus, even at the largest water pool size, the lifetime of ThT is seen to be longer in the case of BHDC RM than that in the AOT RM. This result clearly indicates that irrespective of the central water pool size, the ThT molecules are more strongly associated with the interfacial region of the BHDC RM than in the AOT RM.

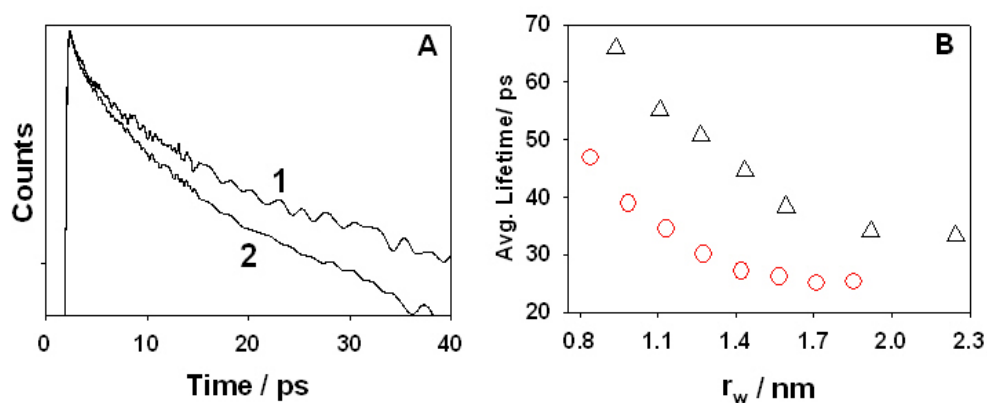


Figure 4.10. (A) Fluorescence decay traces of ThT in (1) BHDC and (2) AOT RM with $r_w = 1.1$ nm. (B) Variation in the average fluorescence lifetime of ThT with the r_w value for AOT(O) and BHDC (Δ) RM.

The nonradiative rate constant, which is a measure of the bond twisting process, was calculated for the dye in both the RMs with different water pool size and are shown in Figure 4.11. It is seen that the rate of bond twisting process gradually increases with an increase in the water pool size. Further, it is observed that the bond twisting rate always remains higher in the case of AOT RM than that in BHDC RM.

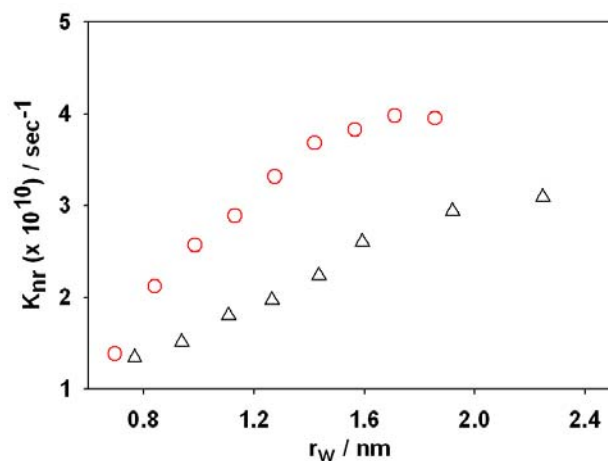


Figure 4.11. Variation in the rate of bond twisting process with the size of the central water pool of AOT(O) and BHDC (Δ) RM.

All these experimental results discussed above clearly indicate that despite having a net positive charge, ThT is more strongly associated with the interface of the positively charged RM than the intuitively expected anionic RM. To understand whether the observed violation in the principle of electrostatic interaction is a general phenomena for self-assembled systems, we have also investigated the association of ThT in AOT and BHDC conventional micelles. Figure 4.12 shows the emission decays for ThT in AOT and BHDC micelle. It is quite evident from the Figure 4.12 that the bond twisting dynamics of ThT is considerably retarded in the AOT micelles as compared to that in the bulk water. This retardation in the bond twisting dynamics in AOT micelles can be easily understood from the fact that the positively charged ThT is likely to get associated with the anionic micelle of AOT primarily due to electrostatic attraction. Due to such an association, the bond twisting process in ThT gets retarded. However, unlike in RM, the bond twisting process in the BHDC normal micelle is seen to be comparable to that in the bulk water. This result clearly indicates that ThT does not get associated with the normal BHDC micelle. Present result is quite expected from the electrostatic point of view as the positively charged molecule will try to avoid the cationic micellar surface and prefer to stay in the water phase.

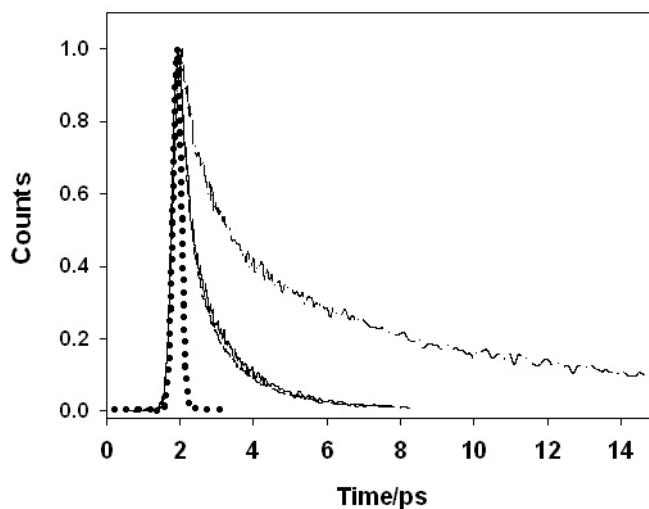


Figure 4.12. Fluorescence decay traces of ThT in water (—), AOT micelle (-.-.-.-.-) and BHDC micelle (-----) the dotted line represents the instrument response function (IRF).

Comparing the results in the RM and in the conventional micelles, it is quite evident that the violation of the principle of electrostatic interaction is not a general phenomena and is quite specific to the RMs. Thus the charged surface formed under the the nano-confinement shows quite extraordinary electrostatic behavior as compared to other normal charged surface. The reason for the observed violation of the electrostatic principle in the nanoconfined water pool can be rationalized in terms of the following possibilities. It is likely that due to the presence of large number of counter ion in the small confined water pool, the electrostatic screening may be operative in the RM. Due to the electrostatic screening the electrostatic repulsion between the positively charged probe and the positively charged interface might be reduced to a considerable extent. In addition, other possible interactions like hydrophobic interaction and the π - π interaction between the aromatic ring of the probe and the BHDC surfactant molecules might also contribute to the stronger association of the probe molecules at the interface of the BHDC RM.

4.4. Conclusion

The effect of confinement on the excited state ultrafast torsional dynamics of Thioflavin-T have been investigated in nanoconfined water pool of AOT reverse micelle. It is demonstrated

that due to the confinement, torsional motion in ThT becomes very sluggish. Due to this sluggish torsional motion, fluorescence enhancements of about 250 times have been observed in the reverse micelle in comparison to that in bulk water. With increase in the water pool size, however, both fluorescence quantum yield and lifetime are seen to decrease non-monotonically. Such a decrease in the fluorescence quantum yield and lifetime has been attributed to the faster torsional motion in the larger water pools of the reverse micelles. It is seen that the torsional motion remains restricted even in a very large water pool. This result has been explained on the basis of the electrostatic interaction between the positively charged probe and the negative surfactant head groups and the effect of the bound water that are unusually sluggish in their movement even in a large water pool of the reverse micelle. The high sensitivity of the fluorescence quantum yield and lifetime on the viscosity of the medium can be useful to design an efficient molecular rotor based on ThT dye.

In cationic reverse micelle, due to the confinement in the nano-space, the electrostatic interaction is modified to such an extent that the principle of electrostatic interaction is overruled. The electrostatic interaction, which is expected to be much stronger than the other interactions like, hydrophobic interaction, π - π interaction, cation- π interaction etc. could be minimized due to the confinement of the large amount of charged species in a small confined space. This result can have far reaching implications in chemical and biological systems. From a more conceptual and fundamental perspective, the results obtained here may herald various interesting applications. For instance, positively charged carriers for drugs are emerging as a promising option owing to their very strong cellular interaction properties and good cellular uptake³²⁰⁻³²² so one can foresee the design of a drug delivery system based on unconventional combination of a positively charged carrier (RM based) and a cationic drug leading to improved drug compatibility and drug stability and in fact these results become even more appealing as Thioflavin-T itself is used as a model drug molecule in various studies.^{323,324}

Further, reverse micellar systems also hold strong promise as a nano-reactor for carrying out chemical reaction and catalysis by exploiting its interfacial properties so one can imagine of the feasibility and/or improved efficiency of a chemical reaction between two similarly charged solutes at a charged interface (cationic in this case) owing to their localization and increased local concentration at the interface which is generally not contemplated.

Chapter 5

Effect of β -CD Nanocavity on the Ultrafast Bond Twisting Dynamics of Thioflavin-T

5.1. Introduction

The notable evolution of supramolecular chemistry over the past decade has resulted, in part, from the advancement in understanding of the host-guest interactions.³²⁵⁻³²⁷ The nature and the structure of the host-guest complexes are of fundamental concern in molecular recognition and are of increasing significance in the applications of supramolecular systems. The nature of the binding forces, the geometry of the intermolecular complexes, and the intermolecular dynamics are the central issues for their applications in synthetic,³²⁸ analytical,³²⁹ and pharmaceutical chemistry.³³⁰ Cyclodextrins (CDs) are the macrocyclic molecules composed of the glucopyranose units possessing a hydrophobic cavity of varying size,^{331,332} and they hold a position of vital importance in supramolecular chemistry. The conformation and orientation of hydroxyl groups in CDs make their external surface hydrophilic, whereas the internal cavity of these molecules is quite hydrophobic in nature. The presence of both hydrophobic interior and hydrophilic exterior makes them suitable and fascinating hosts for supramolecular chemistry and for studying the spectroscopy and dynamics of several molecular systems as guests in aqueous solution.¹³⁷ The remarkable ability of the CDs to form inclusion complexes with a

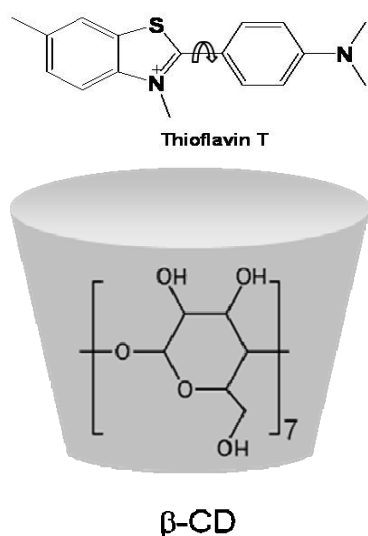
variety of organic molecules has motivated the researchers for past few decades to study such inclusion complexes as they can serve as the miniature models for understanding the action of enzymes,^{332,333} mimicking the reactions in biosystems,³³² and so forth. The chemical reactivity of the guest molecules can be modified remarkably through their incorporation into the CD cavities.^{334,335} The reduced polarity and the restricted space inside the CD cavity influences the photophysical and photochemical properties of an encapsulated guest.¹³⁵⁻¹³⁷ Although, there are extensive literature reports on the structural features of the host-guest complexes, the dynamical behavior of the guest molecules in the ultrafast time regime have received very limited attention in the host-guest chemistry.³³⁶⁻³³⁹

Femtosecond studies of encapsulated molecules in the nanocavities can provide direct information on the relationship between time and space domains of molecular relaxations.³⁴⁰ Using femtosecond time-resolved techniques and selecting the size and nature of the molecular container offered by the host to the guest, one can be able to explore and control the spectroscopy and dynamics of guest molecules.^{341,342} Further, exploring the ultrafast dynamics in different cages may help us to better understand the catalytic mechanism inside these cavities, like those involved in enzymes and zeolites.

In previous Chapter we have seen that the bond twisting dynamics in excited state of ThT molecule undergoes a remarkable change in a restricted environment. Our earlier studies in different homogeneous solvents has shown that the bond twisting process in ThT effectively introduces a very fast non-radiative decay channel for the excited ThT molecule resulting its emission yield to be extremely low.^{279,293} Knowledge of the ultrafast dynamics of the photoexcited ThT molecule under different biomimetic environment is very essential in order to understand the underlying mechanism for the enhancement of the fluorescence emission yield of ThT in confined environment, especially in amyloid fibril. Incorporation of such biologically potent molecules in different biomimetic environments has attracted the interest of

researchers because the studies of such systems can furnish the important clues regarding the noncovalent intermolecular forces operative at the molecular level.

In the present study we examine the effect of confinement of the β -cyclodextrin (β -CD) nanocavity on the ultrafast bond twisting dynamics of ThT using femtosecond fluorescence upconversion technique. The aim of this study is to understand the underlying process that takes place in ThT in the sub-picosecond time regime and how it is modified on the encapsulation of the dye in a macrocyclic nanocavity. Detail analysis of the time-resolved emission spectra including time dependent changes in the peak frequency, width of the emission spectra (FWHM) and asymmetry of the emission spectra have also been carried out and the results are compared with that in bulk water to get insight of the relaxation dynamics in the excited ThT molecules.²⁷⁹



Scheme 5.1. Molecular structure of Thioflavin T and β - cyclodextrin

5.2. Experiments and Methods

The source and purification of ThT are given in Chapter 2. β -CD was purchased from TCI Mark, Tokyo and was used as received. Nanopure water (conductivity less than $0.1 \mu\text{S cm}^{-1}$) was used for all sample preparations. All the measurements were carried out using freshly prepared solution of the dye in β -cyclodextrin. The instrument used for ground-state

absorption, steady-state fluorescence and ultrafast fluorescence decay measurements are discussed in Chapter 2. The emission spectra were corrected for the wavelength dependent instrument responses as discussed in Chapter 2 (*cf.* Section 2.3.1).

5.3. Results and Discussion

5.3.1. Steady-state measurements

The emission spectra of ThT at different β -CD concentrations were measured and are presented in Figure 5.1A. It is seen from Figure 5.1A that the emission intensity of ThT gradually increases with an increase in the β -CD concentrations in the solution. ThT is known to be weakly fluorescent in bulk water due to the presence of very efficient nonradiative bond-twisting process in its excited state.^{239,258,279,293} As mentioned in Chapter 3 that the twisting around the central C-C bond results in the formation of twisted intramolecular charge transfer (TICT) state, which is much weaker fluorescent than the locally excited (LE) state of ThT molecule.^{279,293} Significant increase in the emission intensity of ThT in the presence of β -CD is a clear indication of inclusion complex formation between ThT and β -CD. Due to the formation of inclusion complex, the space available for the bond twisting process in ThT becomes limited. Thus, due to the confinement effect of the β -CD cavity, the bond twisting process in ThT is retarded significantly resulting an increase in its emission yield. Further, the reduced polarity inside the β -CD nanocavity is also not favourable for the charge separation process in the ThT molecule to produce the TICT state. Thus, due to lower propensity for the charge separation, the formation of TICT state will be also reduced due to the inclusion of ThT into β -CD nanocavity. This less propensity to form the TICT state also adds to the observed increase in the emission yield of ThT in the presence of β -CD nanocavity.

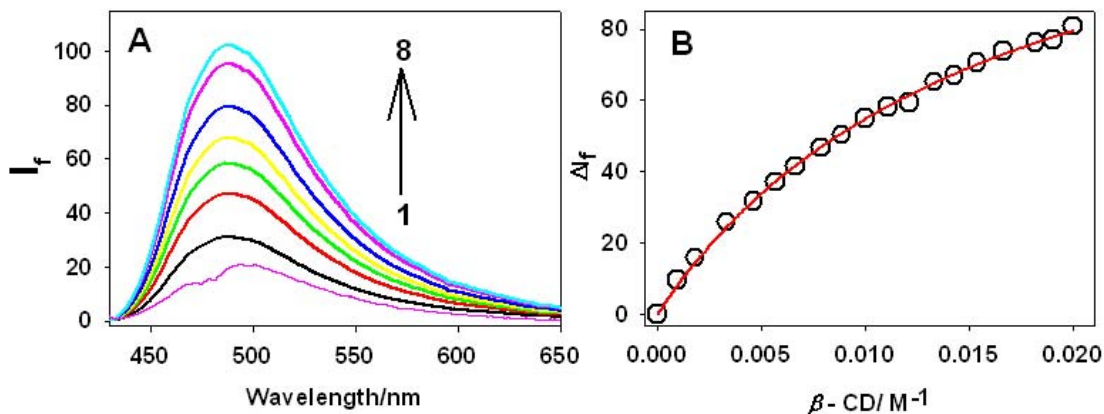


Figure 5.1. (A) Steady-state emission spectra ($\lambda_{\text{ex}}=410$ nm) of Thioflavin-T ($7 \mu\text{M}$) at different β -CD concentrations: (1) 0.0 (2) 2.0 (3) 3.3 (4) 5.7 (5) 7.8 (6) 11.1 (7) 16.0 and (8) 18.0 mM. (B) Fluorescence titration curve (1:1 binding model) for ThT• β CD system.

In order to understand the strength of binding and also the stoichiometric compositions of the ThT- β -CD inclusion complexes, the changes in the fluorescence intensity of the ThT with the varying β -CD concentration was analyzed using the 1:1 complexation model which provided satisfactory fitting results. In these experiments, keeping the total dye concentration $[\text{ThT}]_0$ same, the observed steady-state fluorescence intensity I_f at any concentration of the host (β -CD) can be expressed as,

$$I_f = I_{\text{ThT}}^0 \frac{[\text{ThT}]_{\text{eq}}}{[\text{ThT}]_0} + I_{\text{ThT}\cdot\beta\text{-CD}}^\infty \frac{[\text{ThT}\cdot\beta\text{-CD}]_{\text{eq}}}{[\text{ThT}]_0} \quad (5.1)$$

where, I_{ThT}^0 is the initial fluorescence intensity of the free dye, $I_{\text{ThT}\cdot\beta\text{-CD}}^\infty$ is the extrapolate fluorescence intensity when all the dye in the solution is converted to ThT• β CD complex, $[\text{ThT}]_0$ is the total concentration of dye (ThT) used and $[\text{ThT}]_{\text{eq}}$ is the equilibrium concentration of the free ThT in the solution. For fitting of the fluorescence titration curves, the changes in fluorescence intensity $\Delta I_f = (I_f - I_{\text{ThT}}^0)$ were estimated and plotted against the total host concentration $[\beta\text{-CD}]_0$ used. Following eq. 5.1, ΔI_f is expressed as,

$$\Delta I_f = \left(1 - \frac{[\text{ThT}]_{\text{eq}}}{[\text{ThT}]_0}\right) \left(I_{\text{ThT}\cdot\beta\text{-CD}}^\infty - I_{\text{ThT}}^0\right) \quad (5.2)$$

where $[\text{ThT}]_{\text{eq}}$ is expressed in terms of the total host concentration $[\beta\text{-CD}]_0$ and the binding constant K_{eq} for the $\text{ThT}\bullet\beta\text{-CD}$ complex by the following equation.

$$[\text{ThT}]_{\text{eq}} = \frac{1}{2K_{\text{eq}}} \left\{ (K_{\text{eq}}[\text{ThT}]_0 - K_{\text{eq}}[\beta\text{-CD}]_0 - 1) + \sqrt{(K_{\text{eq}}[\text{ThT}]_0 + K_{\text{eq}}[\beta\text{-CD}]_0 + 1)^2 - 4(K_{\text{eq}})^2[\text{ThT}]_0[\beta\text{-CD}]_0} \right\} \quad (5.3)$$

The binding constant (K_{eq}) for ThT- β CD complex as obtained from the nonlinear fitting of the titration curve (*cf.* Figure 5.1B) using equation 5.2 is found to be $78\pm 5 \text{ M}^{-1}$. This binding constant value for ThT is quite low and is very similar to those obtained for other cationic dye molecules of similar size with cyclodextrin hosts.³⁴³⁻³⁴⁵ Such a low value of K_{eq} indicates only a partial encapsulation of the dye inside the β -CD nanocavity. The observed weak binding of ThT with β -CD could be explained from the relative size of the guest and the host molecules. Since the overall length of ThT (14.0 \AA along long axis³⁴⁶) is much larger than the height of the β -CD cavity ($\sim 7.9 \text{ \AA}$ ^{125,134}), only a part of ThT molecule can only be accommodated into the β -CD cavity, resulting a weak binding. Due to the partial encapsulation of the dye, the bond twisting around the central C-C bond of ThT is still feasible though retarded to some extent and thus the ThT- β CD complex shows relatively less fluorescence enhancement as compared to those observed for ThT dye in other confined environments.^{197,239,279}

5.3.2. Time-resolved measurements

To understand the confinement effect of β -CD nanocavity on the bond twisting process in the excited state of ThT, we carried out detail time-resolved fluorescence measurements of the dye in the presence of varying β -CD concentration. Decay traces measured at the emission peak (490 nm) of ThT in the presence of different concentration of β -CD are shown in Figure 5.2. The transient decay for ThT in bulk water is also shown in Figure 5.2 for comparison. It is evident from Figure 5.2 that the fluorescence decay gradually becomes slower with the increasing concentration of β -CD. All the transient decays were seen to follow a non-exponential kinetics. Similar non-exponential kinetics is also observed for ThT emission in

bulk water due to the presence of barrierless bond twisting process.²⁷⁹ Such non-exponential decay kinetics is also reported in the literature for several other molecules which can undergo barrierless nonradiative decay processes (like cis-trans isomerization, bond twisting, etc.) in their excited state.^{267,347} Due to the non-exponential decay kinetics, it is quite difficult to assign any specific decay constant to any specific process in the excited state of the dye. Further, it is noticed that besides having a long decay component in the presence of β -CD, there are also some ultrafast components in the decay traces, which are quite comparable to those observed in the bulk water (*cf.* Figure 5.2). These results are in the line of the fact that the binding constant of ThT with β -CD is reasonably less. Thus, under such circumstances, it is expected that a reasonable amount of ThT remains in the free state, which behave very similar to that in bulk water.

Due to the presence of the non-exponential decay kinetics, we rely on the average fluorescence lifetime values to understand the effect of β -CD nanocavity on the photophysical behavior of ThT dye. Thus, the average lifetime of ThT in aqueous solution at different β -CD concentration were calculated and are shown in the inset of Figure 5.2.

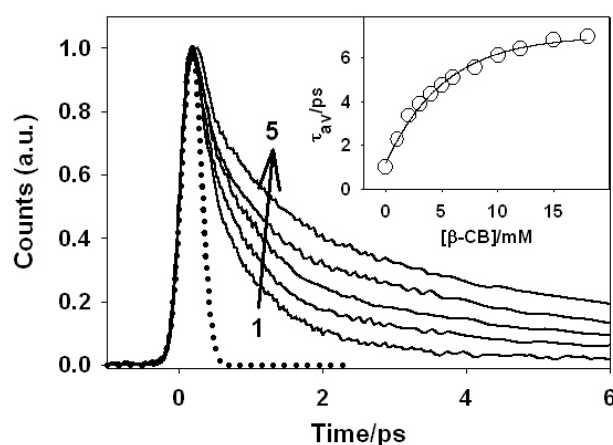


Figure 5.2. Fluorescence transient ($\lambda_{\text{ex}}=410$ nm, $\lambda_{\text{em}}=490$ nm) of ThT in water in the presence of different concentrations of β -CD: (1) 0.0, (2) 2.0, (3) 4.0, (4) 8.0 and (5) 18.0 mM. The dotted line shows the IRF. **Inset:** Variation in average lifetime (τ_{avg}) of ThT with increasing β -CD concentration.

It is to be noted from this fig that the average lifetime of ThT gradually increases with an increase in the β -CD concentration. Such an increase in the average lifetime in the presence of

β -CD suggests that the confinement of ThT in the β -CD cavity provides a restriction towards the torsional motion in the excited ThT molecule.

In bulk water, the bond twisting around the central C-C single bond of ThT take place in the LE state to form TICT state with a time constant of ~ 570 fs.²⁷⁹ To see how the encapsulation of the dye into β -CD cavity affect this LE to TICT state conversion, we have carried out detail wavelength dependent time-resolved fluorescence measurements for aqueous solution of ThT containing 15 mM β -CD and the results are shown in Figure 5.3. It is evident from this figure that the transient fluorescence decays are strongly dependent on the emission wavelengths. Similar wavelength dependent features in the emission decay traces have also been observed for ThT in other media (*cf.* Chapter 3 and 4).²⁷⁹ The average lifetime monitored at the emission maxima (490 nm) for ThT in 15 mM β -CD solution is found to be ~ 6.8 ps which is much longer than that observed in the bulk water (~ 1 ps).²⁷⁹ Similarly, at all the emission wavelengths the decay traces were found to be considerably slower as compared to that in bulk water.

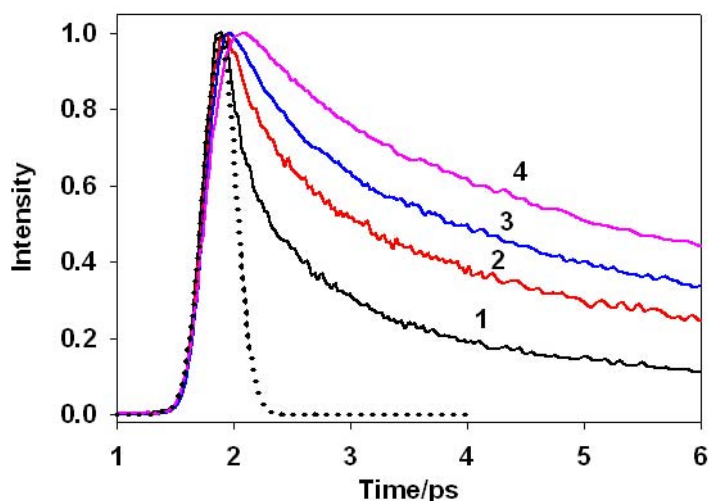


Figure 5.3. Fluorescence transient of ThT in aqueous solution containing 15 mM β -CD at different emission wavelengths: (1) 440 nm, (2) 490 nm, (3) 540 nm, (4) 600 nm. The dotted line shows the IRF.

To understand the torsional dynamics inside the nanocavity of β -CD, wavelength-dependent fluorescence decays were transformed to time-resolved emission spectra (TRES) following the

procedure proposed by Maroncelli and Fleming.³⁹ The TRES thus constructed for ThT in 15 mM aqueous β -CD solution are shown in Figure 5.4A. It is evident from this figure that along with a drastic reduction in the emission intensity, the emission spectra shows a gradual red shift with the time. For better realization of the observed shift in the emission frequency with time, the emission spectra at each time delay was normalized to the same peak intensity and is plotted in Figure 5.4B. The red shift in the emission spectra with time is now very clearly indicated in Figure 5.4B. Thus a Stokes' shift of $\sim 700\text{ cm}^{-1}$ have been observed for ThT in 15 mM β -CD solution within 20 ps time span following the photoexcitation process. To be mentioned that in bulk water, the corresponding dynamic Stokes' shift was observed to be $\sim 600\text{ cm}^{-1}$, quite similar to that observed in the presence of β -CD.

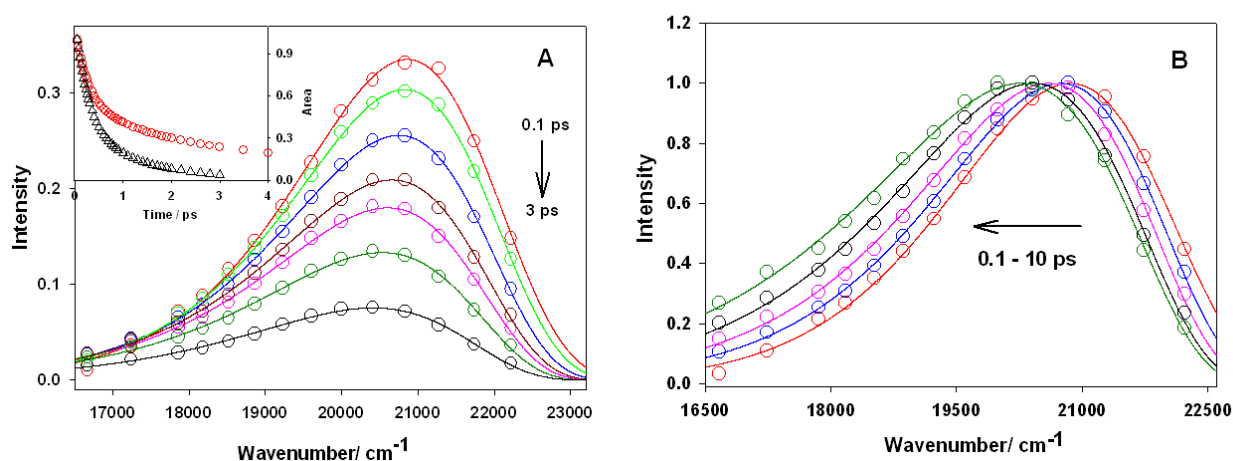


Figure 5.4. (A) Time-resolved emission spectrum (TRES) of ThT in 15 mM β -CD solution at different times. The circles are the experimental data points and the solid lines are lognormal fit to the data points. **Inset:** Variation in area under the curve with time: ThT in water (Δ), ThT in 15 mM β -CD solution (\circ). (B). Intensity normalized TRES at different times.

As mentioned earlier, the observed dynamic Stokes' shift for ThT is due to an intramolecular relaxation process in the excited state of ThT rather than the solvent relaxation process.^{279,293}

The possibility of solvent relaxation process in the present case was excluded on the basis of the substantial reduction in the population of the excited dye within experimental time window and lack of any significant solvatochromism for ThT molecule as discussed in Chapter 3.²⁷⁹

The inset of Figure 5.4A shows the variation in the integrated area under the emission spectra

for ThT in bulk water and in aqueous solution containing 15 mM β -CD. Thus, for ThT in β -CD solution, within 2 ps time window the area under the emission spectra decays by $\sim 70\%$. Though this reduction in the integrated area is relatively less compared to that observed for ThT in bulk water ($\sim 93\%$ within 2 ps time), yet the 70% reduction in the excited state population within 2 ps time span is significantly large to be accounted by the solvent relaxation process. Such large decrease in the area under the time-resolved emission spectra for ThT in different media is understood to be mainly due to the ultrafast intramolecular relaxation caused by the torsional motion in the excited ThT molecule. The fact that reduction in the population for the excited ThT in β -CD cavity is relatively less as compared to that in bulk water is a clear evidence of the retardation in the torsional motion of the excited dye inside the β -CD cavity as compared to that in bulk water. These results clearly indicate that the observed dynamic Stokes' shift in the present system is not due to the solvent relaxation process but due to intramolecular relaxation process. Such dynamic Stokes' shifts due to different intramolecular processes like bond-twisting, trans-cis isomerization etc. in the excited states of the dyes have in fact been reported in the literature.^{280-284,348} Thus, we infer that the observed dynamic Stokes' shift for ThT in β -CD nanocavity also originates from the intramolecular torsional relaxation process operative in the excited state of the dye.

A careful examination of Figure 5.4B reveals that along with the shift in the peak position there is a concomitant spectral broadening, especially at the red edge of the emission spectra while the shape in the blue edge remains effectively unchanged. Such changes in the spectral shape at one side of the spectra are also supported from the fact that the asymmetry parameter (b in equation 3.2; Chapter 3) for the present system changes from -0.35 at 0.1 ps to -0.50 at 20 ps. Similar spectral changes have been observed earlier for photoactive yellow protein where the chromophore based on coumaric acid shows the spectral broadening bearing the asymmetry at the red edge of the spectra.²⁸⁴ To unfold the reason behind the changes in the

spectral shape along with the changes in the emission frequency with time, the area under the emission spectra at different time were normalized and are plotted in Figure 5.5.

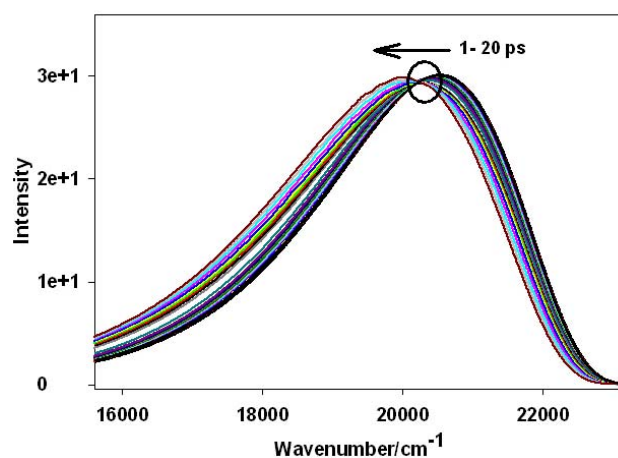


Figure 5.5. Time-resolved area normalized emission spectrum (TRANES) for ThT in 15 mM β -CD solution.

From this time-resolved area normalized emission spectra (TRANES)^{268,269} it is obvious that the emission spectra undergo a definite red shift with time. Another noteworthy observation from Figure 5.5 is the presence of an isoemissive point in the TRANES. The existence of such an isoemissive point in TRANES usually indicates the presence of two emitting species in the system.^{268,269} Appearance of such an isoemissive point in the TRANES have been observed for ThT in water medium and has been explained on the basis of the fact that due to the bond twisting process in the excited state a weakly emissive TICT state is formed at the expense of the LE state of the dye.²⁷⁹ Due to the formation of the weakly emissive TICT state, which is found to emit at longer wavelength region as compared to that of LE state,²⁹³ broadening at the red edge of the emission spectra takes place. This selective broadening at one side of the emission spectra thus results in the increase of the asymmetry parameter with time. Therefore, we can infer that the observed changes in the shape of the emission spectra for ThT in β -CD nanocavity are due to the formation of an emissive TICT state from the LE state of the dye.

The variation in the emission peak frequency with time is presented in Figure 5.6. The change in the peak frequency for ThT in bulk water is also shown in Figure 5.6 for comparison. It is evident from Figure 5.6 that the rate of change in the peak frequency for ThT

in β -CD is much slower as compared to that in bulk water. However, the change in peak frequency for ThT in β -CD follows a bi-exponential kinetics in contrast to the mono-exponential kinetics observed in case of bulk water.²⁷⁹ The time constants obtained in case of β -CD are 0.45 ps (42%) and 8.5 ps (58%). The shorter time constant obtained in the present system is very close to that obtained for bulk water (0.57 ps).²⁷⁹ Appearance of bi-exponential decay kinetics for the peak frequency in the present system can be explained on the basis of the fact that the binding constant value for the formation of the inclusion complex between ThT and β -CD is reasonably low. Due to such low binding constant, it is quite expected that a considerable amount of ThT molecule in this solution will not get associated with the β -CD and remain free in the bulk water phase. Thus, ThT molecules which are free in the bulk phase will undergo very fast bond twisting process as compared to those associated with the β -CD nanocavity. Thus, the shorter time constant (0.45 ps) obtained from the peak frequency variation could be assigned to those ThT molecules which are not associated with the β -CD cavity and the longer component is responsible for those ThT molecules that has formed inclusion complexes with the β -CD nanocavity. Considering the binding constant value of 78 M^{-1} , the percentage of ThT molecules that are expected to remain in the free state in the presence of 15 mM β -CD is $\sim 45\%$. This estimate is in good agreement with the percentage contribution of the shorter time constant (42%) observed from the analysis of the peak frequency shift with time. These results further confirm that the fast decay component in the peak frequency is mainly due to those ThT molecules that are not associated with the β -CD nanocavity.

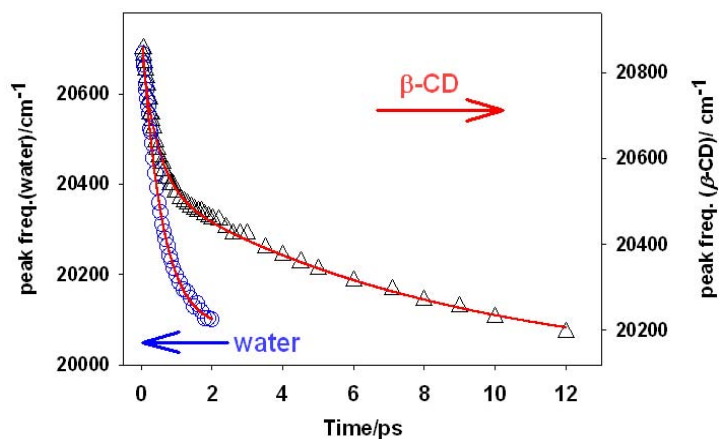


Figure 5.6. Variation in the peak frequency with time for ThT in water (O) and in 15 mM β -CD solution (Δ).

As already indicated there is a distinct spectral broadening for ThT- β CD system with time. To understand the underlying processes involved, the changes in the width of the emission spectra (FWHM) with time were also analyzed. The variation in the FWHM with time for ThT in β -CD solution is shown in Figure 5.7 along with those for ThT in bulk water. It is evident from this figure that the variation in the FWHM is much slower for ThT in β -CD solution as compared to that in bulk water. Like the time dependent changes in the peak frequency, the variation in the FWHM with time also follows a bi-exponential decay kinetics, with time constants of 0.48 ps (35 %) and 8.7 ps (65%). The fast time constant is very similar to that observed for the ThT in bulk water and can be attributed to the free ThT molecules. The longer time constant (8.7 ps) is seen to be similar to that obtained from the analysis of the changes in the peak frequency with time. The similar rate constants for the changes in the peak frequency and the FWHM of the emission spectra clearly indicate that these changes are due to the same intramolecular process, which we attribute to the bond twisting dynamics around the central C-C single bond in the excited ThT molecule. The longer time constant (8.5 ps) for the LE to TICT conversion in the β -CD solution as compared to that in bulk water (0.57 ps) clearly indicates that due to the formation of the inclusion complexes, the bond twisting process for ThT in the β -CD nanocavity is considerably hindered.

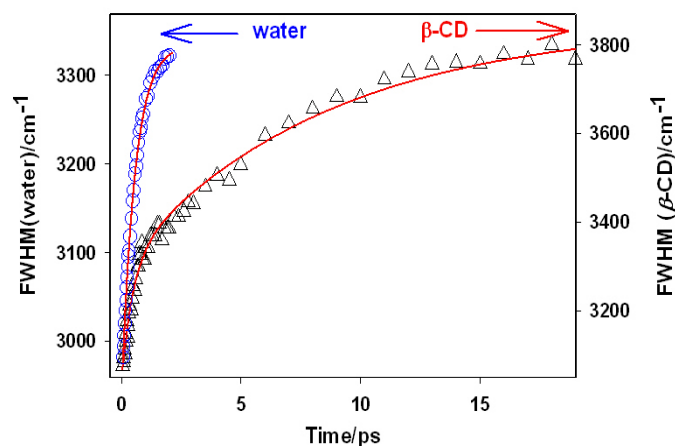


Figure 5.7. Variation in the width of the spectrum (FWHM) with time for ThT in water (O) and in 15 mM β -CD solution (Δ).

5.4. Conclusions

The excited-state torsional relaxation dynamics of ThT in β -CD nanocavity has been investigated following fluorescence up-conversion measurements. ThT forms 1:1 inclusion complex with β -CD and such inclusion complex formation affects the torsional relaxation process of the excited ThT dye leading to an enhancement of its fluorescence intensity. The longer average lifetime of ThT in the presence of β -CD also confirms the inclusion complex formation. TRES analysis indicates the presence of dynamic Stokes' shift as well as changes in the spectral shape with time. TRANES analysis shows the appearance of an isoemissive point, suggesting the formation of an emissive TICT state. The decay of the peak frequency, growth in the spectral width and the decrease in emission intensity were found to be slower in the presence of β -CD compared to that of the bulk water. These substantiate the effect of confinement of β -CD cavity on the ultrafast bond-twisting dynamics of the amyloid fibril sensing dye ThT. Present results shine light on the behavior of the potential biological probe molecule ThT in the confined environment in very short time scale and can be relevant to the behavior of many similar molecules in chemical and biological nanocavity.

Chapter 6

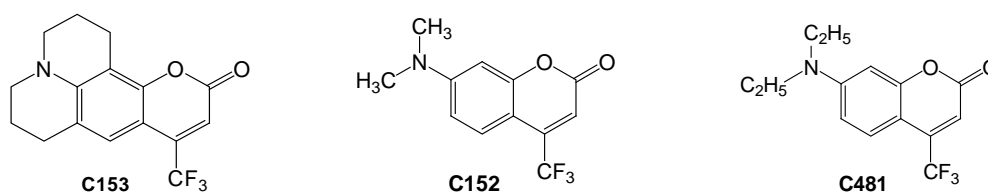
Quantitative Distinction between Competing Intramolecular Bond Twisting & Solvent Relaxation Dynamics

6.1. Introduction

Dynamic Stokes' shift measurements for solvent relaxation study have been applied extensively to understand the structure and dynamics of different chemical and biological systems.³⁴⁹⁻³⁵¹ For example, this method has been used to understand the nature of water molecules in different microheterogeneous media, like micelles,^{352,353} vesicles,³⁵⁴ and also in bio-molecules, like DNA³⁵⁵⁻³⁵⁷ and proteins.^{358,359} Wide varieties of fluorescence probes have been used to understand the solvent relaxation dynamics and consequently the nature of the local environments. A judicious choice of a fluorescent probe for solvent relaxation studies largely depends on the nature of the microenvironment under investigation. A major bottleneck in studying solvent relaxation dynamics with large probe molecules is the interference of several intramolecular processes in the excited probe that takes place in the similar time-scale of the solvent relaxation dynamics. The competing intramolecular processes that can significantly influence the solvent relaxation measurements are twisting of a functional group around a bond, cis-trans isomerization, etc. This poses a tremendous challenge to experimentalists in distinguishing various contributions of the different relaxation processes on the dynamic Stokes' shift. In order to understand the actual dynamics of the solvent relaxation

process, it is very essential to separate out the contribution of the interfering intramolecular processes from the solvent relaxation process.

The aim of the present study is to find out a methodology to quantitatively distinguish and separate out the effect of such competing intramolecular processes from the solvent relaxation process. To demonstrate this methodology, ultrafast fluorescence transient measurements have been carried out in acetonitrile solution with three different coumarin dyes, namely C153, C481 and C152 (*cf.* Scheme 6.1 for molecular structures), as probes. Coumarin dyes have been extensively used as fluorescence probes for solvent relaxation studies, primarily because of the large Stokes' shifts and strong solvent polarity dependent fluorescence properties of these molecules.³⁶⁰ Among these dyes, C153 is the most popular probe for solvent relaxation studies,^{40,361} because its rigid molecular structure ensures the absence of any interfering intramolecular relaxation process.



Scheme 6.1. Molecular Structure of the dyes

Unlike C153, however, the C481 and C152 dyes can participate in a fast twisting motion involving their free amino group and it can compete with the solvent relaxation process. Detailed photophysical studies in different organic solvents indicate that in polar solvents the excited states of C481 and C152 molecules decay much faster as compared to C153.³⁶²⁻³⁶⁵ This fast decay in C481 and C152 has been attributed to nonradiative transition due to twisting of the N,N-dialkyl groups around the carbon-nitrogen bond (*cf.* Scheme 6.1) in the excited states. Unlike, C481 and C152, no such bond twisting is possible for C153, due to the presence of rigid julolidyl group in the latter molecule. This additional bond twisting process in the excited state of C481 and C152 can modulate the measured solvent relaxation times from the dynamic

Stokes' shift measurements. Acetonitrile have been selected as solvent because its polarity is sufficient to induce bond twisting process in the excited states of C481 and C152.³⁶⁵ It has been reported in the literature that the solvent relaxation time measured with C152 is much faster as compared to C153.³⁶⁶ However, the reason for this faster solvent relaxation with C152 has not been discussed explicitly. In the present study time-resolved fluorescence transient measurements have been carried out to differentiate two competing processes, namely intramolecular bond twisting process and solvent relaxation process. A method has been proposed for the first time to quantitatively extract the ultrafast time constant for such an intramolecular process that is hidden or mingled up with the solvent relaxation process.

6.2. Experiments and Methods

Steady-state fluorescence measurements were made in Hitachi spectrofluorimeter (model F-4500). The emission spectra were corrected for the wavelength dependent instrument responses. All measurements were made at magic angle condition. All samples were excited with 400 nm light. Time-resolved fluorescence measurements were carried out using a femtosecond fluorescence upconversion instrument discussed earlier (*cf.* Chapter 2). In the present study the second harmonic of Ti-sapphire laser pulses (410 nm, 50 fs, 88 MHz) was used for the sample excitation. All coumarin dyes were from Exciton and used as received. Spectroscopic grade acetonitrile from Spectrochem, India was used as received.

6.3. Results & Discussion

Fluorescence transient decays at different wavelength intervals were measured using fluorescence upconversion technique for all three dyes. Representative fluorescence decays measured for C153 in acetonitrile solvent at the blue and red side of the emission spectrum are shown in Figure 6.1. It is evident from this figure that the transient fluorescence decay is strongly dependent on the wavelength at which it has been monitored. All the transient decays

can be fitted to a multi-exponential function convoluted to the instrument response function (IRF). At shorter wavelength, the transient decay has a very short time component, which increases with an increase in the monitoring wavelength. At red side of the fluorescence spectrum, the fast decay component is absent and it is replaced by a fast rise component. Thus, for the fluorescence transients, the decay components (both time constant and amplitude) are strongly wavelength dependent. It is reported in the literature that this wavelength dependent decay of the C153 in polar solvents, including acetonitrile, is due to the time dependent motion of the solvent molecules around the photoexcited probe molecule.^{367,368} Similar observations have also been made with the other two coumarin dyes, namely C481 and C152.

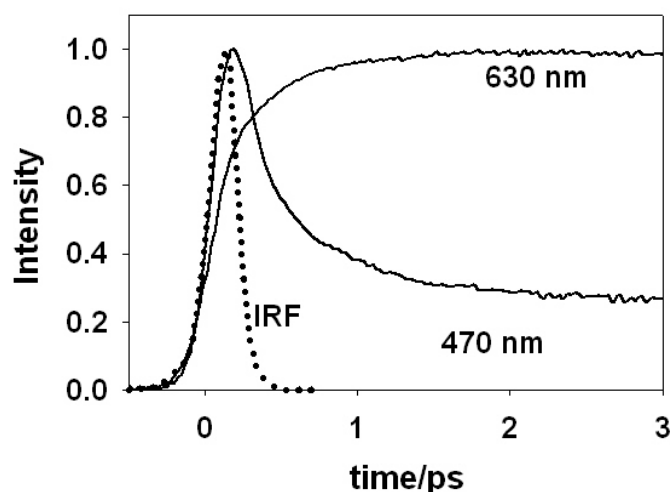


Figure 6.1. Transient fluorescence decay for C153 at 470 and 630 nm. The dotted line shows the instrument response function (IRF).

Time-resolved fluorescence spectra for all three dyes have been reconstructed from transient decays following the method proposed by Maroncelli and Flemming.³⁶⁷ Reconstructed time-resolved spectra thus obtained for three dyes are shown in the Figure 6.2. It is evident from this figure that for all three dyes the emission maxima shift to lower frequency with time along with a concomitant decrease in the emission intensity.

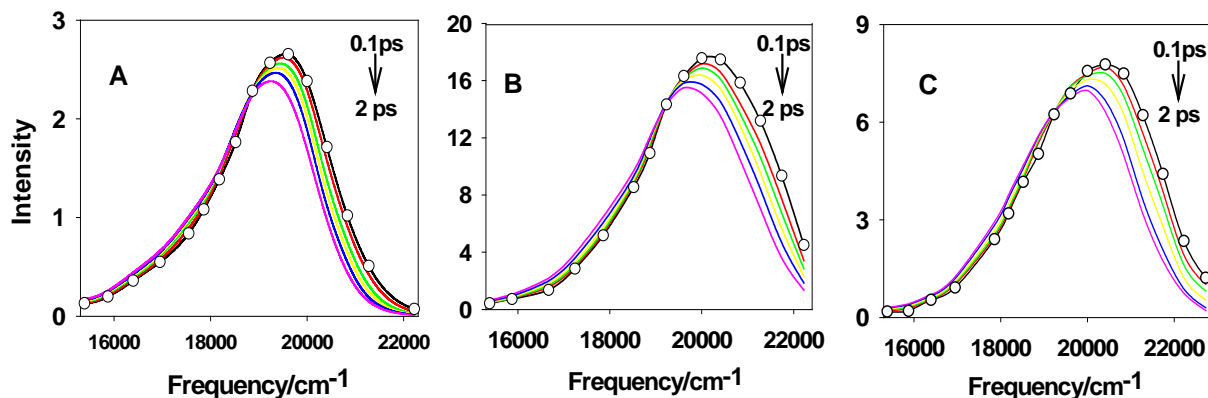


Figure 6.2. Reconstructed time-resolved fluorescence spectra for (A) C153, (B) C481 and (C) C152. Spectra shown are for time 0.1-2 ps. The points in each panel indicate the wavenumbers where the transient emissions are recorded.

To quantify the temporal changes of the emission frequency, the mean frequency or first moments (ω_1) of these transient spectra, as calculated by using eq. 6.1, were correlated with time.

$$\omega_1 = \frac{1}{\omega_0} \int_0^{\infty} \nu I(\nu) d\nu \quad (6.1)$$

where,

$$\omega_0 = \int_0^{\infty} I(\nu) d\nu \quad (6.2)$$

Figure 6.3 shows the variation of the mean frequency of the transient spectra with time for all three dyes. The changes in the mean frequency for C153, according to literature, are solely due to solvent relaxation process.^{367,368} Observed changes in the mean frequency with time for C153 was fitted with a bi-exponential function and the two solvent relaxation time constants thus estimated are 0.39 (45%) and 1.1 (55%) ps. The average solvent relaxation time is accordingly calculated as ~ 0.78 ps, which is in good agreement with the reported value.³⁶⁸ The appearance of the bi-exponential nature of the frequency shift with time has been noted earlier for different other solvents.³⁶⁶⁻³⁶⁹ The non-single exponential nature of the frequency shifts is due to the differences in the responses of the solvent molecules that are directly in contact to the probe than those situated away from the probe. Due to molecular nature of the solvent and

the probe, the dielectric response is different for these two types of solvent molecules. For this reason, the Debye nature of the dielectric response of the solvent is not valid in real systems and they show non-single exponential nature of the solvent responses.

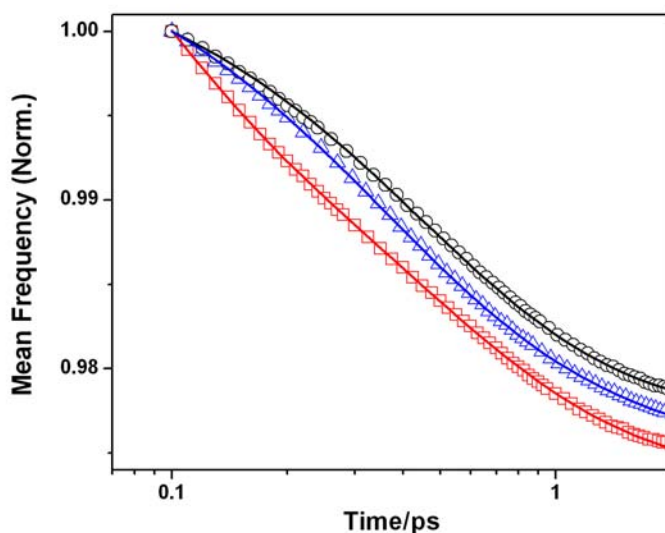


Figure 6.3. Change in the mean frequency of the transient emissions with time for (○) C153, (□) C481 and (△) C152 in acetonitrile solution. Points are calculated from the reconstructed spectra and the solid lines are the multi-exponential fitting to the data points .

The standard solvent relaxation theory predicts that the frequency of the emission spectra will shift with time without changing the shape of the spectra.³⁷⁰⁻³⁷⁴ To check this prediction all the time-resolved emission spectra of C153 have been plotted in Figure 6.4A after removing the frequency shift with time and normalizing the area under each of the emission spectra. It is evident from Figure 6.4A that the spectral shapes do not change with time for C153 dye, which is in accordance with the standard solvent relaxation theory. From these results we can infer that the observed change in the mean frequency for C153 in acetonitrile is solely associated with the solvent relaxation process. Following the procedure mentioned above for C153, when the variation of mean frequency with time for C481 and C152 are analyzed, it results in the average solvent relaxation times as about 0.47 and 0.62 ps, respectively, which are significantly shorter compared to that obtained with C153.

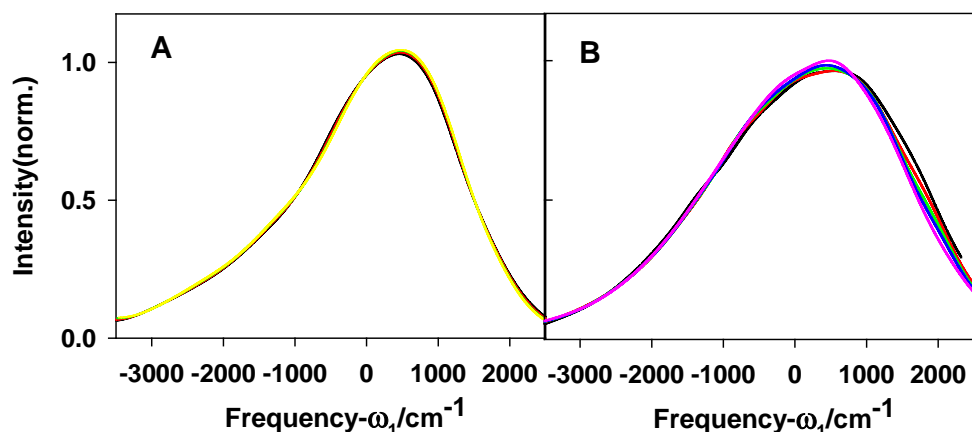


Figure 6.4. Reconstructed transient fluorescence spectrum for (A) C153 and (B) C152 at different times (0.1-2 ps). Each spectrum have been moved along frequency axis to remove the time dependent spectral shift and the area under all spectra have been normalized for comparison.

These apparently rapid changes in the mean frequency with time for C481 and C152 cannot be explained on the basis of the solvent relaxation process alone. According to continuum dielectric theory,³⁷⁵⁻³⁷⁸ the motion of solvent molecules around a probe is independent of the nature of the probe used and solely depends on the nature of the solvent molecules involved. Chapman et al.³⁷² have measured the solvent relaxation times with 16 different probes in 1-propanol solution and observed that the solvent relaxation times measured with 11 out of 16 probes (including C153 and C152) are similar as expected from continuum dielectric theory. For the remaining five probes, however, the solvent relaxation times are found to be shorter by about 2-fold and have been explained due to specific H-bonding interaction of these probes with the solvent molecules. Since a similar specific interaction is not expected in the present systems, the differences observed in the changes of the mean frequencies for the three dyes studied must be related to some other factors than the specific solute-solvent interaction.

As mentioned earlier, presence of a fast bond twisting process in the excited state of a probe can interfere with the solvent relaxation process and accordingly an apparently rapid dynamics of the fluorescence Stokes' shifts can be observed. Thus, the apparently faster solvent relaxation rate with C481 and C152 dyes is attributed to the interference of the fast

intramolecular relaxation to the solvent relaxation process. To check how this fast intramolecular bond twisting process can affect the observed changes in the emission mean frequency we have compared the shape of the emission spectra for C152 and C481 at different times. Figure 6.4B shows such a plot for C152, where the emission spectra have been plotted after removing the frequency shift with time and normalizing the area under the emission curve at each time. It is clearly evident from Figure 6.4B that in contrary to the standard solvent relaxation theory, the shapes of the emission spectra do change with time for C152. Similar observation has also been made for C481. To check how the spectral shape for these two dyes changes with time we have also plotted the width (FWHM) of the emission spectra for these two dyes at different times in Figure 6.5. It is clearly evident from Figure 6.5 that the shape of the spectra becomes narrower with time for C152 and C481. The spectral shape changes up to ~ 0.4 ps and 0.8 ps for C481 and C152, respectively, and after that the shape of the spectrum remains almost unchanged with time as predicted by the standard solvent relaxation theory. This clearly indicates that beside the solvent relaxation process, there is an additional process that takes place in these two dyes causing the observed changes in the shape of the spectra in the initial times. The changes in the spectral shape due to the twisting of a chemical bond and subsequent formation of a rotamer have been reported in the literature.³⁷⁹

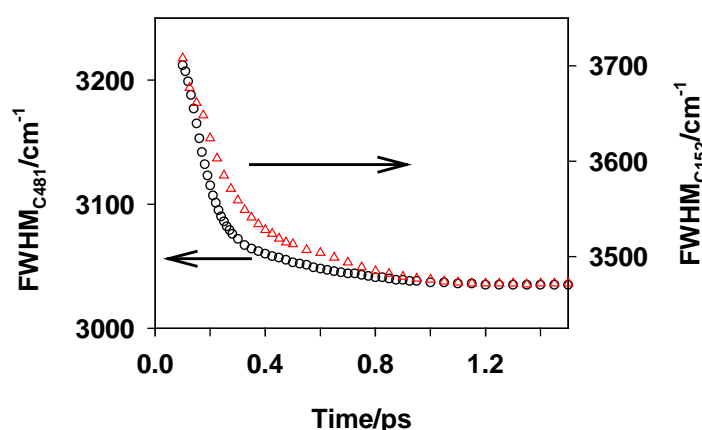


Figure 6.5. Changes in the spectral width of the emission spectra at different times for (○) C481 and (△) C152.

Another interesting point to be noted from Figure 6.4B is that the changes in the spectral shape mostly occur at the blue side of the emission spectra. As the intensity at the blue side of the spectra decreases, the mean frequency of the spectra moves faster to the red side of the spectra. Because of this we observe an increase in the rate of mean frequency shift for C481 and C152 compared to C153 dye. It is also evident from Figure 6.5 that the change in the spectral width for C481 is much faster than that for C152. Because of these, the change in the mean frequency is also found to be faster for C481 than C152 and hence an apparently faster solvent relaxation.

In the present circumstances with C481 and C152 dyes, since the effect of intramolecular bond twisting and solvent relaxation processes are mingled up with the dynamics Stokes' shift, resolving the dynamics of these two relaxation processes is not straight forward. In fact, in the literature, so far no clear methodology has been suggested to resolve the dynamics of such two interfering processes. In the present study, to extract the rate constant for the bond twisting process in C481 and C152, the total fluorescence intensity was plotted against time as shown in Figure 6.6. The total fluorescence intensity, $I(t)$, was calculated by measuring the area under the fluorescence spectra at different times. It is seen that $I(t)$ does not decay exponentially with time. Such non-exponential decay of the fluorescence intensity along with the changes in the mean frequency for C153 in 1-propanol at lower temperature has been explained by Agmon on the basis of the inhomogeneous solvent distribution around the excited dye.³⁸⁰ Their results are supported by the fact that the width of the transient emission spectra decreases with time due to distribution of the lifetimes resulting from the inhomogeneity in the system. However, in the present case it is seen that the shape of the transient emission spectra of C153 do not change with time (*cf.* Figure 6.4A). This eliminates the possibility of inhomogeneity in the present systems. The appearance of the non-exponential decay in $I(t)$, for the present systems, can be easily explained on the basis of the time-dependent shift in the emission frequency. One of the consequences of Einstein's equation for radiative transition is that the rate of this process depends on the emission frequency. Because of the non-equilibrium solvent relaxation in the

excited state, the emission frequency is a function of time. This makes the radiative decay rate, k_r , also time dependent and it should follow a relation like,³⁸¹

$$k_r(t) \propto \langle \nu^3(t) \rangle \quad (6.3)$$

where,

$$\langle \nu^3(t) \rangle = \frac{\int I(\nu, t) d\nu}{\int I(\nu, t) d\nu / \nu^3(t)} \quad (6.4)$$

It is evident from eq. 6.3 that if the solvent relaxation process causes an observable shift in the emission spectra, one would expect that k_r should also be time-dependent accordingly. On the basis of this model the variation of the total fluorescence intensity can be expressed by the following equation.³⁸²

$$I(t) = Ak_r(t) \exp[-k_{nr}t - \int_0^t k_r(\tau) d\tau] \quad (6.5)$$

where, A is the proportionality constant and k_{nr} is the nonradiative decay rate constant. In eq. 6.5 k_{nr} denotes the nonradiative intramolecular conversion from S_1 to S_0 state of the dye. Detail photophysical studies show that this S_1 - S_0 nonradiative process are very slow ($\sim 1 \times 10^8 \text{ s}^{-1}$)³⁶² for all the three dyes used in the present study as compared to our experimental time window. Thus, we may neglect the effect of k_{nr} on the fluorescence intensity decay for the three dyes in the present time scales of measurements. Maroncelli et al. have also shown that eq. 6.5 can be fitted suitably for some coumarin dyes in *i*-propanol after neglecting the contribution of k_{nr} .³⁸²

Our experimental data was fitted using eq. 6.5 (without the k_{nr} term) by a least square fitting method and the fitted curves are shown in Figure 6.6. It is seen that the decay of $I(t)$ for C153 can be fitted quite satisfactorily with eq. 6.5. This result reinforces that the observed non-exponential decay of $I(t)$ for C153 is solely due to the solvent relaxation induced shift in the emission frequency. However, it is evident from Figure 6.6 that the experimental data for C481 and C152 do not fit well with eq. 6.5.

As mentioned earlier, the twisting of the amino groups in the excited states of C481 and C152 dyes, results in the formation of dark twisted intramolecular charge transfer (TICT) states.^{17,18} Formation of these dark states with the twisting of the amino group results in the decrease of the transition dipole moment and hence a decrease in the observed emission intensity. To incorporate this effect, eq. 6.5 has to be modified as in eq. 6.6.

$$I(t) = Ak_r(t) \exp\left[-\int_0^t k_r(\tau) d\tau\right] + B \exp(-kt) \quad (6.6)$$

where B is a pre-exponential term and k is the rate constant for the additional decay process, i.e. the bond twisting process.

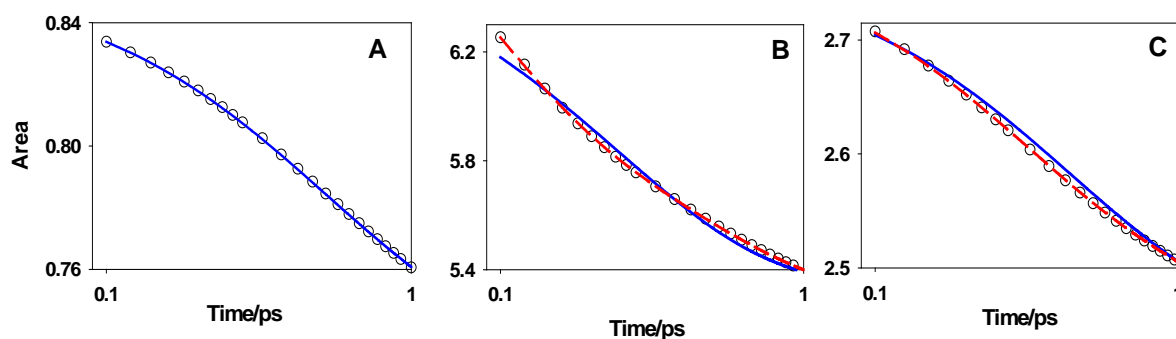


Figure 6.6. Changes in the integrated intensity of (A) C153, (B) C481 and (C) C152 as a function of time. The solid lines are the fitted data according to the eq. 6.5. The dashed lines for coumarin-481 and coumarin-152 are the fitted data according to the eq. 6.6

The experimental data for C481 and C152 have been fitted with eq. 6.6 and the results are shown in Figure 6.6. It is very evident from this figure that the introduction of the additional exponential decay term in eq. 6.6 satisfactorily fit the experimental data for C481 and C152. These results confirm that the observed change in the total intensity for C481 and C152 is a consequence of the combined effect of two processes, i.e. the intramolecular twisting process and the solvent relaxation process. The decay times ($1/k$) for the twisting processes thus estimated are 70 & 230 fs for C481 and C152, respectively.

The rate constant for the twisting process thus measured can be used to estimate the solvent relaxation time from the experimental frequency shift data obtained with C481 and C152. As it is mentioned earlier, due to the presence of bond twisting process, the apparent

solvent relaxation time becomes faster for these dyes. The variation of the mean frequency with time for these two dyes was fitted with a tri exponential function, where one of the decay time was fixed to that obtained for the twisting process. After using this methodology the other two time constants for solvent relaxation process are obtained as 0.45 ps (49%), 1.35 ps (39%) and 0.33 ps (26%), 1.1 ps (65%), respectively, for C481 and C152. The average solvent relaxation times thus calculated are 0.75 and 0.80 ps, respectively. These estimated solvent relaxation times are in good agreement with that obtained with C153 and also to those reported in the literature in acetonitrile solvent.³⁶⁸ Thus, using this methodology, as discussed in this article, it is possible to distinguish two competing ultrafast processes that mutually interfere with each other to affect the observed spectral or kinetic measurements. It is also possible to quantitatively extract the rate constant for the individual processes by adopting this methodology.

From the present results it is indicated that the bond twisting process for C481 is much faster than that of C152. This is in fact expected from the structural point of view of the two dyes. In case of C481, the 7-amino group has two ethyl substituents, which are stronger electron donating in nature as compared to methyl substituents in C152. This makes the twisted charge transfer state energetically more stable for C481 than for C152. Moreover, formation of the twisted state releases more steric hindrance in C481 than in C152, due to the bulkier N-ethyl substituents in the former dye compared to the N-methyl substituents in the latter. It is thus realized that the better stabilization of the twisted state in C481 drives the bond twisting process to occur faster compared to C152. This is also in accordance with the results obtained from photophysical studies of the two dyes in different solvents.³⁶⁵ The fluorescence quantum yield for C481 and C152 in acetonitrile solution are reported to be 0.08 and 0.22 respectively.³⁶⁵ These fluorescence quantum yield are much lower compared to those of the other coumarin dyes. This lowering of the quantum yield for C481 and C152 is attributed to the twisted state mediated nonradiative de-excitation channel. These fluorescence quantum

yield results also indicate that the formation of the twisted state is more favorable for C481 as compared to C152, an inference similar to that made from the present study.

6.4. Conclusion

In brief, present results indicate that the intramolecular bond twisting process largely interfere with the dynamic Stokes' shift for C481 and C152, causing the observed solvent relaxation dynamics apparently faster. Following the procedure of time dependent changes in the integrated intensity of the time-resolved emission spectra and using Einstein's theory of radiative decay rate, we are able to separate out the dynamics of the bond twisting process from the solvent relaxation process. This procedure can be applied to differentiate and quantitatively estimate the rate of an intramolecular process that is otherwise hidden or mingled up with the solvent relaxation process.

Chapter 7

Effect of Electrostatic Interaction on the Probe Migration in Polymer-Surfactant Supramolecular Assembly: A Solvent and Rotational Relaxation Study

7.1. Introduction

Pluronics are the triblock copolymers made up of poly ethyleneoxide (EO) and poly propyleneoxide (PO) blocks with general molecular formula $(EO)_n-(PO)_m-(EO)_n$. These water soluble non-ionic surfactants have attracted considerable attention in the last two decades, partly because of their complex behavior in solution^{141-146,156,157} and partly because of their wide range of industrial applications, as detergent, lubricant and emulsifier.^{147-153,383,384} Their unique behavior in aqueous solution and their low toxicity have made these polymers highly useful in many pharmaceutical formulations.^{147,149-153,383} Because of the formation of microheterogeneous media of varying physical dimensions and characteristics, these polymers have also been used extensively for the fabrication of different nanostructures.³⁸⁵⁻³⁸⁸

Besides the absence of the polar head groups, unlike in the conventional surfactants, pluronics also form micelles in aqueous solution due to the differential solubility characteristics of EO and PO units in water.^{141-144,146,156,157,164} However, these class of polymers form micelles in water only above a certain concentration, known as the critical micelle concentration (CMC) and also above a certain temperature, known as the critical micellar

temperature (CMT). Because of the differences in the solubility of the EO and PO units, the CMT of a pluronic largely depends on its composition, or more specifically on its EO/PO ratio. As the water solubility of EO is higher than that of PO, CMT of a pluronic increases with an increase in the EO/PO ratio. For example the CMT of 5% w/v solution of two pluronics, F88 (n=103 & m=39) and P123 (n=20 & m=70), are 30.5 and 12.5 °C, respectively.¹⁴² Note that the EO/PO ratio for F88 and P123 are 2.64 and 0.29, respectively. This indicates that a pluronic with lower value of the EO/PO ratio favours the micellization process of the polymer. The micellization process and the structure of pluronic micelles have been studied extensively using different techniques, like neutron scattering,^{144,145,162,163} X-ray scattering,¹⁶⁵ light scattering,^{146,157,162,163,165,166} absorption¹⁶⁷ and fluorescence measurements.^{142,168,169} It is understood that pluronic micelles are formed with a water free hydrophobic core consisting of the PO blocks, which is surrounded by the outer shell of hydrated EO blocks, commonly known as the corona region. Though extensive studies have been carried out on the structural aspects of these micellar systems, studies on the dynamical processes in these micelles are very limited. Using fluorescence anisotropy measurements, Dutt et al. have recently reported the results on the rotational dynamics of a solubilized probe in different phases of the pluronic micelles.^{170-173,389} Grant et al. have demonstrated from anisotropy measurements that a suitable molecular probe can be used as a local reporter for the different regions of the copolymer micelles.^{175,176} Relaxation of the water molecules in different regions of pluronic micelles have recently been reported by Bhattacharya et al.¹⁷⁷⁻¹⁷⁹ and Kumbhakar et al.¹⁸⁰⁻¹⁸² All these studies indicate that the dynamical processes in these micelles largely depend on the EO/PO ratios of the polymers.

In several industrial applications, pluronics are often used in combination with low molecular weight ionic surfactants.^{183,184} This feature has prompted experimental studies on the solution behavior of these mixed surfactant systems.^{185,186} Presence of two different classes of surfactants results in the formation of complex microheterogeneous systems, whose properties

and solution behavior are essential to be known to use them in a formulation. Interaction of pluronics with low molecular weight ionic surfactants like sodium dodecyl sulphate (SDS), cetyl trimethyl ammonium chloride (CTAC), etc. have been studied quite extensively by using light scattering,^{162,165,166} neutron scattering,¹⁶² and calorimetric methods.^{166,187-189} These studies show that the pluronic micelles form unique supramolecular assemblies in the presence of an ionic surfactant, for example, SDS.^{162,165,166} In these supramolecular assemblies, it is understood that the hydrophobic chains of the ionic surfactant molecules are dissolved in the core of the pluronic micelles and the charged head groups of the surfactants are placed at the peripheral region of the core, projecting into the hydrated corona region of the micelles.¹⁶² Because of this unique structure of these assemblies, a charged layer is developed inside these micelles. Accordingly, any solute having a charge opposite to that of the charged layer inside these supramolecular assemblies, can experience an electrostatic attraction towards the core-corona interface of the micelles. The extent of the electrostatic attraction will naturally depend on the concentration of the ionic-surfactant in these systems. Due to the presence of such an electrostatic attraction, the solute can move from the surface to the interior of the micelle.

In most of the applications of microheterogeneous media, a solute is dissolved in the micellar phase and the effectiveness of the dissolved solute for a desired process largely depends on the physical and chemical properties of the species in the micellar media. As pluronics can be obtained with wide range of EO/PO ratios,^{142,156,157} they can form micelles with wide range of dimensions of their core and the corona regions. These systems can thus provide a wide range of microenvironments for the dissolved solutes. Because of the availability of wide range of microenvironments in these micelles, the solutes may also have quite different physical and chemical properties depending on their locations in the micelle. Thus, by changing the position of a solute in these micelles, it is possible to modulate the physical as well as the chemical properties of the solute in these microheterogeneous systems. In the present work we have studied the effect of ionic surfactant on the localization site of a

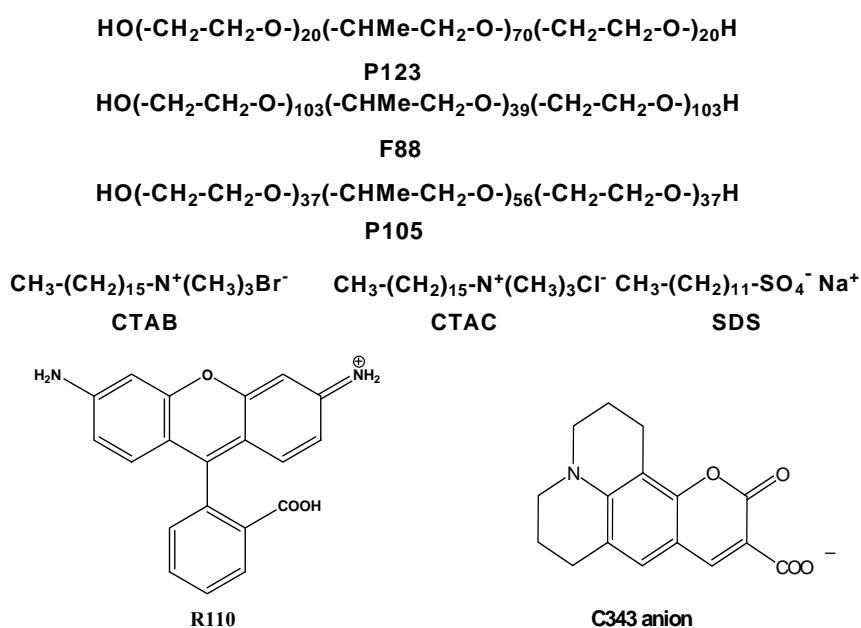
solubilized molecule in a polymer-surfactant supramolecular assembly. Our aim is to see if the location of the solute in the micelle can be changed by changing the polymer-surfactant composition of the supramolecular systems. Additionally, we also investigate how the photophysical properties of the solubilized dye and the structure of water molecules around the dye in the micelle change with a change in the dye location in the supramolecular system. For this purpose, we have used pluronic P123 (EO₂₀-PO₇₀-EO₂₀), F88 (EO₁₀₃-PO₃₉-EO₁₀₃) and P105 (EO₃₇-PO₅₆-EO₃₇) as the copolymers, CTAC and CTAB (Cetyl trimethyl ammonium bromide) as the surfactants and coumarin-343 (C343, *cf.* Scheme 7.1 for molecular structure) as the molecular probe.

7.2. Experiments and Methods

P123 (EO₂₀-PO₇₀-EO₂₀), P105 (EO₃₇-PO₅₆-EO₃₇), CTAC and CTAB were obtained from Aldrich. F88 (EO₁₀₃-PO₃₉-EO₁₀₃) was a gift from BASF Corporation, Edison, New Jersey, USA. C343 was purchased from Exciton and was used as received. Stock solution of block copolymers were prepared by taking 0.1 gm of solid polymer for P123 and 0.05 gm of solid polymer for F88 and P105 per ml of nanopure water (conductivity <0.1 μS cm⁻¹), obtained from a Millipore Gradient A10 system. The solution was stirred for about 24 hours with a magnetic stirrer. To make polymer-surfactant supramolecular system, requisite amount of surfactant solution was added to the polymer solution maintaining the polymer concentration same in all the cases. C343 was added directly to the polymer solution and stirred for 4-6 hours. Concentration of the dye in the polymer solution was kept very low (1-2.5 μM as calculated from the absorbance of the dye) so that the possibility of having more than one dye in a micelle is negligible. All experiments with P123 were carried out at 25⁰C. It was shown earlier that the critical micellar temperature (CMT) for 5% w/v F88 is ~35⁰C,^{175,176,390} and thus, all the experiments with F88 were carried out at 40⁰C to ensure complete micellization. Similarly all experiments with P105 (CMT for 5% w/v is 20.3⁰C³⁹¹) were carried out at 30⁰C to ensure the

complete micellization of the polymer. Molecular structures of the chemicals used in the present study are given in scheme 7.1.

Ground-state absorption and steady-state fluorescence measurements were carried out using a Shimadzu spectrophotometer, (model UV-160A) and a Hitachi spectrofluorimeter, (model F-4500) respectively. The emission spectra were corrected for the wavelength dependent instrument responses as discussed in Chapter 2 (*cf.* Section 2.3.1).



Scheme 7.1. Molecular structures of chemicals used in the present study

The time-resolved fluorescence measurements were carried out using a TCSPC spectrometer from IBH, UK (*cf.* Chapter 2 section 2.4.1). A 408 nm diode laser (1 MHz repetition rate) was used for sample excitation. The instrument response function (IRF) was measured by collecting the scattered excitation light from the suspended TiO_2 particles in water. The IRF thus measured was ~ 100 ps with an MCP-PMT detector & ~ 230 ps with a PMT based detector. For solvation dynamics studies, fluorescence transients were collected at 10 nm interval to cover the entire range of the fluorescence spectrum of the dye. All the fluorescence transients were collected at magic angle (54.7°) as discussed in Chapter 2. Time-

resolved fluorescence anisotropy was measured with the procedure given in Chapter 2. The temperature of the solution was controlled by using a thermoelectric controller (model DS) from IBH, UK.

Small Angle Neutron Scattering (SANS) measurements were carried out using the facility at DHRUVA reactor, Trombay, INDIA. The mean incident wavelength (λ) of the neutron was 5.2 Å with $\Delta\lambda/\lambda = 15\%$. The scattered neutrons were measured for the scattering vector (q) range of 0.02-0.3 Å⁻¹. The measured SANS data were corrected for the background, the empty cell contribution and the transmission, and were presented on an absolute scale using the standard protocols. Correction due to the instrumental smearing was also taken into account throughout the data analysis. All SANS measurements were carried out in D₂O media.

The differential pulse polarography (DPP) study was carried out using a Eco chemie potentiostat, AUTOLAB-100, fitted with the VA663 stand. Details of the DPP measurements are discussed in Chapter 2.

7.3. Results and Discussion

7.3.1. P123-CTAC system

7.3.1.1. Ground-state absorption and steady-state fluorescence studies

The present probe, C343, can exist either in the neutral or in the anionic form, depending on the pH of the medium. To characterize the prototropic form of C343 in P123 micellar solution, both ground-state absorption and steady-state emission spectra of the dye were first recorded at different pH in aqueous solution. Figure 7.1 shows the absorption and emission spectra of C343 at different pH in aqueous solution along with those in P123 micelle for comparison. At pH 3, the absorption and the emission maxima of C343 appear at 450 nm and 488 nm, respectively. Comparing with the literature reports, it is evident that at pH ~3, the dye C343 exists in its neutral form.⁹⁸ The absorption and emission maxima of C343 in aqueous solution

at pH 9.5 appear at 424 nm and 485 nm, respectively. These values match very nicely with the reported absorption and emission peak positions for the anionic form of the dye.⁹⁸ This implies that the dye C343 exists in its anionic form at pH 9.5. Absorption and emission spectra of C343 dye in P123 micellar solution are also shown in Figure 7.1 for comparison. It is evident from Figure 7.1 that the absorption and emission characteristics of C343 dye in P123 micellar solution are very similar to those of the anionic form of the dye in aqueous solution. From the present results it can be inferred that in P123 micellar solution the dye C343 mainly exists in its anionic form. It is to be noted that the absorption and emission spectra of C343 in water at neutral pH also indicate that the dye preferentially exists in its anionic form. Through detailed photophysical studies, Levinger et al. have shown that in a reverse micelle also the dye C343 exclusively exists in its anionic form.^{96,98,99,392}

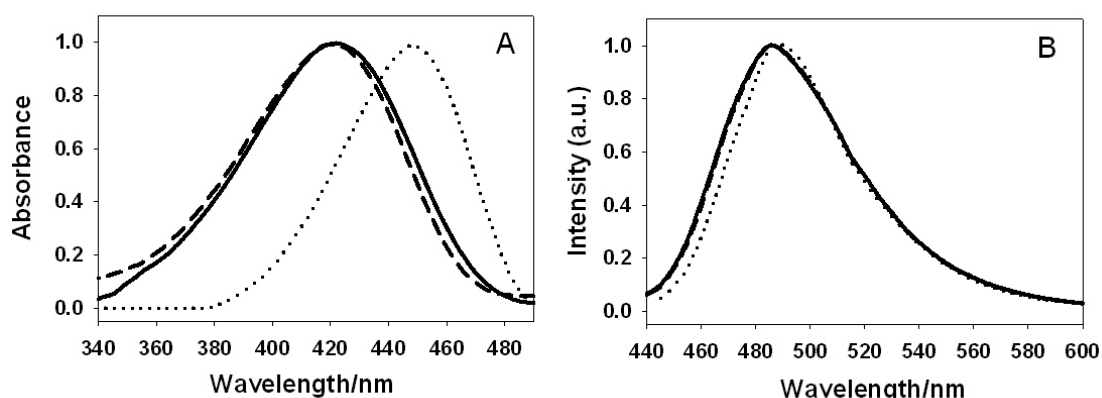


Figure 7.1. Normalized absorption (A) and emission (B) spectra of C343 at different pH in water, pH=3.5 (.....), pH=9.5 (-----), and in P123 micellar solution (—).

Surfactant induced changes in the pK_a values have been reported in the literature.³⁹³ So to confirm whether the pK_a of the probe changes in the present micellar system, we have also carried out pH dependent absorption studies in neat water, in P123 micellar solution and in P123-CTAC mixed micellar solution with [CTAC]/[P123] ratio of ~ 0.4 . The absorbance vs pH plots for the peak position of the neutral form of C343 in these three media are shown in Figure 7.2.

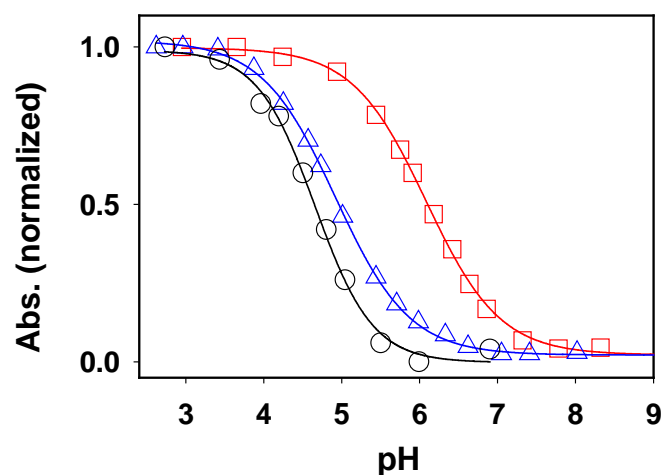


Figure 7.2. The absorbance vs pH plots for the peak position of the neutral form of C343 in water (○), P123 micellar solution (□) and P123-CTAC (△) mixed solution with [CTAC]/[P123] ratio of 0.4. Absorbances at the lowest pH used for the three systems were normalized to unity for comparison.

The pK_a values calculated from the inflection points of these curves are 4.5, 6 and 4.9 in water, P123 and P123-CTAC media, respectively. These results clearly indicate that at the experimental pH=8.1 used in the present study for P123 and P123-CTAC micellar solution, the dye C343 is always present in the anionic form.

The effect of added CTAC on the emission spectra of C343 in P123 micellar solution was studied systematically and the results are shown in Figure 7.3. It is seen that, as the concentration of CTAC is increased in P123 micellar solution, the emission peak of C343 gradually shifts towards the blue region. This hypsochromic shift of the emission spectra of C343 indicates a decrease in the micropolarity around the probe in the micelle on increasing the CTAC concentration. This can possibly happen if the dye initially resides at the surface region of the P123 micelle and then experiences a gradual shift in its location towards the more nonpolar region of the micellar corona on increasing the CTAC concentration in the supramolecular assembly. This is further corroborated by the time-resolved fluorescence measurements, as discussed in the following section.

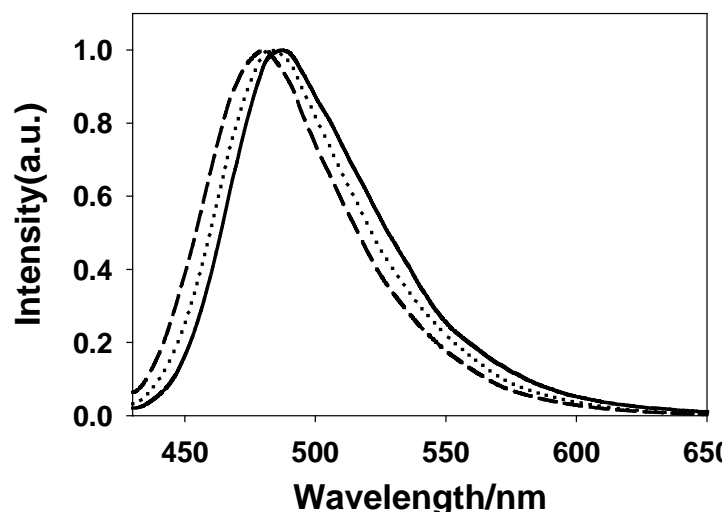


Figure 7.3. Normalized steady-state emission spectra of C343 in P123 micellar solution at different CTAC/P123 molar ratio: 0 (—), 0.06 (·····) and 0.5 (- - -).

7.3. 1.2. Solvent relaxation studies in P123-CTAC system

With an increase in the CTAC concentration in P123 micellar solution if the dye experiences a gradual shift towards the more interior of the micellar corona region, it should also find a concomitant change in the water structure around the probe molecule in the micellar environment. To investigate this aspect, we carried out solvent relaxation studies in the P123-CTAC mixed micellar system. Figure 7.4 shows the fluorescence transients for C343 dye in P123 micellar solution at two different emission wavelengths. At the blue side of the emission spectrum, 440 nm, the transient trace shows a fast decay component whereas at the red side of the emission spectrum, 610 nm, it shows a fast growth component followed by a slower decay. The fast decay at the blue side and fast growth at the red side of the emission spectrum are the signatures of the solvent relaxation process occurring for the present system in the measured time scale.

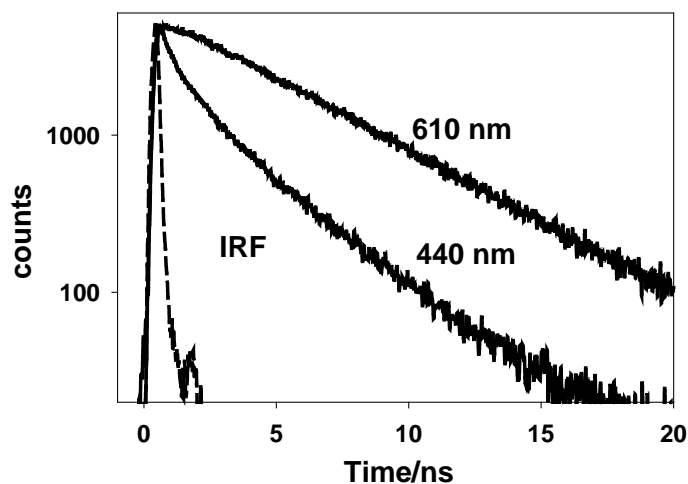


Figure 7.4. Fluorescence transients of C343 in P123 micellar solution at the blue side (440 nm) and red side (610 nm) of C343 emission spectrum in P123 micelle. The dashed line represents the IRF.

Time-resolved emission spectra (TRES) were reconstructed from the transient decay recorded at different emission wavelengths following the procedure suggested by Maroncelli and Fleming.³⁶⁷ The TRES thus reconstructed for C343 dye in P123 micellar solution (in the absence of CTAC) are shown in Figure 7.5A. As indicated from Figure 7.5A the spectra slowly move towards lower frequency region with a concomitant decrease in the emission intensity. To clearly observe the changes in the emission frequency with time and also to know more details about the emissive species, the area under these TRES were normalized and are plotted in Figure 7.5B. From this time-resolved area-normalized emission spectra (TRANES),^{394,395} it is evident that the spectra undergo a clear red shift with time. However, it is interestingly observed from TRANES that there is an isoemissive point (see inset of Figure 7.5B) for these spectra. The existence of such an isoemissive point in TRANES normally suggests that there are two type of emitting species present in the system.^{394,395} Presence of two emitting species in the present system can be perceived from the following consideration. As C343 exists in its anionic form in P123 micellar solution, there is a possibility that a small fraction of the dye might also be present in the bulk water phase though the major fraction of the dye will be dissolved in the P123 micellar phase. Presence of the probe in both micellar and bulk water phases can certainly lead to the appearance of an isoemissive point as observed in TRANES in

Figure 7.5B. The presence of a small fraction of C343 dye in the bulk water phase along with the major fraction associated with the micellar phase has also been reported in other pluronic micelle, F88,^{175,176} and also in AOT reverse micelles.^{96,98,99}

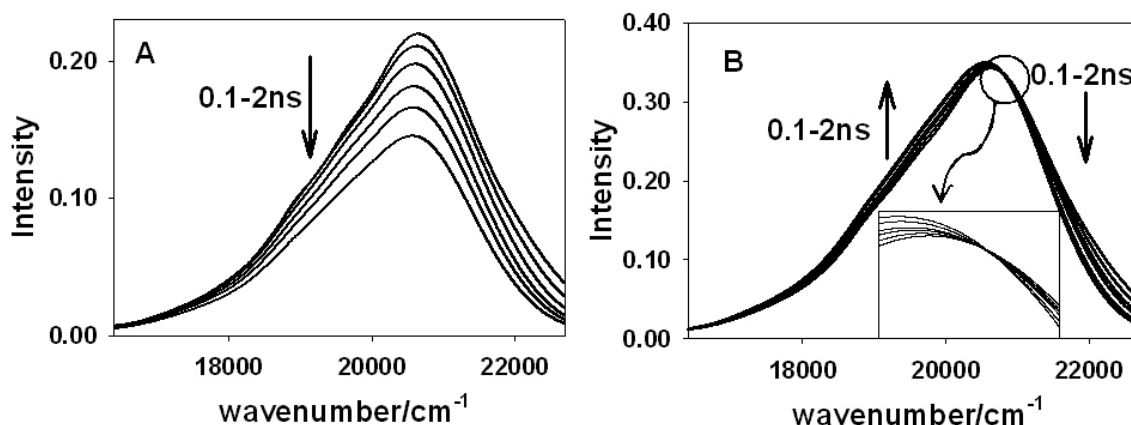


Figure 7.5. (A) Time-resolved emission spectra (TRES) and (B) Time-resolved area normalized emission spectra (TRANES) of C343 in P123 micellar solution.

The TRES were also constructed for P123 micellar solution in the presence of different CTAC concentrations. Figure 7.6A shows the TRES for C343 dye in P123-CTAC supramolecular system for CTAC/P123 molar ratio of 0.5. TRANES for the same system were also reconstructed and are shown in Figure 7.6B. It is to be noted that similar to pure P123 micellar solution, a red shift in the emission spectra with time is also observed for P123-CTAC supramolecular system. However, unlike in pure P123 micellar system, no isoemissive point is observed in the TRANES for the P123-CTAC supramolecular assembly. The absence of isoemissive point indicates that there is only one type of emissive species present in the solution when CTAC is added to the P123 micellar solution. It is likely that in the P123-CTAC supramolecular assembly all the dye is effectively solubilized in the micellar phase.

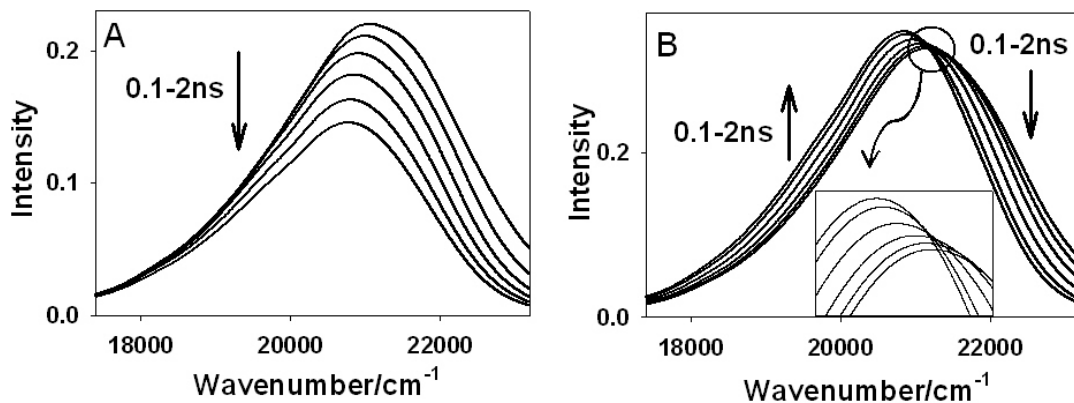


Figure 7.6. (A) Time-resolved emission spectra (TRES) and (B) Time-resolved area normalized emission spectra (TRANES) of C343 in P123 micellar solution at CTAC/P123 molar ratio of 0.5.

To quantify the shifts in the TRES, we calculated the mean frequency (ω_1) for the spectra at different time using the following equation.

$$\omega_1 = \frac{1}{\omega_0} \int_0^{\infty} \bar{\nu} I(\bar{\nu}) d\bar{\nu} \quad (7.1)$$

where, $I(\bar{\nu})$ is the intensity at the emission frequency $\bar{\nu}$ and ω_0 is the integrated intensity given by the following equation.

$$\omega_0 = \int_0^{\infty} I(\bar{\nu}) d\bar{\nu} \quad (7.2)$$

The variations of the normalized mean frequency, $\omega_1(t)/\omega_1(t=0)$, at different concentrations of CTAC in P123 micellar system are shown in Figure 7.7. The changes in the normalized ω_1 values with time are seen to fit well with a tri-exponential function of the following form.

$$\omega_1(t) = \sum_{i=1}^3 a_{si} \exp(-t/\tau_{si}) \quad (7.3)$$

where a_{si} and τ_{si} are the amplitude and time constant, respectively, for the i^{th} decay component.

The average solvation time, $\langle\tau_s\rangle$, was calculated using the following equation.

$$\langle \tau_s \rangle = \frac{\sum_{i=1}^3 a_{si} \tau_{si}^2}{\sum_{i=1}^3 a_{si} \tau_{si}} \quad (7.4)$$

The individual decay component along with the average solvation times, calculated according to equation 7.4, are given in Table 7.1 for C343 dye in P123 micellar solution at different CTAC/P123 molar ratios. It is indicated from the present results that the contribution of the shorter component of the solvation process effectively increases on increasing the CTAC concentration (*cf.* Figure 7.7 & Table 7.1).

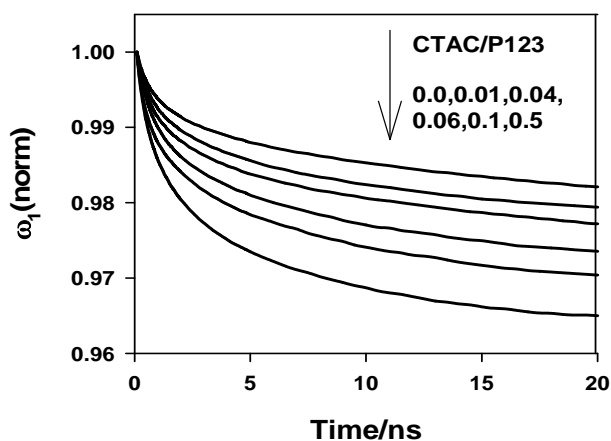


Figure 7.7. Plot of the normalized mean frequency, ω_1 , for C343 dye in P123 micellar solution at different CTAC/P123 molar ratios.

It is expected that if the probe gradually shifts its location from the micellar surface to the deeper corona region of the micelle with an increase in the CTAC concentration, the contribution of the unresolved ultrafast solvation component arising due to the solvent molecules at the micellar surface region should gradually decrease. This point becomes more evident when we consider the total observed Stokes' shifts in the present systems, as will be discussed latter. In the present context it is interesting to consider the changes in the average solvation time with CTAC concentration. Figure 7.8A shows the variation in the average solvation time with CTAC concentration. It is interestingly seen that with an increase in

the CTAC concentration the average solvation time increases and effectively reaches to a limiting value at a CTAC/P123 molar ratio of ~0.15.

Table 7.1. Solvation dynamics results and the estimates of the expected and the observed Stokes' shifts for C343 dye in CTAC/P123 mixed micellar system.

$\frac{[CTAC]}{[P123]}$	a_1 (%)	τ_1 (ns)	a_2 (%)	τ_2 (ns)	a_3 (%)	τ_3 (ns)	$\langle \tau_s \rangle$ (ns)	Stokes' shift (cm ⁻¹)		
								expected ($\Delta\omega_s^{total}$)	observed ($\Delta\omega_s^{obs}$)	$\Delta\omega_s^{%o}$
0	0.07	0.12	6.67	0.54	92.96	4.11	3.86	2297	326	14.2
0.01	1.81	0.29	7.73	0.75	90.46	4.24	3.90	2170	386	17.8
0.04	2.93	0.31	5.59	0.81	91.48	4.30	3.99	2170	433	20.0
0.06	3.36	0.37	6.17	0.89	90.47	4.50	4.14	2127	511	24.0
0.11	2.63	0.30	6.02	0.88	91.35	4.71	4.36	2084	565	27.1
0.22	2.37	0.26	6.47	0.86	91.16	4.78	4.42	2041	630	30.9
0.34	2.64	0.29	7.97	0.98	89.39	4.80	4.38	2041	640	31.4
0.56	2.58	0.24	8.31	0.91	89.11	4.82	4.38	2041	688	33.7

$$* a_i \% = 100 \times a_{si} \tau_{si} / \sum_{i=1}^3 a_{si} \tau_{si}$$

An important point to be considered in the present context is the extent of the missing Stokes' shifts due to the limited time resolution (0.3 ns) of the present experimental setup. With the present measurements, it is expected that there will always be a significant part of the dynamics Stokes' shifts that will remain unobserved. To estimate the extent of this missing Stokes' shifts, the expected total Stokes' shift values were first calculated following the method proposed by Fee and Maroncelli.³⁵ Thus, the absorption and emission spectra of the probe in a nonpolar solvent (cyclohexane) and in the present micellar solution, the total expected Stokes' shift values were calculated using the following equation.

$$\Delta\omega_s^{total} = [\omega_{abs}^m - \omega_{em}^m] - [\omega_{abs}^{CH} - \omega_{em}^{CH}] \quad (7.5)$$

where ω_{abs}^m and ω_{abs}^{CH} are the absorption frequencies and ω_{em}^m and ω_{em}^{CH} are the emission frequencies of the probe in the micellar solution and in cyclohexane, respectively. These total expected Stokes' shifts along with the Stokes' shifts observed from the measured TRES are given in Table 7.1. The percentages of the total Stokes' shifts thus observed in the present study at different CTAC concentrations are also presented in Table 7.1. Figure 7.8B shows the variation in the percentage Stokes' shifts observed as a function of CTAC/P123 molar ratio. It is evident from Figure 7.8A and 7.8B, that the variation of the average solvation time with CTAC concentration corresponds very nicely with that of the percentage Stokes' shifts observed in the present systems.

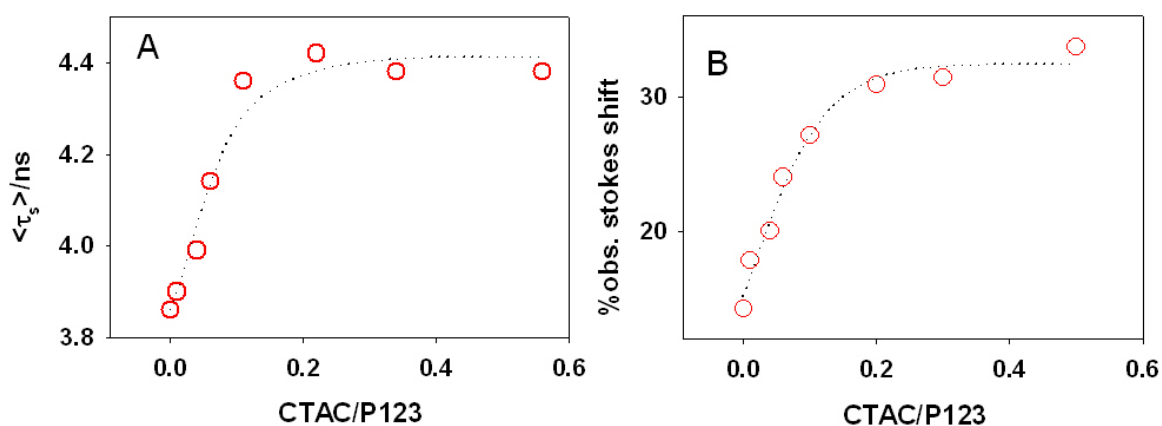


Figure 7.8. Variation in the (A) average solvation time and (B) percentage Stokes' shifts observed with the CTAC/P123 molar ratio.

Detail X-ray and light scattering studies on P123 micellar system in the presence of ionic surfactant have suggested the formation of unique supramolecular assemblies, where the surfactant molecules undergo dissolution into the P123 micelles.^{162,165,166} It is proposed that the long hydrocarbon chain of the ionic surfactant dissolves deep into the PO core of the P123 micelle and the charged head group of the surfactant resides at the boundary of the PO core protruded into the hydrated corona region.¹⁶²

With such a structure of the supramolecular assemblies, the variations in the solvent relaxation parameters and the changes in the percentage Stokes' shifts for C343 are the

manifestations of the changes in the probe location in such assemblies as a function of CTAC concentration. In the absence of CTAC, the anionic form of C343 dye preferentially resides at the surface region of P123 micelle. As CTAC is added to P123 micellar solution, due to the formation of the above supramolecular assemblies, the periphery of the PO core of the micelle becomes a positively charged layer. Since the probe is negatively charged, this positively charged layer will thus impart an electrostatic attraction for the probe leading the dye to undergo a gradual change in its location from the micellar surface to the interior of the micellar corona region. This will result in a gradual change in its photophysical properties as well as in the solvent relaxation parameters as observed experimentally.

Decrease in $\Delta\omega_s^{total}$ value (*cf.* Table 7.1) certainly indicates that the dye gradually moves towards a less polar microenvironment in P123 micelle as CTAC concentration is increased in the solution. Further, the increase in the $\Delta\omega_s^{obs}$ value (*cf.* Table 7.1) suggests that the extent of the missing dynamic Stokes' shift (due to ultrafast solvation component) gradually decreases with CTAC concentration in P123 micellar solution. Such a situation can happen when the anionic probe C343 initially resides at the surface of P123 micelle and gradually shifts deeper into the micellar corona region on increasing the CTAC concentration.

The increase in the percentage Stokes' shift observed with an increase in the CTAC concentration is also a clear manifestation of the movement of the probe in the present systems. When the probe resides at the micellar surface, it is partially exposed to bulk water. As the solvent relaxation for the bulk water is very fast, much faster than the time-resolution of our instrument, the ultrafast component of the Stokes' shifts, which arise mainly due to the libration motion of the water molecules in the bulk phase, will be missed in our measurements. On addition of CTAC, the probe moves inside the micellar media and thus the contribution of the librational motion of the bulk water on the dynamic Stokes' shift decreases and accordingly we could observe a much higher percentage of the total Stokes' shifts. Moreover, presence of

an isoemissive point in the TRANES in pure P123 micelle but the absence of such an isoemissive point for CTAC-P123 micellar system clearly indicate that whatever free probe molecules were initially present in the bulk water in pure P123 micellar solution actually enters into the micellar phase due to the electrostatic interaction of the positively charged layer in the P123-CTAC mixed micellar system with the negatively charged C343 dye.

7.3.1.3. Rotational relaxation studies in P123-CTAC Systems

To understand more about the movement of the probe in the polymer-surfactant supramolecular assemblies, time-resolved fluorescence anisotropy measurements were carried out to understand how the microenvironment of the probe changes in P123 micelle on addition of CTAC. Fluorescence anisotropy decays for C343 in P123 micellar solution at different CTAC concentrations are shown in Figure 7.9A. The anisotropy decay for C343 in bulk water is also shown in Figure 7.9A for comparison. To be mentioned, however, that the exact reorientation time for C343 in bulk water could not be estimated correctly because it is much shorter than the time-resolution of our TCSPC instrument.

The fluorescence anisotropy decays for C343 in P123 micellar solutions are seen to fit well with a bi-exponential function of the following form.

$$r(t) = \sum_{i=1}^2 a_{ri} \exp(-t / \tau_{ri}) \quad (7.6)$$

where a_{ri} and τ_{ri} are the amplitude and rotational time constant, respectively, for the i^{th} decay component. The average rotational relaxation time, $\langle \tau_r \rangle$, was calculated using the following equation.

$$\langle \tau_r \rangle = \frac{\sum_{i=1}^2 a_{ri} \tau_{ri}^2}{\sum_{i=1}^2 a_{ri} \tau_{ri}} \quad (7.7)$$

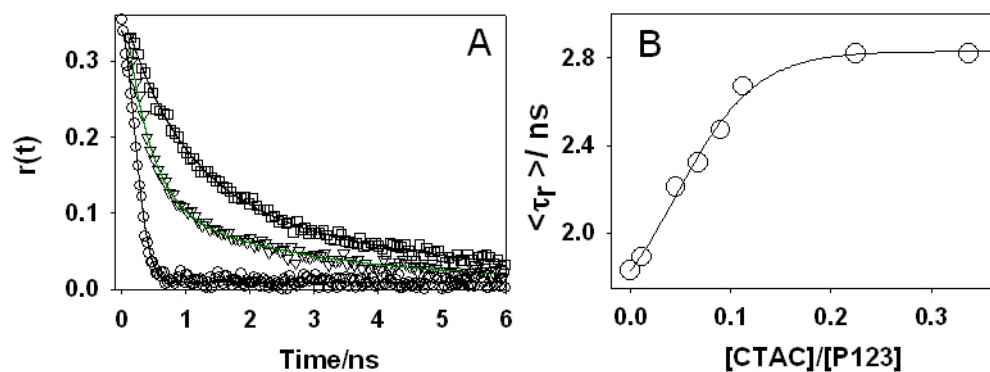


Figure 7.9. (A) Fluorescence anisotropy decay, $r(t)$, for C343 in water (O) and in P123 micelle at different CTAC/P123 molar ratio: (Δ) 0.0 and (\square) 0.34. (B) Variation of the average rotational relaxation time, $\langle\tau_r\rangle$, for C343 in P123 micelle with varying CTAC/P123 molar ratio. Solid line is the best fitted smooth curve among the data points.

All the fitting parameters including $\langle\tau_r\rangle$ values for C343 dye in P123 micellar solution at different CTAC concentrations are presented in Table 7.2. The variation in the $\langle\tau_r\rangle$ values with CTAC concentration is presented in Figure 7.9B. It is obvious from Figure 7.9A and Table 7.2, that the reorientation time of the probe is much slower in P123 micellar solution compared to that in bulk water. This result clearly indicates that the probe, C343, gets preferentially bound to the micellar phase, most likely at the surface region of the micelle, because the probe is anionic in nature. Even though a charged dye has some tendency to be partitioned into the water phase, due to the presence of the large hydrophobic group in C343, the percentage of the dye present in the bulk water phase is expected to be much less. Accordingly, the contribution of the dye in bulk water phase is expected to be very small in the observed anisotropy decay.

From Figure 7.9B it is evident that the reorientation time of C343 increases with CTAC concentration and reaches a plateau when the CTAC/P123 molar ratio reaches a value of ~ 0.15 . This result can be explained on the basis of the formation of the supramolecular assembly mentioned earlier. As C343 is anionic in nature, it experiences an electrostatic attraction by the positively charged layer developed inside the P123 micelle on addition of CTAC. This electrostatic interaction leads to the movement of the anionic probe from the

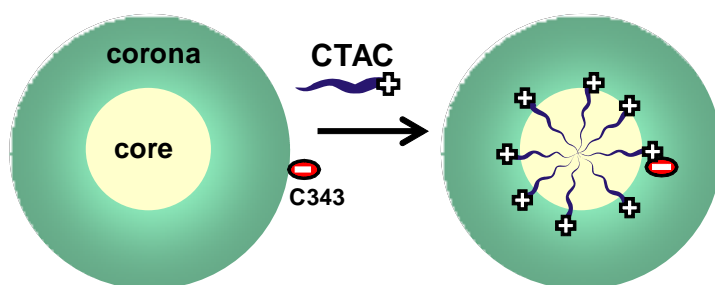
surface region to the interior region of the micelle. Thus, the increase in the reorientation time of the probe with an increase in the CTAC concentration in P123 micelle is due to the following two reasons: (i) the microviscosity experienced by the probe in the interior of the micelle is much higher than that at the micellar surface and (ii) the electrostatic interaction between probe and the charged layer inside the micelle acts against the rotational motion of the probe. Thus, the $\langle\tau_r\rangle$ value of the dye undergoes a gradual increase on increasing the CTAC concentration in P123 micelle.

Table 7.2: Time-resolved anisotropy parameters with varying [CTAC]/[P123] molar ratio.

CTAC/P123 molar ratio	τ_{r1} (ns)	a_1	τ_{r2} (ns)	a_2	τ_{av} (ns)
0	0.37	0.30	2.46	0.70	1.83
0.011	0.32	0.20	2.28	0.80	1.89
0.045	0.44	0.17	2.57	0.83	2.21
0.067	0.48	0.19	2.75	0.81	2.32
0.089	0.47	0.15	2.83	0.85	2.48
0.112	0.69	0.20	3.16	0.80	2.67
0.225	0.62	0.19	3.32	0.81	2.81
0.337	0.71	0.20	3.32	0.80	2.80

The detail structural study by Jansson et al.^{165,166} has shown that the changes in the micellar characteristics, like the core and the micellar radius, are only marginal, even up to the CTAC/P123 molar ratio of ~ 0.5 . Recently Mali et al.³⁸⁹ have suggested that the addition of CTAC does not change the characteristics of the P123 micelle any significantly. These authors have shown that the reorientation time of a cationic dye, which resides at the micellar surface, remains almost unchanged on addition of CTAC up to ~ 0.5 CTAC/P123 molar ratio. This clearly indicates that even if there is a marginal change in the P123 micellar characteristic due to the addition of CTAC, it does not cause any significant change in the reorientation time for a probe that resides at the surface of the micelle. As the anionic probe, C343 is also reported to

reside at the micellar surface under normal circumstances.^{98,175} The observed increase in the reorientation time with CTAC concentration thus clearly suggests that the observed result is not related to the changes in the micellar characteristics but is mainly due to the changes in the location of the probe in the supramolecular assembly formed by the special arrangement of CTAC into the P123 micelle. These changes in the probe location in the supramolecular assembly with an increase in the CTAC concentration can be presented as in Scheme 7.2. To understand the general applicability of this phenomenon, studies have also been carried out using other polymer-surfactant systems as are discussed in the following sections.



Scheme 7.2. Schematic representation of the changes in the location of an anionic solute with the addition of a cationic co-surfactant in a neutral micelle.

7.3.2. Studies on F88-CTAB mixed micellar system

As the characteristics of the pluronic micelles are largely dependent on their EO/PO ratios and pluronics form micelles with wide range of dimensions of their core and corona regions, these systems can provide a wide range of microenvironments for the dissolved solute. With this perspective, in the present work, we have extended our studies using another block copolymer system, F88 (EO₁₀₃-PO₃₉-EO₁₀₃), in the presence of a cationic surfactant CTAB, to investigate the modulation in the properties of a dissolved solute. To be mentioned here that F88 has a much thicker corona region than P123, as the EO/PO ratio is much higher for F88 than P123.

7.3.2.1. Small angle neutron scattering (SANS) studies

To understand about the nature of interaction between F88 and CTAB, we carried out SANS studies using 5% w/v F88 solution (in D₂O) in the absence and presence of CTAB. Figure 7.10 shows the SANS patterns for 5% w/v F88 solution at two different CTAB concentrations. As reported in the case of SDS-pluronic system,¹⁶² in the present case also the addition of CTAB leads to a decrease in the scattering cross section, and a shift in the peak position to a higher q value. Recent NMR and SANS studies on mixed pluronic-ionic surfactant systems suggest that the hydrophobic chain of ionic surfactants are dissolved in the hydrophobic core of the pluronic micelles to avoid unfavorable interaction with the water molecules.^{162,396} Based on this report, we have analyzed our SANS data assuming that the hydrophobic chains of CTAB also get dissolved in the hydrophobic core of the F88 micelles and the charged head groups reside at the interface of the core and corona region, as reported for the P123-SDS system.¹⁶² This consideration gave us a good fit to the experimental SANS data, suggesting the absence of any second type of aggregates in the form of pure CTAB micelles. The solid lines in Figure 7.10 represent the fitted data according to the above mixed micellar model. Parameters obtained from the fit are summarized in Table 7.3. It is seen from Table 7.3 that like in the case of other surfactant-pluronic systems, the core radius (R_{cm}) decreases with an increase in the CTAB concentration due to an increase in the hydrophilic character of the micellar system in the presence of the ionic surfactants. The micellar volume fraction, ϕ , remains effectively unchanged with the increase in the CTAB concentration. Thus, the SANS results clearly support the formation of a supramolecular structure due to the addition of CTAB to F88 micellar solution.

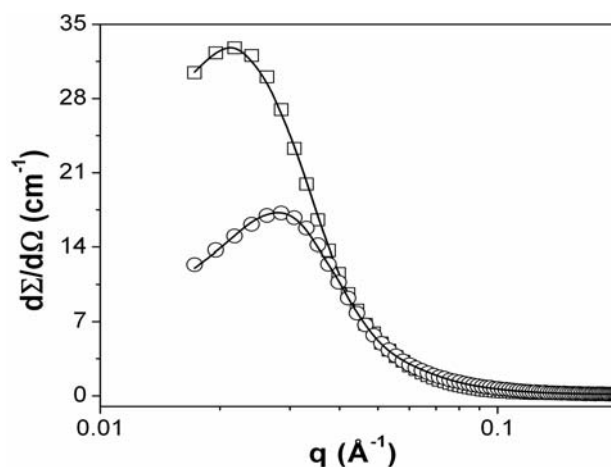


Figure 7.10. SANS data of the F88 solutions with different CTAB/F88 molar ratio (0 (□) and 0.5 (○)). The solid lines are fit to the data using a mixed micellar model as discussed in text.

Table 7.3. The core radius (R_{cm}), the hard sphere radius (R_{hs}), the volume fraction (ϕ) and the polydispersity ($\Delta R_c/R_{cm}$) of the micelles in 5% w/v F88 solutions with different CTAB concentrations. The scattering length densities used to fit the data are $0.603 \times 10^{10} \text{ cm}^{-2}$, $0.343603 \times 10^{10} \text{ cm}^{-2}$ and $6.38603 \times 10^{10} \text{ cm}^{-2}$ for EO, PO and D_2O , respectively.

CTAB/F88 molar ratio	Core Radius R_{cm} (nm)	Hard Sphere Radius R_{hs} (nm)	Volume Fraction ϕ	Polydispersity $\Delta R_c/R_{cm}$ (%)
0.0	3.26 ± 0.02	11.7 ± 0.1	0.23 ± 0.01	25 ± 0.1
0.5	2.58 ± 0.02	9.8 ± 0.2	0.26 ± 0.02	27 ± 0.1

7.3.2.2. Absorption and fluorescence studies in F88-CTAB system

The pH dependent absorption studies were carried out for C343 dye in F88 micellar solution to find out the prototropic form of the dye in the micellar solution. Figure 7.11 shows the pH dependent changes in the absorbance at the absorption peak of the neutral form of C343 in F88 micellar solution (450 nm), resulting its pK_a value as 5.4. The pK_a value for C343 in water is 4.6.⁹⁸ An upward shift in the pK_a value of a solute in a micellar solution as compared to that in bulk water is well documented and has also been observed by us in P123 micelle described in section 7.3.1.³⁹³

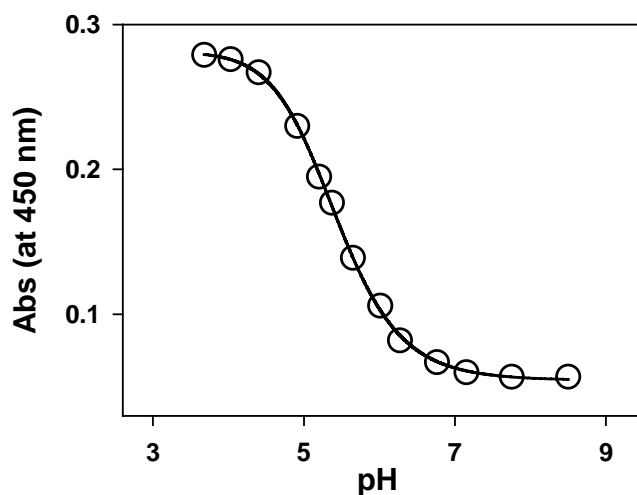


Figure 7.11. Changes in absorbance of the C343 dye (at 450 nm) with the changes in the pH of the 5% w/v F88 solution.

As we have seen in the case of P123, the presence of an ionic surfactant, CTAC, lowers the pK_a value of C343 dissolved in the micellar media. A similar situation is also expected in the F88-CTAB system. Thus, because of the decrease in the pK_a value in the presence of cationic surfactant, the nature of the prototropic form of C343 in F88 micellar solution should also not change from its anionic form with the addition of CTAB, if the pH of the solution is kept significantly higher than 5.4. In the present study, the pH of the F88 solution used for all optical and SANS studies was kept about 7.2. Thus, we assume that C343 exists exclusively in its anionic form in all the experimental solutions even in the presence of CTAB.

Steady-state emission spectra of C343 in F88 micellar solution were recorded at different CTAB concentrations to understand the possible changes in the microenvironment for the probe on the addition of CTAB. Observed results, as shown in Figure 7.12, indicate that with an increase in the CTAB concentration, the emission spectra of C343 gradually shift towards the shorter wavelength, similar to that observed in the case of P123-CTAC systems. Such a hypsochromic shift in the emission spectra suggests that the polarity of the microenvironment around the probe decreases gradually on increasing the CTAB concentration in the F88 micellar solution.

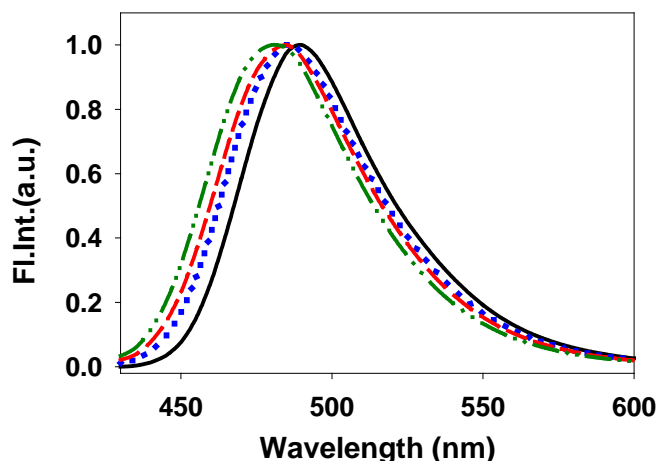


Figure 7.12. Steady-state emission spectra of C343 in 5% w/v F88 solution at different CTAB/F88 molar ratio: 0.0 (—), 0.1 (·····), 0.2 (- - -) and 0.5 (- · - ·).

7.3.2.3. Rotational relaxation Studies in F88-CTAB systems

To explore the details of the changes in the microenvironment of the dye with the added CTAB in F88 micellar solution, we carried out time-resolved fluorescence anisotropy measurements in the present systems. The changes in the anisotropy decay for C343 in F88 solution at different CTAB concentration are shown in Figure 7.13A. The anisotropy decay for C343 in bulk water, which is very fast compared to those in F88-CTAB solutions, is also shown in Figure 7.13A for a comparison. Significantly slower anisotropy decay for the dye in F88 solution suggests that C343 preferentially resides in the micellar phase, as also inferred in the case of P123 micelle. As indicated from Figure 7.13A, the anisotropy decay gradually becomes slower with an increase in the CTAB concentration in F88 solution. The anisotropy decays for the present systems were fitted with a bi-exponential function as given by equation 7.6 and fitting parameters along with the average rotational relaxation time, τ_{av} , (*cf.* eq. 7.7) are listed in Table 7.4. The variation in the τ_{av} values with the CTAB concentration is shown in Figure 7.13B. The τ_{av} initially increases and then saturates to a limiting value at a CTAB/F88 molar ratio of about 0.4. The increase in the τ_{av} clearly indicates that the probe gradually experiences more frictional force in the F88 micellar media with an increase in the CTAB concentration.

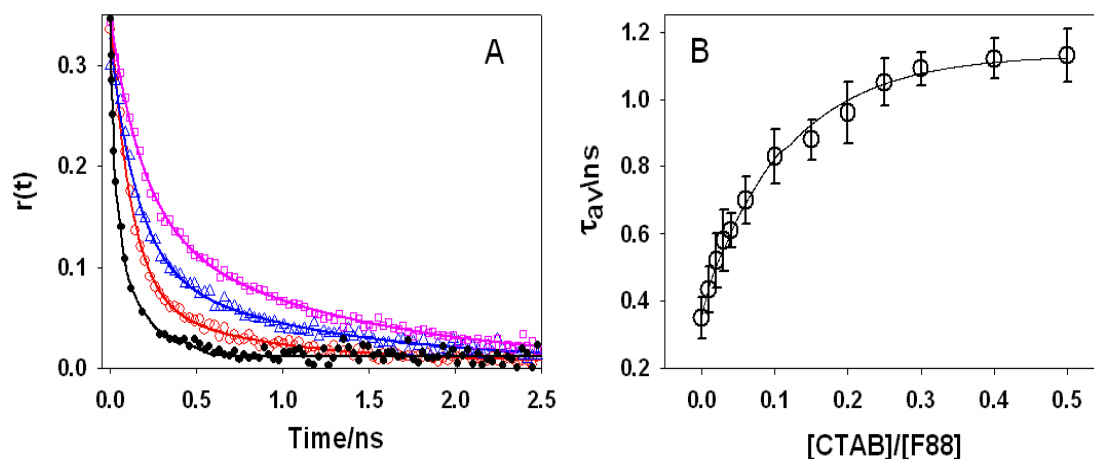


Figure 7.13 (A) Fluorescence anisotropy decay for C343 dye in water (●) and in F88 micellar solution at different CTAB/F88 molar ratio: (○) 0.0, (△) 0.1 and (□) 0.3. (B) Variation of the average reorientation time for C343 dye in F88 micellar solution with the CTAB/F88 molar ratio.

Table 7.4. Time-resolved anisotropy parameters with varying [CTAB]/[F88] molar ratio

CTAB/F88 molar ratio	τ_{r1} (ns)	a_1	τ_{r2} (ns)	a_2	τ_{av} (ns)
0.00	0.15	0.38	0.48	0.62	0.35±0.06
0.01	0.07	0.30	0.74	0.70	0.43±0.07
0.02	0.08	0.30	0.77	0.70	0.52±0.08
0.03	0.08	0.29	0.78	0.71	0.58±0.09
0.04	0.08	0.29	0.82	0.71	0.61±0.05
0.06	0.07	0.22	0.88	0.78	0.70±0.07
0.10	0.09	0.21	1.03	0.79	0.83±0.08
0.15	0.09	0.15	1.02	0.85	0.88±0.06
0.20	0.09	0.15	1.12	0.85	0.96±0.09
0.25	0.12	0.15	1.22	0.85	1.05±0.07
0.30	0.12	0.13	1.23	0.87	1.09±0.05
0.40	0.14	0.13	1.27	0.87	1.12±0.06
0.50	0.17	0.14	1.29	0.86	1.13±0.08

Results from SANS studies indicated the formation of unique supramolecular assembly for F88-CTAB systems where the hydrophobic chain of CTAB molecule is dissolved in the core

of F88 micelle and the charged head group of CTAB resides at the interface region of the core and corona of the micelle. Formation of such assemblies causes a positively charged layer to be developed inside the F88 micelle. The charge density of this layer increases gradually as the CTAB concentration is increased. As the probe C343 is anionic in nature, it experiences an electrostatic attraction by the positively charged layer inside the micelle and thus leads to a gradual movement of the probe from the micellar surface to its interior on increasing the CTAB concentration. Thus, the increase in the τ_{av} value for the probe with an increase in the CTAB concentration in F88 micelle is firstly due to the increasing microviscosity at the interior of the micelle and secondly, due to the increase in the electrostatic interaction between the negatively charged probe and the positively charged layer inside the micelle. The probe movement from the micellar surface to its interior is also responsible for the observed hypsochromic shift in its emission spectra with the addition of CTAB (*cf.* Figure 7.12). The surface of the micelle is exposed to the bulk water and thus has higher dielectric constant as compared to that in the interior of the micelle. Decrease in the dielectric constant of the microenvironment due to the change in the location of the probe results in the observed changes in the photophysical properties.

As indicated by the SANS study, there are some changes in the micellar characteristics due to the addition of CTAB to F88 solution. To check whether these changes in the micellar characteristics have any effect on the rotational motion of the probe, we also measured the reorientation time of a cationic dye, Rhodamin-110 (R110) in F88 micellar solution at different CTAB concentration. It is reported that like C343, R110 also resides preferentially at the surface of the pluronic micelles.³⁸⁹ The average reorientation time for R110 in F88 at CTAB/F88 molar ratios of 0 and 0.5 are found to be effectively the same, ~ 0.34 ns. This reorientation time for R110 is also very similar to that observed for C343 dye in F88 solution in the absence of CTAB (*cf.* Table 7.4). These results indicate that the microenvironment of C343 and R110 are very similar in F88 micellar solution in the absence of CTAB. Similar

reorientation time for R110 in F88 micellar solution at different CTAB concentrations clearly indicates that the dye always resides at the micellar surface and the small changes in the F88 micellar characteristics due to the addition of CTAB, do not change the reorientation time of this probe. As R110 is a positively charged dye, there will be no electrostatic attraction between CTAB and R110 and thus there is no effective movement of R110 in F88 micelle due to the formation of the supramolecular assembly on addition of CTAB. It is thus evident that the observed changes in the reorientation times for anionic C343 in F88 micellar solution, on addition of CTAB, is not due to the changes in the micellar characteristics, but certainly due to the changes in the location of the probe inside the micelle.

To understand the effect of counterion of the surfactant on the above phenomenon, we also carried out detailed ground-state absorption, steady-state emission and time-resolved anisotropy measurements with F88-CTAC system at different CTAC/F88 ratio and the results were found to be quite similar to that of F88-CTAB system. This indicates the nature of the counterion of the surfactant does not affect the modulation of the solute location in the block copolymer-surfactant supramolecular assemblies.

7.3.2.4. Dynamic Stokes' shift measurements in F88-CTAC system.

As understood, the position of the probe, C343, in F88 micellar phase changes on changing the concentration of CTAB and CTAC in the similar manner. Since the microenvironment around the probe changes gradually, on addition of CTAB/CTAC, the solvent relaxation experienced by the probe in these systems should also depend on the surfactant concentration. To explore this aspect, we carried out a detailed dynamic Stokes' shift measurement in F88-CTAC supramolecular assembly using C343 as the probe. The time-resolved emission spectra (TRES) constructed for C343 in F88 micellar solution are shown in Figure 7.14A. It is to be noted that along with the decrease in the emission intensity with time there is also a small but concomitant red shift in the emission peak.

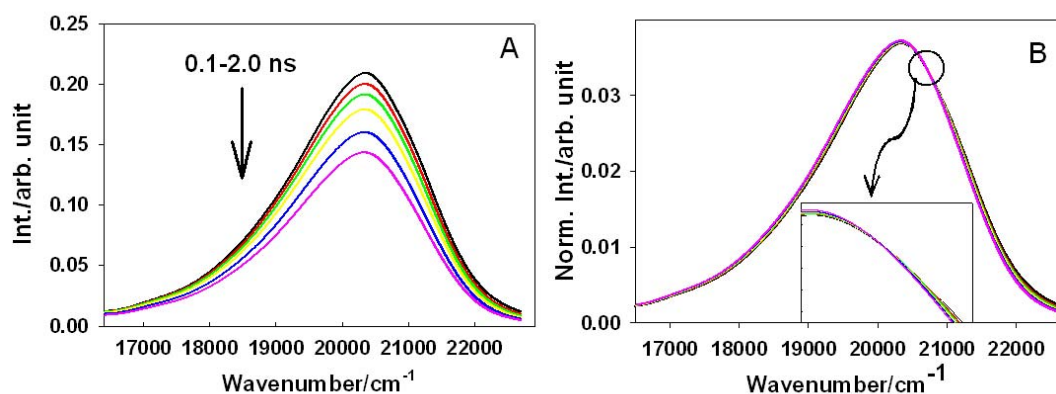


Figure 7.14. (A) Time-resolved emission spectra (TRES) and (B) time-resolved area normalized emission spectra (TRANES) of C343 in F88 micellar solution at different time (0.1 ns to 2 ns).

The time-resolved area normalized emission spectra (TRANES) were also constructed for this system, as shown in Figure 7.14B, where an isoemissive point is clearly indicated. The appearance of such isoemissive point suggests that two emissive species are present in the system.^{394,395} As in the case of P123 system (*cf.* section 7.3.1.2) the two emissive species in the present case is also attributed to the partitioning of the probe between the micelle and the bulk water phases. It is evident from Figure 7.15 that like in F88 system, in F88-CTAC system also with time there is a gradual shift in the emission peak toward the lower frequency. A comparison of Figure 7.14A and 7.15A clearly indicates that the frequency shift in the emission spectra is relatively large in the presence of CTAC. Another important difference between F88 and F88-CTAC system is the absence of an isoemissive point for TRANES in the latter case (*cf.* Figure 7.15B). The absence of an isoemissive point in the F88-CTAC system clearly indicates that there is only one emissive species in the solution. It is inferred that the presence of CTAC in F88 micelle help to take all the dyes in the solution into the micellar phase. These results are in accordance with the results obtained in the time-resolved anisotropy measurements in F88-CTAC system and are also qualitatively similar to the results obtained for P123-CTAC system discussed earlier (*cf.* Section 7.3.1.2).

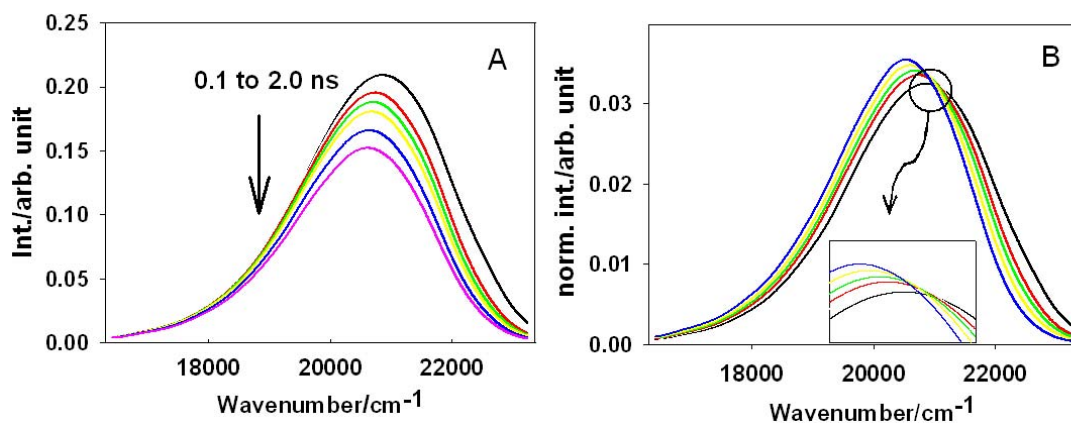


Figure 7.15. (A) Time-resolved emission spectra (TRES) and (B) time-resolved area normalized emission spectra (TRANES) of C343 in F88 micellar solution at CTAC/F88 molar ratio of 0.5 at different time (0.1 ns to 2 ns).

As mentioned, the extent of frequency shift in the TRES is relatively larger in the case of F88-CTAC system as compared to that in F88 system. To estimate the relative amount of the dynamic Stokes' shift observed in the present systems, we first calculated the expected total dynamic Stokes' shift using equation 7.5. Total expected Stokes' shift ($\Delta\omega_s^{total}$) and the observed Stokes' shift ($\Delta\omega_s^{obs}$) values for the present systems are tabulated in Table 7.5. Percentage of the total Stokes' shift observed ($\Delta\omega_s^{\%obs}$) are also shown in Table 7.5. It is evident from Table 7.5 that the $\Delta\omega_s^{total}$ value decreases gradually while the $\Delta\omega_s^{obs}$ and accordingly $\Delta\omega_s^{\%obs}$ value increases gradually as we increase the CTAC concentration in the F88 solution.

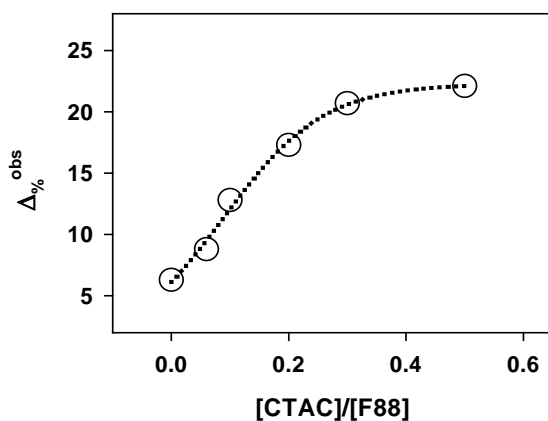


Figure 7.16. Plot of the percentage of Stokes' shift observed ($\Delta\omega_s^{\%obs}$) for C343 dye in the F88 micellar solution as a function of CTAC/F88 molar ratio.

Table 7.5. Solvation parameters with varying CTAC/F88 molar ratio

[CTAC]/[F88]	Stokes' shift		
	$\Delta\omega_s^{total} / \text{cm}^{-1}$	$\Delta\omega_s^{obs} / \text{cm}^{-1}$	$\Delta\omega_s^{\%obs}$
0.00	2339.9	146.6	6.3
0.06	2297.2	201.2	8.8
0.10	2238.0	287.8	12.8
0.20	2195.5	379.0	17.3
0.30	2152.8	445.0	20.7
0.50	2127.1	470.4	22.1

The variation of the $\Delta\omega_s^{\%obs}$ with the added CTAC concentration are shown in Figure 7.16.

Like in P123-CTAC case, these changes can also be explained on the basis of the formation of the F88-CTAC supramolecular assembly. In the absence of CTAC the dye resides at the micellar surface where the solvent relaxation is quite fast and due to the limited time resolution of our instrument we miss a large part of the expected total Stokes' shift. Thus, the observed Stokes' shift is quite less in this case. As we increase the concentration of CTAC in F88 micelle, the probe gradually moves from the surface to its interior and accordingly the solvent relaxation experienced by the probe becomes gradually slower. This causes the observed Stokes' shift to increase gradually on increasing the CTAC concentration. This is also supported by the decrease in the total expected Stokes' shift ($\Delta\omega_s^{total}$) with the increasing CTAC concentration. It happens because the dye experiences less polar environment on its movement into the interior of the micelle with the increasing CTAC concentration.

It is interesting at this point to compare the surfactant to pluronic ratios for F88-CTAC system and P123-CTAC system to achieve the saturation limit in the reorientation time and in the observed dynamic Stokes' shifts. The ratio is about 0.4 for F88-CTAC (*cf.* Fig 7.15B & 7.18) and 0.2 for P123-CTAC (*cf.* Fig 7.8 & 7.13, respectively). The larger CTAC concentration required for F88-CTAC to achieve the limiting effects than P123-CTAC system

can be explained on the basis of the EO block sizes of these two pluronic polymers. For pluronic micelles the corona region is mainly composed of the hydrated EO blocks. The numbers of EO units are 20 and 103 for P123 and F88, respectively. The presence of large number of EO units in F88 results in a much thicker corona region as compared to P123 micelle. Thus the reported corona thickness for F88 and P123 micelle are 46 Å and 6 Å, respectively.^{156,236,390} Because of the larger corona thickness, the electrostatic interaction between the probe and the positive layer in the micelle is weaker in F88-CTAC system than in P123-CTAC system at any particular CTAC concentration. Thus, to pull the negatively charged probe molecule from the micellar surface to the interior of the micelle, much higher concentration of CTAC is required in the former case than the latter. As pluronics are available with wide range of EO block sizes, it is possible to provide different microenvironment to the dissolve solute in a single pluronic micelle. Thus from the present results it can be suggested that by proper choice of the pluronics and with the proper concentration of the ionic surfactant, the microenvironment of a dissolve solute can be modulated suitably over a wide range, which in turn can be used to modulate their physical and chemical properties over a wide range for different applications.

7.3.3. Studies on P105-CTAB mixed micellar systems

Comparing the results of P123-CTAB and F88-CTAB systems, it was indicated that the movement of the probe C343 in these assemblies is dependent on the thickness of the micellar corona region. To explore this aspect further, we carried out both dynamic Stokes' shift and time-resolved anisotropy measurements with another pluronic, namely P105, which has an intermediate corona thickness (31 Å³⁹⁷) as compared to that of F88 (46 Å²³⁶) and P123 (6 Å¹⁸²) micelles. Figure 7.17A shows the fluorescence anisotropy decays for C343 in P105-CTAB system with different CTAB/P105 molar ratio. Similar to P123-CTAC and F88-CTAB cases, in the P105-CTAB system also, the anisotropy decay becomes slower with an increase in the

CTAB concentration. Table 7.6 list different rotational times and their percentage contributions along with average rotational times τ_{av} . Figure 7.17B plots the τ_{av} values as a function of CTAB/P105 molar ratios. It is evident from Figure 7.17B that the reorientation time increases with the CTAB concentration and reaches a saturation at a CTAB/P105 molar ratio of ~ 0.3 . To be mentioned that similar saturation for CTAC/P123 and CTAC/F88 systems were attained at the surfactant/pluronic molar ratios of 0.15 and 0.4 respectively.

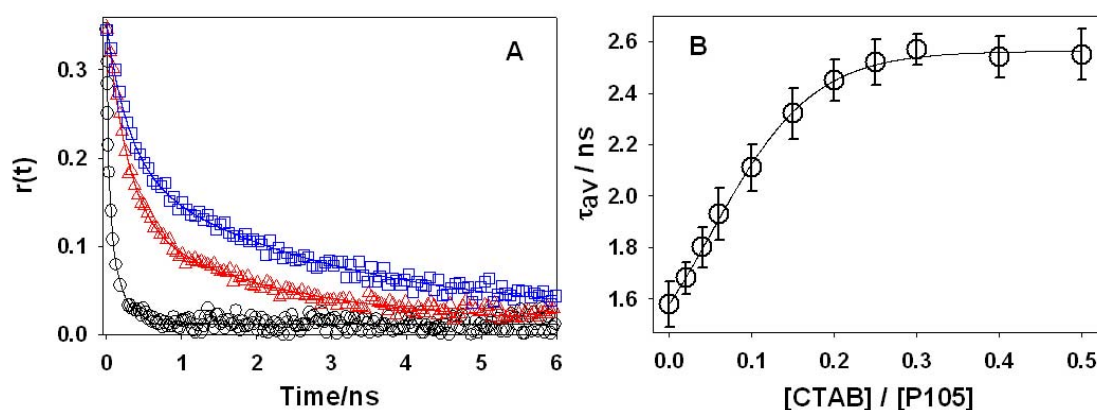


Figure 7.17. (A) Fluorescence anisotropy decay for C343 dye in water (o) and in P105 micellar solution at different CTAB/P105 molar ratio (Δ) 0.0 and (\square) 0.25 (B) Variation of average reorientation time for C343 dye in P105 micellar solution with the CTAB/P105 molar ratio.

Table 7.6. Time-resolved anisotropy parameters with varying [CTAB]/[P105] molar ratio

CTAB/P105 molar ratio	τ_{r1} (ns)	a_1	τ_{r2} (ns)	a_2	τ_{av} (ns)
0	0.32	0.26	2.02	0.74	1.58 \pm 0.09
0.02	0.36	0.26	2.15	0.74	1.68 \pm 0.06
0.04	0.38	0.22	2.20	0.78	1.80 \pm 0.08
0.06	0.39	0.21	2.34	0.79	1.93 \pm 0.10
0.1	0.39	0.19	2.52	0.81	2.11 \pm 0.09
0.15	0.38	0.16	2.70	0.84	2.33 \pm 0.10
0.2	0.46	0.19	2.92	0.81	2.45 \pm 0.08
0.25	0.40	0.15	2.90	0.85	2.52 \pm 0.09
0.3	0.42	0.15	2.95	0.85	2.57 \pm 0.06
0.4	0.44	0.17	2.97	0.83	2.54 \pm 0.08
0.5	0.40	0.15	2.93	0.85	2.55 \pm 0.10

These results clearly indicate that relatively large number of CTAB molecules are required to pull the probe molecules from the micellar surface to its interior as the corona thickness of the micelle increases. Figure 7.18 shows a correlation plot for the limiting CTAB concentration with the thickness of the corona region. It is seen from this figure that the limiting surfactant concentration and the corona thickness follow a nice linear correlation. These results clearly indicate that as we increase the thickness of the corona region, the electrostatic attraction between the probe at the micellar surface and the positively charged layer inside the micelle will be relatively weaker. Because of this, a relatively higher charge density, and consequently a larger CTAB concentration is required to pull the anionic C343 from the surface to the interior of the micelle.

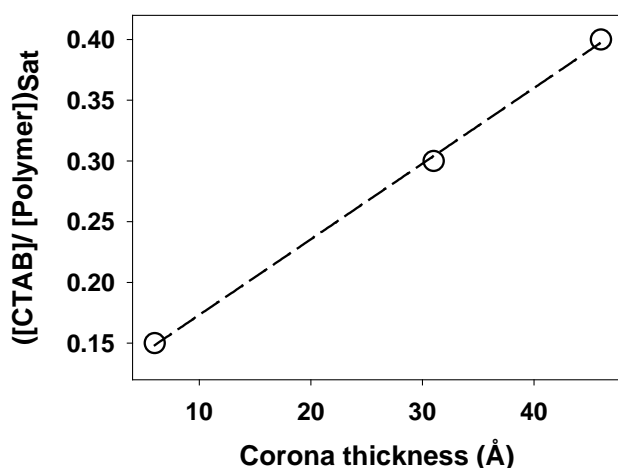


Figure 7.18. Figure shows the linear correlation between the limiting value of surfactant/polymer molar ratio and the thickness of corona region of the block copolymer.

The TRES and TRANES for C343 in P105 micelle following dynamic Stokes' shift measurement procedure are shown in Figure 7.19A and 7.19B respectively. Like P123-CTAC and F88-CTAC systems, in the present case also there is a time-dependent red shift in the TRES and the appearance of an isoemissive point in the TRANES. On addition of CTAB in P105 micelle, the isoemissive point disappear and the observed dynamic Stokes' shift ($\Delta\omega_s^{obs}$) increases, as shown in Figure 7.20A & 7.20B.

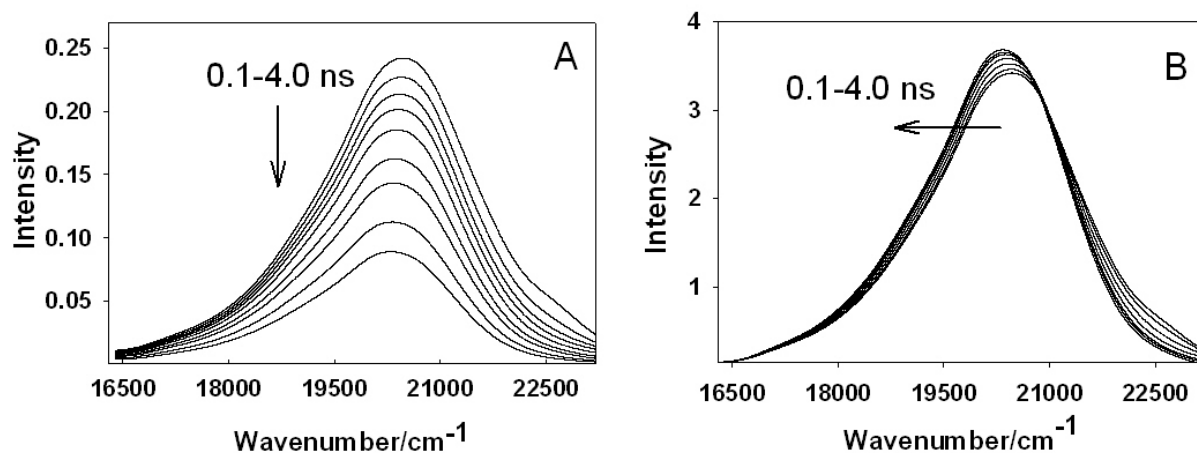


Figure 7.19. (A) Time-resolved emission spectra (TRES) and (B) Time-resolved area normalized emission spectra (TRANES) for C343 in P105 micellar solution.

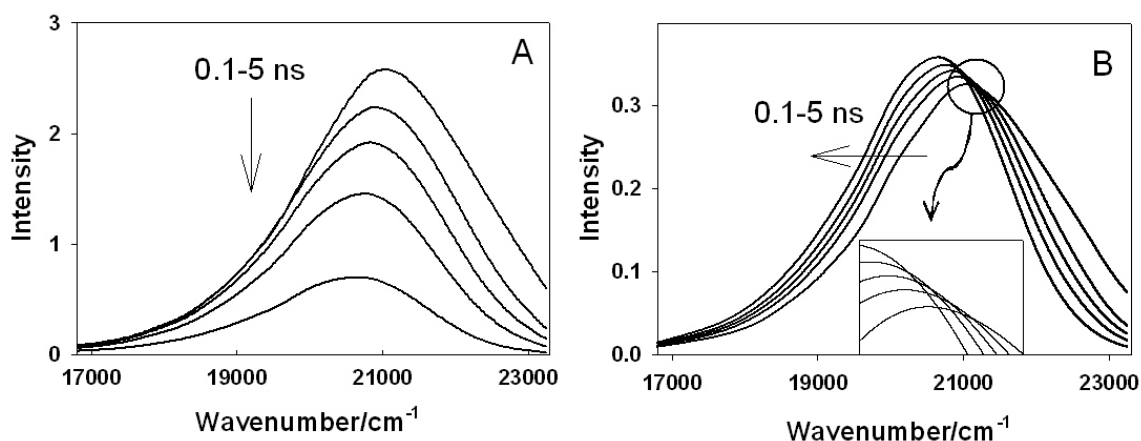


Figure 7.20. (A) Time-resolved emission spectra (TRES) and (B) Time-resolved area normalized emission spectra (TRANES) for C343 in P105 micellar solution at CTAB/P105 molar ratio of 0.4.

Table 7.7 lists $\Delta\omega_s^{total}$, $\Delta\omega_s^{obs}$ and $\Delta\omega_s^{\%obs}$ values of P105-CTAB systems at different CTAB/P105 ratios. The changes in the $\Delta\omega_s^{\%obs}$ with the increasing CTAB/P105 ratio are plotted in Figure 7.21. It is evident from Figure 7.21 that $\Delta\omega_s^{\%obs}$ also initially increases but ultimately reaches to a saturation value at a CTAB/P105 molar ratio of ~ 0.3 . Observed changes in the $\Delta\omega_s^{\%obs}$ value with CTAB concentration is suitably explained considering the movement of the probe from the micellar surface to interior by the electrostatic attraction of the charged positive layer developed in the P105-CTAB assembly for the negatively charged probe C343.

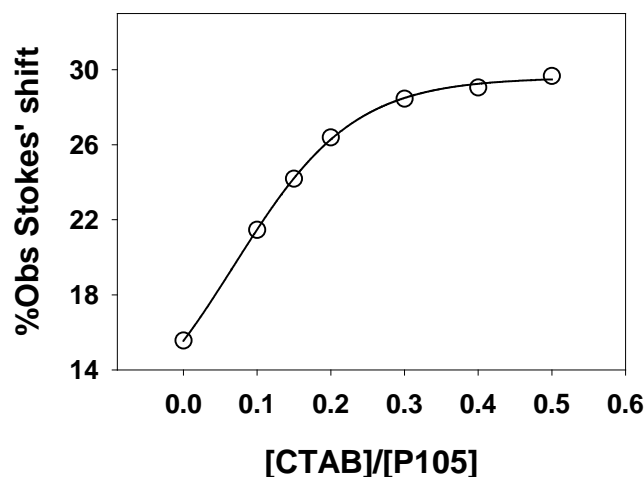


Figure 7.21. Variation in the percentage Stokes' shift observed for C343 dye in P105 micellar solution with the CTAB/P105 molar ratio.

Table 7.7. Dynamic Stokes' shift of C343 in P105 micelle at different CTAB concentrations.

$\frac{[CTAB]}{[P105]}$	Dynamic Stokes' shift		
	$\Delta\omega_s^{total} / \text{cm}^{-1}$	$\Delta\omega_s^{obs} / \text{cm}^{-1}$	$\Delta\omega_s^{\%obs}$
0.00	2423	378	15.6
0.10	2255	485	21.5
0.15	2170	525	24.2
0.20	2084	550	26.4
0.30	2065	588	28.5
0.40	2041	592	29.0
0.50	2035	605	29.7

7.3.4. Effect of addition of SDS on the solute location in the polymer-surfactant assembly

Further to understand the effect of repulsive electrostatic force on the location of the probe, we have also carried out the time-resolved anisotropy measurements in P105-SDS micellar system. Figure 7.22 shows the temporal anisotropy decay profile for C343 in P105-SDS system at two different SDS concentrations. It is clearly indicated from Figure 7.22 that similar to the R110 probe (positively charged) in F88-CTAB mixed micellar system discussed

earlier, there is no change in the anisotropy decay profile for C343 dye (negatively charged) in P105 micelle on addition of the anionic surfactant, SDS. It is thus indicated that the anionic surfactant does not cause any movement for the anionic probe C343 in the P105-SDS supramolecular assembly, as in these cases the probe always reside at the micellar surface. Similar observation have also been made for C343 dye in F88-SDS system.

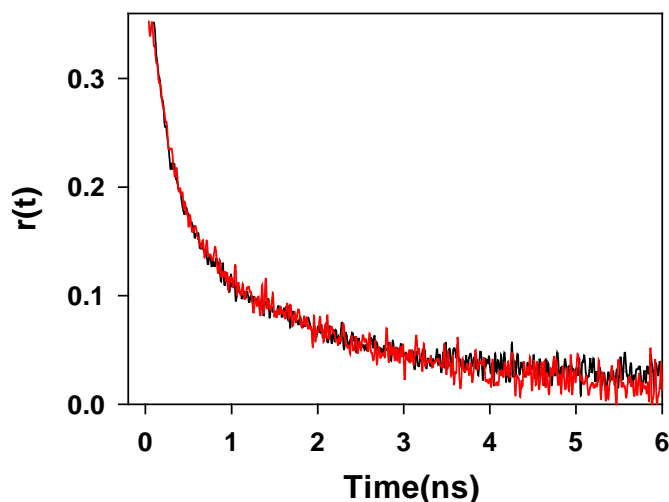


Figure 7.22. The anisotropy decay for C343 in P105-SDS supramolecular assemblies at different SDS/P105 molar ratio : (—) 0 and (—) 0.3.

7.3.5. Tuning the chemical reactivity in the nanocontainer

Microheterogeneous media like micelles can be considered as the nano-reactors/nano-containers, and have been used widely in various applications, e.g. as a confined media for organic synthesis,³⁹⁸⁻⁴⁰⁰ as a template for nanostructures,³⁸⁵⁻³⁸⁸ as drug carrier systems,⁴⁰¹⁻⁴⁰³ etc. In all these applications, the solute of interest is dissolved into the nano sized confined micellar media, and the efficiency of the desired process is determined largely by the physical and the chemical properties of the entrapped solute in these nano-reactors. Among other chemical processes, redox reactions are the most important processes involved in many of these applications. Even the pharmacological activity of certain molecules is believed to be related to their redox properties.⁴⁰⁴ Thus, controlling the reactivity of a chemical species by changing its redox behavior is always a desire to chemists. The most conventional route for

modulating the redox behavior of a molecule is its chemical modification/substitution. However, in this chemical route, the other important chemical properties of the species may get changed, which may result in some other unwanted chemical effects. Changing the chemical reactivity by some physical means is always a challenging task to chemists. After understanding that by controlling the surfactant/polymer ratio the location of the solute in these supramolecular assemblies can be controlled, which in turn can provide a control over its physicochemical properties, we wanted to explore if this can actually be realized to tune the redox potential accordingly to modulate the chemical reactivity of the entrapped solute.

Differential pulse polarography studies were carried out for C343 dye in P123 micellar solution at different CTAC concentration to investigate the effect of co-surfactant on the redox behavior of the solute. Differential pulse polarograms for C343 at different CTAC concentration are presented in Figure 7.23A. The peak potential of C343 in pure P123 micelle appears at -1.381 V. However, as we gradually increase the CTAC concentration, the polarographic peak gradually shifts towards the less negative potential. Thus, the peak potential of the dye measured at a CTAC/P123 molar ratio of ~ 0.2 is about -1.298 V. The variation in the peak potential (V_p) for the dye as a function of CTAC concentration in P123 micelle is shown in Figure 7.23B. A gradual change in the peak potential clearly indicates that the solute C343 gradually becomes stronger oxidant as the CTAC concentration is increased in the P123 micellar solution. It is also evident from Figure 7.23B that the redox potential of the solute tends to reach a limiting value at a CTAC/P123 molar ratio of ~ 0.15 . This implies that the property of the present solute does not change any further beyond a CTAC/P123 molar ratio of ~ 0.15 . The change in the redox characteristics of C343 is associated with only a little change in its absorption and fluorescence spectra. These results indicate that the addition of CTAC to the P123 micellar solution do not cause any change in the chemical nature of the dye and it is believed that the changes in the redox characteristics of the solute is due to the

changes in the microenvironment around the solute in P123 micelle as a function of CTAC concentration.

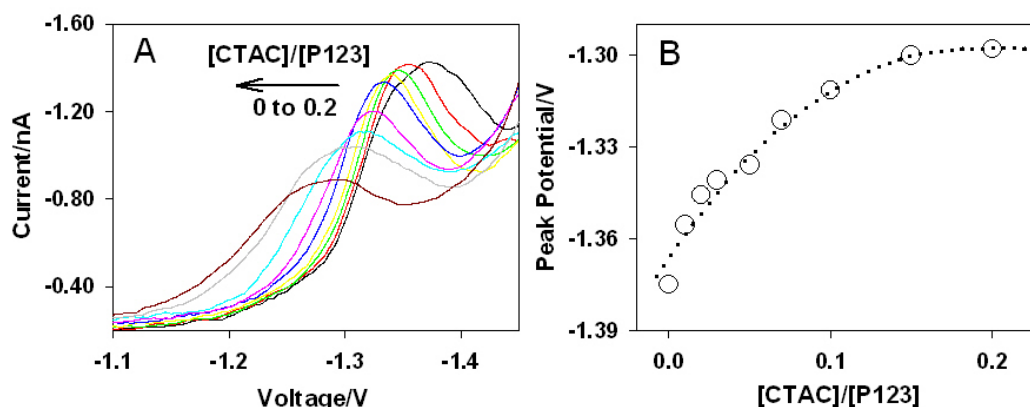


Figure 7.23. (A) Differential pulse polarograms and (B) variation of the peak potential (V_p) of C343 in P123 micellar solution at different CTAC concentration. The CTAC/P123 molar ratios used are 0.0, 0.01, 0.02, 0.03, 0.05, 0.07, 0.10, 0.15 and 0.20. Solid line is the best fitted smooth curve among the data points.

To understand whether the observed changes in the redox potentials are correlated with the changes observed in the rotational relaxation times, we have plotted, in the Figure 7.24, the changes in the peak potential vs. the changes in the reorientation time of the probe due to the addition of CTAC in the P123 micellar solution. It is clearly evident from this figure that the changes in the peak potential and the changes in reorientation time are linearly correlated to each other. This observation clearly indicates that the reason for the observed changes in the peak potentials is the same as that of the observed changes in the reorientation times of the probe in the present systems. The decrease in the polarographic current with an increase in the CTAC concentration, as indicated from Figure 7.23A, is a manifestation of the formation of the supramolecular assembly with P123 micelle. On increasing [CTAC]/[P123] ratio, more and more CTAC molecules are incorporated into P123 micelles, resulting an increase in the average weight of the micelles,⁴⁰⁵ and accordingly their diffusion in the solution becomes sluggish. As the polarographic current is directly related to the diffusion of the micelles, the

current should decrease with an increase in the CTAC concentration, as observed experimentally.

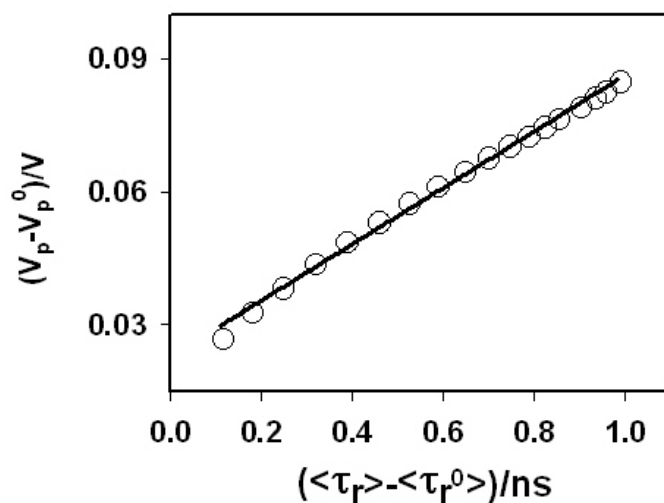


Figure 7.24. Plot for the differences in the peak potentials ($V_p - V_p^0$) vs the differences in the reorientation times ($\langle \tau_r \rangle - \langle \tau_r^0 \rangle$) of C343 in P123 micellar solution obtained at different CTAC additions. V_p^0 & $\langle \tau_r^0 \rangle$ are the peak potential and average reorientation time of C343 in P123 micellar solution in the absence of CTAC and their values are -1.381V and 0.3 ns, respectively. The solid line is the best fitted straight line through the data points.

The increase in the oxidation power of the probe, C343, on gradual increase in the CTAC concentration, is also a manifestation of the electrostatic interaction between head group of CTAC and the reduced form of the probe molecule.⁴⁰⁶ On reduction, the probe C343 becomes more negatively charged and hence gets stabilized in P123-CTAC supramolecular assembly due to the electrostatic attraction between oppositely charged species. This additional stabilization of the reduced form of C343 leads to an increase in the oxidation power of the dye in the supramolecular assembly.

Present study shows that in the supramolecular assembly, which can be considered as a nano-reactor, the location of the solute and consequently its redox potential can be tuned by changing the composition of these assemblies. As the chemical reactivity of a solute largely depends on its redox potential, the former can be controlled by a suitable choice of the composition of these nano-reactors. This phenomenon can also be utilized in other polymer-

surfactant systems and can find possible applications in various applied areas, like chemical synthesis in micellar media, biological activity of drug, etc.

7.4. Conclusions

It is demonstrated from the present study that the position of a suitable anionic probe in pluronic micellar phase can be changed by adding a positively charged co-surfactant CTAC or CTAB. It is indicated from SANS studies that the addition of ionic surfactant to a pluronic micellar solution results in the formation of unique supramolecular assemblies where the hydrocarbon chain of the surfactant molecules reside in the core of the pluronic micelle and the ionic head group of the surfactant resides at the core-corona interface. The positively charged layer thus formed in the CTAC-pluronic and CTAB-pluronic mixed micelles pulls the anionic probe from the micellar surface to their interior. Because of the availability of wide range of microenvironments in these micelles, the solutes can display quite different physical and chemical properties depending on its location in the micelle. Thus, by changing the position of a solute in these micelles, it is possible to modulate the physical as well as the chemical properties of the solute in these microheterogeneous systems. In one of the present systems, the probe migration has been shown to tune the redox potential of the solute by changing the composition of the supramolecular assembly. As the chemical reactivity of the solute largely depends on the redox potential, it can be controlled usefully by suitable selection of the composition of these supramolecular nanoreactors.

Present study further indicates that the effectiveness of a surfactant molecule to move a dissolved solute molecule from the surface to the interior of the micelle is largely determined by the thickness of the corona region, which in turn depends on the EO block size of the block copolymer used. It can be inferred from the present study, that by a proper selection of the polymer and the ionic surfactant, a suitably charged solute can be placed at different locations inside the mixed micelles simply by changing the concentration of the added surfactant. From

the studies with different pluronics it is indicated that the concentration of the ionic surfactant required to drag an oppositely charged probe molecule into the interior of the micelles is linearly correlated with the thickness of the corona region of the micelles used. By controlling the position of the solute in the micellar system, it is thus possible to tune the physical as well as chemical properties of the solute, which may have several applications, especially in the chemical synthesis and controlled drug release systems.

REFERENCES

- (1) Fleming, G. R. *Chemical Applications of Ultrafast Spectroscopy* Oxford University: Oxford, 1986.
- (2) Glasstone, S.; Laidler, K. J.; Eyring, H. *The Theory of Rate Processes* McGraw-Hill: New York, 1941.
- (3) Barbara, P. F.; Walker, G. C.; Smith, T. P. *Science* **1992**, *256*, 975.
- (4) Vos, M. H.; Rappaport, F.; Lambry, J. C.; Breton, J.; Martin, J. L. *Nature (London)* **1993**, *363*, 320.
- (5) Akesson, E.; Bergstrom, H.; Sundstrom, V.; Gillbro, T. *Chem. Phys. Lett.* **1986**, *125*, 385.
- (6) Ben-Amotz, D.; Harris, C. B. *Chem. Phys. Lett.* **1985**, *119*, 305.
- (7) Ben-Amotz, D.; Harris, C. B. *J. Chem. Phys.* **1987**, *86*, 5433.
- (8) Ben-Amotz, D.; Jeanloz, R.; Harris, C. B. *J. Chem. Phys.* **1987**, *86*, 6119.
- (9) Cremers, D. A.; Windsor, M. W. *Chem. Phys. Lett.* **1980**, *71*, 27.
- (10) Doust, T. *Chem. Phys. Lett.* **1983**, *96*, 522.
- (11) Engh, R. A.; Petrich, J.; Fleming, G. R. *J. Phys. Chem.* **1985**, *89*, 618.
- (12) Mentzel, R.; Hoganson, C. W.; Windsor, M. W. *Chem. Phys. Lett.* **1985**, *120*, 29.
- (13) Rettig, W.; Vogel, M.; Lippert, E.; Otto, H. *Chem. Phys.* **1986**, *108*, 381.
- (14) Sundstrom, V.; Gillbro, T. *J. Chem. Phys.* **1984**, *81*, 3463.
- (15) Sundstrom, V.; Gillbro, T.; Bergstrom, H. *Chem. Phys.* **1982**, *73*, 439.
- (16) Glasbeek, M.; Zhang, H. *Chem. Rev.* **2004**, *104*, 1929.
- (17) Grabowski, Z. R. *Pure Appl. Chem.* **1992**, *64*, 1249.
- (18) Grabowski, Z. R. *Pure Appl. Chem.* **1993**, *65*, 1751.
- (19) Rotkiewicz, K.; Grellmann, K. H.; Grabowski, Z. R. *Chem. Phys. Lett.* **1973**, *19*, 315.
- (20) Grabowski, Z. R.; Rotkiewicz, K.; Rettig, W. *Chem. Rev.* **2003**, *103*, 3899 and references there in.
- (21) Corrie, J. E. T.; Munasinghe, V. R. N.; Rettig, W.; . *J. Heterocycl. Chem.* **2000**, *37*, 1447.
- (22) Bagchi, B.; Fleming, G. R. *J. Phys. Chem.* **1990**, *94*, 9.

- (23) Glasbeek, M.; Zhang, H.; van der Meer, M. J. *Journal of Molecular Liquids* **2000**, *86*, 123.
- (24) Tachiya, M.; Murata, S. *J. Am. Chem. Soc* **1994**, *116*, 2434.
- (25) Bagchi, B.; Gayathri, N. *Adv. Chem. Phys.* **1999**, *1*, 107.
- (26) Agmon, N.; Hopfield, J. J. *Chem. Phys.* **1983**, *78*, 6947.
- (27) Ernst, O. P.; Bartl, F. J. *ChemBioChem* **2002**, *3*, 968.
- (28) Stenkamp, R. E.; Teller, D. C.; Palczewski, K. *ChemBioChem* **2002**, *3*, 963.
- (29) Unger, V. M.; Hargrave, P. A.; Baldwin, J. M.; Schertler, G. F. X. *Nature* **1997**, *389*, 203.
- (30) Haupts, U.; Tittor, J.; Oesterhelt, D. *Annu. Rev. Biophys. Biomol. Struct.* **1999**, *28*, 367.
- (31) Andel, F.; Hasson, K. C.; Gai, F.; Anfinrud, P. A.; Mathies, R. A. *Biospectroscopy* **1997**, *3*, 421.
- (32) Quail, P.; Boylan, M. T.; Parks, B. M.; Short, T. W.; Xu, Y.; Wagner, D. *Science* **1995**, *268*, 675.
- (33) Bhattacharyya, K.; Bagchi, B. *J. Phys. Chem. A* **2000**, *104*, 10603.
- (34) Castner, E. W.; Fleming, G. R.; Bagchi, B.; Maroncelli, M. *J. Chem. Phys.* **1988**, *89*, 3519.
- (35) Fee, R. S.; Maroncelli, M. *Chem. Phys.* **1994**, *183*, 235.
- (36) Fee, R. S.; Milsom, J. A.; Maroncelli, M. *J. Phys. Chem.* **1991**, *95*, 5170.
- (37) Hara, K.; Kuwabara, H.; Kajimoto, O. *J. Phys. Chem. A* **2001**, *105*, 7174.
- (38) Maroncelli, M. *J. Mol. Liq.* **1993**, *57*, 1.
- (39) Maroncelli, M.; Fleming, G. R. *J. Chem. Phys.* **1987**, *86*, 6221.
- (40) Maroncelli, M.; Macinnis, J.; Fleming, G. R. *Science* **1989**, *243*, 1674.
- (41) Nandi, N.; Bhattacharyya, K.; Bagchi, B. *Chem. Rev.* **2000**, *100*, 2013.
- (42) Riter, E. R.; Willard, D. M.; Levinger, N. E. *J. Phys. Chem. B* **1998**, *102*, 2705.
- (43) Sarkar, N.; Datta, A.; Das, S.; Bhattacharyya, K. *J. Phys. Chem.* **1996**, *100*, 15483.
- (44) Sen, P.; Mukherjee, S.; Halder, A.; Bhattacharyya, K. *Chem. Phys. Lett.* **2004**, *385*, 357.
- (45) Willard, D. M.; Riter, R. E.; Levinger, N. E. *J. Am. Chem. Soc.* **1998**, *120*, 4151.
- (46) van der Zwan, G.; Hynes, J. T. *J. Phys. Chem.* **1985**, *89*, 4181.

- (47) Chandra, A.; Bagchi, B. *Chem. Phys. Lett.* **1990**, *165*, 93.
- (48) De, T.; Maitra, A. *Adv. Colloid Interface Sci.* **1995**, *59*, 95.
- (49) Luisi, P. L.; Giomini, M.; Pileni, M. P.; Robinson, B. H. *Biochim. Biophys. Acta* **1988**, *947*, 209.
- (50) Paul, B. K.; Moulik, S. P. *J. Dispers. Sci. Technol.* **1997**, *18*, 301.
- (51) Pileni, M. P. *J. Phys. Chem.* **1993**, *97*, 6961.
- (52) Silber, J. J.; Biasutti, A.; Abuin, E.; Lissi, E. *Adv. Colloid Interface Sci.* **1999**, *82*, 189.
- (53) Uskokovic, V.; Drogenik, M. *Adv. Colloid Interface Sci.* **2007**, *133*, 23.
- (54) Shrestha, L. K.; Sato, T.; Dulle, M.; Glatter, O.; Aramaki, K. *J. Phys. Chem. B* **2010** *114*, 12008.
- (55) Shrestha, L. K.; Shrestha, R. G.; Oyama, K.; Matsuzawa, M.; Aramaki, K. *J. Phys. Chem. B* **2009**, *113*, 12669.
- (56) Luisi, P. L.; Straub, B. E. *Reverse Micelles: Biological and Technological Relevance of Amphiphilic Structures in Apolar Media*; Plenum Press: New York, 1984.
- (57) Corbeil, E. M.; Levinger, N. E. *Langmuir* **2003**, *19*, 7264.
- (58) Correa, N. M.; Biasutti, M. A.; Silber, J. J. *J. Colloid Interface Sci.* **1995**, *172*, 71.
- (59) Garcia-Rio, L.; Hervella, P. *Chemistry* **2006**, *12*, 8284.
- (60) Hickey, S.; Lawrence, M. J.; Hagan, S. A.; Buckin, V. *Langmuir* **2006**, *22*, 5575.
- (61) Lopez, F.; Cinelli, G.; Ambrosone, L.; Colafemmina, G.; Ceglie, A.; Palazzo, G. *Colloid Surf. A* **2004**, *237*, 49.
- (62) Nagarajan, R.; Ruckenstein, E. *Langmuir* **1991**, *7*, 2934.
- (63) Palazzo, G.; Lopez, F.; Giustini, M.; Colafemmina, G.; Ceglie, A. *J. Phys. Chem. B* **2003**, *107*.
- (64) Pant, D.; Levinger, N. E.; . *Langmuir* **2000**, *16*, 10123.
- (65) Rodriguez, J.; Marti, J.; Guardia, E.; Laria, D. *J. Phys. Chem. B* **2007**, *111*, 4432.
- (66) Sando, G. M.; Dahl, K.; Owrutsky, J. C. *J. Phys. Chem. B* **2005**, *109*, 4084.
- (67) Schubert, K. V.; Kaler, E. W. *Ber. Bunsen-Ges. Phys. Chem.* **1996**, *100*, 190.
- (68) Strey, R.; Glatter, O.; Schubert, K. V.; Kaler, E. W. *J. Chem. Phys.* **1996**, *105*, 1175.
- (69) Willard, D. M.; Levinger, N. E. *J. Phys. Chem. B* **2000**, *104*, 11075.

- (70) Zhu, D. M.; Feng, K. I.; Schelly, Z. A. *J. Phys. Chem.* **1992**, *96*, 2382.
- (71) Zulauf, M.; Eicke, H. F. *J. Phys. Chem.* **1979**, *83*, 480.
- (72) Christopher, D. J.; Yarwood, J.; Belton, P. S.; Hills, B. P. *J. Colloid Interface Sci.* **1992**, *152*, 465.
- (73) D'Angelo, M.; Onori, G.; Santucci, A. *J. Phys. Chem.* **1994**, *98*, 3189.
- (74) Faeder, J.; Ladanyi, B. M. *J. Phys. Chem. B* **2000**, *104*, 1033.
- (75) Jain, T. K.; Varshney, M.; Maitra, A. *J. Phys. Chem.* **1989**, *93*, 7409.
- (76) Li, Q.; Weng, S. F.; Wu, J. G.; Zhou, N. F. *J. Phys. Chem. B* **1998**, *102*, 3168.
- (77) Moran, P. D.; Bowmaker, G. A.; Cooney, R. P.; Bartlett, J. R.; Woolfrey, J. L. *Langmuir* **1995**, *11*, 738.
- (78) Valero, M.; Sanchez, F.; Gomez-Herrera, C.; Lopez-Cornejo, P. *Chem. Phys.* **2008**, *345*, 65.
- (79) Venables, D. S.; Huang, K.; Schmuttenmaer, C. A. *J. Phys. Chem. B* **2001**, *105*, 9132.
- (80) Dokter, A. M.; Woutersen, S.; Bakker, H. J. *Proc. Natl. Acad. Sci. USA* **2006**, *103*, 15355.
- (81) Piletic, I. R.; Moilanen, D. E.; Spry, D. B.; Levinger, N. E.; Fayer, M. D. *J. Phys. Chem. A* **2006**, *110*, 4985.
- (82) Piletic, I. R.; Tan, H. S.; Fayer, M. D. *J. Phys. Chem. B* **2005**, *109*, 21273.
- (83) Tan, H. S.; Piletic, I. R.; Fayer, M. D. *J. Chem. Phys.* **2005**, *122*, 174501.
- (84) Fioretto, D.; Freda, M.; Mannaioli, S.; Onori, G.; Santucci, A. *J. Phys. Chem. B* **1999**, *103*, 2631.
- (85) Freda, M.; Onori, G.; Paciaroni, A.; Santucci, A. *J. Mol. Liq.* **2002**, *101*, 55.
- (86) Ikushima, Y.; Saito, N.; Arai, M. *J. Colloid Interface Sci.* **1997**, *186*, 254.
- (87) MacDonald, H.; Bedwell, B.; Gulari, E. *Langmuir* **1986**, *2*, 704.
- (88) Temsamani, M. B.; Maeck, M.; Hassani, I. E.; Hurwitz, H. D. *J. Phys. Chem. B* **1998**, *102*, 3335.
- (89) Zhong, Q.; Baronavski, A. P.; Owrutsky, J. C. *J. Chem. Phys.* **2003**, *119*, 9171.
- (90) Chattopadhyay, A.; Mukherjee, S.; Raghuraman, H. *J. Phys. Chem. B* **2002**, *106*, 13002.
- (91) Correa, N. M.; Levinger, N. E. *J. Phys. Chem. B* **2006**, *110*, 13050.
- (92) Hazra, P.; Chakrabarty, D.; Sarkar, N. *Langmuir* **2002**, *18*, 7872.

- (93) Hazra, P.; Sarkar, N. *Phys. Chem. Chem. Phys.* **2002**, *4*, 1040.
- (94) Munson, C. A.; Baker, G. A.; Baker, S. N.; Bright, F. V. *Langmuir* **2004**, *20*, 1551.
- (95) Pant, D.; Riter, R. E.; Levinger, N. E. *J. Chem. Phys.* **1998**, *109*, 9995.
- (96) Riter, R. E.; Kimmel, J. R.; Undiks, E. P.; Levinger, N. E. *J. Phys. Chem. B* **1997**, *101*, 8292.
- (97) Riter, R. E.; Undiks, E. P.; Kimmel, J. R.; Levinger, N. E. *J. Phys. Chem. B* **1998**, *102*, 7931.
- (98) Riter, R. E.; Undiks, E. P.; Levinger, N. E. *J. Am. Chem. Soc.* **1998**, *120*, 6062.
- (99) Riter, R. E.; Willard, D. M.; Levinger, N. E. *J. Phys. Chem. B* **1998**, *102*, 2705.
- (100) Shirota, H.; Horie, K. *J. Phys. Chem. B* **1999**, *103*, 1437.
- (101) Spry, D. B.; Goun, A.; Glusac, K.; Moilanen, D. E.; Fayer, M. D. *J. Am. Chem. Soc.* **2007**, *129*, 8122.
- (102) Baruah, B.; Roden, J. M.; Sedgwick, M.; Correa, N. M.; Crans, D. C.; Levinger, N. E. *J. Am. Chem. Soc.* **2006**, *128*, 12758.
- (103) Baruah, B.; Swafford, L. A.; Crans, D. C.; Levinger, N. E. *J. Phys. Chem. B* **2008**, *112*, 10158.
- (104) Carlstrom, G.; Halle, B. *Langmuir* **1988**, *4*, 1346.
- (105) Hauser, H.; Haering, G.; Pande, A.; Luisi, P. L. *J. Phys. Chem.* **1989**, *93*, 7869.
- (106) Wong, M.; Thomas, J. K.; Nowak, T. *J. Am. Chem. Soc.* **1977**, *99*, 4730.
- (107) Boned, C.; Peyrelasse, J.; Moha-Ouchane, M. *J. Phys. Chem.* **1986**, *90*, 634.
- (108) Eastoe, J.; Towey, T. F.; Robinson, B. H.; Williams, J.; Heenan, R. K. *J. Phys. Chem.* **1993**, *97*, 1459.
- (109) Harpham, M. R.; Ladanyi, B. M.; Levinger, N. E.; Herwig, K. W. *J. Chem. Phys.* **2004**, *121*, 7855.
- (110) Abel, S.; Sterpone, F.; Bandyopadhyay, S.; Marchi, M. *J. Phys. Chem. B* **2004**, *108*, 19458.
- (111) Derecskei, B.; Derecskei-Kovacs, A.; Schelly, Z. A. *Langmuir* **1999**, *15*, 1981.
- (112) Faeder, J.; Albert, M. V.; Ladanyi, B. M. *Langmuir* **2003**, *19*, 2514.
- (113) Harpham, M. R.; Ladanyi, B. M.; Levinger, N. E. *J. Phys. Chem. B* **2005**, *109*, 16891.
- (114) Senapati, S.; Berkowitz, M. L. *J. Chem. Phys.* **2003**, *118*, 1937.

- (115) Cringus, D.; Lindner, J.; Milder, M. T. W.; Pshenichnikov, M. S.; Vchringer, P.; Wiersma, D. A. *Chem. Phys. Lett.* **2005**, *408*, 162.
- (116) Levinger, N. E. *Science* **2002**, *298*, 1722.
- (117) Lakowicz, J. R. *Principle of fluorescence spectroscopy*; Plenum Press: New York, 2006.
- (118) *Encyclopedia of Supramolecular Chemistry*; Marcel Dekker: New York, 2004.
- (119) Easton, C. J.; Lincoln, S. F. *Modified Cyclodextrins- Scaffolds and Templates for Supramolecular Chemistry*; Imperial College Press: London, 1999.
- (120) Liu, Y.; Chen, Y. *Acc. Chem. Res.* **2006**, *39*, 681.
- (121) Rekharsky, M. V.; Inoue, Y. *Chem. Rev.* **1998**, *98*, 1875.
- (122) Uekama, K.; Hirayama, F.; Irie, T. *Chem. Rev.* **1998**, *98*, 2045.
- (123) Breslow, R.; Dong, S. D. *Chem. Rev.* **1998**, *98*, 1997.
- (124) Chen, Y.; Liu, Y. *Chem. Soc. Rev.* **2010**, *39*, 495.
- (125) D'Souza, V. T.; Bender, M. L. *Acc. Chem. Res.* **1987**, *20*, 146.
- (126) Breslow, R. *Science* **1982**, *218*, 532.
- (127) Tabushi, I.; . *Acc. Chem. Res.* **1982**, *15*, 66.
- (128) Saenger, W. *Angew. Chem. Int. Ed. Engl.* **1980**, *19*, 344.
- (129) Murakami, Y.; Kikuchi, J.; Hisaeda, Y.; Hayashida, O. *Chem. Rev.* **1996**, *96*, 721.
- (130) Harper, J. B.; Easton, C. J.; Lincoln, S. F. *Curr. Org. Chem.* **2000**, *4*, 429.
- (131) Loftsson, T.; Jarvinen, T. *Adv. Drug Delivery Rev.* **1999**, *36*, 59.
- (132) Shinoda, T.; Kagatani, S.; Maeda, A.; Konno, Y.; Hashimoto, H.; Hara, K.; Fujita, K.; Sonobe, T. *Drug Dev. Ind. Pharm.* **1999**, *25*, 1185.
- (133) Ogoshi, T.; Harada, A. *Sensors* **2008**, *8*, 4961.
- (134) Li, S.; Purdy, W. C. *Chem. Rev.* **1992**, *92*, 1457.
- (135) Cho, D. W.; Kim, Y. H.; Kang, S. G.; Yoon, M. *J. Phys. Chem.* **1994**, *98*, 558.
- (136) Cox, G. S.; Turro, N. J. *J. Am. Chem. Soc.* **1984**, *106*, 422.
- (137) Douhal, A. *Chem. Rev.* **2004**, *104*, 1955.
- (138) Hamai, S. *J. Phys. Chem. B* **1997**, *101*, 1707.

- (139) Mallick, A.; Haldar, B.; Chattopadhyay, N. *J. Photochem. Photobiol. B* **2005**, *78*, 215.
- (140) Singh, M. K.; Pal, H.; Koti, A. S. R.; Sapre, A. V. *J. Phys. Chem. A* **2004**, *108*, 1465.
- (141) Alexandridis, P.; Hatton, T. A. *Colloids Surf. A* **1995**, *96*, 1.
- (142) Alexandridis, P.; Holzwarth, J. F.; Hatton, T. A. *Macromolecules* **1994**, *27*, 2414.
- (143) Goddard, E. D. *J. Colloid Interface Sci.* **2002**, *256*, 228.
- (144) Mortensen, K.; Brown, W.; Norden, B. *Phys. Rev. Letts.* **1992**, *68*, 2340.
- (145) Mortensen, K.; Pederson, J. S. *Macromolecules* **1993**, *26*, 805.
- (146) Zhou, Z.; Chu, B. *J. Colloid Interface Sci.* **1988**, *126*, 171.
- (147) Alakhov, V. Y.; Kabanov, A. V. *Expert Opin. Invest. Drugs* **1998**, *7*, 1453.
- (148) Bahadur, P.; Riess, G. *Tenside, Surfactants, Deterg.* **1991**, *28*, 173.
- (149) Batrakova, E. V.; Han, H. Y.; Miller, D. W.; Kabanov, A. V. *Pharm. Res.* **1998**, *15*, 1525.
- (150) Guzman, M.; Garcia, F. F.; Molpeceres, J.; Aberturas, M. R. *Int. J. Pharm.* **1992**, *80*, 119.
- (151) Kabanov, A.; Zhu, J.; Alakhov, V. *Adv. Genet.* **2005**, *53*, 231.
- (152) Park, T. G.; Cohen, S.; Langer, R. *Parm. Res.* **1992**, *9*, 37.
- (153) Yokoyama, M. *Crit. Rev. Therapeutic Drug Carrier Syst.* **1992**, *9*, 213.
- (154) Wang, H.; Lin, W.; Fritz, K.; Scholes, G.; Winnik, M.; Manners, I. *J. Am. Chem. Soc.* **2007**, *129*, 12924.
- (155) Wang, H.; Patil, A. J.; Liu, K.; Petrov, S.; Mann, S.; Winnik, M. A.; Manners, I. *Adv. Mater.* **2009**, *21*, 1805.
- (156) Chu, B.; Zhou, Z. Physical chemistry of polyoxyalkylene block copolymer surfactants. In *Nonionic surfactants*; Nace, V. M., Ed.; Marcel Dekker: New York, 1996; Vol. 60; pp 67.
- (157) Wanka, G.; Hoffmann, H.; Ulbricht, W. *Macromolecules* **1994**, *27*, 4145.
- (158) Brown, W.; Schillen, K.; Almgren, M.; Hvidt, S.; Bahadur, P. *J. Phys. Chem.* **1991**, *95*, 1850.
- (159) Wanka, G.; Hoffmann, H.; Ulbricht, W. *Colloid. Polym. Sci.* **1990**, *268*, 101.
- (160) Malmsten, M.; Lindman, B. *Macromolecules* **1992**, *25*, 5440.
- (161) Rassing, J.; Attwood, D. *Int. J. Pharm.* **1983**, *13*, 47.

- (162) Ganguly, R.; Aswal, V. K.; Hassan, P. A.; Gopalakrishnan, I. K.; Kulshreshth, S. K. *J. Phys. Chem. B* **2006**, *110*, 9843.
- (163) Ganguly, R.; Aswal, V. K.; Hassan, P. A.; Gopalakrishnan, I. K.; Yakhmi, J. V. *J. Phys. Chem. B* **2005**, *109*, 5653.
- (164) Mortensen, K.; Brown, W. *Macromolecules* **1993**, *26*, 4128.
- (165) Jansson, J.; Schillen, K.; Nilsson, M.; Soderman, O.; Fritz, G.; Bergmann, A.; Glatter, O. *J. Phys. Chem. B* **2005**, *109*, 7073.
- (166) Jansson, J.; Schillen, K.; Olofsson, G.; Silva, R. C. d.; Loh, W. *J. Phys. Chem. B* **2004**, *108*, 82.
- (167) Lopes, J. R.; Loh, W. *Langmuir* **1998**, *14*, 750.
- (168) Alexandridis, P.; Nivaggioli, T.; Hatton, T. A. *Langmuir* **1995**, *11*, 1468.
- (169) Nakashima, K.; Anzai, T.; Fujimoto, Y. *Langmuir* **1994**, *10*, 658.
- (170) Dutt, G. B. *J. Phys. Chem. B* **2005**, *109*, 4923.
- (171) Mali, K. S.; Dutt, G. B. *J. Chem. Sci.* **2007**, *119*, 147.
- (172) Mali, K. S.; Dutt, G. B.; Ganguly, R.; Mukherjee, T. *J. Chem. Phys.* **2005**, *123*, 144913.
- (173) Mali, K. S.; Dutt, G. B.; Mukherjee, T. *J. Phys. Chem. B* **2007**, *111*, 5878.
- (174) Nad, S.; Kumbhakar, M.; Pal, H. *J. Phys. Chem. A* **2003**, *107*, 4808.
- (175) Grant, C. D.; DeRitter, M. R.; Steege, K. E.; Fadeeva, T. A.; Castner, E. W. *Langmuir* **2005**, *21*, 1745.
- (176) Grant, C. D.; Steege, K. E.; Bunagan, M. R.; Castner, E. W. *J. Phys. Chem. B* **2005**, *109*, 22273.
- (177) Ghosh, S.; Adhikari, A.; Mandal, U.; Dey, S.; Bhattacharyya, K. *J. Phys. Chem. C* **2007**, *111*, 8775.
- (178) Mandal, U.; Adhikari, A.; Dey, S.; Ghosh, S.; Mondal, S. K.; Bhattacharyya, K. *J. Phys. Chem. B* **2007**, *111*, 5896.
- (179) Sen, P.; Ghosh, S.; Sahu, K.; Mondal, S. K.; Roy, D.; Bhattacharyya, K. *J. Chem. Phys.* **2006**, *124*, 204905.
- (180) Kumbhakar, M. *J. Phys. Chem. B* **2007**, *111*, 12154.
- (181) Kumbhakar, M.; Ganguly, R. *J. Phys. Chem. B* **2007**, *111*, 3935.
- (182) Kumbhakar, M.; Geol, T.; Nath, S.; Mukherjee, T.; Pal, H. *J. Phys. Chem. B* **2006**, *110*, 25646.

- (183) Pancheri, E. J.; Mao, M. H. K. Comprising anionic surfactant polymeric nonionic surfactant and betaine surfactant US Patent, 1992.
- (184) Schafer, R. Use of pluronic surfactant to enhance the cleaning effect of pancreatin on contact lenses US Patent, 1997.
- (185) Sastry, N. V.; Hoffmann, H. *Colloid Surf. A* **2004**, *250*, 247.
- (186) Tama, K. C.; Wyn-Jones, E. *Chem. Soc. Rev.* **2006**, *35*, 693.
- (187) Li, Y.; Xu, R.; Bloor, D. M.; Holzwarth, J. F.; Wyn-Jones, E. *Langmuir* **2000**, *16*, 10515.
- (188) Li, Y.; Xu, R.; Couderc, S.; Bloor, D. M.; Holzwarth, J. F.; Wyn-Jones, E. *Langmuir* **2001**, *17*, 5742.
- (189) Silva, R. C. d.; Olofsson, G.; Schille'n, K.; Loh, W. *J. Phys. Chem. B* **2002**, *106*, 1239.
- (190) Stsiapura, V. I.; Maskevich, A. A.; Kuzmitsky, V. A.; Turoverov, K. K.; Kuznetsova, I. M. *J. Phys. Chem. A* **2007**, *111*, 4829.
- (191) Chiti, F.; Dobson, C. M. *Annu. Rev. Biochem.* **2006**, *75*, 333.
- (192) Gestwicki, J. E.; Crabtree, G. R.; Graef, I. A. *Science* **2004**, *306*, 865.
- (193) Gilead, S.; Gazit, E. *Angew. Chem. Int. Ed.* **2004**, *43*, 4041.
- (194) Mishra, R.; Winter, R. *Angew. Chem. Int. Ed.* **2008**, *47*, 6518.
- (195) Maskevich, A. A.; Stsiapura, V. I.; Kuzmitsky, V. A.; Kuznetsova, I. M.; Povarova, O. I.; Uversky, V. N.; Turoverov, K. K. *J. Proteome Res.* **2007**, *6*, 1392.
- (196) LeVine, H., III. *Protein Sci.* **1993**, *2*, 404.
- (197) Raj, C. R.; Ramaraj, R. *Photochem. Photobio.* **2001**, *74*, 752.
- (198) Schirra, R. *Chem. Phys. Letts.* **1985**, *119*, 463.
- (199) Birks, J. B. *Photo Physics of Aromatic Molecules*; Wiley-Interscience: New York, 1970.
- (200) Gilbert, A.; Baggott, J.; Wagner, P. J. *Essential of Molecular Photochemistry*; Blackwell science Inc.: Cambridge, USA, 1991.
- (201) Lackowicz, J. R. *Principles of fluorescence spectroscopy*, 3rd ed.; Springer: New York, 2006.
- (202) Rohatgi-Mukherjee, K. K. *Fundamentals of Photochemistry*; Wiley Eastern Ltd: India, 1986.
- (203) Velapoldi, R. A.; Mielenz, K. D. *Standard Reference Materials: A fluorescence standard reference material: Quinine sulfate dihydrate* **1980**, Nat. Bur. Stand. (US) Spec. Publ. 260.

- (204) Becker, W. *Advanced time correlated single photon counting technique*; Springer: New York, 2005.
- (205) Demas, J. N. *Excited state lifetime measurement*; Academic press: New York, 1983.
- (206) O'Connor, D. V.; Phillips, D. *Time Correlatated Single Photon Counting*; Academic: New York, 1984.
- (207) Ware, W. R. Creation and detection of the Excited State; Lamola, A. A., Ed.; Marcel Dekker: New York, 1971; Vol. 1, Part A. .
- (208) Bevington, P. R. *Data Reduction and Error Analysis for the Physical Sciences*; McGraw-Hill: New York, 1969.
- (209) Gedcke, D. A.; McDonald, W. J. *Nucl. Instrum. Meth.* **1967**, *55*, 377.
- (210) Gedcke, D. A.; McDonald, W. J. *Nucl. Instrum. Meth.* **1968**, *58*, 253.
- (211) Haugen, G. R.; Wallin, B. W.; Lytle, J. E. *Rev. Sci. Instrum.* **1972**, *50*, 64.
- (212) Yguerabide, J. *Meth. Enzymol* **1972**, *26*, 498.
- (213) McKinnon, A. E.; Szabo, A. G.; Miller, D. R. *J. Phys Chem.* **1977**, *81*, 1564.
- (214) O'Connor, D. V.; Ware, W. R.; Andre, J. C. *J. Phys. Chem.* **1979**, *83*, 1333.
- (215) Ware, W. R.; Doemeny, L. J.; Nemzek, T. L. *J. Phys Chem.* **1973**, *77*, 2083.
- (216) Ito, M.; Kume, H.; Oba, K. *IEEE Trans. Nucl. Sci.* **1984**, *NS-31*, 408.
- (217) Singh, P. K.; Kumbhakar, M.; Ganguly, R.; Aswal, V. K.; Pal, H.; Nath, S. *J. Phys. Chem. B* **2010**, *114*, 3818.
- (218) Singh, P. K.; Kumbhakar, M.; Pal, H.; Nath, S. *J. Phys. Chem. B* **2008**, *112*, 7771.
- (219) Singh, P. K.; Kumbhakar, M.; Pal, H.; Nath, S. *J. Phys. Chem. B* **2009**, *113*, 1353.
- (220) Singh, P. K.; Satpati, A. K.; Kumbhakar, M.; Pal, H.; Nath, S. *J. Phys. Chem. B* **2008**, *112*, 11447.
- (221) Bebelaar, D. *Rev. Sci. Instrum.* **1986**, *57*, 1116.
- (222) Duguay, M. A. *Progress in Optics* Amsterdam, Netherlands, 1976; Vol. XIV.
- (223) Duguay, M. A.; Hansen, J. M. *Opt. Commun* **1969**, *1*, 254.
- (224) Kahlow, M. A.; Jarzeba, W.; DuBruil, T. P.; Barbara, P. F. *Rev. Sci. Instrum.* **1988**, *59*, 1098.
- (225) Mahr, H.; Hirsch, M. D. *Opt. Commun.* **1975**, *13*, 96.
- (226) Shah, J. *IEEE J. Quant. Elect.* **1988**, *24*, 276.

- (227) Becke, A. D. *J. Chem. Phys.* **1993**, *98*, 5648.
- (228) Lee C; Yang W; Parr, R. G. *Phys. Rev. B* **1998**, *37*, 785.
- (229) Frisch, M. J.; Trucks, G. W.; Schlegel, H. B.; al., e. GAUSSIAN 03; Gaussian, Inc.: Wallingford, CT, 2004.
- (230) Barone, V.; Cossi, M. *J. Phys. Chem. A* **1998**, *102*, 1995.
- (231) Aswal, V. K.; Goyal, P. S. *Current Sci.* **2000**, *79*, 947.
- (232) Chen, S. H.; Lin, T. L. Colloidal solutions. In *Methods of experimental physics: neutron scattering*; Price, D. L., Skold, K., Eds.; Academic Press: New York, 1987; Vol. 23B; pp 489.
- (233) Pedersen, J. S. *J. Appl. Cryst.* **2000**, *33*, 637.
- (234) Ashcroft, N. W.; Leckner, J. *Phys. Rev.* **1966**, *145*, 83.
- (235) Kinnig, D. J.; Thomas, E. L. *Macromolecules* **1984**, *17*, 1712.
- (236) Jain, N. J.; Aswal, V. K.; Goyal, P. S.; Bahadur, P. *J. Phys. Chem. B* **1998**, *102*, 8452.
- (237) Percus, J. K.; Yevick, G. J. *Phys. Rev.* **1958**, *110*, 1.
- (238) Aswal, V. K.; Kohlbrecher, J. *Chem. Phys. Lett.* **2006**, *425* 118.
- (239) Singh, P. K.; Kumbhakar, M.; Pal, H.; Nath, S. *J. Phys. Chem. B* **2009**, *113*, 8532.
- (240) Ban, T.; Yamaguchi, K.; Goto, Y. *Acc. Chem. Res.* **2006**, *39*, 663.
- (241) Cabaleiro-Lago, C.; Quinlan-Pluck, F.; Lynch, I.; Lindman, S.; Minogue, A. M.; Thulin, E.; Walsh, D. M.; Dawson, K. A.; Linse, S. *J. Am. Chem. Soc.* **2008**, *130*, 15437.
- (242) Vetri, V.; Canale, C.; Relini, A.; Librizzi, F.; Militello, V.; Gliozzi, A.; Leone, M. *Biophys. Chem.* **2007**, *125*, 184.
- (243) Khurana, R.; Coleman, C.; Ionescu-Zanetti, C.; Carter, S. A.; Krishna, V.; Grover, R. K.; Roy, R.; Singh, S. *J. Struct. Biol.* **2005**, *151*, 229.
- (244) Groenning, M.; Olsen, L.; Weert, M. v. d.; Flink, J. M.; Frokjaer, S.; Jørgensen, F. S. *J. Struct. Biol.* **2007**, *158*, 358.
- (245) Kitts, C. C.; Bout, D. A. V. *J. Phys. Chem. B* **2009**, *113*, 12090.
- (246) Abedini, A.; Meng, F.; Raleigh, D. P. *J. Am. Chem. Soc.* **2007**, *129*, 11300.
- (247) Soldi, G.; Bemporad, F.; Chiti, F. *J. Am. Chem. Soc.* **2008**, *130*, 4295.
- (248) Yagi, H.; Ban, T.; Morigaki, K.; Naiki, H.; Goto, Y. *Biochem.* **2007**, *46*, 15009.
- (249) Yona, R. L.; Mazeres, S.; Faller, P.; Gras, E. *Chem. Med. Chem.* **2008**, *3*, 63.

- (250) Friedhoff, P.; Schneider, A.; Mandelkow, E.-M.; Mandelkow, E. *Biochemistry* **1998**, *37*, 10223.
- (251) Raj, C. R.; Ramaraj, R. *J. Photochem. Photobio. A: Chem.* **1999**, *122*, 39.
- (252) Sabate, R.; Lascu, I.; Saupe, S. J. *J. Struct. Biol.* **2008**, *162*, 387.
- (253) Stsiapura, V. I.; Maskevich, A. A.; Kuzmitsky, V. A.; Uversky, V. N.; Kuznetsova, I. M.; Turoverov, K. K. *J. Phys. Chem. B* **2008**, *112*, 15893.
- (254) Jurczok, M.; Plaza, P.; Martin, M. M.; Rettig, W. *J. Phys. Chem. A* **1999**, *103*, 3372.
- (255) Vogel, M.; Rettig, W. *Ber. Bunsen-Ges. Phys. Chem.* **1985**, *89*, 962.
- (256) Loutfy, R. O. *macromolecules* **1981**, *14*, 270.
- (257) Saha, S. K.; Purkayastha, P.; Das, A. B.; Dhara, S. *J. Photochem. Photobio. A: Chem.* **2008**, *199*, 179.
- (258) Voropai, E. S.; Samtsov, M. P.; Kaplevskii, K. N.; Maskevich, A. A.; Stepuro, V. I.; Povarova, O. I.; Kuznetsova, I. M.; Turoverov, K. K.; Fink, A. L.; Uverskiid, V. N. *J. Appl. Spec.* **2003**, *70*, 868.
- (259) Aldrich Library of ¹³C and ¹H FT NMR Spectra; Aldrich, 1993.
- (260) Neunert, G.; Polewski, P.; P.Walejko; Markiewicz, M.; S.Witkowski; Polewski, K. *Spectrochim. Acta Part A* **2009**, *73*, 301.
- (261) Manno, M.; Giacomazza, D.; Newman, J.; Martorana, V.; Biagio, P. L. S. *Langmuir* **2010**, *26*, 1424.
- (262) Nad, S. Studies on photoinduced electron transfer and charge transfer processes in solution phase. Doctoral Thesis, University of Bombay, 2002.
- (263) Weast, R. C. *CRC Handbook of Chemistry and Physics*; The Chemical Rubber Co., 1970.
- (264) Dutt, G. B.; Srivatsavoy, V. J. P.; Sapre, A. V. *J. Chem. Phys.* **1999**, *111*, 9705.
- (265) Liley, P. E.; Makita, T.; Tanaka, Y. Properties of Inorganic and Organic Fluids; Ho, C. Y., Ed.; Hemisphere: New York, 1988.
- (266) Changenet, P.; Zhang, H.; van der Meer, M. J.; Glasbeek, M.; Plaza, P.; Martin, M. M. *J. Phys. Chem. A* **1998**, *102*, 6716.
- (267) van der Meer, M. J.; Zhang, H.; Glasbeek, M. *J. Chem. Phys.* **2000**, *112*, 2878.
- (268) Koti, A. S. R.; Krishna, M. M. G.; Periasamy, N. *J. Phys. Chem. A* **2001**, *105*, 1767.
- (269) Koti, A. S. R.; Periasamy, N. *J. Chem. Phys.* **2001**, *115*, 7094.
- (270) Rocker, C.; Heilemann, A.; Fromherz, P. *J. Phys. Chem.* **1996**, *100*, 12172.

- (271) Volchkov, V. V.; Hoa, G. H. B.; Kossanyi, J. A.; Gromov, S. P.; Alfimov, M. V.; Uzhinov, B. M. *J. Phys. Org. Chem.* **2005**, *18*, 21.
- (272) Huang, Y.; Cheng, T.; Li, F.; Huang, C.-H.; Wang, S.; Huang, W.; Gong, Q. *J. Phys. Chem. B* **2002**, *106*, 10041.
- (273) Veldhoven, E. v.; Zhang, H.; Rettig, W.; Brown, R. G.; Hepworth, J. D.; Glasbeek, M. *Chem. Phys. Lett.* **2002**, 363 189.
- (274) Hawe, A.; Sutter, M.; Jiskoot, W. *Pharm. Res.* **2008**, *25*, 1487.
- (275) Loutfy, R. O.; Arnold, B. A. *J. Phys. Chem.* **1982**, *86*, 4205.
- (276) Oster, G.; Nishijima, Y. *J. Am. Chem. Soc.* **1956**, *78*, 1581.
- (277) Dzwolak, W.; Pecul, M. *FEBS Letts.* **2005**, *579*, 6601.
- (278) Fodera, V.; Groenning, M.; Vetri, V.; Librizzi, F.; Spagnolo, S.; Cornett, C.; Olsen, L.; Weert, M. v. d.; Leone, M. *J. Phys. Chem. B* **2008**, *112*, 15174.
- (279) Singh, P. K.; Kumbhakar, M.; Pal, H.; Nath, S. *J. Phys. Chem. B* **2010**, *114*, 2541.
- (280) Aberg, U.; Akesson, E.; Alvarez, J. L.; Fedchenia, I.; Sundstrom, V. *Chem. Phys.* **1994**, *183*, 269.
- (281) Changuenet, P.; Zhang, H.; van der Meer, M. J.; Hellingwerf, K. J.; Glasbeek, M. *Chem. Phys. Lett.* **1998**, *282*, 276.
- (282) Chosrowjan, H.; Mataga, N.; Nakashima, N.; Imamaoto, Y.; Tokunaga, F. *Chem. Phys Lett.* **1997**, *270*, 267.
- (283) Du, M.; Fleming, G. R. *Biophys. Chem.* **1993**, *48*, 101.
- (284) Kandori, H.; Sasabe, H. *Chem. Phys. Lett.* **1993**, *216*, 126.
- (285) Yartsev, A.; Alvarez, J. L.; Aberg, U.; Sundstrom, V. *Chem. Phys. Lett.* **1995**, *243*, 281.
- (286) Levinger, N. E.; Riter, R. E. Solvation Dynamics at Liquid Interfaces. In *Liquid Interfaces in Chemical, Biological, and Pharmaceutical Applications*; Volkov, A. G., Ed.; Marcel Dekker: New York, 2001; pp 399.
- (287) Zhang, J.; Bright, F. V. *J. Phys. Chem.* **1991**, *95*, 7900.
- (288) Pileni, M. P. *Structure and Reactivity of Reverse Micelles*; Elsevier: New York, 1989.
- (289) Kotlarchyk, M.; Hum, J. S.; Chen, S. H. *J. Phys. Chem.* **1986**, *89*, 4382.
- (290) Mukherjee, K.; Moulik, S. P. *Langmuir* **1993**, *9*, 1727.
- (291) Kumar, S.; Singh, A. K.; Krishnamoorthy, G.; Swaminathan, R. *J. Fluoresc.* **2008**, *18*, 1199.

- (292) Srivastava, A.; Singh, P. K.; Kumbhakar, M.; Mukherjee, T.; Chattopadhyay, S.; Pal, H.; Nath, S. *Chem. Eu. J.* **2010**, *16*, 9257.
- (293) Singh, P. K.; Kumbhakar, M.; Pal, H.; Nath, S. *J. Phys. Chem. B* **2010**, *114*, 5920.
- (294) Jaraudias, J. *J. Photochem.* **1980**, *13*, 35.
- (295) Velsko, S. P.; Fleming, G. R. *Chem. Phys.* **1982**, *65*, 59.
- (296) Hasegawa, M.; Sugimura, T.; Suzaki, Y.; Shindo, Y.; Kitahara, A. *J. Phys. Chem.* **1994**, *98*, 2120.
- (297) Keh, E.; Valeur, B. *J. Colloid Interface Sci.* **1981**, *79*, 465.
- (298) Borsarelli, C. D.; Braslavsky, S. E. *J. Phys. Chem. B* **1997**, *101*, 6036.
- (299) Zinsli, P. E. *J. Phys. Chem.* **1979**, *83*, 3223.
- (300) Bhattacharyya, K. *Acc. Chem. Res.* **2003**, *36*, 95.
- (301) Choudhury, S. D.; Kumbhakar, M.; Nath, S.; Sarkar, S. K.; Mukherjee, T.; Pal, H. *J. Phys. Chem. B* **2007**, *111*, 8842.
- (302) Chang, C. W.; Lu, Y. C.; Wang, T. T.; Diao, E. W. G. *J. Am. Chem. Soc.* **2004**, *126*, 10109.
- (303) Kim, J.; Park, S.; Scherer, N. F. *J. Phys. Chem. B* **2008**, *112*, 15576.
- (304) Westenhoff, S.; Beenken, W. J. D.; Friend, R. H.; Greenham, N. C.; Yartsev, A.; Sundstrom, V. *Phys. Rev. Letts.* **2006**, *97*, 166804.
- (305) Jain, T. K.; Varshney, M.; Maitra, A. *J. Phys. Chem.* **1989**, *93*, 7409.
- (306) Haidekker, M. A.; Theodorakis, E. A. *Org. Biomol. Chem.* **2007**, *5*, 1669.
- (307) Caselli, M.; Mangone, A.; Traini, A. *Ann. Chim.* **1998**, *88*, 299.
- (308) Ueda, M.; Kimura, A.; Wakida, T.; Yoshimura, Y.; Schelly, Z. A. *J. Colloid Interface Sci.* **1994**, *163*, 515.
- (309) Caselli, M.; Daniele, V.; Mangone, A.; Paolillo, P. *J. Colloid Interface Sci.* **2000**, *221*, 173.
- (310) Caselli, M.; Mangone, A.; Paolillo, P.; Traini, A.; . *Ann. Chim.* **2002**, *92*, 501.
- (311) Gunaseelan, K.; Romsted, L. S.; Gonzalez-Romero, E.; Bravo-Diaz, C. *Langmuir* **2004**, *20*, 3047.
- (312) Hung, H.-C.; Chang, G.-G. *J. Chem. Soc., Perkin Trans.* **1999**, *2*, 2177.
- (313) Lissi, E. A.; Abuin, E. B.; Rubio, M. A.; Ceron, A. *Langmuir* **2000**, *16*, 178.
- (314) Sarma, S.; Dutta, R. K. *J. Surfactants Deterg.* **2005**, *8*, 277.

- (315) Singh, A. K.; Majumdar, N. *J. Photochem. Photobiol. B: Biol.* **1995**, *30*, 105.
- (316) Correa, N. M.; Biasutti, M. A.; Silber, J. J. *J. Colloid Interface Sci.* **1996**, *184*, 570.
- (317) McNeil, R.; Thomas, J. K. *J. Colloid Interface Sci.* **1981**, *83*, 57.
- (318) Abuin, E.; Lissi, E.; Duarte, R.; Silber, J. J.; Biasutti, M. A. *Langmuir* **2002**, *18*, 8340.
- (319) Sato, C.; Kikuchi, K. *J. Phys. Chem.* **1992**, *96*, 5601.
- (320) Bilensoy, E. *Expert Opin Drug Deliv.* **2010**, *7*, 795.
- (321) Janes, K. A.; Fresneau, M. P.; Marazuela, A.; Fabra, A.; Alonso, M. J. *Journal of Controlled Release* **2001**, *73*, 255.
- (322) Teng, X. R.; Shchukin, D. G.; ohwald, H. M. *Langmuir* **2008**, *24*, 383.
- (323) Hartig, W.; Paulke, B. R.; Varga, C.; Seeger, J.; Harkany, T.; Kacza, J. *Neuroscience Letters* **2003**, *338*, 174.
- (324) Maezawa, I.; Hong, H. S.; Liu, R.; Wu, C. Y.; Cheng, R. H.; Kung, M. P.; Kung, H. F.; Lam, K. S.; Oddo, S.; LaFerla, F. M.; Jin, L. W. *Journal of Neurochemistry* **2008**, *104*, 457.
- (325) *Supramolecular Chemistry*; Balzani, V.; DeCola, L., Eds.; Kluwer Academic Publishers: Dordrecht, Netherlands, 1992.
- (326) Komiyama, M.; Shigekawa, H. In *Comprehensive Supramolecular Chemistry*; Atwood, J. L., Davies, J. E. D., MacNicol, D. D., Vögtle, F., Eds.; Pergamon: New York, 1996; Vol. 3; pp 401.
- (327) *Frontiers in Supramolecular Chemistry and Photochemistry*; Schneider, H. J.; Durr, H., Eds.; VCH: Weinheim, 1992.
- (328) *Cyclodextrin Chemistry*; Bender, M. L.; Komiyama, M., Eds.; Springer Verlag: Berlin, 1978.
- (329) *Comprehensive Supramolecular Chemistry*; Szejtli, J.; Osa, T., Eds.; Elsevier: New York, 1996; Vol. 3.
- (330) Davis, M. E.; Brewster, M. E. *Nature Reviews Drug Discovery* **2004**, *3*, 1023.
- (331) Hapiot, F.; Tilloy, S.; Monflier, E. *Chem. Rev.* **2006**, *106*, 767.
- (332) Villalonga, R.; Cao, R.; Fragoso, A. *Chem. Rev.* **2007**, *107*, 3088.
- (333) Saenger, W. *Angew. Chem. Int. Ed. Engl.* **1980**, *19*, 344.
- (334) Dasaratha Reddy, G.; Ramamurthy, V. *J. Org. Chem.* **1987**, *52*, 3952.
- (335) Shayira Banu, H.; Lalitha, A.; Pitchumani, K.; Srinivasan, C. *Chem. Commun.* **1999**, 607.

- (336) Chachisvilis, M.; Garcia-Ochoa, I.; Douhal, A.; Zewail, A. H. *Chem. Phys. Lett.* **1998**, *293*, 153.
- (337) Douhal, A.; Fiebig, T.; Chachisvilis, M.; Zewail, A. H. *J. Phys. Chem. A* **1998**, *102*, 1657.
- (338) Flachenecker, G.; Behrens, P.; Knopp, G.; Schmitt, M.; Siebert, T.; Vierheilig, A.; Wirnsberger, G.; Materny, A. *J. Phys. Chem. A* **1999**, *103*, 3854.
- (339) Varnavski, O.; Goodson, T. T. *Chem. Phys. Lett.* **2000**, *320*, 688.
- (340) Zewail, A. *J. Phys. Chem. A* **2000**, *104*, 5660.
- (341) Douhal, A. Femtochemistry in Nanocavities. In *Femtochemistry*; De Schryver, F. C., De Feyter, S., Schweitzer, G., Eds.; Wiley-VCH: Weinheim, 2001.
- (342) Zhong, D.; Douhal, A.; Zewail, A. H. *Proc. Natl. Acad. Sci. U.S.A.* **2000**, *97*, 14056.
- (343) Ashanagar, A.; Naseri, N. G.; B., K. *E-Journal of Chemistry* **2007**, *4*, 550.
- (344) Sarkar, D.; Bose, D.; Mahata, A.; Ghosh, D.; Chattopadhyay, N. *J. Phys. Chem. B* **2010**, *114*, 2261.
- (345) Yuan, Z.; Zhu, M.; Han, S. *Analytica Chimica Acta* **1999**, *389*, 291.
- (346) Groenning, M. *J. Chem. Biol.* **2010**, *3*, 1.
- (347) Changenet, P.; Zhang, H.; Meer, M. J. v. d.; Glasbeek, M. *J. Phys. Chem. A* **1998**, *102*, 6716.
- (348) Yartsev, A.; Alvarez, J. L.; Aberg, U.; Sundstrom, V. *Chem. Phys. Lett.* **1995**, *243*.
- (349) Nandi, N.; Bhattacharyya, K.; Bagchi, B. *Chem. Rev.* **2000**, *100*, 2013.
- (350) Raguraman, H.; Kelkar, D. A.; Chattopadhyay, A. Novel insights in to protein structure and dynamics utilizing the red edge excitation shift approach. In *Reviews in Fluorescence*; Geddes, C. D., Lakowicz, J. R., Eds.; Springer: New York, 2005; pp 199.
- (351) Chudoba, C.; Nibbering, E. T. J.; Elsaesser, T. *Phys. Rev. Lett.* **1998**, *81*, 3010.
- (352) Shirota, H.; Tamoto, Y.; Segawa, H. *J. Phys. Chem. A* **2004**, *108*, 3244.
- (353) Kumbhakar, M.; Nath, S.; Pal, H.; Sapre, A. V.; Mukherjee, T. *J. Chem. Phys.* **2003**, *119*, 388.
- (354) Duttachoudhury, S.; Kumbhakar, M.; Nath, S.; Pal, H. *J. Chem. Phys.* **2007**, *127*, 194901.
- (355) Brauns, E. B.; Madaras, M. L.; Coleman, R. S.; Murphy, C. J.; Berg, M. A. *Phys. Rev. Lett.* **2002**, *88*, 158101.

- (356) Andreatta, D.; Lustres, J. L. P.; Kovalenko, S. A.; Ernsting, N. P.; Murphy, C. J.; Coleman, R. S.; Berg, M. A. *J. Am. Chem. Soc.* **2005**, *127*, 7270.
- (357) Andreatta, D.; Sen, S.; Lustres, J. L. P.; Kovalenko, S. A.; Ernsting, N. P.; Murphy, C. J.; Coleman, R. S.; Berg, M. A. *J. Am. Chem. Soc.* **2006**, *128*, 6885.
- (358) Pierce, D. W.; Boxer, S. G. *J. Phys. Chem. B* **1992**, *96*, 5560.
- (359) Pal, S. K.; Peon, J.; Zewail, A. H. *Proc. Natl. Acad. Sci. USA*. **2002**, *99*, 1763.
- (360) Jones II, G.; Jackson, W. R.; Konaktanaporn, S. *Opt. Commun.* **1980**, *33*, 315.
- (361) Jimenez, R.; Fleming, G. R.; Kumar, P. V.; Maroncelli, M. *Nature* **1994**, *369*, 471.
- (362) Jones II, G.; Jackson, W. R.; Helpert, A. M. *Chem. Phys. Lett.* **1980**, *72*, 391.
- (363) Jones II, G.; Jackson, W. R.; Choi, C.; Bergmark, W. R. *J. Phys. Chem.* **1985**, *89*, 294.
- (364) Rettig, W. *Angew Chem. Int. Ed. Engl.* **1986**, *25*, 971.
- (365) Nad, S.; Kumbhakar, M.; Pal, H. *J. Phys. Chem. A* **2003**, *107*, 4808.
- (366) Jarzeba, W.; Walker, G. C.; Johnson, A. E.; Barbara, P. F. *Chem. Phys.* **1991**, *152*, 57.
- (367) Maroncelli, M.; Fleming, G. R. *J. Chem. Phys.* **1987**, *86*, 6221.
- (368) Kahlow, M. A.; Kang, T. J.; Barbara, P. F. *J. Chem. Phys.* **1988**, *88*, 2372.
- (369) Maroncelli, M. *J. Mol. Liq.* **1993**, *57*, 1.
- (370) Lakowitz, J. R. *Principle of Fluorescence Spectroscopy*, 3rd ed.; Springer: New York, 2006.
- (371) Gearheart, L. A.; Somoza, M. M.; Rivers, W. E.; Murphy, C. J.; Coleman, R. S.; Berg, M. A. *J. Am. Chem. Soc.* **2003**, *125*, 11812.
- (372) Chapman, C. F.; Fee, R. S.; Maroncelli, M. *J. Phys. Chem.* **1995**, *99*, 4811.
- (373) Spry, D. B.; Goun, A.; Fayer, M. D. *J. Phys. Chem. A* **2007**, *111*, 230.
- (374) Smith, N. A.; Meech, S. R.; Rubtsov, I. V.; Yoshihara, K. *Chem. Phys. Letts.* **1999**, *303*, 209.
- (375) Wyman, J. J. *J. Am. Chem. Soc.* **1936**, *58*, 1485.
- (376) Bakshiev, N. G. *Opt. Spectrosc.* **1964**, *16*, 446.
- (377) Barbara, P. F.; Jarzeba, W. *Advan. Photochem.* **1990**, *15*, 1.
- (378) Bagchi, B.; Oxtoby, D. W.; Fleming, G. R. *Chem. Phys.* **1984**, *86*, 257.

- (379) Röcker, C.; Heilemann, A.; Fromherz, P. *J. Phys. Chem.* **1996**, *100*, 12172.
- (380) Agmon, N. *J. Phys. Chem.* **1990**, *94*, 2959.
- (381) Birks, J. B. *Photophysics of Aromatic Molecules*; Wiley: New York, 1970.
- (382) Maroncelli, M.; Fee, R. S.; Chapman, C. F.; Fleming, G. R. *J. Phys. Chem.* **1991**, *95*, 1012.
- (383) Nakashima, K.; Bahadur, P. *J. Controlled Release* **2002**, *82*, 189.
- (384) Schmolka, I. R. *J. Am. Oil Chem. Soc.* **1980**, *59* 322.
- (385) Forster, S.; Antonietti, M. *Adv. Mater.* **1998**, *10*, 195.
- (386) Förster, S.; Konrad, M. *J. Mater. Chem.* **2003**, *13*, 2671.
- (387) Sakai, T.; Alexandridis, P. *Langmuir* **2005**, *21*, 8019.
- (388) Zhao, D.; Huo, Q.; Feng, J.; Chmelka, B. F.; Stucky, G. D. *J. Am. Chem. Soc.* **1998**, *120*, 6024.
- (389) Mali, K. S.; Dutt, G. B.; Mukherjee, T. *J. Chem. Phys.* **2007**, *127*, 1549041.
- (390) Verma, P.; Nath, S.; Singh, P. K.; Kumbhakar, M.; Pal, H. *J. Phys. Chem. B* **2008**, *112*, 6363.
- (391) Ma, J.; Guo, C.; Tang, Y.; Xiang, J.; Chen, S.; Wang, J.; Liu, H. *J. Colloid Interface Sci.* **2007**, *312*, 390.
- (392) Willard, D. M.; Riter, R. E.; Levinger, N. E. *J. Am. Chem. Soc.* **1998**, *120*, 4151.
- (393) Kalyanasundaram, K. *Photochemistry in microheterogeneous systems*; Academic Press Inc.: Orlando, 1987.
- (394) Koti, A. S. R.; Krishna, M. M. G.; Periasamy, N. *J. Phys. Chem. A* **2001**, *105*, 1767.
- (395) Koti, A. S. R.; Periasamy, N. *J. Chem. Phys.* **2001**, *115*, 7094.
- (396) Almgren, M.; Stam, J. V.; Lindblad, C.; Li, P.; Stilbs, P.; Bahadur, P. *J. Phys. Chem.* **1991**, *95*, 5677.
- (397) Yang, L.; Alexandridis, P. *Langmuir* **2000**, *16*, 4819.
- (398) Klier, J.; Tucker, C. J.; Kalantar, T. H.; Green, D. P. *Adv. Mater.* **2000**, *12*, 1751.
- (399) Lindström, U. M. *Chem. Rev.* **2002**, *102*, 2751.
- (400) Vriezema, D. M.; Aragono's, M. C.; Elemans, J. A. A. W.; Cornelissen, J. J. L. M.; Rowan, A. E.; Nolte, R. J. M. *Chem. Rev.* **2005**, *105*, 1445.

- (401) Kabanova, A. V.; Batrakovaa, E. V.; Alakhovb, V. Y. *J. Controlled Release* **2002**, *82*, 189.
- (402) Kataoka, K.; Harada, A.; Nagasaki, Y. *Adv. Drug. Deliver. Rev.* **2001**, *47*, 113.
- (403) Lavasanifar, A.; Samuel, J.; Kwon, G. S. *Adv. Drug Delivery Rev.* **2002**, *54*, 169.
- (404) Sereda, G.; Heukelom, J. V.; Koppang, M.; Ramreddy, S.; Collins, N. *Beilstein J. Org. Chem.* **2006**, *2*, 26.
- (405) Parry, E. P.; Osteryoung, R. A. *Anal. Chem.* **1965**, *37*, 1634.
- (406) Prado-Gotor, R.; Jimenez, R.; Perez-Tejeda, P.; Lopez-Lopez, M.; Sanchez, F. *Chem. Phys.* **2001**, *263*, 139.

LIST OF PUBLICATIONS

1. Quantitative Distinction between Competing Intramolecular Bond Twisting & Solvent Relaxation Dynamics: An Ultrafast Study

Prabhat K. Singh, Sukhendu Nath, Manoj Kumbhakar, A. C. Bhasikuttan, and Haridas Pal

J. Phys. Chem. A, 112, 5598–5603, 2008.

2. Effect of electrostatic interaction on the location of molecular probe in polymer-surfactant supramolecular assembly: A solvent relaxation study

Prabhat K. Singh, Manoj Kumbhakar, Haridas Pal, and Sukhendu Nath

J. Phys. Chem. B, 112, 7771-7777, 2008.

3. A Nanoreactor for Tuning the Chemical Reactivity of a Solute

Prabhat K. Singh, A. K. Satpati, Manoj Kumbhakar, Haridas Pal, and Sukhendu Nath

J. Phys. Chem. B (Letter), 112, 11447–11450, 2008. (**Art work appeared as the cover page**)

4. Ultrafast Torsional Dynamics of Protein binding dye, Thioflavin T, in Nanoconfined Water Pool

Prabhat K. Singh, Manoj Kumbhakar, Haridas Pal, and Sukhendu Nath

J. Phys. Chem. B, 113, 8532–8538, 2009.

5. Modulation in the solute location in block copolymer-surfactant supramolecular assembly: A time resolved fluorescence study

Prabhat K. Singh, Manoj Kumbhakar, Haridas Pal, and Sukhendu Nath

J. Phys. Chem. B, 113, 1353-1359, 2009.

6. Change in the location of a solute in Pluronic- surfactant supramolecular assembly: A fluorescence and neutron scattering study

Prabhat K. Singh, Manoj Kumbhakar, Rajib Ganguly, V. K. Aswal, Haridas Pal, and Sukhendu Nath

J. Phys. Chem. B, *114*, 3818-3826, 2010.

7. Ultrafast Bond Twisting Dynamics in Amyloid Fibril Sensor

Prabhat K. Singh, Manoj Kumbhakar, Haridas Pal, and Sukhendu Nath

J. Phys. Chem. B, *114*, 2541-2546, 2010.

8. Viscosity effect on the ultrafast bond twisting dynamics in an amyloid fibril sensor : Thioflavin- T

Prabhat K. Singh, Manoj Kumbhakar, Haridas Pal, and Sukhendu Nath

J. Phys. Chem. B, *114*, 5920-5927, 2010.

9. Identifying the bond responsible for the fluorescence modulation in amyloid fibril sensor

Anvita Srivastava, **Prabhat K. Singh**, Manoj Kumbhakar, Tulsi Mukherjee, Subrata Chattopadhyay, Haridas Pal and Sukhendu Nath

Chem Euro J., *16*, 9257-9263, 2010

10. Confined Ultrafast Torsional Dynamics of Thioflavin-T in a Nanocavity

Prabhat K. Singh, Manoj Kumbhakar, Haridas Pal, and Sukhendu Nath

Phys. Chem. Chem. Phys., 2011 (Accepted)

11. Nano-confined Charged Layer Defy the Rule of Electrostatic Interaction

Prabhat K. Singh, Manoj Kumbhakar, Haridas Pal, and Sukhendu Nath

(Communicated)